

Alma Mater Studiorum – Università di Bologna

DOTTORATO DI RICERCA

Scienze Farmaceutiche

Ciclo XXI

Settore scientifico disciplinare di afferenza: CHIM/08

**DESIGN AND SYNTHESIS OF NOVEL
NON PEPTIDOMIMETIC BETA-SECRETASE
INHIBITORS IN THE TREATMENT
OF ALZHEIMER'S DISEASE**

Presentata da: **Dott. Riccardo Matera**

Coordinatore Dottorato

Chiar.mo Prof.
Maurizio Recanatini

Relatore

Chiar.ma Prof.ssa
Anna Minarini

Correlatore

Chiar.mo Prof.
Carlo Melchiorre

Esame finale anno 2009

Table of Contents

Abstract	page	1
1. Introduction	page	3
1.1. Alzheimer's Disease (AD)	page	5
1.1.1. The cholinergic deficit in AD	page	6
1.1.2. The "amyloid cascade hypothesis"	page	11
1.1.2.1. β -Amyloid-based therapeutics	page	14
1.1.3. Oxidative stress in AD	page	19
1.1.4. Neuroinflammation	page	23
1.2. β -Secretase (BACE1)	page	24
1.3. BACE1 inhibitors	page	30
1.3.1. Transition-state analogues: from peptidomimetics to small molecules inhibitors	page	31
1.3.2. Non-transition-state-derived small molecules	page	40
1.4. Alternative therapeutic approaches to targeting β -secretase	page	44
1.5. Multi Target Directed Ligands to combat AD	page	46
References	page	50
2. Aim of the thesis	page	63
2.1. Design of heterocycles-based BACE1 inhibitors	page	63
2.2. Design of δ -aminocyclohexane carboxylic acid-based BACE1 inhibitors	page	69
References	page	73
3. Chemistry	page	75
3.1. Synthesis of heterocycles-based BACE1 inhibitors	page	75
3.2. Synthesis of δ -aminocyclohexane carboxylic acid-based BACE1 inhibitors	page	85
References	page	89

4. Biology	page	91
4.1. BACE1 inhibition	page	91
4.1.1. Method A: Panvera substrate and Invitrogen enzyme	page	92
4.1.2. Method B: Casein-FITC substrate and Invitrogen enzyme	page	92
4.1.3. Method C: M-2420 substrate and Sigma enzyme	page	93
4.1.4. BACE1 fluorogenic substrate evaluation	page	94
4.2. Cathepsin D inhibition	page	94
4.3. AChE and BChE inhibition	page	94
4.4. Inhibition of AChE-induced A β aggregation	page	95
4.5. Animal studies	page	95
References	page	97
5. Results and Discussion	page	99
5.1. Biological evaluation of tetrahydroacridine-, rivastigmine- and caproctamine-based compounds (1-10)	page	99
5.2. Biological evaluation of 4-aminoquinoline- and 4-aminoquinazoline-based compounds (11-27)	page	104
5.3. Synthesis of δ -aminocyclohexane carboxylic acid-based BACE1 inhibitors	page	112
References	page	116
6. Experimental Section	page	117
6.1. Chemistry	page	117
6.2. Biology	page	154
6.2.1. BACE1 inhibition	page	154
6.2.2. Cathepsin D inhibition	page	156
6.2.3. AChE and BChE inhibition	page	157
6.2.4. Inhibition of AChE-induced A β aggregation	page	157
6.2.5. Animal studies	page	158
References	page	159

Abstract

The aspartic protease BACE1 (β -amyloid precursor protein cleaving enzyme, β -secretase) is recognized as one of the most promising targets in the treatment of Alzheimer's disease (AD). The accumulation of β -amyloid peptide ($A\beta$) in the brain is a major factor in the pathogenesis of AD. $A\beta$ is formed by initial cleavage of β -amyloid precursor protein (APP) by β -secretase, therefore BACE1 inhibition represents one of the therapeutic approaches to control progression of AD, by preventing the abnormal generation of $A\beta$. For this reason, in the last decade, many research efforts have focused at the identification of new BACE1 inhibitors as drug candidates. Generally, BACE1 inhibitors are grouped into two families: substrate-based inhibitors, designed as peptidomimetic inhibitors, and non-peptidomimetic ones. The research on non-peptidomimetic small molecules BACE1 inhibitors remains the most interesting approach, since these compounds hold an improved bioavailability after systemic administration, due to a good blood-brain barrier permeability in comparison to peptidomimetic inhibitors.

Very recently, our research group discovered a new promising lead compound for the treatment of AD, named lipocrine, a hybrid derivative between lipoic acid and the AChE inhibitor (AChEI) tacrine, characterized by a tetrahydroacridinic moiety. Lipocrine is one of the first compounds able to inhibit the catalytic activity of AChE and AChE-induced amyloid- β aggregation and to protect against reactive oxygen species. Due to this interesting profile, lipocrine was also evaluated for BACE1 inhibitory activity, resulting in a potent lead compound for BACE1 inhibition. Starting from this interesting profile, a series of tetrahydroacridine analogues were synthesised varying the chain length between the two fragments. Moreover, following the approach of combining in a single molecule two different pharmacophores, we designed and synthesised different compounds bearing the moieties of known AChEIs (rivastigmine and caproctamine) coupled with lipoic acid, since it was shown that dithiolane group is an important structural feature of lipocrine for the optimal inhibition of BACE1. All the tetrahydroacridines, rivastigmine and caproctamine-based compounds, were evaluated for BACE1 inhibitory activity in a FRET (fluorescence resonance energy transfer) enzymatic assay (test A). With the aim to enhancing the biological activity of the lead compound, we applied the molecular simplification approach to design and synthesize novel heterocyclic compounds related to lipocrine, in which the tetrahydroacridine moiety was replaced by 4-amino-quinoline or 4-amino-quinazoline rings. All the

synthesized compounds were also evaluated in a modified FRET enzymatic assay (test B), changing the fluorescent substrate for enzymatic BACE1 cleavage. This test method guided deep structure-activity relationships for BACE1 inhibition on the most promising quinazoline-based derivatives. By varying the substituent on the 2-position of the quinazoline ring and by replacing the lipoic acid residue in lateral chain with different moieties (i.e. *trans*-ferulic acid, a known antioxidant molecule), a series of quinazoline derivatives were obtained. In order to confirm inhibitory activity of the most active compounds, they were evaluated with a third FRET assay (test C) which, surprisingly, did not confirm the previous good activity profiles. An evaluation study of kinetic parameters of the three assays revealed that method C is endowed with the best specificity and enzymatic efficiency. Biological evaluation of the modified 2,4-diamino-quinazoline derivatives measured through the method C, allow to obtain a new lead compound bearing the *trans*-ferulic acid residue coupled to 2,4-diamino-quinazoline core endowed with a good BACE1 inhibitory activity ($IC_{50} = 0.8 \mu\text{M}$). We reported on the variability of the results in the three different FRET assays that are known to have some disadvantages in term of interference rates that are strongly dependent on compound properties. The observed results variability could be also ascribed to different enzyme origin, varied substrate and different fluorescent groups. The inhibitors should be tested on a parallel screening in order to have a more reliable data prior to be tested into cellular assay. With this aim, preliminary cellular BACE1 inhibition assay carried out on lipocrine confirmed a good cellular activity profile ($EC_{50} = 3.7 \mu\text{M}$) strengthening the idea to find a small molecule non-peptidomimetic compound as BACE1 inhibitor. In conclusion, the present study allowed to identify a new lead compound endowed with BACE1 inhibitory activity in submicromolar range. Further lead optimization to the obtained derivative is needed in order to obtain a more potent and a selective BACE1 inhibitor based on 2,4-diamino-quinazoline scaffold.

A side project related to the synthesis of novel enzymatic inhibitors of BACE1 in order to explore the pseudopeptidic transition-state isosteres chemistry was carried out during research stage at Université de Montréal (Canada) in Hanessian's group. The aim of this work has been the synthesis of the δ -aminocyclohexane carboxylic acid motif with stereochemically defined substitution to incorporating such a constrained core in potential BACE1 inhibitors. This fragment, endowed with reduced peptidic character, is not known in the context of peptidomimetic design. In particular, we envisioned an alternative route based on an organocatalytic asymmetric conjugate addition of nitroalkanes to cyclohexenone in presence of D-proline and *trans*-2,5-dimethylpiperazine. The enantioenriched obtained 3-(α -nitroalkyl)-cyclohexanones were further functionalized to give the corresponding δ -nitroalkyl cyclohexane carboxylic acids. These intermediates were elaborated to the target structures 3-(α -aminoalkyl)-1-cyclohexane carboxylic acids in a new readily accessible way.

Chapter 1

Introduction

A case report presented by Alois Alzheimer on November 1907¹ in a neurology conference showed the clinical observation of a 51-years old woman affected by a new disorder, later named as Alzheimer's disease (AD). The patient showed progressive cognition and memory impairment, reduced comprehension, aphasia, unpredictable behaviour and disorientation associated with evident histopathological findings such as miliary foci, several fibrils and typical plaques. Even though these clinical observations still remain nowadays the major characteristics of the disease, scientific community had to wait nearly 60 years to formulate a first hypothesis on the aetiology of the disorder. Indeed, in the late 70s it was shown that cholinergic neurons and synapses of the basal forebrain are selectively lost in AD patients' brain, accounting for the development of cognitive impairments. These findings constituted the premises for the so-called "cholinergic hypothesis" of AD, which proposed cholinergic enhancement as an approach for improving cognitive function in AD.² This paradigm has so far produced the majority of therapeutic agents (cholinesterase inhibitors) acting as cognition enhancers but representing only palliative remedies.³ Among cholinesterase inhibitors, donepezil, galantamine and rivastigmine became the standard for the disease, whereas memantine, a non competitive NMDA antagonist, reached the market in 2007.

Nowadays, is fully recognized that β -amyloid ($A\beta$) deposits in senile plaques represent the triggering event in the pathogenesis of AD whereas neurofibrillary tangles (NFT), consisting mainly of paired helical filaments of abnormally phosphorylated τ protein may be an important secondary event linked to neurodegeneration⁴ (Figure 1). These two pathological hallmarks strengthen the well-known "amyloid cascade hypothesis". The seminal discovery that $A\beta$ is a principal component of neuritic plaque has spurred intense search to investigate the molecular mechanism involved in $A\beta$ secretion and neurotoxicity. Certainly, reducing the production of $A\beta$ or increasing its clearance are attractive strategies for the treatment of AD.⁵ In addition, several

lines of evidence support a concomitant role of oxidative stress, metal ion dishomeostasy and inflammation⁶ in AD. Consequently it is not trivial to state that these hypotheses are not mutually exclusive, rather, they complement each other, intersecting at a high level of complexity.

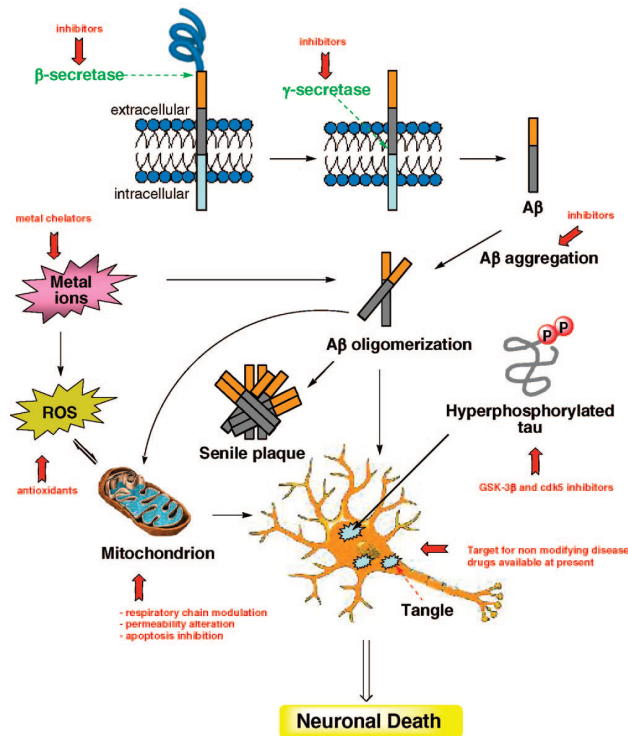


Figure 1. Possible molecular causes of neuronal death and protective mechanisms in AD. The central event in AD pathogenesis is an imbalance between A β production and clearance.⁷

According to amyloid cascade hypothesis, the main research involves decreasing A β production with β -secretase and γ -secretase inhibitors and α -secretase activators, preventing and reversing A β aggregation using metal ion modulators and antifibrillating agents, or promoting A β clearance and degradation through immunization. Among these therapeutic strategies, β -secretase (beta-site amyloid precursor protein cleaving enzyme or BACE1) is recognized as one of the most promising targets for a disease-modifying treatment of AD controlling the onset and progression of AD. Thus, BACE1 inhibitors might reduce β -amyloid by treating the aetiology of pathology and not just the symptoms of the disorder.

In view of the complexity of AD and the involvement of multiple and interconnected pathological pathways, a combination of therapeutic agents may result in a more effective strategy of treatment than monotherapy. Besides the combination of known drugs, acting on

diverse imbalanced mechanisms, new therapeutic approaches are based on the development of multifunctional molecule able to inhibit BACE1 and interfere with other pathological event, in order to address this unmet medical need and to slow or perhaps even halt the course of the disease.

1.1. Alzheimer's disease (AD)

Alzheimer's disease (AD) is a progressive neurodegenerative brain disorder clinically characterized by a global decline of cognitive function accompanied by behavioural impairment and decreasing ability to perform basic daily activities. The cognitive symptoms caused by gradual damage memory and inability to learn include memory loss, disorientation, incapacity to make judgments, reasoning and communicate with the social environment. Initially, short-term memory is affected, due to neuronal dysfunction and degeneration in the hippocampus and amygdala. As the disease progresses, neurons degenerate and die in other cortical regions of the brain leading to dramatic changes in personality and behaviour, such as anxiety, suspiciousness, depression or agitation, as well as delusions or hallucinations.⁸ Despite accurate neurophysiological tests, useful diagnostic tools for an early diagnosis of AD are still not available; however verbal memory, executive control, and associated learning are recognized as the first impaired functions in AD patients. Moreover, a decrease in attentional ability could appear in the early stages of the disease. Diagnosis of AD requires *post-mortem* examination of the brain, which must contain sufficient numbers of “plaques” and “tangles” to qualify as affected by AD.⁹ Indeed, the two major neuropathological hallmarks of AD are: (a) the deposition of extracellular neuritic A β plaques that reside in hippocampal and cerebral cortical regions, and (b) the intracellular NFT that occupy much of the cytoplasm of pyramidal neurons.^{10,11} These two proteins seem to be at the root of the pathogenesis of the disease.¹²

Nevertheless, the neuronal death is the trigger event that accounts for the development of cognitive impairments. In particular, cholinergic neurons and synapses in the nucleus basalis, hippocampus and entorhinal cortex are lost and their projection to the cerebral cortex are marked with decreased level of acetylcholine (ACh) and its biosynthetic key enzyme, choline acetyltransferase (ChAT).¹³ The disease spreads from specific limbic regions to the hippocampus, neocortex (regions that are associated with higher mental function) and several ACh, serotonin (5-HT) and noradrenaline (NA) subcortical nuclei.^{14,15} Although loss of ACh-

releasing neurones has been associated with diminished cognitive function, recent evidence indicates that neuronal loss is also linked to non-cognitive changes in behaviour.¹⁶ Other neurotransmitters systems such as dopamine (DA), histamine and neuropeptides are compromised in AD and undergo severe atrophy throughout the course of disease.¹⁷

Glutamate excitotoxicity is also hypothesised to play a role in AD. Glutamate is the primary excitatory neurotransmitter in the brain and overstimulation of glutamate receptors can cause seizures and neurodegeneration. In particular, blocking the voltage dependent NMDA glutamate receptor allow blocking excessive stimulation at NMDA receptors. Based on these finding, a non competitive low-affinity NMDA receptor antagonist, memantine, is now available for the treatment of moderate to severe AD and is effective in patients with concomitant cholinesterase inhibitor use.¹⁸

Inflammation, evidenced by the activation of microglia and astroglia, is another hallmark of AD and is an important source of oxidative stress in AD patients; particularly the induction of superoxide production (“oxidative burst”). The inflammatory process occurs mainly around the amyloid plaques and is characterized by pro-inflammatory substances released from activated microglia.¹⁹ Reactive oxygen species (ROS) are the most prominent molecules in the inflammatory process, along with prostaglandins, interleukin 1 β (IL-1 β), interleukin 6 (IL-6), macrophage-colony stimulating factor (M-CSF) and tumour necrosis factor (TNF)- α .^{20,21,22} In addition to morphological alterations, AD is associated also with a markedly impaired cerebral glucose metabolism.²³

1.1.1. The cholinergic deficit in AD

In the 70s and 80s, it was discovered that ACh synthesis, ACh levels, and cholinergic receptors were greatly reduced in AD brain.²⁴ Furthermore, the progressive neuronal cell loss in AD is associated with region-specific brain atrophy involving ACh system. These findings, combined with the known role of ACh in memory and attentional processing,²⁵ led to the so-called “cholinergic hypothesis”.²⁶

The origin of the cholinergic theory derives mainly from the effect produced by natural anticholinergic agents, such as atropine and scopolamine. Low doses of scopolamine could produce a pattern of cognitive disorders that generally paralleled those seen in elderly volunteers. A series of publications using non human primates strengthen the observation that the

scopolamine induced memory loss closely matched the consistent deficit that naturally occurs in aged monkeys.^{27,28} These findings led to the first demonstration that age related memory loss in aged monkeys could be pharmacologically reduced using the acetylcholinesterase enzyme (AChE) inhibitor, physostigmine.²⁹ A large number of pharmacological studies have shown³⁰ that ACh receptor antagonists such as scopolamine reduce performance of animals in learning and memory tasks; these deficits can be reversed by AChE-inhibitors (AChEIs). The role of cholinergic neurons in the processes subserving learning and memory has been further validated by the *post mortem* neurochemical findings associated with AD pathology.¹⁷

Loss of basal forebrain cholinergic neurons is demonstrated by the reduction in number of cholinergic markers, such as ChAT, AChE, and presynaptic M₂ muscarinic and nicotinic receptors. These findings were almost simultaneously reported by three different laboratories^{31,32,33} and these cholinergic markers changes are highly correlated with the clinical degree of dementia observed in AD.³⁴ Nowadays, there are supporting evidences showing that the cholinergic projection from the nucleus basalis of Meynert to areas of the cerebral cortex is affected early, and most severely, in brains from Alzheimer patients.³⁵ Learning and memory deficits observed in patients with AD are, at least partially, caused by the dysfunction of basal forebrain cholinergic neurons in early stages of AD.

Another metabolic step associated with cholinergic transmission is the robustly deficient activity in AD brain, namely that catalyzed by pyruvate dehydrogenase complex.^{36,37} This enzyme provides the acetyl coenzyme A, the final product of the glycolytic pathway, required for the synthesis of acetylcholine. Pyruvate derived from glycolytic metabolism serves as an important energy source in neurons.³⁸ Therefore, the inhibition of pyruvate production, for example, by glucose depletion, is considered a crucial factor leading to acetyl-CoA deficits in AD brains.

Based on the findings that (a) AD patients have reduced levels of the enzyme choline acetyltransferase and of the neurotransmitter ACh, compared to healthy elderly people and (b) ACh is hydrolyzed by AChE, AChEIs were the first drug class successfully introduced for the treatment of AD (Fig. 2).

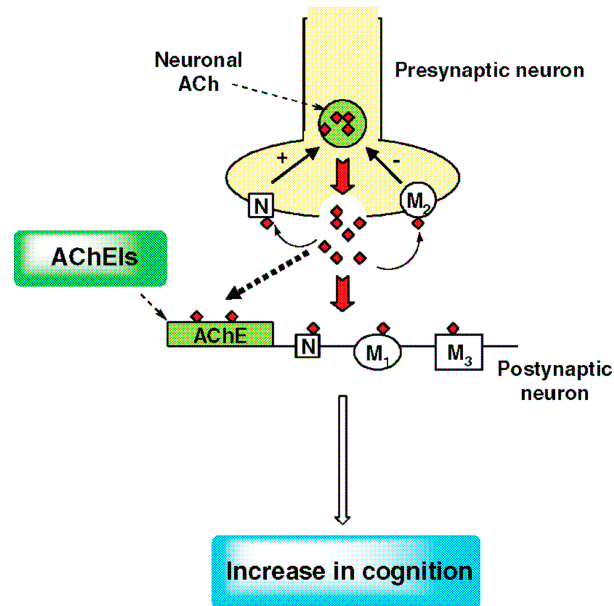


Figure 2. Mechanism of action of ACh at a cholinergic synapse. ACh is released in the synaptic cleft where it activates both postsynaptic and presynaptic cholinergic receptors [nicotinic (N) and muscarinic (M)] leading to an increase of cholinergic transmission, which results in cognition improvement. ACh is removed from the synapse by the action of the enzyme AChE, which is the target of the available AChEIs for AD treatment.⁷

Cognition Enhancer therapeutics

The cholinergic hypothesis has provided the first rational framework for treatment strategies of cognitive dysfunction in AD, so it has led to the development of new medicines and numerous ACh-mimetics are under clinical development.^{26,39,40} Inhibiting AChE, is the most common approach. AChEIs were the first drug class successfully introduced for the treatment of Alzheimer's patients. In fact, in 1993, the AChEI tacrine, was the first drug to be approved for the treatment of AD, now rarely used because of its hepatotoxicity. Later, three other AChEIs, donepezil, rivastigmine, and galantamine reached the market, becoming the standard for AD therapy for their better profiles. To these AChEIs, recently, memantine, a non-competitive NMDA antagonist, was added for AD treatment (Fig. 3).

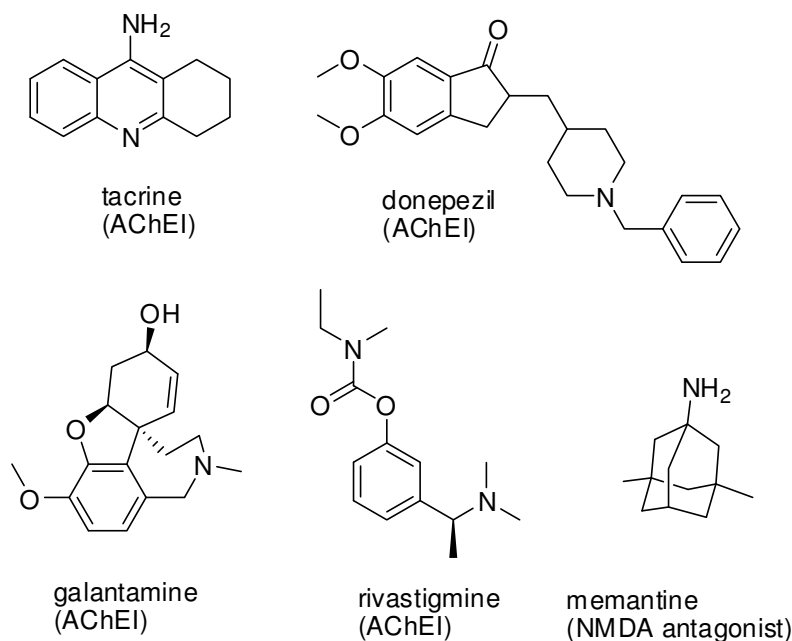


Figure 3. Chemical structures of the five drugs available for AD treatment (mechanism of action indicated in parentheses).

In addition to AChE inhibition, rivastigmine inhibits butyrylcholinesterase (BChE), and galantamine allosterically modulates nicotinic receptors, although the importance of these additional activities is unknown.⁴¹ Although AChEIs are widely used, only 25-50% of patient respond to the therapy.⁴² Current work in the field is directed at identifying therapeutics that combine AChE inhibition with other mechanism.⁴³ One example is phenserine, an AChEI that reduces $\text{A}\beta$ in preclinical models.⁴⁴ Huperzine A, derived from a Chinese herb, has neuroprotective activity in addition to AChE inhibition.⁴⁵ Dimebon has several known activities in addition to AChE inhibition: histamine and NMDA antagonism and inhibition of mitochondrial permeability transition pores.⁴⁶

In addition to AChEIs, efforts to increase cholinergic neurotransmission using M_1 agonists, M_2 antagonists, and nicotinic agonists have been investigated. Postsynaptic M_1 receptors are spared in AD brain,²⁴ while most M_2 receptors are presynaptic autoreceptors that inhibit ACh release.⁴⁷ For these reasons M_1 agonist and M_2 antagonist are sought for AD. Although M_1 agonist development began at the same time as AChEIs, no M_1 agonists are approved for AD. The reason for the absence of successful M_1 agonists for AD may be related to the lack of M_1 selectivity and resultant intolerable effects. Some M_1 agonists such as NGX-267, P-58 and sabcomeline are under clinical trials. Among the second generation selective M_1 agonists that have been recently developed, AF267B effectively reduced the two major hallmark

neuropathological lesions and rescued the cognitive deficits in a novel triple transgenic model of AD.⁴⁸ On the other hand, M₂ antagonist are currently under development.⁴⁹

Nicotinic agonists are also being developed as cognition enhancer based on the cholinergic hypothesis and epidemiologic data showing a reduced incidence of AD in smokers.⁵⁰ Unlike M₁ receptors, both $\alpha 4\beta 7$ and $\alpha 7$ nicotinic receptor subtypes, implicated in learning and memory processes, are decreased in AD.⁵¹ Nicotinic agonist and partial agonist acting at both nicotinic receptor subtypes improve performance in attention and working memory tasks.⁵²

Indirect means to enhance cholinergic and other neurotransmission are also being investigated for AD. Serotonin-6 (5-HT₆) receptor antagonists enhance signalling of ACh, glutamate, aspartate, dopamine and GABA, probably via their effects on interneurons.⁵³

Definitely, according to the cholinergic hypothesis of AD, the use of cholinomimetic agents, able to compensate for ACh deficit should allow alleviation of the symptoms of the disease. Indeed, with the sole exception of memantine, the other four commercialized anti-Alzheimer drugs (tacrine, donepezil, rivastigmine, and galantamine) are AChEIs. One of the most commonly voiced objection against cholinergic hypothesis is the palliative nature of AChEIs based strategy. Despite reduction in ACh pathways has been shown in biopsies from patients within a year of onset of symptoms,⁵⁴ it is not completely clear if the cholinergic deficit occurs early in the course of the disease or it is a consequence of other pathological events. It seems clear that the AChEIs capability to relieve symptoms of AD may depend on the integrity of the neuronal cholinergic system and, in severe cases, there may be an insufficient ACh release to allow AChEIs to be effective.

Moreover, significant variability existed in the response to the AChEIs treatment, with some subjects apparently unresponsive at any dose tested. While the ultimate goal for AD treatment would obviously involve the pathogenesis and aetiology of the disease, clinical use of AChEIs have shown a temporary stabilization of cognitive impairment and delaying in the need for patients' placement in nursing homes by several months. Despite the controversial debate upon the cholinergic hypothesis and the development of several new approaches to the treatment of AD not related to the modulation of cholinergic activity, this theory is far from being considerate merely an historical approach. Some investigators have recently reported an apparent retardation of the progression of the neurodegeneration process in patients treated with AChEIs. Furthermore, the finding that non classical modulation of AChE activity can interfere with the accumulation and precipitation of A β , hence, downstream, with the deposition of senile plaques,

could afford a rational link between the two more important strategies of AD cure.⁵⁵ Preclinical studies identified unexpected mechanisms of action of the anticholinesterasic drugs, underlying that they may tackle alterations in A β precursor protein (APP) processing in *in vitro* and *ex vivo* systems. Specifically, convincing results substantiate a consistent relationship between cholinergic activation and changes in APP metabolism (see following section 1.1.2). In parallel, the recent discovery of the so-called “non-classical function”⁵⁶ of AChE has renewed interest in the search for novel AChEIs, expanding their potential as real disease-modifying agents.^{57,58,59} In particular, it has been reported that AChE might act as a “pathological chaperone” in inducing A β aggregation through the direct interaction of its peripheral anionic site (PAS) with fibrils of the peptide.⁶⁰ This has led scientists to reconsider this enzyme as a target that mediates two important effects in the neurotoxic cascade, that is, A β fibrils formation and ACh breakdown.

The neuroprotective effects exhibited by some currently commercialized AChEIs not only due to the mere cholinomimetic mechanisms confirm that cholinergic hypothesis could still represent a rationale for promising disease-modifying anti-Alzheimer drug candidates and not only for palliative treatment of AD.

1.1.2. The “amyloid cascade hypothesis”

The amyloid cascade hypothesis, proposed more than 25 years ago,^{61,62} postulates that the initiating molecule in AD is A β , ultimately leading to neuronal degeneration and dementia. The hypothesis, strengthened by pathological evidences, claims that amyloid- β 42 (A β 42) plays an early and crucial role in all cases of AD. A β 42 forms aggregates that are thought to initiate a pathogenic cascade.⁵ In fact, the overproduction of A β peptide, or failure to clear this peptide, leads to AD primarily through A β deposition, which is presumed to be involved in neurofibrillary tangle formation, therefore tau aggregation may be an important secondary event related to neurodegeneration.

Extracellular amyloid plaques, consisting predominantly of A β 42, and intraneuronal neurofibrillary tangles, consisting of an aggregated form of the neuronal protein tau, are the two pathological hallmarks of AD. These resulting lesions are then associated with cell death, which is reflected in memory impairment and, at the end, to dementia, as shown in figure 4.

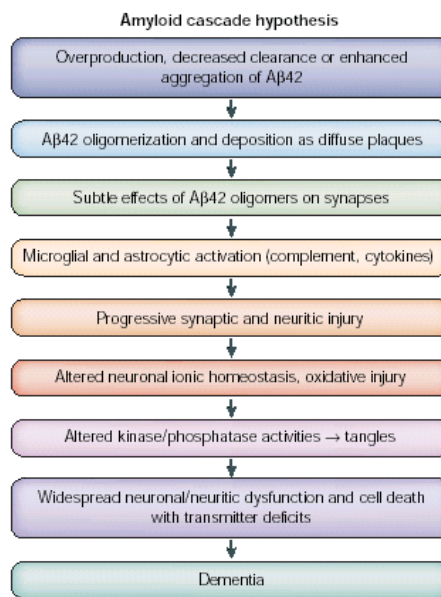


Figure 4. The sequence of pathogenic events that are thought to lead to AD.⁶³

Genetic analysis of the rare familial autosomal dominant AD with early onset has led to the identification of three genes (i.e. those encoding APP, presenilin1 and presenilin2) that, when mutated, lead to the development of AD.⁶⁴ The great majority of these mutations increases Aβ42 production, which is therefore assumed to play a causal role in disease pathogenesis.^{65,66} By contrast, the cause of sporadic late-onset AD remains unknown. Based on the similarities in the pathology and clinical presentation of familial early and sporadic late-onset AD, it is widely accepted that Aβ42 also plays a crucial role in sporadic AD. Although Aβ42 overproduction does not appear to be the primary event in disease pathogenesis, accumulation of Aβ42 in the central nervous system (CNS) can be attributed to enhanced aggregation of Aβ42, decreased clearance of Aβ42 or other factors.

Aβ is generated proteolytically from a large transmembrane protein amyloid precursor protein (APP) by sequential action of two proteases, β-secretase and γ-secretase (Fig. 5).

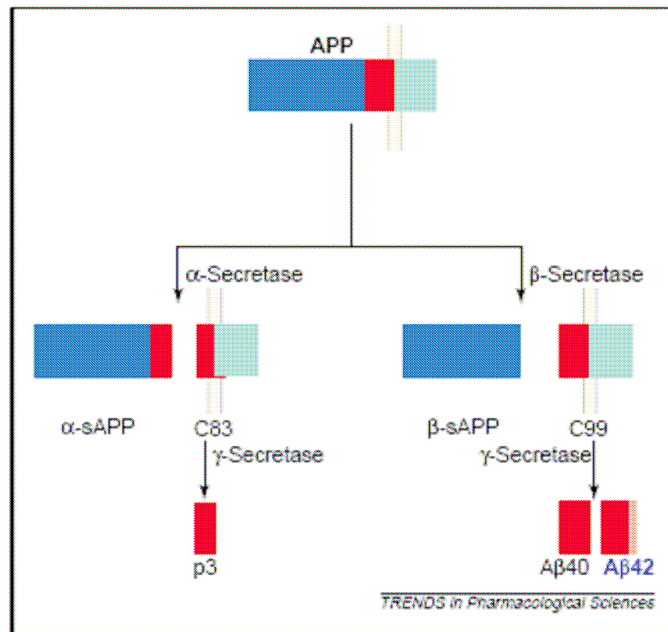


Figure 5. Schematic representation of APP and its metabolites, relevant to AD.⁶⁷

The first cleavage of APP is carried out by β -secretase (also called β -site APP cleaving enzyme or BACE)^{68,69} releasing a large soluble fragment (β -sAPP). The carboxyterminal fragment C99 peptide is then cleaved by γ -secretase complex at several positions, leading to the formation of A β 40 and the pathogenic A β 42. Alternatively, cleavage of the protein by α -secretase allows for the release of a large fragment, α -APPs, which is not amyloidogenic. The C-terminal C83 peptide is metabolized to p3 by γ -secretase. After A β formation from APP cleavage, the monomers deposit and aggregate (or aggregate and deposit) in extracellular insoluble plaques, whereas soluble A β is thought to undergo a conformational change to high β -sheet content, which renders it prone to aggregate into soluble oligomers and larger insoluble fibrils in plaques. In this process, the fibrillogenic A β 42 isoform triggers the misfolding of other A β species. Currently, the nature of the neurotoxic A β species is very difficult to define because monomers, soluble oligomers, insoluble oligomers, and insoluble amyloid fibrils are expected to accumulate and exist in dynamic equilibrium in the brain. Initially, only A β deposited in plaques was assumed to be neurotoxic, but more recent findings suggest that soluble oligomers might be the central players. Afterward, A β may exert its neurotoxic effects in a variety of ways, including disruption of mitochondrial function via binding of the A β -binding alcohol dehydrogenase protein,⁷⁰ induction of apoptotic genes through inhibition of Wnt44 and insulin signalling,⁷¹ formation of ion channels,⁷² stimulation of the stress-activated protein kinases (SAPK)

pathway⁷³ or activation of microglia cells leading to the expression of pro-inflammatory genes, an increase in reactive oxygen species (ROS), and eventual neuronal toxicity and death.⁷⁴

Recently, it has become clear that, in addition to forming extracellular aggregates, A β (or its precursor APP) has complicated intracellular effects involving a variety of subcellular organelles, including mitochondria. Soluble A β localizes to mitochondria and interferes with their normal functioning, causing overproduction of ROS, inhibiting respiration and ATP production and damaging the structure of mitochondria.⁷⁵ These data offer a potential explanation for the well-established observation that mitochondrial function and energy metabolism are perturbed early in AD.⁷⁶

1.1.2.1. β -Amyloid-based therapeutics

The amyloid cascade hypothesis spurred an intense search to address the overwhelming issue of the overproduction and aggregation of neurotoxic form of A β . The attention of research community was focussed on the enzymes responsible for liberating the A β 42 residue segment of APP and on the physical and immunological mechanisms that inhibit aggregation. As a matter of fact, amyloid-based therapeutics include α -secretase stimulators, BACE1 inhibitors, γ -secretase inhibitors and modulators, aggregation blockers, catabolism inducers and anti-A β biologics (Fig. 6).

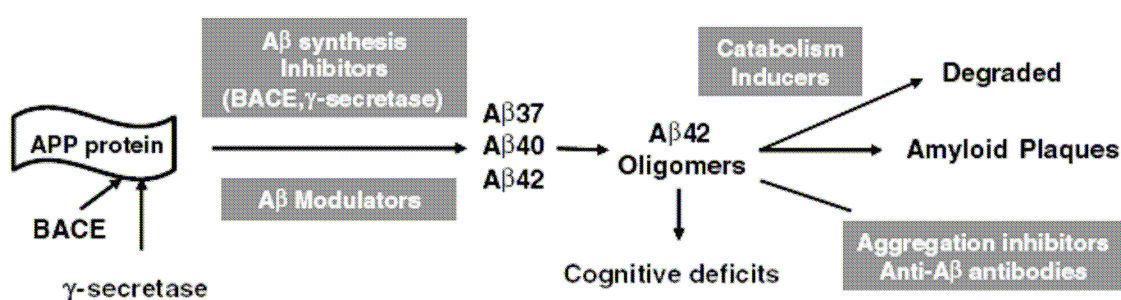


Figure 6. The formation of A β by cleavage of APP and its conversion to A β oligomers and amyloid plaques is shown. Potential therapeutic approaches to decrease A β toxicity are indicated in the shaded boxes.⁷⁷

Firstly, the APP processing pathway outlines immediately three putative strategies to reduce A β generation, actively pursued for more than a decade: inhibition of β and γ -secretase and stimulation of α -secretase. In order to synthesize selective and potent modulators of these proteases, research has focused its attention on the structural and functional features of these enzymes.

α -Secretase stimulation

α -Secretase pathway stimulation might lead to a reduction of the APP substrates available for A β formation, activating non-amyloidogenic sAPP α . Moreover, α -secretase is stimulated also by AChEIs via selective muscarinic activation inducing the translation of APP mRNA with the final goal of restricting amyloid fibre assembly. Three members of the ADAM family (“a disintegrin and metalloproteinase”) ADAM-10, ADAM-17 and ADAM-9 have been proposed as α -secretases. To date, it is accepted that each of these enzymes acts as a physiologically relevant α -secretase. Genetic studies revealed that ADAM-10 is a key protein involved in neurogenesis and axonal extension.^{78,79} This underlines the positive, neuroprotective role of ADAM-10 and thus of α -secretase like cleavage activity in the metabolic processing of APP.

In addition to ADAMs, perhaps other membrane-associated metalloproteinases contribute to the shedding of APP. Stimulation of α -secretase activities can be achieved via several signalling cascades including phospholipase C, phosphatidylinositol 3-kinase and serine/threonine-specific kinases such as protein kinases C, and mitogen activated protein kinases. Direct activation of protein kinase C and stimulation of distinct G protein-coupled receptors are known to increase α -secretase processing of APP. Agonists for M₁ muscarinic receptors and serotonin 5-HT₄ receptors are currently in clinical trials to test their efficiency in the treatment of AD.^{80,81}

β -Secretase inhibition

β -Secretase, also called BACE1 is a membrane bound aspartic protease specifically abundant in brain, which forms, together with its homologue BACE2, a new branch of the pepsin family⁶⁸ (for details, see following section 1.2). The enzyme catalyzes the cleavage of APP to produce N-terminus of A β peptides. The data suggesting BACE1 is the enzyme relevant to AD-related APP processing are strong, and have recently been reviewed along with other aspect of BACE biology.⁸² Inhibition of BACE holds promise for the production of safe anti-amyloid therapy, as transgenic mice lacking the BACE gene produce little or no A β , and do not display any robust negative phenotype.^{67,83}

For these reasons β -secretase appears to be an excellent drug target, even if the absence of toxicity in mice does not prove absence of human toxicity. Although the biology of BACE1 inhibition seems to be a promising line in inquiry, inhibitors development is proving to be

challenging.⁸⁴ Research regarding BACE1 inhibitors has been strengthened by the large amount of information available on other aspartic protease, in particular on the highly investigated HIV-1 protease. Furthermore, the crystal structure of BACE1 active domain bound to a peptidomimetic inhibitor has been reported, opening new possibility of rational drug design⁸⁵ (for details, see following section 1.3).

γ -Secretase inhibition and modulation

γ -Secretase is responsible for the final cut of the APP to produce the A β peptide implicated in the pathogenesis of AD. Thus, this protease is a top target for the development of AD therapeutics. γ -Secretase is a complex of four different integral membrane proteins, with the multi-pass presenilin being the catalytic component of a novel intramembrane-cleaving aspartyl protease. A number of inhibitors of the γ -secretase complex have been identified, including peptidomimetics that block the active site, helical peptides that interact with the initial substrate docking site, and other, less peptidomimetic, more drug-like compounds. To date, one peptidomimetic γ -secretase inhibitor (DAPT) has advanced into late-phase clinical trials for the treatment of AD, but serious concerns remain. γ -Secretase cleaves other substrates besides APP, the most notorious being the Notch receptor that is required for many cell differentiation events.⁸⁶ Because proteolysis of Notch by γ -secretase is essential for Notch signalling, interference with this process by γ -secretase inhibitors can cause severe toxicities. γ -Secretase inhibitors may cause abnormalities in the gastrointestinal tract, thymus and spleen in rodents.⁸⁷ Thus, the potential of γ -secretase as therapeutic target likely depends on the ability to selectively inhibit A β production without hindering Notch proteolysis. The discovery of compounds capable of such allosteric modulation of the protease activity has revived γ -secretase as an attractive target. Structural modification of these γ -secretase modulators has allowed to discover and advance one compound in late-phase clinical trials, renewing interest in γ -secretase as a therapeutic target.^{88,89} Small molecules that shift A β 42 to shorter A β species, were discovered while investigating the mechanism for the reduced prevalence of AD among users of non-steroidal anti-inflammatory drugs (NSAIDs).⁹⁰ Subsequent studies have shown that certain NSAIDs modulate A β synthesis due to binding to γ -secretase.⁹¹ Despite this mechanism, A β do not cause Notch toxicities.⁹² The most advanced γ -secretase modulator, *R*-flurbiprofen, is in phase III clinical trials.⁹³ Unlike *S*-flurbiprofen, *R*-flurbiprofen does not inhibit cyclooxygenase and, consequently, does not cause the gastrointestinal side effects due to cyclooxygenase

inhibition.

A β -aggregation inhibitors and A β -degradation stimulators

The biosynthesis of A β and secretases activity are modulated by several other factors, which could be considered as potential target candidates in AD treatment. Several A β aggregation inhibitors have been discovered. The compound 3-amino-1-propanesulfonic acid (3APS) was identified based on the observation that glycosaminoglycans stimulate A β aggregation. 3APS binds monomeric A β , decreases A β deposition in transgenic mice,⁹⁴ and reduces cerebrospinal fluid A β in human.⁹⁵

An essential role for metals in A β aggregation⁹⁶ led to the discovery of small molecule chelator that perturbs A β -metal binding. The antibiotic clioquinol partially dissolves plaques *in vitro* and prevented plaque deposition in transgenic mice, whereas a second generation chelating agent (PBT2) is in phase II.⁹⁷ Scyllo-inositol binds an A β oligomer to inhibit further aggregation and toxicity,⁹⁸ and reduces plaque deposition and cognitive deficits in transgenic mouse model.⁹⁹ One potential issue for aggregation inhibitors is a shift in the equilibrium between less toxic aggregated forms to more toxic soluble intermediates, such as protofibrils.¹⁰⁰

Method to stimulate A β degradation are an additional approach to decrease A β oligomers.^{101,102} For example somatostatin¹⁰³ and plasminogen activator inhibitor-1 (PAI-1) can indirectly increase neprilysin and plasmin activity, respectively, which leads to increased degradation of A β .

Anti-amyloid immunotherapy

Anti-amyloid immunotherapy for AD has received considerable attention after Elan Corporation's publication,¹⁰⁴ which reported that amyloid pathology was reduced in APP transgenic mouse model after vaccination with aggregated A β 42. First described in 1999, immunotherapy uses anti-A β antibodies to lower brain amyloid levels. Active immunization, in which A β is combined with an adjuvant to stimulate an immune response producing antibodies and passive immunization, in which antibodies are directly injected, were shown to lower brain amyloid levels and improve cognition in multiple transgenic mouse models. Mechanisms of action were studied in these mice and revealed a complex set of mechanisms that depended on the type of antibody used. When active immunization advanced to clinical trials a subset of

patients developed meningoencephalitis; an event not predicted in mouse studies. However, it was suspected that a T-cell response due to the type of adjuvant used was the cause of the meningoencephalitis and studies in mice indicated alternative methods of vaccination. Passive immunization has also advanced to phase III clinical trials on the basis of successful transgenic mouse studies. Reports from the active immunization clinical trial indicated that, indeed, amyloid levels in brain were reduced.¹⁰⁵ The performance of anti-A β antibodies in transgenic mouse models of AD showed they are delivered to the CNS, clearing A β plaques and protecting the mice from learning and age-related memory deficits.

As immunotherapy is at the crossroads of immunology and the nervous system, a deeper understanding of the A β peptide clearance mechanism may lead to an optimized therapeutic approach to the treatment of AD. Antibodies generated with the first-generation vaccine might not have the desired therapeutic properties to target the "correct" mechanism, however, new immunological approaches are now under consideration.¹⁰⁶

Hyperphosphorylated tau protein and tau-based therapeutics

Neurofibrillary tangles (NFT) in AD brain consist of paired helical filaments of hyperphosphorylated, conformationally altered tau (τ) proteins. Tau binds and stabilizes microtubules, while hyperphosphorylated τ from AD brain disrupt microtubule structure.¹⁰⁷ The presence of NFT in AD and their correlation with cognitive status suggest an important role in dementia.¹⁰⁸ Phosphorylation within the microtubule binding domain of τ protein results in its reduced ability to stabilize microtubules assembly, leading to the disruption of neuronal transport and eventually to faster synaptic loss and cell death. Dephosphorylation of τ protein isolated from NFT restores its ability to bind with neuronal microtubules, indicating that the mechanisms regulating phosphorylation/dephosphorylation kinetics are perturbed in AD. Reducing τ phosphorylation via inhibition of kinases is a major therapeutic strategy based on the presence of hyperphosphorylated τ in the brain.

The nature of protein kinases, phosphatases, and τ sites involved in this lesion has recently been elucidated, suggesting that activation of phosphoserine/phosphothreonine protein phosphatase-2A (PP-2A) or inhibition of both glycogen synthase kinase-3 β (GSK3 β) and cyclin-dependent protein kinase 5 (cdk5) might be required to inhibit AD neurofibrillary degeneration.¹⁰⁹ In particular, recent data also suggest that GSK3 β inhibition plays a significant role in synaptic plasticity, which may be involved in learning and memory. GSK3 β inhibition

suppresses long term depression and consolidated long-term potentiation.^{110,111} Many small molecules acting as GSK3 β inhibitors have been designed and one of those inhibitors, developed by Neuropharma, is in phase I clinical trials for AD.^{112,113,114}

Reduction in τ levels and increased catabolism of abnormal forms of τ are also therapeutic strategies for AD. Heat shock protein 90 (Hsp90) inhibitors were identified in a cellular screens for small molecule that decreases total τ levels.¹¹⁵ The Hsp90 inhibitors PU-DZ8 and EC102 reduce phospho- τ but not total τ , in two tauopathy models.^{116,117} A useful therapeutic window for Hsp90 inhibitors in AD may be possible because EC102 binds higher affinity to AD brain tissue from affected areas.¹¹⁸

Furthermore, the discovery that NFTs in AD brain are made up of the microtubule (MT)-associated protein τ and the evidence that the toxic amyloid peptides in AD can lead to τ hyperphosphorylation and cytoskeletal dystrophy support the assertion that disruption of the MT network is an early signalling event in neurodegenerative cascades. Therefore, drugs that can moderate such signals through interactions with MTs would protect neurons against A β toxicity. Drugs targeted to MTs are currently used as anti-cancer agents, due to their blockade of cell proliferation and induction of cell death. However, it is accepted that low concentrations of compounds that help to stabilize MTs, do indeed protect post-mitotic neurons challenged with various toxic stimuli. Therefore cytoskeletal network actually serves as a sensor for the overall state of the neurons and a first-line transducer of stress signals. Drugs that can moderate initiation of such early signalling events do protect against disruption of the cytoskeleton and neuritic dystrophy in neuronal cell cultures. Moreover, microtubule stabilizing agents protect cultured neuron from A β 42, chloroquine, and glutamate induced toxicity.^{119,120,121} Paclitaxel reverse deficit in fast axonal transport, increased microtubule numbers, and improved motor deficits in transgenic mice with tauopathy in the spinal cord.¹²² These observations suggest that drugs able to protect the integrity of the cytoskeletal network can have significant and novel effects on signalling events in specific cellular contexts.¹²³

1.1.3. Oxidative stress in AD

Oxidative stress, perturbed calcium regulation and mitochondrial impairment are major alterations involved in functional and structural abnormalities in synapses and axons in AD. Oxidative damage is present within the brain of AD patients and is observed within every class

of biological macromolecules. Oxidative injury may develop secondary to excessive oxidative stress resulting from A β -induced free radicals, mitochondrial abnormalities, inadequate energy supply, inflammation, or altered antioxidant defences. Oxidative stress is thought to have a causative role in the pathogenesis of AD.¹²⁴ Support for this hypothesis has also been provided by the current notion that, while AD is probably associated with multiple aetiologies and pathogenic phenomena, all these mechanisms seem to share oxidative stress as a unifying factor.

Oxidative stress occurs when the oxidative balance is disturbed, that is, excessive production of ROS to cellular antioxidant defences. The brain is particularly vulnerable to oxidative stress because it is rich in unsaturated fatty acids, moreover it is a highly oxidative organ consuming 20% of the body's oxygen despite accounting for only 2% of the total body weight. With normal ageing the brain accumulates metals ions such iron (Fe), zinc (Zn) and copper (Cu). Consequently the brain is abundant in antioxidants to control and prevent the detrimental formation of ROS generated via Fenton chemistry involving redox active metal ion reduction and activation of molecular oxygen.¹²⁵

The early involvement of oxidative stress in AD is demonstrated by oxidative modifications of lipids,^{126,127} proteins,¹²⁸ and nucleic acids¹²⁹ in brains from AD patients, and also in cellular and animal models of AD. Oxidative stress-modified molecules are detected not only in extracellular plaques, but also within cells. For example, elevated concentration of 4-hydroxynonenal (4-HNE), a marker of lipid peroxidation, is found in A β .¹³⁰ Oxidized RNA nucleoside 8-hydroxyguanosine is significantly increased in neurons from the frontal cortex of familial AD with a mutation in presenilin-1 (PS-1) or APP gene.¹²⁹ Moreover, the activity of a mitochondrial enzyme α -ketoglutarate dehydrogenase (KGDH) complex is reduced in brains of AD patients. KGDH complex is sensitive to various oxidants whether they are added to cells or generated internally in cells.¹³¹

Together, these data support oxidative stress serving as an early event that leads to the development of cognitive disturbances and pathologic features observed in AD. The origin of these ROS is also critical to understanding how they might alter gene transcription. There are several major sites of ROS production in the cells, including mitochondria. The major source of radicals during unstressed conditions is not clear, but during pathologic conditions, mitochondria seem to be a major source and they represent the primary target of ROS.

Among the pathways acting in generating ROS, the major role has played by the metal ions via activation of molecular oxygen. Besides this function in oxidative stress, copper, together

with other metal ions, influences the protein aggregation processes that are critical in most neurodegenerative diseases. For example, APP and A β are able to bind and reduce copper, which forms a high-affinity complex with A β , promoting its aggregation, and A β neurotoxicity depends on catalytically generated H₂O₂ by A β -copper complexes *in vitro*. Moreover, lipid peroxidation induced by A β , impairs the function of ion-motive ATPases, glucose and glutamate transporters, and also GTP-binding proteins as the result of covalent modification of the proteins by the 4-HNE. By disturbing cellular ion homeostasis and energy metabolism, relatively low levels of membrane-associated oxidative stress can render neurons vulnerable to excitotoxicity and apoptosis. The dysfunction and degeneration of synapses in AD may involve A β -induced oxidative stress, because exposure of synapses to A β impairs the function of membrane ion and glutamate transporters and compromises mitochondrial function by an oxidative-stress-mediated mechanism (Fig. 7).

Oxidative modifications of τ by 4-HNE and other ROS can promote its aggregation and may thereby induce the formation of NFT. A β can also cause mitochondrial oxidative stress and dysregulation of Ca²⁺ homeostasis, resulting in impairment of the electron transport chain, increased production of superoxide anion radical and decreased production of ATP. Superoxide is converted to H₂O₂ by the activity of superoxide dismutases (SOD) and superoxide can also interact with nitric oxide (NO) via nitric oxide synthase (NOS) to produce peroxynitrite (ONOO \cdot). Interaction of H₂O₂ with Fe²⁺ or Cu⁺ generates the hydroxyl radical (OH \cdot), a highly reactive oxyradical and potent inducer of membrane-associated oxidative stress that contributes to the dysfunction of the endoplasmic reticulum.¹³²

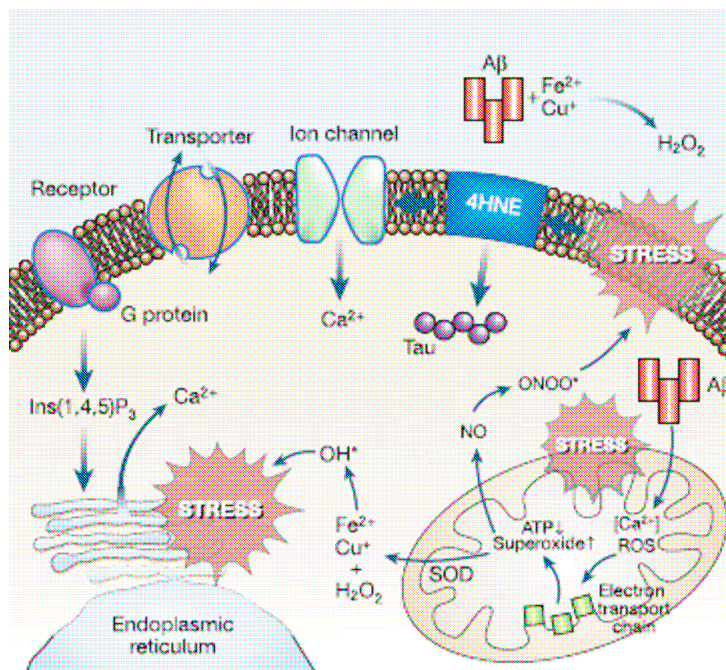


Figure 7. The neurotoxic action of A β involves generation of ROS and disruption of cellular calcium homeostasis.¹³²

Therefore, therapeutic strategies preventing oxidative damage and stimulating mitochondria are currently pursued.¹³³ The use of the peroxisome proliferator-activated receptor- γ (PPAR γ) agonist rosiglitazone, an anti-diabetic drug, now in phase III clinical trials, is one potential method to stimulate mitochondrial metabolism.^{134,135} The metal ions accumulated in the amyloid deposits of AD brains could be partially disassembled by metal chelators.¹³⁶ Some of them, such as clioquinol and desferrioxamine have had some success in altering the progression of AD symptoms.

Potential antioxidants include mitoquinone,⁹⁷ vitamin E, and natural polyphenols, such as extracts from Ginkgo biloba, green tea, wine, blueberries, and curcumin (phase II).¹³⁷ Nevertheless, clinical trials with vitamin E, Ginkgo biloba extract, and omega-3 fatty acids have not shown strong beneficial effects in AD patients.^{138,139,140} Since several antioxidant agents may be required for significant benefits for AD,¹³⁷ clinical trials are in progress using a combination of vitamin E, vitamin C, α -lipoic acid, and coenzyme Q.¹⁴¹

In particular, α -lipoic acid (LA) is a naturally occurring precursor of an essential cofactor for mitochondrial enzymes, including pyruvate dehydrogenase (PDH) and KGDH. LA has been shown to have a variety of properties which can interfere with pathogenic principles of AD.³⁸ LA showed relevant antioxidant activities: LA chelates redox-active transition metals, thus inhibiting

the formation of hydroxyl radicals and also scavenges ROS, thereby increasing the levels of reduced glutathione. Via the same mechanisms, down-regulation redox-sensitive inflammatory processes is also achieved. Furthermore, LA can scavenge lipid peroxidation products such as 4-HNE and acrolein. Besides these antioxidant, carbonyl scavenging and metal chelating activities, LA increases ACh production by activation of ChAT and increases glucose uptake, thus supplying more acetyl-CoA for the production of ACh. The reduced form of LA, dihydrolipoic acid (DHLA), is the active compound responsible for most of these beneficial effects. (*R*)- α -LA can be applied instead of DHLA, as it is reduced by mitochondrial lipoamide dehydrogenase, a part of the PDH complex. These multiple properties make LA suitable to be a promising tool in slowing AD progression.

1.1.4. Neuroinflammation

Neuroinflammation of CNS cells has been recognized as an invariable feature of all neurodegenerative disorders. In AD, among CNS cells, microglia have received special interest. Microglia are activated by A β to produce cytokines, chemokines, and neurotoxins that are potentially toxic and therefore may contribute to neuronal degeneration. However, recent findings suggest that microglia may play a neuroprotective role in AD. This highlights the potential risk of using the inhibition of monocyte/macrophage recruitment as a therapeutic strategy and argues for caution in the pursuit of this approach.¹⁴²

In this field, a cytokine modulator, VP-025 is developed and is now entering phase II clinical trials for AD.⁹⁷ Rosiglitazone may have also anti-inflammatory effects and A β reducing properties.¹⁴³ The lipid-lowering statins may also have some anti-inflammatory effects, and initial clinical results with atorvastatin have been promising.¹⁴⁴

Another approach involves stimulation of the neuronal cannabinoid receptor-1 (CB-1), which shows activity of neuroinflammation.¹⁴⁵ In contrast, some data suggests that stimulation of the inflammatory response may be beneficial in AD.^{146,147} Although most inflammation in AD is usually associated with A β due to the localization of activated astrocytes and microglia with plaques, inflammation may also play a role in tau-mediated aspects of the disease. A role for tau-mediated inflammation is suggested by recent work using an aggressive tauopathy model where inflammatory markers in microglia and neurons are increased prior to the development of tangles.¹⁴⁸

Interestingly, modulation of inflammation is nowadays one of the most dynamic areas in the search for new therapeutic targets for AD and related neurodegenerative disorders.¹⁴⁹

1.2. β -Secretase (BACE1)

Nowadays, β -Secretase (BACE1) is universally recognized as the first protease that processes APP in the pathway leading to the production of A β . This hypothesis has been carefully confirmed by scientific community during the last decade. Actually, from the initial discovery that A β was a normal proteolytic product of APP, it was supposed that two enzymes must exist to cleave small products (1-40/42 peptides) from its larger single transmembrane precursor protein. The unknown enzyme cleaving APP at the beginning of A β , prior to aminoacid 1, was called β -secretase. In 1992, the discovery that patients affected by a rare autosomal dominant forms of AD, show a Swedish APP (APP_{SWE}) double mutation, located at -2 and -1 (Lys⁶⁷⁰ \rightarrow Asn/Met⁶⁷¹ \rightarrow Leu) of the β -secretase site,¹⁵⁰ drew attention to the possibility that this mutation could cause AD. Therefore, it was supposed APP_{SWE} would have been more favourable to β -secretase cleavage. This was strengthened in studies showing that APP_{SWE} significantly enhanced the proteolytic activity of β -secretase causing a 10 fold increase in A β production.¹⁵¹ Following an intensive search to identify β -secretase, an aspartic protease fitting all the requirements for β -secretase was identified in 1999 and 2000 by several groups.^{68,152,153,154,155} This protease was named memapsin-2, and Asp-2 and is now more commonly referred to as BACE1 (β -site APP cleaving enzyme 1). Soon after the discovery of BACE1, a homologue was described and identified.¹⁵⁶ The gene identified was named memapsin-1 and is also referred to as Asp-1, ALP-56, CDA-13, DRAP (Down's region aspartic protease), but is now more commonly called BACE2. Both BACE1 and BACE2 can process APP at the β -site, but BACE2 has a preference to cleave between aminoacids 19 and 20 of the A β sequence, thus precluding A β formation. A number of studies provide strong evidence that BACE1 is the major β -secretase responsible for A β generation in the brain. Thus BACE1 cleaves at the β and also the β' site (between aminoacid 10 and 11 of A β) of APP and has a higher preference to cleave APP_{SWE}.^{68,152,153,154} BACE1 mRNA has highest expression levels in the mammalian brain,¹⁵⁷ and is found in organelles of the secretory pathway displaying optimal activity at pH = 4.5,¹⁵⁸ which is consistent with its detection in acidic organelles of the endosomes and trans-Golgi network

where A β is predominantly generated.^{151,159,160} The most interesting discovery was to assess that targeted deletion of BACE1 in APP transgenic mice completely abolishes the production and deposition of A β .^{83,161,162}

BACE1 and BACE2 are the newest described members of the A1 aspartic protease family, commonly known as the pepsin family. Human aspartic proteases of this family include pepsin, cathepsin-E, cathepsin-D, renin, pepsinogen-C and napsin. The BACE proteins represent a novel subgroup of this family, being the first reported aspartic proteases to contain a transmembrane domain and carboxyl terminal extension,¹⁵⁷ and also possessing unique disulphide bridge distribution.^{163,164} The eight known functional human A1 aspartic proteases vary in genomic structure.

Main features of A1 aspartic proteases are their bilobar structure, with an essential catalytic Asp dyad located at the interface of the homologous N- and C-terminal lobes, with maximal enzyme activity occurring in an acidic environment. These Asp residues activate water molecules to mediate nucleophilic attack on the substrate peptide bond,¹⁶⁵ and mutation of the catalytic active site aspartic residues abolishes enzyme activity. For BACE1 the Asp dyad locates at aminoacids, 93-96 (D*TGS) and 289-292 (D*SGT). A1 aspartic proteases are usually synthesised as inactive pre-pro-enzymes (zymogens), where pro-domain removal is necessary for enzymatic activity. However, this is not the case for BACE1, which possesses enzymatic activity.¹⁶⁶ BACE1 is synthesised with a pro-sequence that is rapidly removed during transit through the Golgi¹⁶⁷ by the action of a furin-like convertase.¹⁶⁸ BACE1 is highly glycosylated,¹⁶⁹ and its carbohydrate chains may favour interaction with its substrate or with glycoproteins that help regulate its activity.

All A1-aspartic proteases have six conserved Cys residues which form three disulphide bridges. BACE1 disulphide bridges maintain correct folding and orientation of BACE, but are not vital to its enzymatic activity.^{163,164} In addition, the unique transmembrane regions of BACE1 and BACE2 confer an evolutionary specialisation, allowing their sequestration to membranes of specific organelles and the plasma membrane. This serves to expose their catalytic lobes to the luminal regions of vesicles such as endosomes or Golgi where the low pH environment sustains their optimal protease activity, while their C-termini are exposed to the cytoplasm, enabling post-translational modification and protein-protein interaction.

Although very short, the cytoplasmic domain of BACE1 plays an important role in orienting BACE1 cellular trafficking and compartmentalization. BACE1 resides in the trans-Golgi

network (TGN) and its endosomes, the main cellular sites of APP processing and A β production.¹⁷⁰

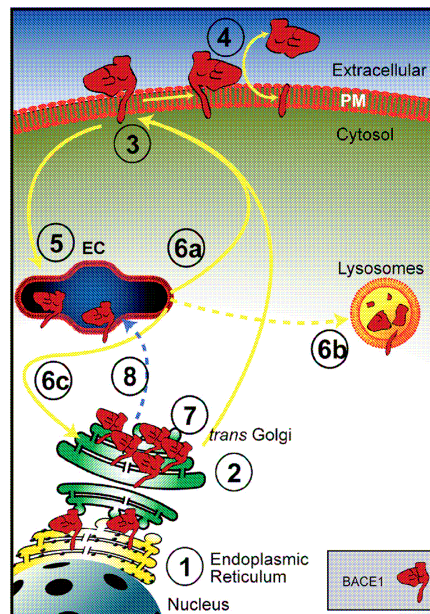


Figure 8. Intracellular trafficking of the BACE1 protein.¹⁷¹ See text for discussion.

As depicting in figure 8, after synthesis, BACE1 resides in the endoplasmic reticulum (1) and is transported to the TGN (2). From this compartment, BACE1 is transported to the plasma membrane (PM) (3) where a small proportion can undergo ectodomain compartment (EC) (5) where the acidic environment provides the optimal condition for the proteolysis of APP. From the endocytic compartments BACE1 can be recycled to directly back to the cell surface (6a), transit to lysosomes for degradation (6b) or retrogradely to the TGN (6c) from where it can be trafficked back to the PM (7). It is also possible that BACE1 can be transported directly from the TGN to endocytic compartments (8).

Insight into the three-dimensional structure of BACE1 is vital to understanding how the enzyme works catalytically, and in developing inhibitors which block BACE1 activity as a therapy for AD. X-Ray crystallography of BACE1 has determined numerous structures of BACE1 complexes, and residues and regions that are important for substrate specificity and proteolysis.^{85, 172,173,174,175,176} To date, there are over 70 known structures of BACE1 in complex with inhibitor, seven without inhibitor and one of BACE2 in the protein data bank.¹⁷⁷ The number of crystal structures of BACE1 is an evidence to the variety of compounds being tested as β -secretase drug candidates (for review see following section 1.3.). The X-ray structure of

BACE1 protease domain was first determined to 1.9Å resolution, with BACE1 bound to an eight residue transition state analogue inhibitor OM99-2 (Fig. 9).⁸⁵

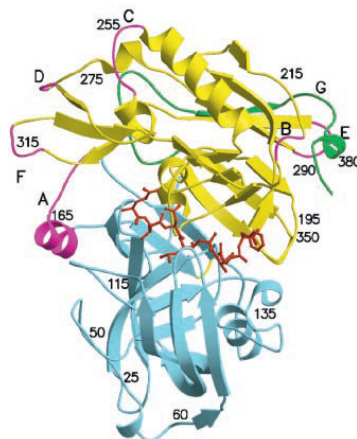


Figure 9. A ribbon model of the crystal structure of BACE1 complexed to inhibitor OM99-2. The N-lobe and C-lobe are blue and yellow, respectively, except the insertion loops, designated A to G in the C-lobe are magenta and the COOH-terminal extension is green. The inhibitor bound between the lobes is shown in red.⁸⁵

OM99-2 (**I**) is a P4-P4' peptide (P4-P3-P2-P1*-P1'-P2'-P3'-P4') based on the aminoacid composition of APP_{SWE} (Glu-Val-Asn-Leu*Ala-Ala-Glu-Phe) but incorporating a non-cleavable hydroxyethylene isostere (*) at P1 and P1', blocking normal proteolytic BACE1 cleavage between the P1 and P1' scissile bond (Fig. 10).

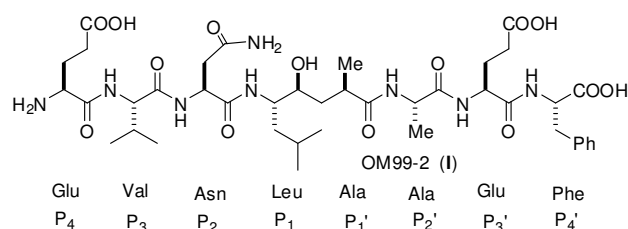


Figure 10. Chemical structure of BACE1 inhibitor OM99-2 with the constituent aminoacids and their subsite designations. The hydroxyethylene transition-state isostere is between P₁ and P₁'.

Further enzyme subsites were identified for BACE1 with enzyme bound to other eight residue¹⁷⁵ and longer transition state inhibitors,¹⁷⁶ and the crystal structure of free BACE1 has been studied.^{172,174} These crystal structure studies show BACE1 has strong conservation with A1 aspartic proteases, for which pepsin is prototypic, and also more recently with BACE2.¹⁷⁸ Ribbon diagrams of the 3D structure described for BACE1, BACE2 and pepsin, describing their major structural features, are shown in figure 11.

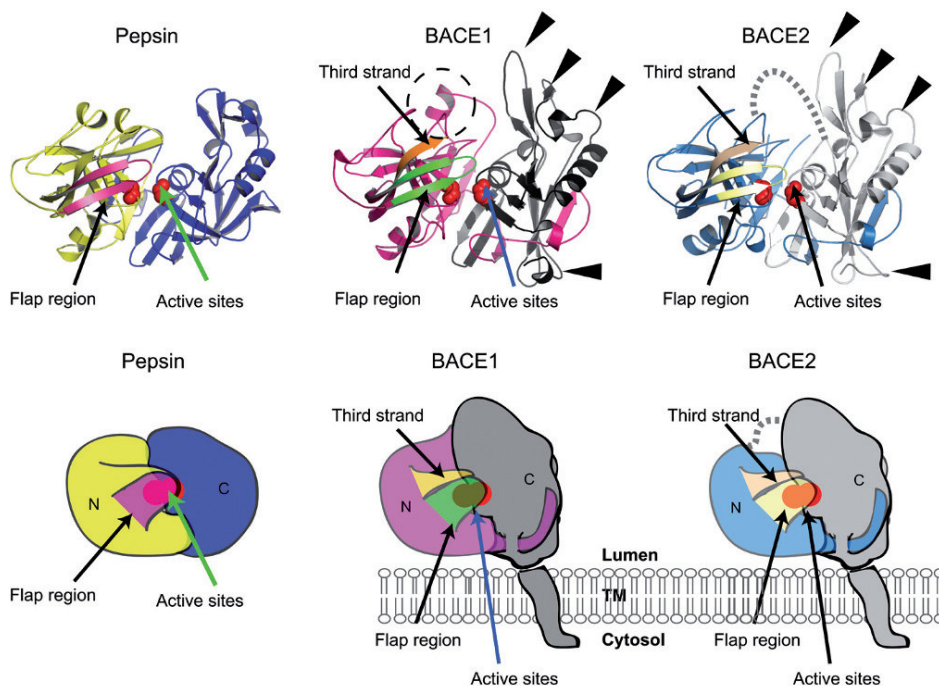


Figure 11. Structural features of BACE1 compared to pepsin and BACE2. The shown cartoon illustrations underneath the ribbon structures represent the surface structures of each protein and a possible orientation of BACE1 and BACE2 to the membrane. The N-terminal lobes of pepsin, BACE1 and BACE2 are coloured gold, magenta and blue, respectively, and the C-terminal catalytic lobes are coloured dark blue, dark grey and silver, respectively. The flap regions of pepsin, BACE1 and BACE2 are shown in their respective colours of purple, green and beige. The third-strands in BACE1 and BACE2 are shown adjacent to the flaps and coloured orange and beige, respectively. The active site aspartates of each enzyme are coloured in red space fill. The BACE1 and BACE2 insertion loops are indicated with arrow heads and the BACE1 insertion helix is highlighted with a hatched circle. The dashed line in BACE2 represents a disordered region in the BACE2 crystal structure.¹⁷¹

Regions of commonality include: the conformation and location of the catalytic Asp dyad in the middle of the active site cleft at the interface between N- and C terminal lobes, and the shielding of the active site by a flexible antiparallel hairpin-loop, known as a flap.^{85,178} Overall accommodation of the eight peptide substrate (P1-P4) residues occurs at enzyme subsites (S1-S4) and P1'-P4' at enzyme subsites S1'-S4' in a similar way to other aspartic proteases. Thus, hydrogen bonds between the active site aspartates and 10 hydrogen bonds from different parts of the active site and flap bond to the substrate/inhibitor backbone in the active site cleft, with a high degree of conservation. There are key differences between the BACE1 crystal structure and other aspartic proteases that may be exploited in BACE inhibitor design. The most obvious difference is the larger molecular surface of BACE1, due to the presence of five insertions (four loops and one helix) all in the C-terminal lobe, in addition to the presence of a 35 residue C-terminal extension, the latter being highly ordered in structure and possibly forming a stem with the transmembrane domain.⁸⁵

In addition, although the general organisation of the active site subsites is similar to other aspartic proteases, their specificity and conformation display key differences.^{85,173,174,175} Moreover, the active site of BACE1 is larger, having additional subsites (S5-S7), and although it works well with the eight substrate residues as is normal for other aspartic proteases, it can also accommodate a greater number of substrate residues (11).¹⁷⁶ The larger opening of the active site occurs due to structural differences near subsites, and the absence of a constricting pepsin helix loop across from the active site.^{85,173,174,175} The S1 and S3 subsites consist mostly of hydrophobic residues and their conformations are very different to pepsin. S4 and S2 are much more hydrophilic than these subsites in other aspartic proteases, where S2 in BACE1 and BACE2 contains Arg (Arg296, Arg310, respectively), absent in other aspartic proteases and linked to more effective cleavage of APP_{SWE} compared to normal APP.^{85,178,179} Subsites S5-S7 localise in the vicinity of the insertion helix, a region also absent in other A1 aspartyl proteases, and is believed to contribute to substrate recognition and transition state binding.¹⁷⁶

The flexible flaps which cover the active sites of all A1 aspartic protease contribute to hydrolytic specificity and substrate access, believed to open to allow substrate/inhibitor access, close when substrate/inhibitor is bound, and open to release hydrolytic products. However, the details of this mechanism are unclear. The BACE1 flap position can differ by 4.5Å-7Å at the tip when comparing free unbound enzyme (Apo) with enzyme bound to transition state inhibitor.^{174,180} A conserved aspartic protease Tyr71 residue in the tip of the flap forms hydrogen bonds with substrates/inhibitors at the P1 and P2' positions of BACE1, thereby mechanistically sealing the flap shut.¹⁷⁴ The open position is narrow and stabilised by intra-flap hydrogen bonds and a hydrogen bond with Tyr71 (Fig. 12).

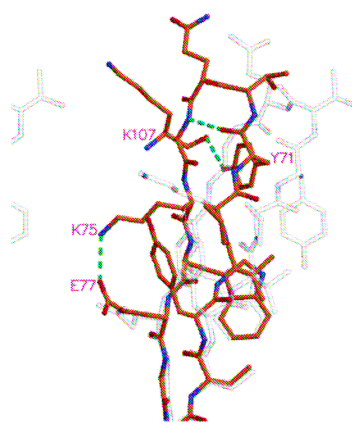


Figure 12. View of the difference in flap positions of free (red) and inhibitor-bound BACE1 (light gray). Three unique hydrogen bonds in the structure of the free BACE1 flap are shown in green dotted lines. Notice the differences between side-chain orientations of Tyr71, Lys75, and Glu77.¹⁷⁴

A parallel side chain region in BACE1 (and also in BACE2), known as the third strand (see fig. 11), forms hydrogen bonds with residues in the flap and active site residues, thereby influencing and stabilising the open or closed state of the enzyme.¹⁷⁴ Another region of flexibility shared between BACE1 and BACE2, most likely important in recognition and processing of APP substrate, is known as the 10s loop,¹⁷⁸ which forms part of the hydrophobic S3 binding pocket (Fig 11). This region can also display flexible conformations in BACE1 when comparing Apo and inhibitor complexed structures,^{85,172,174} and displays subtle differences in aminoacid composition between BACE1 and BACE2 (Fig. 11) and may be involved in their substrate discrimination.¹⁷⁸ Examination of the interaction of the P4-P4' peptide inhibitor based on the mutant aminoacid composition of APP_{SWE} (Glu-Val-Asn-Leu*Ala-Ala-Glu- Phe) with BACE1's active site gives information about why this substrate displays a 60-fold increase in affinity of APP_{SWE} over that of normal wild-type APP to cause AD.⁸⁵ Firstly, mutant P1-Leu is closely packed against P3-Val and both have considerable hydrophobic contacts with BACE1, especially true for P1-Leu, part of which encompasses its interaction the Tyr71 at the flap tip. This hydrophobic interaction would likely be much more unfavourable with P1-Met in the normal APP substrate. Furthermore, the side-chain of mutant P2-Asn is H-bonded to P4-Glu and interacts strongly with Arg296 within the S2 subsite, both interactions would be much less favourable with the positively charged P2-Lys in normal APP. Together, the information gained on the unique structural features of BACE1 through investigating crystal structure is lending to the rational design of inhibitor drugs,¹⁸¹ incorporating such information on unique subsite-inhibitor interaction and flap control.

Definitely, crystal structures of BACE1 inhibitors complexes have revealed much about the nature of protein-ligand interactions, and information regarding the nature of binding sites obtained by this approach has been of critical importance in the design and development of inhibitors that will be effective drugs in treatment of AD.

1.3. BACE1 inhibitors

The availability of structural data from the extracellular domain of BACE1 has greatly enhanced the design of potential inhibitors. The conceptual basis of such a design elements has traditionally relied on mimicking the tetrahedral transition state of the enzyme-substrate complex

with a suitable surrogate. The first generation of BACE1 transition state inhibitors using peptidomimetics based on APP_{SWE} with non-cleavable isosteres have been employed to determine the crystal structure of the enzyme, and to understand BACE1 substrate and inhibitor interactions at the active site. Although these inhibitors potently inhibit BACE1 activity and provide information for inhibitor design, they are unfortunately too large to penetrate the blood brain barrier (BBB) and to be functional as drug candidates. Thus, ideally β -secretase inhibitors should be 700 kDa or smaller, in addition to having high lipophilicity, in order to penetrate the BBB and to access neuronal membranes, in particular the membranes of subcellular organelles where BACE1 resides. Improvements in the design of the above inhibitors have reduced their mass and increased their specificity, but they remain ineffective in permeating cell membranes. Moreover, a certain selectivity towards other aspartic proteases has to be pursued, in particular towards BACE2, for its close specificity to β -secretase,¹⁸² and cathepsin D (CatD), for its ubiquitous presence in nearly all the cells.

Definitely, in order to obtain a practical BACE1 inhibitor, we need to keep in mind that such a compound has to be directed to cells, and maintain the feature of permeating neuronal membrane and in particular the membranes of subcellular organelles where BACE1 resides. To this aim selective cell penetrable BACE1 inhibitors, non-peptidomimetic ligands or compounds bearing penetratin¹⁸³ or carrier peptide¹⁸⁴ sequences are being explored.

Very recently, one of the most intriguing approach dealt with the inhibition of BACE1 by membrane targeting: specifically a transition state inhibitor was linked to a sterol moiety allowing to reach active BACE1 found in endosomes increasing its local membrane concentration.¹⁸⁵

The area of drug development for BACE1 inhibition has been addressed in several excellent recent reviews.^{186,187,188,189}

1.3.1. Transition-state analogues: from peptidomimetics to small-molecules inhibitors

Substrate analogues have generally been used as starting point in the development of aspartic protease inhibitors and the search for BACE1 inhibitors has taken advantage of the efforts invested in the development of inhibitors for renin and HIV protease.¹⁹⁰ The inhibitor is designed as structural analogue of the transition state occurring when an appropriate substrate is cleaved by the aspartic proteases. The non-hydrolysable isostere mimics the transition state avoiding to

be cleaved by aspartic protease and definitely inhibiting the enzyme.

Statines

Sinha *et al.*¹⁵² were the first to report the use of a peptidic inhibitor based on the APP sequence. This was the tetradecapeptide Lys-Thr-Glu-Glu-Ile-Ser-Glu-Val-*LeuStatine*-Val-Ala-Glu-Phe-OH, (**II**) (known as STA-200) corresponding to APP residues 588-599 of the human APP₆₉₅ sequence harbouring the Swedish mutation (Fig. 13).



Figure 13. Statine core and STA-200 inhibitor (Leu-Statine isostere is highlighted in dashed circle).

STA-200 contained a modification at the cleavage site, with the introduction of a statine ((3*S*, 4*S*)-4-amino-3-hydroxy-6-methylheptanoic), an unusual amino acid that was found to behave as a transition state isostere in the inhibition of pepsin by the microbial aspartic protease inhibitors of the pepstatin family.¹⁹¹ The incorporation of statine increased binding affinity of the peptide for BACE1 by three orders of magnitude. The residue Asp₅₉₆ was also replaced by Val resulting in a 30 nM inhibition of BACE1. The use of a bis-statine central core has further provided high affinity inhibitors for BACE1.¹⁹² From these seminal discoveries, medicinal chemistry development at Elan and Boehringer-Ingelheim created smaller statine-containing molecules.^{193,194} Recent results of the biological assays for the Boehringer inhibitors indicate *in vitro* IC₅₀ < 30 μM.¹⁹⁴

Hydroxyethylene derivatives

As already cited, Tang and Ghosh and researchers at the Oklahoma Medical Research Foundation used homostatine (or hydroxyethylene, HE) as an isostere to design the octapeptide analogue Glu-Val-Asn-*Leu*Ala* Ala Glu-Phe, OM99-2 (Fig. 10), in which the cleavable bond Leu-Asp (BACE1 cleavage site) is replaced with HE isostere, to create a transition state mimic. This peptide inhibits BACE1 with $K_i = 1.6$ nM. In fact, a hydroxyethylene isostere in the backbone of the synthetic protease inhibitor has performed an admirable role in the design of a potential inhibitor. Starting from this crystal structure of a BACE1-OM99-2 complex (Fig. 9), reported by the Tang and Ghosh⁸⁵ groups in 2000, valuable insights gleaned from this structural information led to the design and synthesis of several other types of both BACE1 inhibitors. Structure refinements provided OM00-3 (**III**) (Glu-Leu-Asp-Leu*Ala-Val- Glu-Phe) with $K_i =$

0.3 nM¹⁹⁵ (Fig.14).

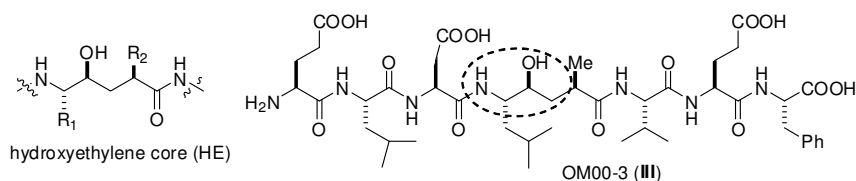
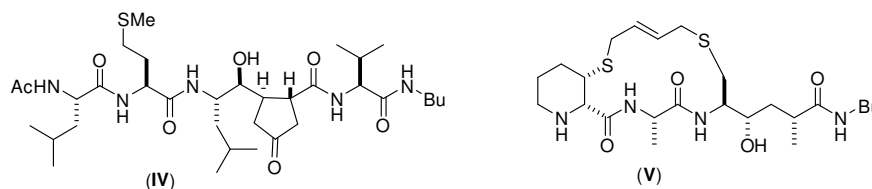
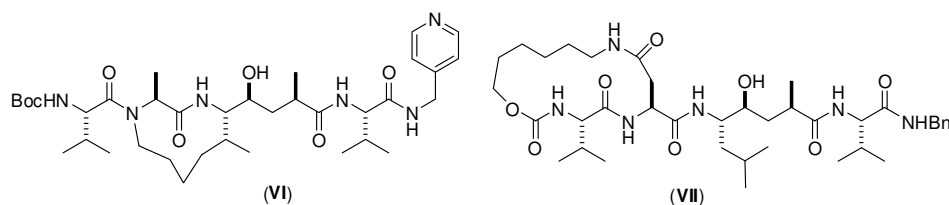


Figure 14. Hydroxyethylene core and OM00-3 inhibitor (HE isostere is highlighted in dashed circle).

Conformationally restricted peptidomimetic BACE1 inhibitors have been reported by several groups. Hanessian and Novartis researchers accomplished some functional modification and appropriate truncation of a synthetic OM99-2 of BACE1 leading to a series of constrained carbocyclic or heterocyclic analogues.¹⁹⁶ The representative compound **IV** displayed an $IC_{50} = 10$ nM in enzymatic assays.

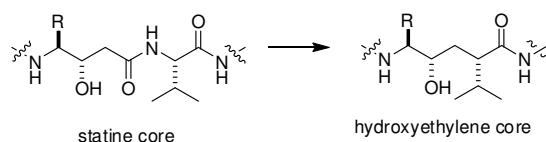


Despite the character of these compounds remains still peptidic, the above structural modifications have produced potent BACE1 inhibitors endowed with excellent potential for selectivity over CatD. Moreover, a series of macroheterocyclic analogues were synthesized in order to establish by macrocyclization the bioactive conformation of these transition state mimic inhibitors, giving a representative compound **V** endowed with an $IC_{50} = 184$ nM in enzymatic assays.¹⁹⁷ The protease inhibitors are designed to mimic essential features of peptides in β -strand conformation because protease substrates have to adopt such extended conformation to be recognized and cleaved by the enzyme. In this topic, macrocyclization has been applied successfully for a number of proteases with the final purpose to improve activity, pharmacokinetic properties and proteolytic stability in comparison to the open chain analogues. Other examples by Lilly¹⁹⁸ (compound **VI**, $IC_{50} = 80$ nM) and Oklahoma / Zapaq¹⁹⁹ (compound **VII**, $IC_{50} = 25$ nM) gave good results in term of enzymatic inhibitory activity. The high resolution X-ray crystal structures of the Novartis and Lilly macrocycles providing further insights into interactions with enzyme.

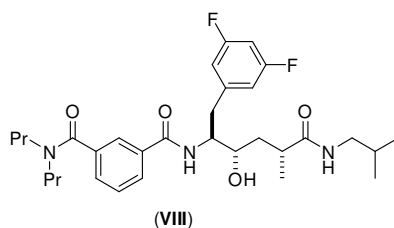


Although peptidomimetics inhibitors are very potent *in vitro*, their large size and their peptidic structure seriously impair their use *in vivo*. Chang *et al.*¹⁸⁴ conjugated such HE inhibitor to a carrier peptide, to improve BBB permeability.

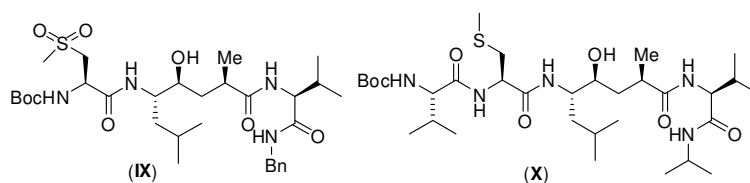
In order to overcome their limited druggability, researchers at Elan Pharm. Inc. developed hydroxyethylene based drug by replacing the statin moiety with the HE core which represents a dipeptide isostere.²⁰⁰



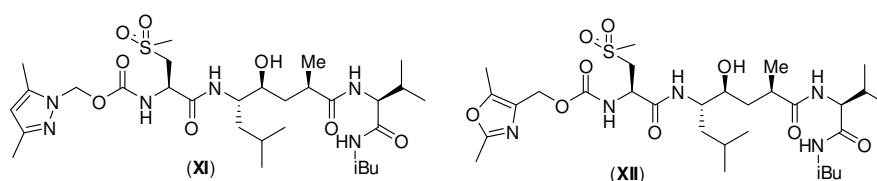
Therefore, a variety of compounds bearing the optimal isophthalamide *N*-terminus of the statin series and different *C* termini at the P1' substituent were synthesized. The HEs were more cell permeable than the statins. The representative compound **VIII** (BACE1 IC₅₀ = 0.03 μM) was less potent than the best statin analogue toward BACE1, but demonstrated a ratio of cell to enzyme activity (EC₅₀/IC₅₀) of 100, (EC₅₀ = 3 μM in HEK-293 cells).



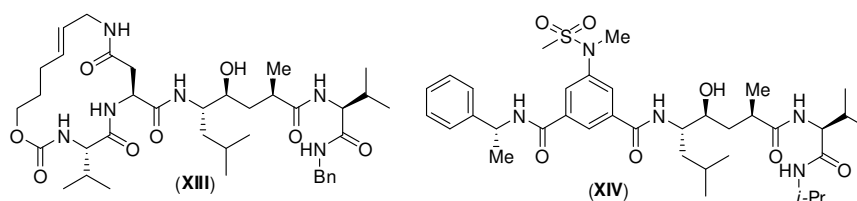
Modification carried out onto original peptidomimetic inhibitor OM99-2 gave interesting results. Size reduction of this inhibitor revealed that the removal of the four outside residues P4, P3, P3' and P4' resulted in greatly reduced potency.²⁰¹ A representative inhibitor is compound **IX**, which, despite well-optimized side chains, has a *K_i* value almost 1000 times higher compared to OM99-2. The inclusion of P3 Val, combined with the optimization of P2 and *C*-terminal blocking group, brought the *K_i* back to the nanomolar level, as represented by compound **X**. Evidence from these studies suggested that, from the structural template derived from OM99-2, high potency could be attained by inhibitors with five subsites, from P3 to P2', resulting in a molecular size of approximately 700 Da.



In search of selectivity towards CatD, researchers in Ghosh group designed a selective inhibitor **XI** with a K_i of 0.3 nM against BACE1; it displayed 1186-fold selectivity over BACE2 and 436-fold selectivity over CatD. Subsequently, they designed inhibitor **XII**, which has demonstrated a K_i of 0.12 nM against β -secretase but with K_i values for BACE2 and CatD greater than 3800-fold and 2500-fold, respectively. The structural basis of selectivity *versus* BACE2 resides mainly in P3-oxazole, which affected a local conformational change better accommodated in BACE1, compared to BACE2.²⁰² The P2-sulfone group in compound **XII** also provides a hydrogen-bonded network in β -secretase that cannot be accommodated in CatD, thus differentiating inhibition potency.



In order to investigate different means to restrain the conformational freedom of the inhibitors, macrocyclic compound were designed. Cyclization of the *N*-terminal portion of the previous inhibitors guided by structure-based design produced cycloamide-urethane derivatives with improved biological properties. A series of (14 to 16)-membered macrocyclic inhibitors were reported¹⁹⁹ resulting in good potency *in vitro* and improved cell penetration. A representative inhibitor **XIII**, ($K_i = 14$ nM) suggests that introduction of rings to constrain the backbone freedom may be pursued.



Further evolution of the inhibitor structures along this line gave rise to compound **XIV**, which contains a substituted isophthalamide ring at P2 and optimized side chains from structure-based design and energy minimization. This inhibitor is potent ($K_i = 1.1$ nM), and has moderately good selectivity (K_i values of 31 nM and 41 nM *versus* BACE2 and CatD, respectively). At 648 Da, it penetrated the cell membrane well and inhibited A β production in cultured cell with an IC_{50} of 39 nM. Recently Ghosh and co-workers reported that **XIV** is active *in vivo*, showing 30% reduction of A β 40 production in Tg2576 transgenic mice after a single intraperitoneal administration (8 mg/kg).²⁰³

Hydroxymethylcarbonyl derivatives

The group of Kiso at Kyoto Pharmaceutical University has used norstatine (hydroxymethylcarbonyl, HMC) (Fig. 15) as alternative isostere to develop potent BACE1 inhibitors. Similarly, they started by designing octapeptide analogues and reported that KMI-008 (**XV**) had an $IC_{50} = 413$ nM in the *in vivo* assay and that could decrease by 38% the secretion of sAPP β from COS-7 cells overexpressing APP.²⁰⁴

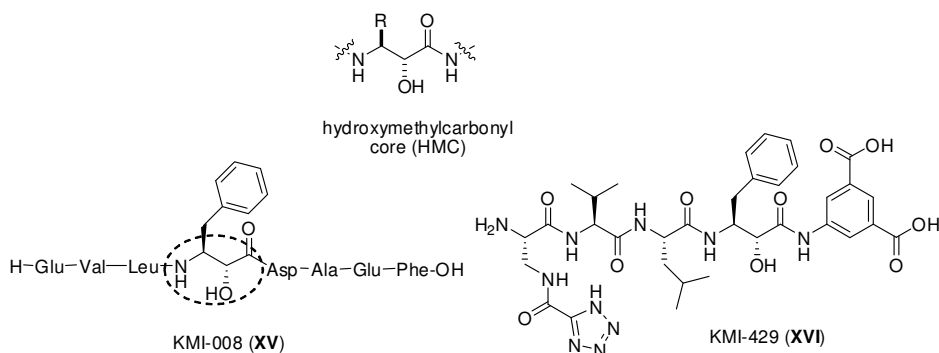
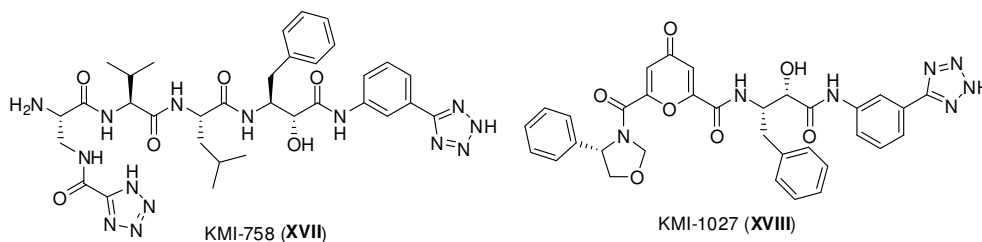


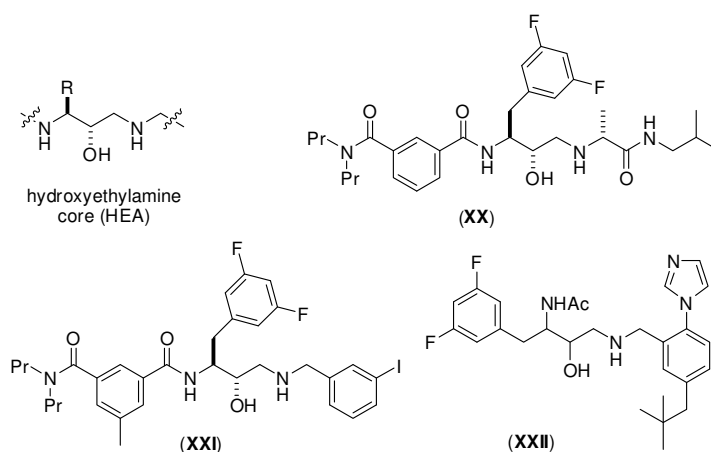
Figure 15. Hydroxymethylcarbonyl core and Kyoto Pharmaceutical University inhibitors (HMC isostere is highlighted in dashed circle).

Norstatine was then replaced with phenylnorstatine²⁰⁵ and introduction of a tetrazole carbonyl in the P4 position provided KMI-429 (**XVI**), with *in vitro* $IC_{50} = 3.9$ nM.²⁰⁶ Biological assays revealed that **XVI** was effective in cells and in animals.²⁰⁷ An IC_{50} value of 42.8 nM was obtained in a cell assay measuring APP β release from BACE1 overexpressing human embryonic kidney (HEK293) cells. Injection of 2.5 nM of KMI-429 (**XVI**) into the hippocampus of Tg2576 transgenic mice caused a 20% decrease of sAPP β . Recent further modification to those compounds include the introduction of carboxylic acid bioisosteres at P1' position, resulting in IC_{50} as low as 1-5 nM²⁰⁸ and elongation of the side chain at P1 position by changing the phenylnorstatine to phenylthionorstatine.²⁰⁹ Further optimization was carried out replacing the acidic moiety of KMI-429 with non acidic hydrogen bonding groups, to give KMI-758 (**XVII**) ($IC_{50} = 14$ nM).²¹⁰ In order to improve cellular inhibitory activity, a series of BACE1 inhibitors possessing a heterocyclic ring at the P₂ position and a 5-membered ring at the P₃ position, were designed. The authors found novel small-molecule and non-peptidic chelidonic BACE1 inhibitor KMI-1027 (**XVIII**) ($IC_{50} = 50$ nM).²¹¹



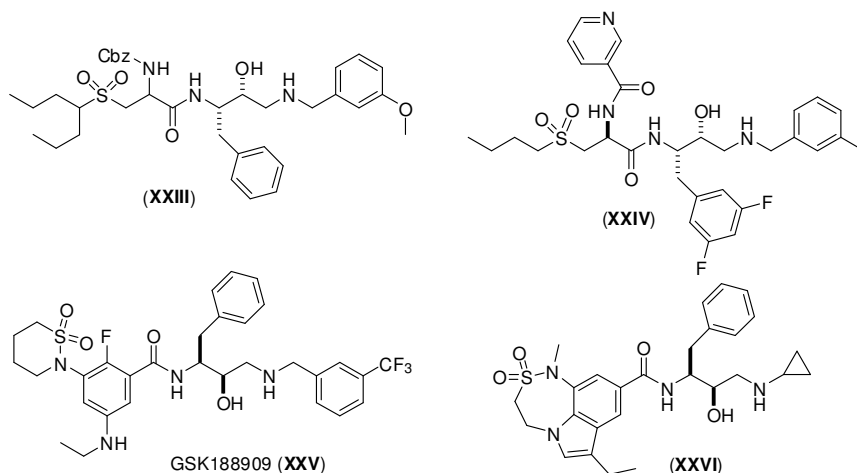
Hydroxyethylamine derivatives

However, the scaffold, which provided the majority of active compounds is the hydroxyethylene (HEA). The HEA transition-state analogue inhibits aspartic proteases, with both the secondary amine and the secondary alcohol interacting with the two catalytic aspartates. The hydroxyethyl secondary amine isostere was an alternative of HE because of the strict preference of BACE for acyclic residues at the S1' subsite, and considering that the majority of CNS drugs contain a basic amine.²¹² This was extensively exploited by Elan-Pharmacia who had claimed some hydroxyalkylamine derivatives as BACE1 inhibitors.²¹³ Compound **XX** (BACE1, $IC_{50} = 0.13 \mu\text{M}$; HEK-293, $EC_{50} = 0.23 \mu\text{M}$; $EC_{50}/IC_{50} = 1.8$) was a potent cellular inhibitor of $A\beta$ production, Compound **XXI** bearing a C-terminal meta-iodo benzyl amine exhibited nanomolar both enzymatic and cellular BACE1 enzyme inhibitory activity (BACE1, $IC_{50} = 5 \text{ nM}$; HEK-293, $EC_{50} = 3 \text{ nM}$; $EC_{50}/IC_{50} = 0.6$).



For compound **XXII**, some *in vivo* studies showed it reduced $A\beta$ levels by 17% in brain cortex and by 47% in plasma, when administered at 100 mg/Kg.²¹⁴ A drawback for this class of compounds was the predicted poor metabolic stability due to microsomal *N*-debenzylation and *N*-depropylation.²¹⁵ By replacing the isophthalate *N*-terminus by acyclic sulfones, the racemic carbobenzyloxy-derivative compound **XXIII** was designed, representing a lead compound

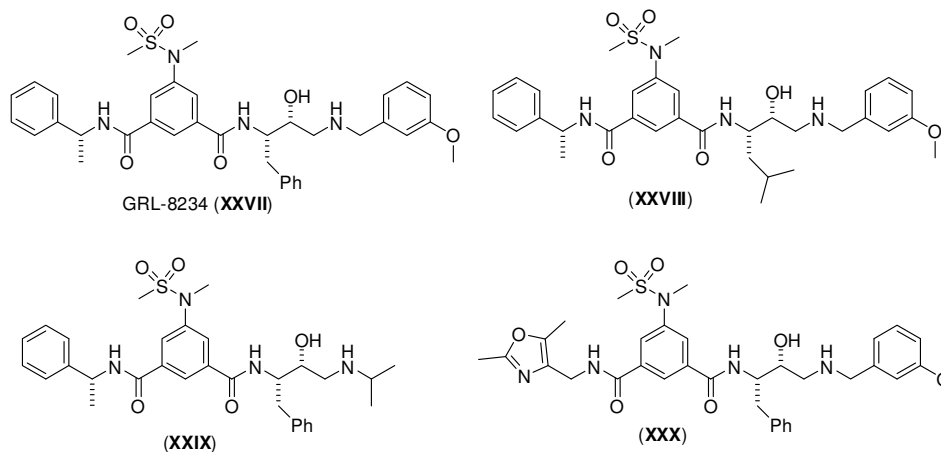
endowed with good enzymatic activity, but more potent inhibitory activity against CatD ($IC_{50} = 67 \text{ nM}$).²¹⁶



Further structure based drug design gave the derivative **XXIV**, with highly improved enzymatic inhibitory activity ($IC_{50} = 2 \text{ nM}$) and cellular potency ($IC_{50} = 1 \text{ nM}$). The X-ray crystal structure of compound **XXIV**-bound to BACE1 highlighted a close association between the pyridyl nitrogen and the Arg235 in the S2 site. The authors suggest that, because CatD S2 pocket is more lipophilic, and consequently is less tolerant of the introduction of polar groups with respect to BACE1, the pyridyl moiety of compound **XXIV** is also the main determinant of improved selectivity *versus* CatD enzyme ($IC_{50} = 474 \text{ nM}$).²¹⁷ Inhibitor **XXV** (GSK188909) was described as the first orally bioavailable BACE1 inhibitor capable of lowering brain A β in APP transgenic mice,²¹⁸ and the studies leading to the discovery of this orally active HEA isostere-based inhibitor have been reported.²¹⁹ GSK188909 inhibited BACE1 activity with an IC_{50} of 5 nM and also showed good selectivity with respect to BACE2, renin, and CatD. It caused a decrease in A β 40 and A β 42 production in cell-based assays expressing both wild-type and Swedish-variant APP sequences ($IC_{50} = 5$ and 30 nM, respectively). When orally administered to TASTPM mice, along with a P-glycoprotein (P-gp) inhibitor, GSK188909 (250 mg/kg) displayed a 68% and 55% decrease in A β 40 and A β 42, respectively. Further optimization led to discover inhibitor **XXVI** incorporating a tricyclic nonprime side and a truncated prime side residues, which showed nanomolar potency in a cell-based assay ($IC_{50} = 19 \text{ nM}$). Moreover, this compound is endowed with good oral bioavailability.²²⁰

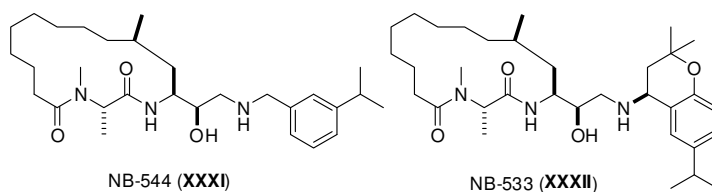
Another interesting example is compound GRL-8234 (**XXVII**),²²¹ that contains a HEA isostere with a P1-phenylmethyl side chain, a functionalized P2-isophthalamide ligand, and a P2'-hydrophobic benzyl derivative. The inhibitor exhibited a BACE1 $K_i = 1.8 \text{ nM}$. Most

strikingly, it has shown a BACE1 cellular $IC_{50} = 1$ nM. This impressive cellular activity is in marked contrast to inhibitors with hydroxyethylene isosteres. The P1-leucine side chain containing inhibitor **XXVIII** ($K_i = 916$ nM) was significantly less potent.



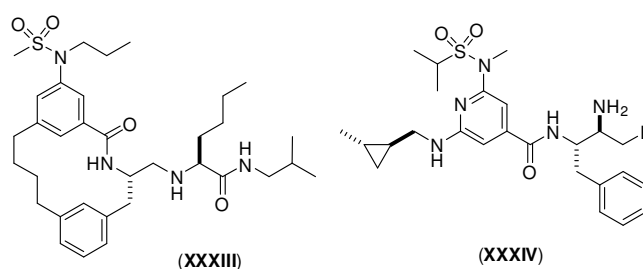
Inhibitor **XXIX** ($K_i = 425$ nM) with a P2'-isopropyl group is also less potent than inhibitor GRL-8234 with a P2'-methoxybenzyl derivative. Similarly, replacement of P3-phenylmethyl derivative gave inhibitor **XXX** which resulted in marked attenuation of activity ($K_i = 552$ nM). The remarkable cellular activity of GRL-8234 may be due to the balance of its lipophilic and basic amine properties. The X-ray crystallographic analysis of protein–ligand structure of GRL-8234 shows that both the hydroxyl group and the secondary amine group form a network of tight hydrogen bonding with the active site aspartic acid residues Asp32 and Asp228. The P2-sulfonamide derivative fits well into the S2-site and makes extensive hydrogen bonding with β -secretase. Inhibitor GRL-8234 has shown good selectivity over other aspartic proteases (39-fold selective over BACE2 and 23-fold selective over CatD) and very relevant *in vivo* properties in transgenic mice. Administration of compound (8 mg/kg i.p.) to Tg2576 mice resulted in up to 65% reduction of A β 40 production after 3 h.

Very recently, researchers at Novartis discovered some macrocycles-based BACE1 inhibitor NB-544 (**XXXI**, $IC_{50} = 27$ nM; cellular-CHO, $IC_{50} = 45$ nM) exchanging the HE to HEA transition state core. Variation of the P' moiety resulted in the macrocyclic inhibitor NB-533 (**XXXII**, $IC_{50} = 2$ nM; cellular-CHO, $IC_{50} = 24$ nM). Both macrocycles not only are highly potent and selective, but show inhibition of BACE1 in the brain of APP_{51/16} transgenic mice, NB-544 after intravenous and NB-533 after oral application.²²²



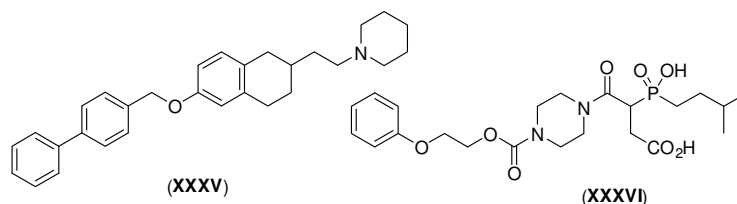
Other isosteres

Sunesis and Merck researchers investigated the effect of introducing an aminoethylene (AE) isostere group as a central scaffold. Crystallization data indicated the amino group can interact with BACE1 active sites aspartates. Furthermore, following a macrocyclization approach, to improve affinity and selectivity, a series of inhibitors were designed based on an isophthalamide scaffold coupled to a reduced amide isostere.²²³ The compound **XXXIII** displayed an enzymatic $IC_{50} = 4$ nM, a cellular $IC_{50} = 76$ nM, and, most important, an improved membrane permeability and reduced P-gp susceptibility. When administered in mouse at a dose of 100 mg/kg i.v., it produced a 25% decrease in A β 40 levels in brain extracts. Merck researchers have also discovered a series of 2,6-diamino-isonicotinamide inhibitors, which bind to S1-S3 pocket of BACE1 active site in conjunction with a primary amine or alcohol group. These are highly potent and selective for BACE1 over CatD. The truncated reduced amino isostere as the aspartate binding element^{224,225} is exemplified by compound **XXXIV**, displaying cellular IC_{50} of 49 nM and *in vivo* activity in transgenic mice expressing human wild-type APP. After intravenous administration of a 50 mg/kg dose of inhibitor **XXXIV**, a maximal reduction of A β 40 (34%) at 3 h from dosing was observed, and the concentration of drug in the brain was 1.9 μ M.²²⁵



1.3.2. Non-transition-state-derived small molecules

In 2001, Takeda Chem. Ind. reported the first novel non-transition-state-derived ligands disclosing new avenues to non-peptidomimetic BACE1 inhibitors.^{226,227} Derivative **XXXV** was found, at that time, the most potent inhibitor among a series of tetralines, and showed $IC_{50} = 0.349$ μ M as determined by a fluorescence assay.



Neurologic, Inc. described non-peptidomimetic phosphinylmethyl and phosphorylmethyl succinic and glutaric acid analogues along with some phosphorous-containing tetrapeptides.^{228,229} Noteworthy, the BACE1 inhibitory activity of the phospho analogues was indirectly associated through measurements of the compounds ability to increase sAPP α (it was expected to increase the pool of non-amyloidogenic derivatives). The activity of **XXXVI** on sAPP α secretion was dose proportional at > 1 nM concentration.

Vertex, in 2002, disclosed hundreds of different heterocycle compounds,²³⁰ whose activity was around micromolar range. Vertex researchers proposed a 3D pharmacophore map of BACE to guide the design of new inhibitors. The compounds described in the invention showed hydrogen-bonding moiety interactions (HB) with the active site and other key residues of BACE, and hydrophobic interactions (HPB) with BACE subsites. Different BACE/inhibitor binding modes were hypothesized involving, for instance, seven features of the inhibitor as shown in figure 16.

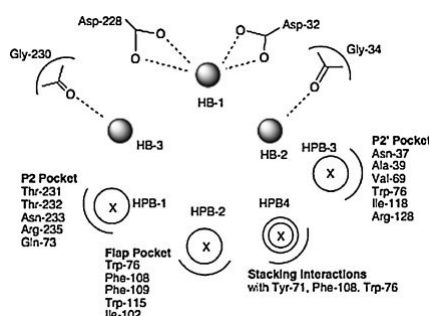
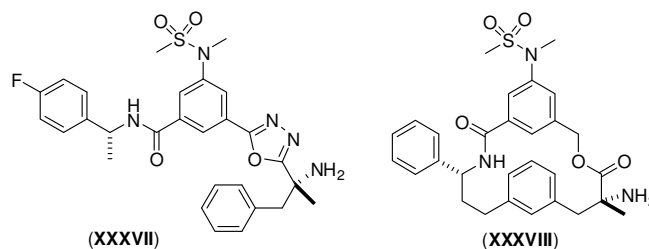


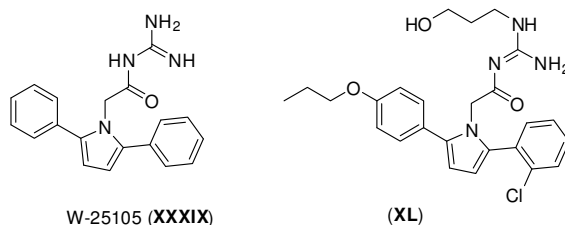
Figure 16. Seven features binding modes with BACE1

One of the most intriguing small-molecule inhibitors deriving from HEA drug design was first disclosed by Merck. In particular, the discovery and optimization of tertiary carbinamine-derived inhibitors²³¹ represented novel non-transition-state-derived ligands incorporating a single primary amine to interact with the catalytic aspartates of the target enzyme. Optimization of this series provided inhibitors with intrinsic and functional potency comparable to evolved transition state isostere derived inhibitors of BACE1. Their optimized inhibitor (**XXXVII**) showed high potency in enzymatic and cellular assays (IC_{50} = 12 and 65 nM, respectively) and good selectivity toward both renin and CatD, but only moderate selectivity toward the high homolog BACE2 (IC_{50} = 620 nM).



Macrocyclization of this series of inhibitors led to lactone **XXXVIII**, which displayed increased potency *versus* BACE1 ($IC_{50} = 2$ nM). Both series of compounds, however, suffer from poor brain penetration, mostly due to high efflux of P-gp.²³²

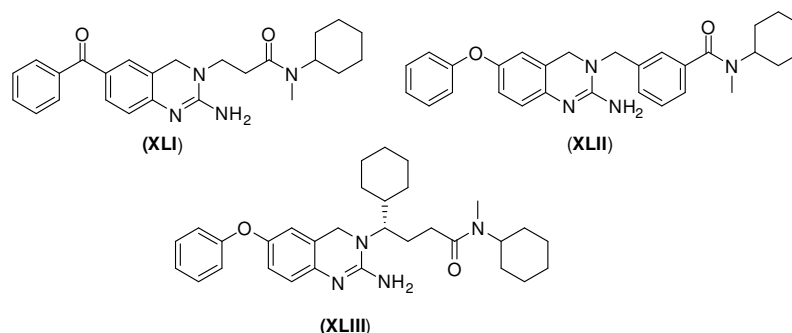
Strategies to discover non-peptidomimetic small-molecule hits, to be optimized as BACE1 inhibitors, mostly involved screening of multimillion libraries of compounds. Wyeth drug discovery team has identified W-25105 (**XXXIX**) as low micromolar BACE1 inhibitor through screening of drug libraries in a high throughput screening (HTS) *in vitro* assay, endowed with activity in cells at 20 μ M. This acylguanidine compound interacts through hydrogen bonding via catalytic aspartates and stabilizes the flap in an open position conformation whereas the polar functionality of the guanidine *N*-substituent extends into the S1' pocket, forming hydrogen-bonding interactions through bridging water molecules.²³³ Optimization of the hit using structure-based design led to the design of compound **XL** which displayed a BACE1 inhibition IC_{50} of 110 nM.



Preliminary structure–activity relationship (SAR) investigations^{234,235} resulted in moderate improvement of BACE1 inhibitory potency, but poor selectivity for BACE2 enzyme and poor permeability, as assessed in a Caco-2 drug transport model, remain major drawbacks of this class of compounds. The poor cellular permeability of the acylguanidine inhibitors could be due to the guanidinyll functionality, and bioisosteric replacement of this group is currently under evaluation.²³⁵

In this regard, a series of bioisosteric 2-amino-3,4-dihydropyrido[3,4-d]pyrimidines showed K_i values in the submicromolar range of concentration.²³⁶ Johnson & Johnson Pharm. focused SAR development on 2-amino-3,4-dihydroquinazoline **XLI** (BACE1 $K_i = 900$ nM). An X-ray structure of BACE1/**XLI** obtained in collaboration with Astex Ther. showed that the side chain

bent back onto itself in a hairpin turn orientation, allowing the *N*-cyclohexyl substituent to occupy the S1 binding pocket, while the flap region of the protein adopted an “open” structure.



Compound **XLI** formed H-bonds with the catalytic aspartates as shown in Fig. 17. Compound **XLII** incorporates a 1,3-disubstituted phenyl ring in the side chain and 6-phenoxy substituent instead of the 6-benzoyl group, was six fold more potent than parent compound **XLI** (BACE1 K_i = 158 nM). To fill the S1' pocket a cyclohexyl was introduced on the (*R*)- α -carbon of the side chain. The (*S*) enantiomer **XLI** inhibited BACE1 with K_i = 11 nM (racemate K_i = 30 nM). Compound **XLIII** displayed modest selectivity for BACE1 over renin and CatD as well as the hERG channel. Compound **XLIII** exhibited excellent potency in a cellular assay, which measures the inhibition of A β 40 secretion in CHO cells transfected with the Swedish familial AD mutant APP. Additionally, **XLIII** lowered A β 40 in plasma by 40–70% in rats after oral administration (30 mg/kg), 3 hr post-dosing.²³⁷

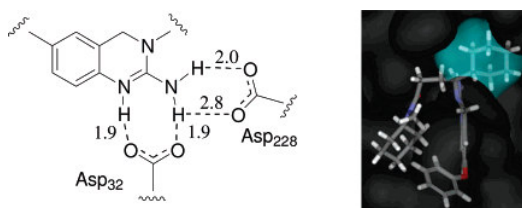
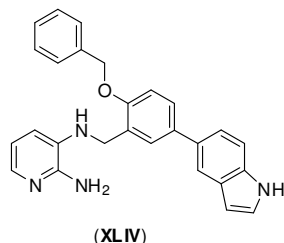


Figure 17. Left: the 2-amino-3,4-dihydroquinazolin-5(1H)-one fragment of **XLI** and the Asp32 and Asp228 sidechains of BACE1, with H-bond distances in Å. Right: the X-ray structure of **XLIII** bound into the enzyme, showing the *R*-cyclohexyl moiety filling the S1' pocket.²³⁷

Astex Ther. used the Pyramid fragment screening methodology to BACE1 to identify by X-ray crystallography three distinct chemotypes (amino-heterocycle, piperidine and aliphatic hydroxyl group) binding to the catalytic aspartates. The fragment hits were endowed with weak BACE1 inhibitory activity but most of them displayed relatively good ligand efficiency. Virtual screening around the aminoheterocycle recognition motif identified an amino-pyridine with increased potency. By means of Pyramid, non-peptidic fragments were identified useful for the

design of new (non-peptidic) BACE1 inhibitor.²³⁸ Structure-based design approaches have led to identification of low micromolar lead compounds that retain these interactions and additionally occupy adjacent hydrophobic pockets of the active site. From this novel medicinal chemistry approach a representative lead **XLIV** ($IC_{50} = 690$ nM) was identified.



1.4 Alternative therapeutic approaches to targeting β -secretase

Most of the effort in the area of targeting BACE1 has been directed toward the development of inhibitors of this protease. Despite significant progress, very few examples of inhibitor drug candidates have been disclosed due to their limited capability to penetrate the blood brain barrier. Therefore, the late generation inhibitors are, as already described, small molecules. For some of them, such as GRL-8234, the ability to penetrate membranes and to inhibit $A\beta$ production is well demonstrated in transgenic mice.¹⁸¹ In 2007, a compound named CTS-21166, belonging to small molecule transition-state analogues, began Phase I of clinical trials handled by CoMentis. However, many of the BACE1 inhibitors developed so far inhibit APP binding to the active site, but underestimate the fact that *in vivo* action of BACE1 on APP hydrolysis would require the participation of many other cellular components and would thus provide alternative opportunities for therapeutic intervention.

However, few therapeutic approaches outside of BACE1 inhibitors have so far been reported. Chang *et al.*²³⁹ explored the idea that neutralizing antibodies against BACE1, generated from the immunization with the protease itself, may be enlisted to reduce $A\beta$ production. Immunization of BACE1 produce polyclonal anti BACE1 antibodies in peripheral system such as plasma. Certain percentage of antibodies penetrates BBB and binds to BACE1 on surface of brain cells. Rapid endocytosis on neuron membrane carries surface molecules to endosome with an optimal pH (4.5) for BACE1 activity. Because enzymatic site of BACE1 is masked by antibodies, BACE1 hydrolysis on APP is prevented. Therefore, production of $A\beta$ is reduced improving the cognitive performance of AD mice (Fig. 18).

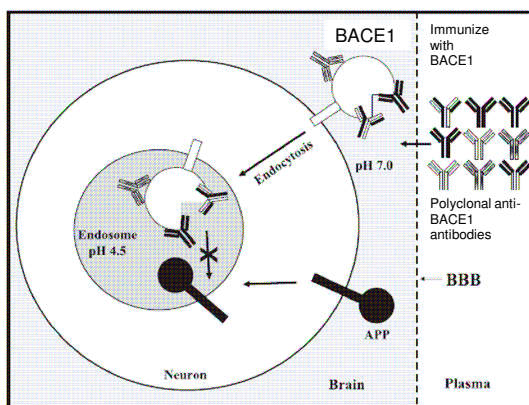


Figure 18. Schematic representation of mechanism for proposed BACE1 immunization.²³⁹

The antibodies in this approach serve as inhibitors for BACE1 activity and thus do not require the participation of immune cells for A β reduction. This may indeed lower the risk of autoimmune response as observed in A β immunization. A conceptually related approach is immunization using peptides derived from the BACE1 cleavage site in APP. A study with AD mice using this approach has shown promise.²⁴⁰

Other strong evidences to deal with are the intracellular trafficking of BACE1 allowing to perform its function of APP hydrolysis and consider endosome as the main location of enzyme activity. Considering this issue might explain the poor results obtained with some inhibitors in cellular assays.²⁴¹

In fact, although ubiquitously expressed, BACE1 mRNA has the highest expression levels in the mammalian brain, and is found in acidic organelles of the endosomes and trans-Golgi network. This is consistent with the discovery that BACE1 cleavage of APP occurs predominantly in endosomes, and that endocytosis of APP and BACE1 is essential for A β production. BACE1 activity and access to substrates is regulated by the composition of lipid raft domains in the membrane bilayer. Endosomes have high lipid raft and cholesterol content, critical in regulating APP endocytosis with increased amyloidogenic processing. In order to overcome this crucial issue, an innovative approach was recently reported, consisting of targeting inhibition to the subcellular compartment where the enzyme is active. A membrane anchored BACE1 transition state inhibitor was synthesized by coupling via a polyglycol linker the inhibitor to a sterol moiety (Figure 19).¹⁸⁵

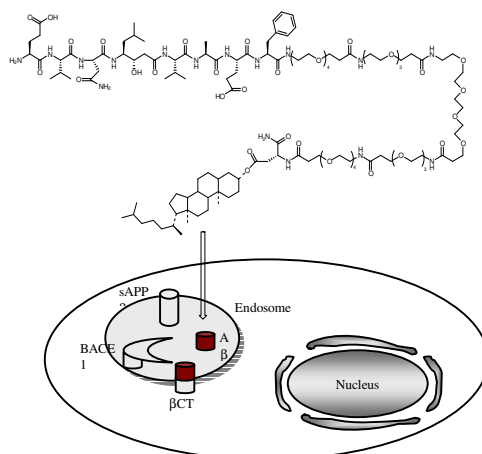


Figure 19. Illustration of sterol-linked BACE1 inhibitor targeting endosome.

This inhibitor efficiently targeted BACE1 in endosomes via endocytosis, significantly enhancing the inhibitor efficacy, both in cell culture and in fly and mouse models of AD. Although it is too early to say whether this approach will lead to a functional drug therapy, the authors postulate that this membrane-tethering strategy might also be useful for designing inhibitors against other disease-associated membrane proteins.

1.5. Multi Target Directed Ligands to combat AD

AD is currently recognized as a complex neurodegenerative disorder with a multifaceted pathogenesis. This may explain why the currently available drugs, developed according to the reductionist paradigm of "one-molecule-one-target," have turned out to be palliative rather than curative.

Different pharmacological approaches offer possible ways of overcoming the problems that arise from the use of such drugs.²⁴² When a single medicine is not sufficient to effectively treat a disease, a multiple-medication therapy (MMT) (also referred to as a "cocktail" or "combination of drugs") may be used. Usually, an MMT is composed of two or three different drugs that combine different therapeutic mechanisms. But this approach might be disadvantageous for patients with compliance problems. A second approach might be the use of a multiple-compound medication (MCM) (also referred to as a "single-pill drug combination"), which implies the incorporation of different drugs into the same formulation in order to simplify dosing regimens and improve patient compliance. Finally, a third strategy is now emerging on the basis of the assumption that a single compound may be able to hit multiple targets. Clearly, therapy with a

single drug that has multiple biological properties would have inherent advantages over MMT or MCM. It would obviate the challenge of administering multiple single-drug entities, which could have different bioavailability, pharmacokinetics, and metabolism. Indeed, if a single molecular species can show a complex ADMET profile, an MMT/MCM approach might be untenable. Furthermore, in terms of pharmacokinetic and ADMET optimization, the clinical development of a drug able to hit multiple targets should not, in principle, be different from the development of any other single lead molecule. It thus offers a much simpler approach than MMT/MCM. In addition, the risk of possible drug-drug interactions would be avoided and the therapeutic regimen greatly simplified in relation to MMT. In light of this, drug combinations that can act at different levels of the neurotoxic cascade offer new hopes toward curing AD and other neurodegenerative diseases.²⁴³ All these considerations are of particular relevance, as one of the major contributions to the attrition rate in drug development continues to be the drug candidate's pharmacokinetic profiling.²⁴⁴ There is, therefore, a strong indication that the development of compounds able to hit multiple targets might disclose new avenues for the treatment of, for example, major neurodegenerative diseases, for which an effective cure is an urgent need and an unmet goal.

Morphy and Rankovic elegantly discuss in recent articles^{242,245,246} “designed multiple ligands” approach to describe compounds whose multiple biological profile is rationally designed to address a particular disease. In parallel, this new paradigm in medicinal chemistry, recently termed by Melchiorre and co-workers⁷ as “multi-target-directed ligand” (MTDL) design strategy (Fig. 20) has been successfully exploited at both academic and industrial levels in the fields of AD²⁴⁷ and similarly complex diseases.^{248,249}

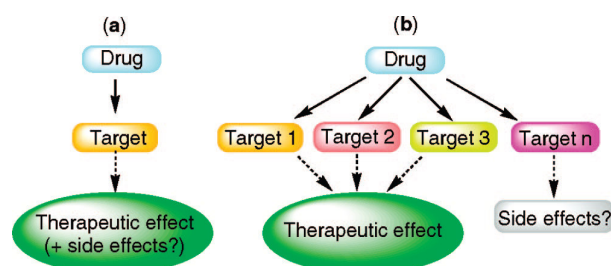


Figure 20. Pathways leading to the discovery of new medications: (a) Target-driven drug discovery approach, that is, the application of the current one-molecule-one-target paradigm. Although this approach has led to many effective drugs able to hit a single target, it is now well-documented that these drugs may represent the exception rather than the rule. (b) MTDLs approach to drug discovery. A drug, could recognize (in principle, with comparable affinities) different targets involved in the cascade of pathological events leading to a given disease. Thus, such a medication would be highly effective for treating multifactorial diseases. The design of such a drug may not be easy because it could also bind targets that are not involved with the disease and could be responsible (although not necessarily) for side effects. With MTDLs, the one-medication-one-disease paradigm finds a practical application.

To obtain novel Multi-Target-Directed Ligands (MTDLs) a design strategy is usually applied in which distinct pharmacophores of different drugs are combined in the same structure to afford hybrid molecules. In principle, each pharmacophore of these new drugs should retain the ability to interact with its specific site(s) on the target and, consequently, to produce specific pharmacological responses that, taken together, should slow or block the neurodegenerative process. One of the most widely adopted approaches in the field has been to modify the molecular structure of an AChEI in order to provide it with additional biological properties useful for treating AD.

However, the selection of a therapeutic target (to seek either a single- or a multi-target-directed ligand) is one of the biggest challenges in designing new molecules for this multifactorial disease.²⁵⁰ Clearly, MTDLs should be targeted against the most important pathophysiological processes. Obviously, better understanding of the complexity of the signalling pathways in which targets are involved is needed. Moreover, it is important to develop new approaches with which to unravel the mechanisms underlying the neurodegenerative process. Knowing that BACE1 is now recognized as one of the most intriguing target in the pathogenesis of AD, conferring to a given molecule an additional property such as BACE1 inhibition could be a useful strategy to seek a multi-target-directed ligand for the treatment of AD.

However, more clues regarding the target seek come from the system biology approach²⁵¹ which may help in addressing how ‘networking’ (collective arrangement, connections, and interactions) of targets influences the final properties of the MTDLs against a given pathological event.^{252,253}

The main criticism to MTDL drug discovery paradigm is that this approach is resource hungry, because the rational design of MTDLs has to deal with the critical issues of affinity balancing and pharmacokinetics. However, as proof of principle, and to support the view that MTDLs are destined to become the mainstream of AD therapeutics in the years to come, could be useful to discuss the biological profile of ladostigil (TV-3326), an MTDL developed by Youdim and co-workers,²⁵⁴ which is currently in phase II clinical trials for AD.

The design of MTDLs is based on the combination of two or more pharmacophores acting on different AD targets. In particular, ladostigil was designed by merging the structures of rivastigmine, an AChEI, and rasagiline, a selective MAO-B inhibitor (Fig. 21).

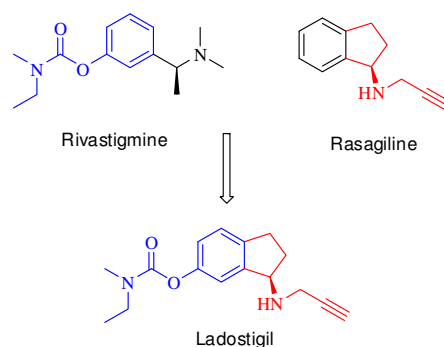


Figure 21. The design strategy leading to the anti-Alzheimer MTDL ladostigil.

Thanks to these chemical features, ladostigil showed the ability to inhibit both cholinesterases (AChE and BChE) and brain monoamine oxidases (MAO-A and -B). The block of MAOs avoids hydrogen peroxide generation, thus preventing the Fenton reaction and the formation of neurotoxic free radical species. In addition, MAO inhibition confers potential antidepressant activity by increasing the levels of dopamine, noradrenaline, and serotonin in the central nervous system.²⁵⁵ Interestingly, in addition to its ability to inhibit MAOs and AChE, ladostigil also showed other supplementary neuroprotective actions, such as APP processing regulation via mitogen-activated protein kinase-signalling pathways, and mitochondrial membrane potential stabilization.^{256,257} Furthermore, ladostigil was a protective agent against oxidative stress-induced neuronal apoptosis, increasing the antioxidant enzymes' expression and catalase activity.²⁵⁸ Ladostigil increased the brain-derived nerve factor (BDNF) mRNA expression, leading to an improved production of BDNF and to a consequent enhanced neuroprotective activity.²⁵⁹ Thanks to this wide MTDL profile, ladostigil can be considered a very promising drug for the treatment of AD.

Definitely, in view of the complexity of AD and the involvement of multiple and interconnected pathological pathways, a combination of therapeutic properties may result in a more effective strategy to address this unmet medical need and to slow or perhaps even halt the course of the disease.

References

- ¹ Alzheimer, A.; Stelzmann, R.A.; Schnitzlein, H.N.; Murtagh, F.R. An English translation of Alzheimer's 1907 paper, "Über eine eigenartige Erkrankung der Hirnrinde". *Clin. Anat.* **1995**, *8*, 429–431.
- ² Bartus, R.T.; Dean, R.L.^{3rd}; Beer, B.; Lippa, A.S. The cholinergic hypothesis of geriatric memory dysfunction. *Science* **1982**, *217*, 408–414.
- ³ Sivaprakasam, K. Towards a unifying hypothesis of Alzheimer's disease: cholinergic system linked to plaques, tangles and neuroinflammation. *Curr. Med. Chem.* **2006**, *13*, 2179–2188.
- ⁴ Kennedy, G.J.; Golde, T.E.; Tariot, P.N.; Cummings, J.L. Amyloid based interventions in Alzheimer's disease. *CNS Spectrums* **2007**, *12*, 1–14.
- ⁵ Hardy, J. and Selkoe, D.J. The amyloid hypothesis of Alzheimer's disease: progress and problems on the road to therapeutics. *Science* **2002**, *297*, 353–356.
- ⁶ Blennow, K.; de Leon, M.J.; Zetterberg, H. Alzheimer's disease. *Lancet* **2006**, *368*, 387–403.
- ⁷ Cavalli, A.; Bolognesi, M.L.; Minarini, A.; Rosini, M.; Tumiatti, V.; Recanatini, M.; Melchiorre, C. Multi-target-directed ligands to combat neurodegenerative diseases. *J. Med. Chem.* **2008**, *14*, 51, 347–72.
- ⁸ Cummings, J.L. Alzheimer's disease. *N. Engl. J. Med.* **2004**, *351*, 56–67.
- ⁹ Braak, H. and Braak, E. Evolution of neuronal changes in the course of Alzheimer's disease. *J. Neural. Transm. Suppl.* **1998**, *53*, 127–140.
- ¹⁰ Merz, P.A., Wisniewski, H.M., Somerville, R.A., Bobin, S.A., Masters, C.L., Iqbal, K. Ultrastructural morphology of amyloid fibrils from neuritic and amyloid plaques. *Acta Neuropathol. (Berl.)* **1983**, *60*, 113–124.
- ¹¹ Braak, H., and Braak, E. Neuropil threads occur in dendrites of tanglebearing nerve cells. *Neuropathol. Appl. Neurobiol.* **1988**, *14*, 39–44.
- ¹² Klafki, H.W.; Staufenbiel, M.; Kornhuber, J.; Wiltfang, J. *Brain* **2006**, *129*, 2840–2855.
- ¹³ Vesey, R.; Birrel, J.M.; Bolton, C.; Chipperfield, R.S.; Blackwell, A.D.; Dening, T.R.; Sahakian, B.J.; *CNS Drugs* **2002**, *16*, 485–500.
- ¹⁴ Pearson, R.C. Cortical connections and the pathology of Alzheimer's disease. *Neurodegeneration*, **1996**, *5*, 429–434
- ¹⁵ Rüb, U.; Del Tredici, K.; Schultz, C.; Thal, D.R.; Braak, E.; Braak, H. The autonomic higher order processing nuclei of the lower brain stem are among the early targets of the Alzheimer's disease-related cytoskeletal pathology. *Acta Neuropathol.* **2001**, *101*, 555–564.
- ¹⁶ Palmer, A.M. Pharmacotherapy for Alzheimer's disease: progress and prospects. *Trends Pharm. Sci.* **2002**, *23*, 426–433.
- ¹⁷ Buccafusco, J.J. *Cognitive Enhancing Drugs* **2004**, 1–10.
- ¹⁸ Tariot, P.N.; Farlow, M.R.; Grossberg, G.T.; Graham, S.M.; McDonald, S.; Gergel, I. Memantine treatment in patients with moderate to severe Alzheimer disease already receiving donepezil; a randomized controlled trial. *JAMA* **2004**, *291*, 317–324.
- ¹⁹ Halliday, G., Robinson, S.R., Shepherd, C.; Kril, J. Alzheimer's disease and inflammation: a review of cellular and therapeutic mechanisms. *Clin. Exp. Pharmacol. Physiol.* **2000**, *27*, 1–8.
- ²⁰ Griffin, W.S.; Sheng, J.G.; Roberts, G.W.; Mrak, R.E. Interleukin-1 expression in different plaque types in Alzheimer's disease: significance in plaque evolution. *J. Neuropathol. Exp. Neurol.* **1995**, *54*, 276–281.
- ²¹ Meda, L.; Cassatella, M.A.; Szendrei, G.I.; Otvos, L.^{Jr}; Baron, P.; Villalba, M.; Ferrari, D.; Rossi, F. Activation of microglial cells by beta-amyloid protein and interferon-gamma. *Nature* **1995**, *374*, 647–650.
- ²² Pachter, J.S. Inflammatory mechanisms in Alzheimer disease: the role of beta-amyloid/glial interactions. *Mol. Psychiatry* **1997**, *2*, 91–95.
- ²³ Alexander, G.E.; Chen, K.; Pietrini, P.; Rapoport, S.I.; Reiman, E.M. Longitudinal PET evaluation of cerebral metabolic decline in dementia: a potential outcome measure in Alzheimer's disease treatment studies. *Am. J. Psychiatry* **2002**, *159*, 738–745.
- ²⁴ Kasa, P.; Rakonczay, Z.; Gulya, K. The cholinergic system in Alzheimer's disease. *Prog. Neurobiol* **1997**, *52*, 511–535.
- ²⁵ Sarter, M. and Bruno, J.P. Trans-synaptic stimulation of cortical acetylcholine and enhancement of attentional

- functions: a rational approach for the development of cognition enhancers. *Behav. Brain Res.* **1997**, 83, 7–14.
- ²⁶ Francis, P.T.; Palmer, A.M.; Snape, M.; Wilcock, G.K. The cholinergic hypothesis of Alzheimer's disease: a review of progress. *J. Neurol. Neurosurg. Psychiatry* **1999**, 66, 137–147.
- ²⁷ Bartus, R.T.; *Recent Advances in Gerontology* (H. Orimo, Ed.) **1978**, 225-228.
- ²⁸ Bartus, R.T.; Dean, R.L.; Flicker, C.; *Psychopharmacology: A third generation of Progress* (E. Usdin, Ed.) **1987**, 219-232.
- ²⁹ Bartus, R.T. Physostigmine and recent memory: effects in young and aged nonhuman primates. *Science* **1979**; *206*, 1087-9.
- ³⁰ Bejar, C.; Wang, R.H.; Weinstock, M. Effect of rivastigmine on scopolamine-induced memory impairment in rats. *Eur. J. Pharmacol.* **1999**, 383, 231–240.
- ³¹ Bowen, D.; Smith, C.; White, P.; Davison, A. Neurotransmitter-related enzymes and indices of hypoxia in senile dementia and other abiotrophies. *Brain* **1976**, 99, 459-469.
- ³² Davies, P.; Maloney, A.J.F. Selective loss of central cholinergic neurons in Alzheimer's disease. *Lancet* **1976**, 1403.
- ³³ Perry, E.K.; Perry, R.H.; Blessed, G.; Tomlinson, B.E. Dietary lecithin supplements in dementia of Alzheimer type. *Lancet* **1977**, 309, 189.
- ³⁴ Nordberg, A. PET studies and cholinergic therapy in Alzheimer's disease. *Rev. Neurol. (Paris)* **1999**, 155 (Suppl 4), S53–S63.
- ³⁵ Nagai, T.; McGeer, P.L.; Peng, J.H.; McGeer, E.G.; Dolman, C.E. Choline acetyltransferase immunohistochemistry in brains of Alzheimer's disease patients and controls. *Neurosci. Lett.* **1983**, 36, 195–199.
- ³⁶ Bubber, P.; Haroutunian, V.; Fisch, G.; Blass, J.P.; Gibson, G.E. Mitochondrial abnormalities in Alzheimer brain: mechanistic implications. *Ann. Neurol.* **2005**, 57, 695–703.
- ³⁷ Gibson, G.E.; Blass, J.P.; Jenden, D.J. Measurement of acetylcholine turnover with glucose used as precursor: evidence for compartmentation of glucose metabolism in brain. *J. Neurochem.* **1978**, 30, 71–76.
- ³⁸ Holmquist, L.; Stuchbury, G.; Berbaum, K.; Muscat, S.; Young, S.; Hager, K.; Engel, J.; Münch, G. *Pharmacol. Ther.* **2007**, 113, 154–164 155.
- ³⁹ Moghul, S. and Wilkinson, D. Use of acetylcholinesterase inhibitors in Alzheimer's disease. *Expert Rev. Neurotherapeutics* **2001**, 1, 61–69.
- ⁴⁰ Benzi, G. and Moretti, A. Is there a rationale for the use of acetylcholinesterase inhibitors in the therapy of Alzheimer's disease? *Eur. J. Pharmacol.* **1998**, 346, 1–13.
- ⁴¹ Raskind, M.A.; Peskind, E.R.; Wessel, T.; Yuan, W. Galantamine in AD: a 6-month randomized, placebo-controlled trial with a 6-month extension. The Galantamine USA-1 Study Group. *Neurology*, **2000**, 54, 2261-2268.
- ⁴² Giacobini, E. Cholinesterase inhibitors stabilize Alzheimer's disease. *Ann. NY Acad. Sci.* **2000**, 920, 321-327.
- ⁴³ Bolognesi, M.L.; Minarini, A.; Rosini, M.; Tumiatti, V.; Melchiorre, C. From dual binding site acetylcholinesterase inhibitors to multi-target-directed ligands (MTDLs): a step forward in the treatment of Alzheimer's disease. *Mini Rev. Med. Chem.* **2008**, 8, 960-967.
- ⁴⁴ Klein, J. Phenserine. *Expert Opin. Invest. Drugs* **2007**, 16, 1087-1097.
- ⁴⁵ Zhang, H.Y.; Yan, H.; Tang, X.C. Non-cholinergic effects of huperzine A: beyond inhibition of acetylcholinesterase. *Cell. Mol. Neurobiol.* **2008**, 28, 173-183.
- ⁴⁶ Doody, R.S.; Gavrilova, S.; Sano, M.; Thomas, R.; Aisen, P.; Bachurin, S.; Seely, L.; Hung, D. Result of one-year randomized, placebo-controlled trial of dimebon for the treatment of mild to moderate Alzheimer's disease. *Alzheimer Dement.* **2007**, 3, 199-200.
- ⁴⁷ Wess, J. Muscarinic acetylcholine receptor knockout mice: novel phenotypes and clinical implications. *Annu. Rev. Pharmacol. Toxicol.* **2004**, 44, 423-450.
- ⁴⁸ Caccamo, A.; Oddo, S.; Billings, L.M.; Green, K.N.; Martinez-Coria, H.; Fisher, A.; LaFerla, F.M. M₁ receptors play a central role in modulating AD-like pathology in transgenic mice. *Neuron* **2006**, 49, 671–682.
- ⁴⁹ Clader, J.W.; Billard, W.; Binch, H.^{3rd}; Chen, L.Y.; Crosby, G.^{Jr}; Duffy, R.A.; Ford, J.; Kozlowski, J.A.; Lachowicz, J.E.; Li, S.; Liu, C.; McCombie, S.W.; Vice, S.; Zhou, G.; Greenlee, W.J. Muscarinic M2 antagonists: anthranilamide derivatives with exceptional selectivity and in vivo activity. *Bioorg. Med. Chem.* **2004**, 12, 319-26.
- ⁵⁰ Fratiglioni, L.; Wang, H.X. Smoking and Parkinson's and Alzheimer's disease: review of the epidemiological studies. *Behavioural. Brain Res.* **2000**, 113, 117-120.
- ⁵¹ Buccafusco, J.J.; Letchworth, S.R.; Bencherif, M.; Lippiello, P.M. Long-lasting cognitive improvement with nicotinic receptor agonists: mechanisms of pharmacokinetic-pharmacodynamic discordance. *Trends Pharmacol. Sci.* **2005**, 26, 352-360.
- ⁵² Dunbar, G.C.; Inglis, F.; Kuchibhatla, R.; Sharma, T.; Tomlinson, M.; Wamsley, J. Effect of ispronicline, a neuronal nicotinic acetylcholine receptor partial agonist, in subjects with age associated memory impairment

(AAMI) *J. Psychopharmacol.* **2007**, *21*, 171-8.

⁵³ Mitchell, E.S.; Neumaier, J.F. 5-HT₆ receptors: a novel target for cognitive enhancement. *Pharmacol. Ther.* **2005**, *108*, 320-33.

⁵⁴ Bowen, D.M.; Benton, J.S.; Spillane, J.A. Choline acetyltransferase activity and histopathology of frontal neocortex from biopsies of demented patients. *J. Neurol. Sci.* **1982**, *57*, 191-202.

⁵⁵ Inestrosa, N.C.; Alvarez, A.; Perez, C.A.; Moreno, R.D.; Vicente, M.; Linker, C.; Casanueva, O.I.; Soto, C.; Garrido, J. *Neuron* **1996**, *16*, 881-891.

⁵⁶ Silman, I.; Sussman, J.L. Acetylcholinesterase: "classical" and "nonclassical" functions and pharmacology. *Curr. Opin. Pharmacol.* **2005**, *5*, 293-302.

⁵⁷ Holzgrabe, U.; Kapkova, P.; Alptuzun, V.; Scheiber, J.; Kugelmann, E. Targeting acetylcholinesterase to treat neurodegeneration. *Expert Opin. Ther. Targets* **2007**, *11*, 161-179.

⁵⁸ Recanatini, M.; Valenti, P. Acetylcholinesterase inhibitors as a starting point towards improved Alzheimer's disease therapeutics. *Curr. Pharm. Des.* **2004**, *10*, 3157-3166.

⁵⁹ Castro, A.; Martinez, A. Targeting beta-amyloid pathogenesis through acetylcholinesterase inhibitors. *Curr. Pharm. Des.* **2006**, *12*, 4377-4387.

⁶⁰ Alvarez, A.; Bronfman, F.; Perez, C.A.; Vicente, M.; Garrido, J.; Inestrosa, N.C. Acetylcholinesterase, a senile plaque component, affects the fibrillogenesis of amyloid-beta-peptides. *Neurosci. Lett.* **1995**, *201*, 49-52.

⁶¹ Hardy, J.; Allsop, D. Amyloid deposition as the central event in the aetiology of Alzheimer's disease. *Trends Pharmacol. Sci.* **1991**, *12*, 383-388.

⁶² Hardy, J.A.; Higgins, G.A. Alzheimer's disease: the amyloid cascade hypothesis. *Science* **1992**, *256*, 184-185.

⁶³ Citron, M. Strategies for disease modification in Alzheimer's disease. *Nat. Rev. Neurosci.* **2004**, *5*, 677-85.

⁶⁴ Tanzi, R.E. and Bertram, L. New frontiers in Alzheimer's disease genetics. *Neuron* **2001**, *32*, 181-184.

⁶⁵ Younkin, S.G. The role of Abeta 42 in Alzheimer's disease. *J. Physiol. (Paris)*, **1998**, *92*, 289-292.

⁶⁶ Selkoe, D.J. Translating cell biology into therapeutic advances in Alzheimer's disease. *Nature* **1999**, *399*, A23-A31.

⁶⁷ Citron M. Beta-secretase inhibition for the treatment of Alzheimer's disease-promise and challenge. *Trends Pharmacol. Sci.* **2004**, *25*, 92-97.

⁶⁸ Vassar, R.; Bennett, B.D.; Babu-Khan, S.; Kahn, S.; Mendiaz, E.A.; Denis, P.; Teplow, D.B.; Ross, S.; Amarante, P.; Loeloff, R.; Luo, Y.; Fisher, S.; Fuller, J.; Edenson, S.; Lile, J.; Jarosinski, M.A.; Biere, A.L.; Curran, E.; Burgess, T.; Louis, J.C.; Collins, F.; Treanor, J.; Rogers, G.; Citron, M. *Science*. **1999**, *286*, 735-741.

⁶⁹ Tang, B.L.; Liou, Y.C. Novel modulators of amyloid-beta precursor protein processing. *J. Neurochem.* **2007**, *100*, 314-323.

⁷⁰ Lustbader, J.W.; Cirilli, M.; Lin, C.; Xu, H.W.; Takuma, K.; Wang, N.; Caspersen, C.; Chen, X.; Pollak, S.; Chaney, M.; Trinchese, F.; Liu, S.; Gunn-Moore, F.; Lue, L. F.; Walker, D.G.; Kuppusamy, P.; Zewier, Z.L.; Arancio, O.; Stern, D.; Yan, S.S.; Wu, H. ABAD directly links Abeta to mitochondrial toxicity in Alzheimer's disease. *Science* **2004**, *304*, 448-452.

⁷¹ Xie, L.; Helmerhorst, E.; Taddei, K.; Plewright, B.; Van Bronswijk, W.; Martins, R. Alzheimer's beta-amyloid peptides compete for insulin binding to the insulin receptor. *J. Neurosci.* **2002**, *22*, RC221.

⁷² Kagan, B.L.; Hirakura, Y.; Azimov, R.; Azimova, R.; Lin, M.C. The channel hypothesis of Alzheimer's disease: current status. *Peptides* **2002**, *23*, 1311-1315.

⁷³ Tamagno, E.; Parola, M.; Guglielmotto, M.; Santoro, G.; Bardini, P.; Marra, L.; Tabaton, M.; Danni, O. Multiple signaling events in amyloid beta-induced, oxidative stress-dependent neuronal apoptosis. *Free Radical. Biol. Med.* **2003**, *35*, 45-58.

⁷⁴ Bamberger, M.E.; Landreth, G.E. Microglial interaction with beta-amyloid: implications for the pathogenesis of Alzheimer's disease. *Microsc. Res. Tech.* **2001**, *54*, 59-70.

⁷⁵ Reddy, P.H.; Beal, M.F. Amyloid beta, mitochondrial dysfunction and synaptic damage: implications for cognitive decline in aging and Alzheimer's disease. *Trends Mol. Med.* **2008**, *14*, 45-53.

⁷⁶ Lin, M.T.; Beal, M.F. Alzheimer's APP mangles mitochondria. *Nat. Med.* **2006**, *12*, 1241-1243.

⁷⁷ Barten, D.M.; Albright, C.F. Therapeutic strategies for Alzheimer's disease. *Mol. Neurobiol.* **2008**, *37*, 171-186.

⁷⁸ Fambrough, D.; Pan, D.; Rubin, G.M.; Goodman, C.S. The cell surface metalloprotease/disintegrin Kuzbanian is required for axonal extension in *Drosophila*. *Proc. Natl. Acad. Sci. USA* **1996**, *93*, 13233-8.

⁷⁹ Rooke, J.; Pan, D.; Xu, T.; Rubin, G.M. KUZ, a conserved metalloprotease-disintegrin protein with two roles in *Drosophila* neurogenesis. *Science* **1996**, *273*, 1227-1231.

⁸⁰ Postina, R. A closer look at alpha-secretase. *Curr. Alzheimer Res.* **2008**, *5*, 179-86.

⁸¹ Bandyopadhyay, S.; Goldstein, L.E.; Lahiri, D.K.; Rogers, J.T. Role of the APP non-amyloidogenic signalling pathway and targeting alpha-secretase as an alternative drug target for treatment of Alzheimer's disease. *Curr. Med.*

Chem. **2007**, *14*, 2848-64.

- ⁸² Vassar, R. Beta-secretase (BACE) as a drug target for Alzheimer's disease. *Adv. Drug Deliv. Rev.* **2002**, *54*, 1589–1602.
- ⁸³ Luo, Y.; Bolon, B.; Kahn, S.; Bennet, B.D.; Babu-Khan, S.; Denis, P.; Fan, W.; Kha, H.; Zhang, J.; Gong, Y.; Martin, L.; Louis, J.C.; Yan, Q.; Richards, W.G.; Citron, M.; Vassar, R. *Nat. Neurosci.* **2001**, *3*, 231-232.
- ⁸⁴ John, V.; Beck, J.P.; Bienkowski, M.J.; Sinha, S.; Heinrikson, R.L. Human beta-secretase (BACE) and BACE inhibitors. *J. Med. Chem.* **2003**, *46*, 4625-30.
- ⁸⁵ Hong, L.; Koelsch, G.; Lin, X.; Wu, S.; Terzyan, S.; Ghosh, A.K.; Zhang, X.C.; Tang, J. Structure of protease domain of memapsin 2 (beta-secretase) complexed with inhibitor. *Science* **2000**, *290*, 150-153.
- ⁸⁶ Imbimbo, B.P. Therapeutic potential of gamma-secretase inhibitors and modulators. *Curr. Top. Med. Chem.* **2008**, *8*, 54-61.
- ⁸⁷ Wong, G.T.; Manfra, D.; Poulet, F.M.; Zhang, Q.; Josien, H.; Bara, T.; Engstrom, L.; Pinzon-Ortiz, M.; Fine, J.S.; Lee, H.J.J.; Zhang, L.; Higgins, G.A.; Parker, E.M. Chronic treatment with the gamma-secretase inhibitor LY-411,575 inhibits beta-amyloid peptide production and alters lymphopoiesis and intestinal cell differentiation. *J. Biol. Chem.* **2004**, *279*, 12876-12882.
- ⁸⁸ Wolfe, M.S. Gamma-Secretase modulators *Curr. Alzheimer Res.* **2007**, *4*, 571-3.
- ⁸⁹ Wolfe, M.S. Inhibition and modulation of gamma-secretase for Alzheimer's disease. *Neurotherapeutics*, **2008**, *5*, 391-398.
- ⁹⁰ Weggen, S.; Eriksen, J.L.; Das, P.; Sagi, S.A.; Wang, R.; Pietrzik, C.U.; Findlay, K.A.; Smith, T.E.; Murphy, M.P.; Bulter, T.; Kang, D.E.; Marquez-Sterling, N.; Golde, T.E.; Koo, H.E. *Nature* **2001**, *414*, 212-216.
- ⁹¹ Clarke, E.E.; Churcher, I.; Ellis, S.; Wrigley, J.D.; Lewis, H.D.; Harrison, T.; Shearman, M.S.; Behr, D. Intra- or intercomplex binding to the gamma-secretase enzyme. A model to differentiate inhibitor classes. *J. Biol. Chem.* **2006**, *281*, 31279–31289.
- ⁹² Czirr, E.; Weggen, S. Gamma-secretase modulation with Abeta42-lowering nonsteroidal anti-inflammatory drugs and derived compounds. *Neurodegener. Dis.* **2006**, *3*, 298–304.
- ⁹³ Geerts, H. Drug evaluation: (R)-flurbiprofen - an enantiomer of flurbiprofen for the treatment of Alzheimer's disease. *IDrugs* **2007**, *10*, 121–133.
- ⁹⁴ Gervais, F.; Paquette, J.; Morissette, C.; Krzykowski, P.; Yu, M.; Azzi, M.; Lacombe, D.; Kong, X.; Aman, A.; Laurin, J.; Szarek, W.A.; Tremblay, P. Targeting soluble Abeta peptide with Tramiprosate for the treatment of brain amyloidosis. *Neurobiol. Aging* **2007**, *28*, 537–547.
- ⁹⁵ Aisen, P.S.; Saumier, D.; Briand, R.; Laurin, J.; Gervais, F.; Tremblay, P.; Garceau, D. A Phase II study targeting amyloid-beta with 3APS in mild-to-moderate Alzheimer disease. *Neurology* **2006**, *67*:1757–1763.
- ⁹⁶ Bush, A.I. and Tanzi, R.E. The galvanization of beta-amyloid in Alzheimer's disease. *Proc. Natl. Acad. Sci. USA* **2002**, *99*, 7317–7319.
- ⁹⁷ Kwon, M.O.; Herrling, P. List of drugs in development for neurodegenerative diseases. Update June 2006. *Neurodegener. Dis.* **2006**, *3*, 148–186.
- ⁹⁸ McLaurin, J.; Golomb, R.; Jurewicz, A.; Antel, J.P.; Fraser, P.E. Inositol stereoisomers stabilize an oligomeric aggregate of Alzheimer amyloid beta peptide and inhibit Abeta-induced toxicity. *J. Biol. Chem.* **2000**, *275*, 18495–18502.
- ⁹⁹ McLaurin, J.; Kierstead, M.E.; Brown, M.E.; Hawkes, C.A.; Lambermon, M.H.; Phinney, A.L.; Darabie, A.A.; Cousins, J.E.; French, J.E.; Lan, M.F.; Chen, F.; Wong, S.S.; Mount, H.T.; Fraser, P.E.; Westaway, D.; StGeorge-Hyslop, P. Cyclohexanehexol inhibitors of Abeta aggregation prevent and reverse Alzheimer phenotype in a mouse model. *Nat. Med.* **2006**, *12*, 801–808.
- ¹⁰⁰ Martins, I.C.; Kuperstein, I.; Wilkinson, H.; Maes, E.; Vanbrabant, M.; Jonckheere, W.; Van Gelder, P.; Hartmann, D.; D'Hooge, R.; DeStrooper, B.; Schymkowitz, J.; Rousseau, F. Lipids revert inert Abeta amyloid fibrils to neurotoxic protofibrils that affect learning in mice. *EMBO J.* **2008**, *27*, 224–233.
- ¹⁰¹ Tanzi, R.E.; Moir, R.D.; Wagner, S.L. Clearance of Alzheimer's Abeta peptide: the many roads to perdition. *Neuron* **2004**, *43*, 605–608.
- ¹⁰² Pangalos, M.N.; Jacobsen, S.J.; Reinhart, P.H. Disease modifying strategies for the treatment of Alzheimer's disease targeted at modulating levels of the beta-amyloid peptide. *Biochem. Soc. Trans.* **2005**, *33*, 553–558.
- ¹⁰³ Saito, T.; Iwata, N.; Tsubuki, S.; Takaki, Y.; Takano, J.; Huang, S.M.; Suemoto, T.; Higuchi, M.; Saido, T.C. Somatostatin regulates brain amyloid beta peptide Abeta42 through modulation of proteolytic degradation. *Nat. Med.* **2005**, *11*, 434–439.
- ¹⁰⁴ Shenck, D.; Barbour, R.; Dunn, W.; Gordon, G.; Grajeda, H.; Guido, T.; Hu, K.; Huang, J.; Johnson-Wood, K.; Khan, K.; Kholodenko, D.; Lee, M.; Liao, Z.; Lieberburg, I.; Motter, R.; Mutter, L.; Soriano, F.; Shopp, G.; Vasquez, N.; Vandevent, C.; Walker, S.; Wogulis, M.; Yednock, T.; Games, D.; Seubert, P. Immunization with amyloid-beta

attenuates Alzheimer-disease-like pathology in the PDAPP mouse. *Nature* **1999**, 400, 173-177.

¹⁰⁵ Wilcock, D.M.; Colton, C.A. Anti-Abeta immunotherapy in Alzheimer's disease; relevance of transgenic mouse studies to clinical trials *J. Alzheimer's Dis.* 2008, 15, 555-569.

¹⁰⁶ Solomon, B. Immunological approaches for amyloid-beta clearance toward treatment for Alzheimer's disease. *Rejuvenation Res.* **2008**, 11, 349-57.

¹⁰⁷ Li, B.; Chohan, M.O.; Grundke-Iqbal, I.; Iqbal, K. Disruption of microtubule network by Alzheimer's abnormally hyperphosphorylated tau. *Acta Neuropathol.* **2007**, 113, 501-511.

¹⁰⁸ Lace, G.L.; Wharton, S.B.; Ince, P.G. A brief history of tau: the evolving view of microtubule-associated protein tau in neurodegenerative disease. *Clin. Neuropathol.* **2007**, 26, 43-58.

¹⁰⁹ Wang, J.Z.; Grundke-Iqbal, I.; Iqbal, K. Kinases and phosphatases and tau sites involved in Alzheimer neurofibrillary degeneration. *Eur. J. Neurosci.* **2007**, 25, 59-6.

¹¹⁰ Hooper, C.; Markevich, V.; Plattner, F.; Killick, R.; Schofield, E.; Engel, T.; Hernandez, F.; Anderton, B.; Rosenblum, K.; Bliss, T.; Cooke, S.F.; Avila, J.; Lucas, J.J.; Giese, K.P.; Stephenson, J.; Lovestone, S. Glycogen synthase kinase-3 inhibition is integral to long-term potentiation. *Eur. J. Neurosci.* **2007**, 25, 81-86.

¹¹¹ Peineau, S.; Taghibiglou, C.; Bradley, C.; Wong, T.P.; Liu, L.; Lu, J.; Lo, E.; Wu, D.; Saule, E.; Bouschet, T.; Matthews, P.; Isaac, J.T.; Bortolotto, Z.A.; Wang, Y.T.; Collingridge, G.L. LTP inhibits LTD in the hippocampus via regulation of GSK3beta. *Neuron* **2007**, 53, 703-717.

¹¹² Churcher, I. Tau therapeutic strategies for the treatment of Alzheimer's disease. *Curr. Top. Med. Chem.* **2006**, 6, 579-595.

¹¹³ Bhat, R.V.; Budd Haerberlein, S.L.; Avila, J. Glycogen synthase kinase 3: a drug target for CNS therapies. *J. Neurochem.* **2004**, 89, 1313-1317.

¹¹⁴ Meijer, L.; Flajolet, M.; Greengard, P.; Pharmacological inhibitors of glycogen synthase kinase 3. *Trends Pharmacol. Sci.* **2004**, 25, 471-480.

¹¹⁵ Dickey, C.A.; Eriksen, J.; Kamal, A.; Burrows, F.; Kasibhatla, S.; Eckman, C.B.; Hutton, M.; Petrucelli, L.; Development of a high throughput drug screening assay for the detection of changes in tau levels-proof of concept with HSP90 inhibitors. *Curr. Alzheimer Res.* **2005**, 2, 231-238.

¹¹⁶ Dickey, C.A.; Kamal, A.; Lundgren, K.; Klosak, N.; Bailey, R.M.; Dunmore, J.; Ash, P.; Shoraka, S.; Zlatkovic, J.; Eckman, C.B.; Patterson, C. Dickson, D.W.; Nahman, N.S.Jr; Hutton, M.; Burrows, F.; Petrucelli, L. The high-affinity HSP90-CHIP complex recognizes and selectively degrades phosphorylated tau client proteins. *J. Clin. Invest.* **2007**, 117, 648-658.

¹¹⁷ Luo, W.; Dou, F.; Rodina, A.; Chip, S.; Kim, J.; Zhao, Q.; Moulick, K.; Aguirre, J.; Wu, N.; Greengard, P.; Chiosis, G. Roles of heatshock protein 90 in maintaining and facilitating the neurodegenerative phenotype in tauopathies. *Proc. Natl. Acad. Sci. USA* **2007**, 104, 9511-9516.

¹¹⁸ Dunmore, J.; Ash, P.; Shoraka, S.; Zlatkovic, J.; Eckman, C.B.; Patterson, C.; Dickson, D.W.; Nahman, N.S.Jr.; Hutton, M.; Burrows, F.; Petrucelli, L. The high-affinity HSP90-CHIP complex recognizes and selectively degrades phosphorylated tau client proteins. *J. Clin. Invest.* **2007**, 117, 648-658.

¹¹⁹ Furukawa, K.; Mattson, M.P.; Taxol stabilizes $[Ca^{2+}]_i$ and protects hippocampal neurons against excitotoxicity. *Brain Res.* **1995**, 689, 141-146.

¹²⁰ Butler, D.; Bendiske, J.; Michaelis, M.L.; Karanian, D.A.; Bahr, B.A. Microtubule-stabilizing agent prevents protein accumulation-induced loss of synaptic markers. *Eur. J. Pharmacol.* **2007**, 562, 20-27.

¹²¹ Michaelis, M.L.; Ansar, S.; Chen, Y.; Reiff, E.R.; Seyb, K.I.; Himes, R.H.; Audus, K.L.; Georg, G.I. {beta}-Amyloid-induced neurodegeneration and protection by structurally diverse microtubule-stabilizing agents. *J. Pharmacol. Exp. Ther.* **2005**, 312, 659-668.

¹²² Zhang, B.; Maiti, A.; Shively, S.; Lakhani, F.; McDonald-Jones, G.; Bruce, J.; Lee, E.B.; Xie, S.X.; Joyce, S.; Li, C.; Toleikis, P.M.; Lee, V.M.; Trojanowski, J.Q. Microtubule-binding drugs offset tau sequestration by stabilizing microtubules and reversing fast axonal transport deficits in a tauopathy model. *Proc. Natl. Acad. Sci. USA* **2005**, 102, 227-231.

¹²³ Michaelis, M.L.; Seyb, K.I.; Ansar, S. Cytoskeletal integrity as a drug target. *Curr. Alzheimer Res.* **2005**, 2, 227-9.

¹²⁴ Liu, Q.; Xie, F.; Rolston, R.; Moreira, P.I.; Nunomura, A.; Zhu, X.; Smith, M. A.; Perry, G. Prevention and treatment of Alzheimer disease and aging: antioxidants. *Mini-Rev. Med. Chem.* **2007**, 7, 171-180.

¹²⁵ Brewer, G.J. Iron and copper toxicity in diseases of aging, particularly atherosclerosis and Alzheimer's disease. *Exp. Biol. Med. (Maywood)* **2007**, 232, 323-335.

¹²⁶ Mattson, M.P.; Chan, S.L.; Duan, W. Modification of brain aging and neurodegenerative disorders by genes, diet, and behavior. *Physiol. Rev.* **2002**, 82, 637-672.

¹²⁷ Floyd, R.A. and Hensley, K. Oxidative stress in brain aging. Implications for therapeutics of neurodegenerative

diseases. *Neurobiol. Aging*. **2002**, *23*, 795–807.

¹²⁸ Smith, C.D.; Carney, J.M.; Starke-Reed, P.E.; Oliver, C.N.; Stadman, E.R.; Floyd R.A., Markesbery, W.R. Excess brain protein oxidation and enzyme dysfunction in normal aging and in Alzheimer disease. *Proc. Natl. Acad. Sci. USA*. **1991**, *88*, 10540–10543.

¹²⁹ Nunomura, A.; Chiba, S.; Lippa, C.F.; Cras, P.; Kalaria, R.N.; Takeda, A., Honda, K.; Smith, M.A.; Perry, G. Neuronal RNA oxidation is a prominent feature of familial Alzheimer's disease. *Neurobiol. Dis.* **2004**, *17*, 108–113.

¹³⁰ Ando, Y.; Brannstrom, T.; Uchida, K.; Nyhlin, N.; Näsman, B.; Suhr, O.; Yamashita, T.; Olsson, T.; El Salhy, M.; Uchino, M. Histochemical detection of 4-hydroxynonenal protein in Alzheimer amyloid. *J. Neurol. Sci.* **1998**, *156*, 172–176.

¹³¹ Kumar, M.J.; Nicholls, D.G.; Andersen, J.K. Oxidative alpha-ketoglutarate dehydrogenase inhibition via subtle elevations in monoamine oxidase B levels results in loss of spare respiratory capacity: implications for Parkinson's disease. *J. Biol. Chem.* **2003**, *278*, 46432–46439.

¹³² Mattson, M.P. Pathways towards and away from Alzheimer's disease. *Nature* **2004**, *430*, 631–639.

¹³³ Sullivan, P.G.; Brown, M.R. Mitochondrial aging and dysfunction in Alzheimer's disease. *Prog. Neuro-psychopharmacol. Biol. Psychiatry* **2005**, *29*, 407–410.

¹³⁴ Roses, A.D.; Saunders, A.M. Perspective on a pathogenesis and treatment of Alzheimer's disease. *Alzheimers Dement.* **2006**, *2*, 59–70.

¹³⁵ Strum, J.C.; Shehee, R.; Virley, D.; Richardson, J.; Mattie, M.; Selley, P.; Ghosh, S.; Nock, C.; Saunders, A.; Roses, A. Rosiglitazone induces mitochondrial biogenesis in mouse brain. *J. Alzheimers Dis.* **2007**, *11*, 45–51.

¹³⁶ Gaggelli, E.; Kozlowski, H.; Valensin, D.; Valensin, G. Copper homeostasis and neurodegenerative disorders (Alzheimer's, prion, and Parkinson's diseases and amyotrophic lateral sclerosis). *Chem. Rev.* **2006**, *106*, 1995–2044.

¹³⁷ Mandel, S.; Amit, T.; Bar-Am, O.; Youdim, M.B.; Iron dysregulation in Alzheimer's disease: multimodal brain permeable iron chelating drugs, possessing neuroprotective-neurorescue and amyloid precursor protein-processing regulatory activities as therapeutic agents. *Prog. Neurobiol.* **2007**, *82*, 348–360.

¹³⁸ Kanowski, S.; Hoerr, R. Ginkgo biloba extract EGb 761 in dementia: intent-to-treat analyses of a 24-week, multi-center, double-blind, placebo-controlled, randomized trial. *Pharmacopsychiatry* **2003**, *36*, 297–303.

¹³⁹ Ames, D.; Ritchie, C. Antioxidants and Alzheimer's disease: time to stop feeding vitamin E to dementia patients? *Int. Psychogeriatr.* **2007**, *19*, 1–8.

¹⁴⁰ Freund-Levi, Y.; Basun, H.; Cederholm, T.; Faxen-Irving, G.; Garlind, A.; Grut, M.; Vedin, I.; Palmblad, J.; Wahlund, L.O.; Eriksdotter-Jonhagen, M. Omega-3 supplementation in mild to moderate Alzheimer's disease: effects on neuropsychiatric symptoms. *Int. J. Geriatr. Psychiatry.* **2008**, *23*, 161–169.

¹⁴¹ www.clinicaltrials.com

¹⁴² El Khoury, J.; Toft, M.; Hickman, S. E.; Means, T. K.; Terada, K.; Geula, C.; Luster, A. D. Ccr2 deficiency impairs microglial accumulation and accelerates progression of Alzheimer-like disease. *Nat. Med.* **2007**, *13*, 432–438.

¹⁴³ Ringheim, G.E.; Szczepanik, A.M. Brain inflammation, cholesterol, and glutamate as interconnected participants in the pathology of Alzheimer's disease. *Curr. Pharm. Des.* **2006**, *12*, 719–738.

¹⁴⁴ Sparks, D.L.; Sabbagh, M.; Connor, D.; Soares, H.; Lopez, J.; Stankovic, G.; Johnson-Traver, S.; Ziolkowski, C.; Browne, P. Statin therapy in Alzheimer's disease. *Acta Neurol. Scand.* **2006**, *185*, 78–86.

¹⁴⁵ Marchalant, Y.; Cerbai, F.; Brothers, H.M.; Wenk, G.L. Cannabinoid receptor stimulation is anti-inflammatory and improves memory in old rats. *Neurobiol. Aging*, **2008**, *29*, 1894–1901.

¹⁴⁶ Wyss-Coray, T. Inflammation in Alzheimer disease: driving force, bystander or beneficial response? *Nat. Med.* **2006**, *12*, 1005–1015.

¹⁴⁷ Morgan, D.; Gordon, M.N.; Tan, J.; Wilcock, D.; Rojiani, A.M. Dynamic complexity of the microglial activation response in transgenic models of amyloid deposition: implications for Alzheimer therapeutics. *J. Neuropathol. Exp. Neurol.* **2005**, *64*, 743–753.

¹⁴⁸ Yoshiyama, Y.; Higuchi, M.; Zhang, B.; Huang, S.M.; Iwata, N.; Saido, T.C.; Maeda, J.; Suhara, T.; Trojanowski, J.Q.; Lee, V.M. Synapse loss and microglial activation precede tangles in a P301S tauopathy mouse model. *Neuron* **2007**, *53*, 337–351.

¹⁴⁹ Piehl, F. Inflammation and neurodegeneration. *Future Neurol.* **2006**, *1*, 95–105.

¹⁵⁰ Mullan, M.; Houlden, H.; Windelspecht, M.; Fidani, L.; Lombardi, C.; Diaz, P.; Rossor, M.; Crook, R.; Hardy, J.; Duff, K.; Crawford, F. A locus for familial early-onset Alzheimer's disease on the long arm of chromosome 14, proximal to the alpha 1-antichymotrypsin gene. *Nat. Genet.* **1992**, *2*, 340–342.

¹⁵¹ Haass, C.; Lemere, C.A.; Capell, A.; Citron, M.; Seubert, P.; Schenk, D.; Lannfelt, L. and Selkoe, D. J. The Swedish mutation causes early-onset Alzheimer's disease by beta-secretase cleavage within the secretory pathway. *Nat. Med.* **1995**, *1*, 1291–1296.

- ¹⁵² Sinha, S.; Anderson, J.P.; Barbour, R.; Basi, G.S.; Caccavello, R.; Davis, D.; Doan, M.; Dovey, H.F.; Frigon, N.; Hong, J.; Jacobson-Croak, K.; Jewett, N.; Keim, P.; Knops, J.; Lieberburg, I.; Power, M.; Tan, H.; Tatsuno, G.; Tung, J.; Schenk, D.; Seubert, P.; Suomensari, S.M.; Wang, S.; Walker, D.; Zhao, J.; McConlogue, L.; John, V. Purification and cloning of amyloid precursor protein beta-secretase from human brain. *Nature* **1999**, *402*, 537-540.
- ¹⁵³ Yan, R.; Bienkowski, M.J.; Shuck, M.E.; Miao, H.; Tory, M.C.; Pauley, A.M.; Brashier, J.R.; Stratman, N.C.; Mathews, W.R.; Buhl, A.E.; Carter, D.B.; Tomasselli, A.G.; Parodi, L.A.; Heinrikson, R.L.; Gurney, M.E. Membrane anchored aspartyl protease with Alzheimer's disease beta-secretase activity. *Nature* **1999**, *402*, 533-537.
- ¹⁵⁴ Hussain, I.; Powell, D.; Howlett, D.R.; Tew, D.G.; Meek, T.D.; Chapman, C.; Gloger, I.S.; Murphy, K.E.; Southan, C.D.; Ryan, D.M.; Smith, T.S.; Simmons, D.L.; Walsh, F.S.; Dingwall, C.; Christie, G. Identification of a novel aspartic protease (Asp 2) as beta-secretase. *Mol. Cell. Neurosci.* **1999**, *14*, 419-427.
- ¹⁵⁵ Lin, X.; Koelsch, G.; Wu, S.; Downs, D.; Dashti, A.; Tang, J. Human aspartic protease memapsin 2 cleaves the beta-secretase site of beta-amyloid precursor protein. *Proc. Natl. Acad. Sci. USA* **2000**, *97*, 1456-1460.
- ¹⁵⁶ Saunders, A.J.; Kim, T.-W.; Tanzi, R.E.; Fan, W.; Bennett, B.D.; Babu-Kahn, S.; Luo, Y.; Louis, J.-C.; McCaleb, M.; Citron, M.; Vassar, R.; Richards, W.G. BACE Maps to Chromosome 11; and a BACE Homolog, BACE2, Reside in the Obligate Down Syndrome Region of Chromosome 21. *Science* **1999**, *286*, 1255a.
- ¹⁵⁷ Bennett, B.D.; Babu-Khan, S.; Loeloff, R.; Louis, J.C.; Curran, E.; Citron, M.; Vassar, R. Expression analysis of BACE2 in brain and peripheral tissues. *J. Biol. Chem.* **2000**, *275*, 20647-20651.
- ¹⁵⁸ Gruninger-Leitch, F.; Schlatter, D.; Kung, E.; Nelbock, P.; Dobeli, H. Substrate and inhibitor profile of BACE (beta-secretase) and comparison with other mammalian aspartic proteases. *J. Biol. Chem.* **2002**, *277*, 4687-4693.
- ¹⁵⁹ Haass, C.; Hung, A.Y.; Schlossmacher, M.G.; Oltersdorf, T.; Teplow, D.B.; Selkoe, D.J. Normal cellular processing of the beta-amyloid precursor protein results in the secretion of the amyloid beta peptide and related molecules. *Ann. N. Y. Acad. Sci.* **1993**, *695*, 109-116.
- ¹⁶⁰ Koo, E. H. and Squazzo, S. L. Evidence that production and release of amyloid beta-protein involves the endocytic pathway. *J. Biol. Chem.* **1994**, *269*, 17386-17389.
- ¹⁶¹ Roberds, S.L.; Anderson, J.; Basi, G.; Bienkowski, M.J.; Branstetter, D.G.; Chen, K.S.; Freedman, S.B.; Frigon, N. L.; Games, D.; Hu, K.; Johnson-Wood, K.; Kappenman, K.E.; Kawabe, T.T.; Kola, I.; Kuehn, R.; Lee, M.; Liu, W.; Motter, R.; Nichols, N. F.; Power, M.; Robertson, D.W.; Schenk, D.; Schoor, M.; Shopp, G.M.; Shuck, M.E.; Sinha, S.; Svensson, K.A.; Tatsuno, G.; Tintrup, H.; Wijsman, J.; Wright, S.; McConlogue, L. BACE knockout mice are healthy despite lacking the primary beta-secretase activity in brain: implications for Alzheimer's disease therapeutics. *Hum. Mol. Genet.* **2001**, *10*, 1317-1324.
- ¹⁶² Cai, H.; Wang, Y.; McCarthy, D.; Wen, H.; Borchelt, D.R.; Price, D.L.; Wong, P.C. BACE1 is the major beta-secretase for generation of Aβ peptides by neurons. *Nat. Neurosci.* **2001**, *4*, 233-234.
- ¹⁶³ Fischer, F.; Molinari, M.; Bodendorf, U.; Paganetti, P. The disulphide bonds in the catalytic domain of BACE are critical but not essential for amyloid precursor protein processing activity. *J. Neurochem.* **2002**, *80*, 1079-1088.
- ¹⁶⁴ Haniu, M.; Denis, P.; Young, Y.; Mendiaz, E.A.; Fuller, J.; Hui, J.O.; Bennett, B.D.; Kahn, S.; Ross, S.; Burgess, T.; Katta, V.; Rogers, G.; Vassar, R.; Citron, M. Characterization of Alzheimer's beta-secretase protein BACE. A pepsin family member with unusual properties. *J. Biol. Chem.* **2000**, *275*, 21099-21106.
- ¹⁶⁵ James, N.M.G. Catalytic pathway of aspartic peptidases. In: *Handbook of Proteolytic Enzymes* Ed. Eds., Elsevier, London. **2004**, 12-19.
- ¹⁶⁶ Shi, J.; Zhang, S.; Tang, M.; Liu, X.; Li, T.; Wang, Y.; Han, H.; Guo, Y.; Hao, Y.; Zheng, K.; Kong, X.; Su, Z.; Tong, Y.; Ma, C. The 1239G/C polymorphism in exon 5 of BACE1 gene may be associated with sporadic Alzheimer's disease in Chinese Hans. *Am. J. Med. Genet. B. Neuropsychiatr. Genet.* **2004**, *124*, 54 - 57.
- ¹⁶⁷ Capell, A.; Steiner, H.; Willem, M.; Kaiser, H.; Meyer, C.; Walter, J.; Lammich, S.; Multhaup, G.; Haass, C. Maturation and pro-peptide cleavage of beta-secretase. *J. Biol. Chem.* **2000**, *275*, 30849-54.
- ¹⁶⁸ Benjannet, S.; Elagoz, A.; Wickham, L.; Mamarbachi, M.; Munzer, J.S.; Basak, A.; Lazure, C.; Cromlish, J.A.; Sisodia, S.; Checler, F.; Chrétien, M.; Seidah, N.G. Post-translational processing of beta-secretase (beta-amyloid-converting enzyme) and its ectodomain shedding. The pro- and transmembrane/cytosolic domains affect its cellular activity and amyloid-beta production. *J. Biol. Chem.* **2001**, *276*, 10879-87.
- ¹⁶⁹ Charlwood, J.; Dingwall, C.; Matico, R.; Hussain, I.; Johanson, K.; Moore, S.; Powell, D.J.; Skehel, J.M.; Ratcliffe, S.; Clarke, B.; Trill, J.; Sweitzer, S.; Camilleri, P. Characterization of the glycosylation profiles of Alzheimer's beta -secretase protein Asp-2 expressed in a variety of cell lines. *J. Biol. Chem.* **2001**, *276*, 16739-48.
- ¹⁷⁰ Huse, J.T.; Pijak, D.S.; Leslie, G.J.; Lee, V.M.; Doms, R.W. Maturation and endosomal targeting of beta-site amyloid precursor protein-cleaving enzyme. The Alzheimer's disease beta-secretase. *J. Biol. Chem.* **2000**, *275*, 33729-37.
- ¹⁷¹ Stockley, J.H.; O'Neill, C. Understanding BACE1: essential protease for amyloid-beta production in Alzheimer's disease. *Cell Mol Life Sci.* **2008**, *65*, 3265-89.

- ¹⁷² Patel, S.; Vuillard, L.; Cleasby, A.; Murray, C.W.; Yon, J. Apo and inhibitor complex structures of BACE (betasecretase). *J. Mol. Biol.* **2004**, *343*, 407-416.
- ¹⁷³ Hong, L.; He, X.; Huang, X.; Chang, W.; Tang, J. Structural features of human memapsin 2 (beta-secretase) and their biological and pathological implications. *Acta. Biochim. Biophys. Sin. (Shanghai)* **2004**, *36*, 787-792.
- ¹⁷⁴ Hong, L. and Tang, J. Flap position of free memapsin 2 (beta-secretase), a model for flap opening in aspartic protease catalysis. *Biochemistry* **2004**, *43*, 4689-4695.
- ¹⁷⁵ Hong, L.; Turner, R.T.^{3rd}; Koelsch, G.; Shin, D.; Ghosh, A.K.; Tang, J. Crystal structure of memapsin 2 (betasecretase) in complex with an inhibitor OM00-3. *Biochemistry* **2002**, *41*, 10963-10967.
- ¹⁷⁶ Turner, R.T.^{3rd}; Hong, L.; Koelsch, G.; Ghosh, A.K.; Tang, J. Structural locations and functional roles of new subsites S5, S6, and S7 in memapsin 2 (beta-secretase). *Biochemistry* **2005**, *44*, 105-112.
- ¹⁷⁷ <http://www.rcsb.org>
- ¹⁷⁸ Ostermann, N.; Eder, J.; Eidhoff, U.; Zink, F.; Hassiepen, U.; Worpenberg, S.; Maibaum, J.; Simic, O.; Hommel, U.; Gerhartz, B. Crystal structure of human BACE2 in complex with a hydroxyethylamine transition-state inhibitor. *J. Mol. Biol.* **2006**, *355*, 249-261.
- ¹⁷⁹ Farzan, M.; Schnitzler, C.E.; Vasilieva, N.; Leung, D.; Choe, H. BACE2, a beta-secretase homolog, cleaves at the beta site and within the amyloid-beta region of the amyloid-beta precursor protein. *Proc. Natl. Acad. Sci. USA* **2000**, *97*, 9712-9717.
- ¹⁸⁰ Gorfe, A.A. and Caffisch, A. Functional plasticity in the substrate binding site of beta-secretase. *Structure* **2005**, *13*, 1487-1498.
- ¹⁸¹ Ghosh, A.K.; Kumaragurubaran, N.; Hong, L.; Koelsch, G.; Tang, J. Memapsin 2 (beta-secretase) inhibitors: drug development. *Curr. Alzheimer Res.* **2008**, *5*, 121-131.
- ¹⁸² Turner, R.T.^{3rd}; Loy, J.A.; Nguyen, C.; Devasamudram, T.; Ghosh, A.K.; Koelsch, G.; Tang, J. Specificity of memapsin 1 and its implications on the design of memapsin 2 (beta-secretase) inhibitor selectivity. *Biochemistry* **2002**, *41*, 8742-6.
- ¹⁸³ Lefranc-Jullien, S.; Lisowski, V.; Hernandez, J.F.; Martinez, J.; Checler, F. Design and characterization of a new cell-permeant inhibitor of the beta-secretase BACE1. *Br. J. Pharmacol.* **2005**, *145*, 228-235.
- ¹⁸⁴ Chang, W.P.; Koelsch, G.; Wong, S.; Downs, D.; Da, H.; Weerasena, V.; Gordon, B.; Devasamudram, T.; Bilcer, G.; Ghosh, A.K.; Tang, J. In vivo inhibition of Abeta production by memapsin 2 (beta-secretase) inhibitors. *J. Neurochem.* **2004**, *89*, 1409-1416.
- ¹⁸⁵ Rajendran, L.; Schneider, A.; Schlechtingen, G.; Weidlich, S.; Ries, J.; Braxmeier, T.; Schwiller, P.; Schulz, J.B.; Schroeder, C.; Simons, M.; Jennings, G.; Knolker, H.J.; Simons, K. Efficient inhibition of the Alzheimer's disease beta-secretase by membrane targeting. *Science* **2008**, *320*, 520-523.
- ¹⁸⁶ Durham, T.B.; Shepherd, T.A. Progress toward the discovery and development of efficacious BACE inhibitors. *Curr. Opin. Drug Discov. Devel.* **2006**, *9*, 776-91.
- ¹⁸⁷ Ghosh, A.K.; Bilcer, G.; Hong, L.; Koelsch, G.; Tang, J. Memapsin 2 (beta-secretase) inhibitor drug, between fantasy and reality. *Curr. Alzheimer Res.* **2007**, *4*, 418-22.
- ¹⁸⁸ John, V. Human beta-secretase (BACE) and BACE inhibitors: progress report. *Curr. Top. Med. Chem.* **2006**, *6*, 569-78.
- ¹⁸⁹ Thompson, L.A.; Bronson, J.J.; Zusi, F.C. Progress in the discovery of BACE inhibitors. *Curr. Pharm. Des.* **2005**, *11*, 3383-404.
- ¹⁹⁰ Eder, J.; Hommel, U.; Cumin, F.; Martoglio, B.; Gerhartz, B. Aspartic proteases in drug discovery. *Curr. Pharm. Des.* **2007**, *13*, 271-85.
- ¹⁹¹ Kunimoto, S.; Aoyagi, T.; Morishima, H.; Takeuchi, T.; Umezawa, H. Mechanism of inhibition of pepsin by pepstatin. *J. Antibiot. (Tokyo)* **1972**, *25*, 251-5.
- ¹⁹² Bridges, K.G.; Chopra, R.; Lin, L.; Svenson, K.; Tam, A.; Jin, G.; Cowling, R.; Lovering, F.; Akopian, T.N.; DiBlasio-Smith, E.; Annis-Freeman, B.; Marvell, T.H.; LaVallie, E.R.; Zollner, R.S.; Bard, J.; Somers, W.S.; Stahl, M.L.; Kriz, R.W. A novel approach to identifying beta-secretase inhibitors: bis-statine peptide mimetics discovered using structure and spot synthesis. *Peptides* **2006**, *7*, 1877-85.
- ¹⁹³ Schostarez, H.J.; Chrisciel, R.A. *PCT Int. Appl.* **2003**, WO03006021.
- ¹⁹⁴ Peters, S.; Fuchs, K.; Eickmeier, C.; Stransky, W.; Dorner-Ciossek, C.; Handschuh, S.; Nar, H.; Klinder, K.; Kostka, M. *PCT Int. Appl.* **2006**, WO06050862.
- ¹⁹⁵ Turner, R.T.^{3rd}; Koelsch, G.; Hong, L.; Castanheira, P.; Ermolieff, J.; Ghosh, A.K.; Tang, J. Subsite specificity of memapsin 2 (beta-secretase): implications for inhibitor design. *Biochemistry* **2001**, *40*, 10001-6.
- ¹⁹⁶ Hanessian, S.; Yun, H.; Hou, Y.; Yang, G.; Bayrakdarian, M.; Therrien, E.; Moitessier, N.; Roggo, S.; Veenstra, S.; Tintelnot-Blomley, M.; Rondeau, J.M.; Ostermeier, C.; Strauss, A.; Ramage, P.; Paganetti, P.; Neumann, U.; Betschart, C. Structure-based design, synthesis, and memapsin 2 (BACE) inhibitory activity of carbocyclic and

heterocyclic peptidomimetics. *J. Med. Chem.* **2005**, *48*, 5175-5190.

¹⁹⁷ Hanessian, S.; Yang, G.; Rondeau, J.M.; Neumann, U.; Betschart, C.; Tintelnot-Blomley, M. Structure-based design and synthesis of macroheterocyclic peptidomimetic inhibitors of the aspartic protease beta-site amyloid precursor protein cleaving enzyme (BACE). *J. Med. Chem.* **2006**, *49*, 4544-4567.

¹⁹⁸ Rojo, I.; Martín, J.A.; Broughton, H.; Timm, D.; Erickson, J.; Yang, H.C.; McCarthy, J.R. Macrocyclic peptidomimetic inhibitors of beta-secretase (BACE): first X-ray structure of a macrocyclic peptidomimetic-BACE complex. *Bioorg. Med. Chem. Lett.* **2006**, *16*, 191-195.

¹⁹⁹ Ghosh, A.K.; Devasamudram, T.; Hong, L.; DeZutter, C.; Xu, X.; Weerasena, V.; Koelsch, G.; Bilcer, G.; Tang, J. Structure-based design of cycloamide-urethane-derived novel inhibitors of human brain memapsin 2 (beta-secretase). *Bioorg. Med. Chem. Lett.* **2005**, *15*, 15-20.

²⁰⁰ Hom, R.K.; Gailunas, A.F.; Mamo, S.; Fang, L.Y.; Tung, J.S.; Walker, D.E.; Davis, D.; Thorsett, E.D.; Jewett, N.E.; Moon, J.B.; John, V. Design and synthesis of hydroxyethylene-based peptidomimetic inhibitors of human beta-secretase. *J. Med. Chem.* **2004**, *47*, 158-164.

²⁰¹ Ghosh, A.K.; Bilcer, G.; Harwood, C.; Kawahama, R.; Shin, D.; Hussain, K.A.; Hong, L.; Loy, J.A.; Nguyen, C.; Koelsch, G.; Ermolieff, J.; Tang, J. Structure-based design: potent inhibitors of human brain memapsin 2 (beta-secretase). *J. Med. Chem.* **2001**, *44*, 2865-2868.

²⁰² Ghosh, A.K.; Kumaragurubaran, N.; Hong, L.; Lei, H.; Hussain, K.A.; Liu, C.F.; Devasamudram, T.; Weerasena, V.; Turner, R.; Koelsch, G.; Bilcer, G.; Tang, J. Design, synthesis and X-ray structure of protein-ligand complexes: important insight into selectivity of memapsin 2 (beta-secretase) inhibitors. *J. Am. Chem. Soc.* **2006**, *128*, 5310-5311.

²⁰³ Ghosh, A.K.; Kumaragurubaran, N.; Hong, L.; Kulkarni, S.S.; Xu, X.; Chang, W.; Weerasena, V.; Turner, R.; Koelsch, G.; Bilcer, G.; Tang, J. Design, synthesis, and X-ray structure of potent memapsin 2 (beta-secretase) inhibitors with isophthalamide derivatives as the P2-P3-ligands. *J. Med. Chem.* **2007**, *50*, 2399-2407.

²⁰⁴ Shuto, D.; Kasai, S.; Kimura, T.; Liu, P.; Hidaka, K.; Hamada, T.; Shibakawa, S.; Hayashi, Y.; Hattori, C.; Szabo, B.; Ishiura, S.; Kiso, Y. KMI-008, a novel beta-secretase inhibitor containing a hydroxymethylcarbonyl isostere as a transition-state mimic: design and synthesis of substrate-based octapeptides. *Bioorg. Med. Chem. Lett.* **2003**, *13*, 4273-6.

²⁰⁵ Kimura, T.; Shuto, D.; Kasai, S.; Liu, P.; Hidaka, K.; Hamada, T.; Hayashi, Y.; Hattori, C.; Asai, M.; Kitazume, S.; Saido, T.C.; Ishiura, S.; Kiso, Y. KMI-358 and KMI-370, highly potent and small-sized BACE1 inhibitors containing phenylnorstatine. *Bioorg. Med. Chem. Lett.* **2004**, *14*, 1527-31.

²⁰⁶ Kimura, T.; Shuto, D.; Hamada, Y.; Igawa, N.; Kasai, S.; Liu, P.; Hidaka, K.; Hamada, T.; Hayashi, Y.; Kiso, Y. Design and synthesis of highly active Alzheimer's beta-secretase (BACE1) inhibitors, KMI-420 and KMI-429, with enhanced chemical stability. *Bioorg. Med. Chem. Lett.* **2005**, *15*, 211-5.

²⁰⁷ Asai, M.; Hattori, C.; Iwata, N.; Saido, T.C.; Sasagawa, N.; Szabó, B.; Hashimoto, Y.; Maruyama, K.; Tanuma, S.; Kiso, Y.; Ishiura, S. The novel beta-secretase inhibitor KMI-429 reduces amyloid beta peptide production in amyloid precursor protein transgenic and wild-type mice. *J. Neurochem.* **2006**, *96*, 533-40.

²⁰⁸ Kimura, T.; Hamada, Y.; Stochaj, M.; Ikari, H.; Nagamine, A.; Abdel-Rahman, H.; Igawa, N.; Hidaka, K.; Nguyen, J.T.; Saito, K.; Hayashi, Y.; Kiso, Y. Design and synthesis of potent beta-secretase (BACE1) inhibitors with P1' carboxylic acid bioisosteres. *Bioorg. Med. Chem. Lett.* **2006**, *16*, 2380-6.

²⁰⁹ Ziora, Z.; Kasai, S.; Hidaka, K.; Nagamine, A.; Kimura, T.; Hayashi, Y.; Kiso, Y. Design and synthesis of BACE1 inhibitors containing a novel norstatine derivative (2R,3R)-3-amino-2-hydroxy-4-(phenylthio)butyric acid. *Bioorg. Med. Chem. Lett.* **2007**, *17*, 1629-33.

²¹⁰ Hamada, Y.; Abdel-Rahman, H.; Yamani, A.; Nguyen, J.T.; Stochaj, M.; Hidaka, K.; Kimura, T.; Hayashi, Y.; Saito, K.; Ishiura, S.; Kiso, Y. BACE1 inhibitors: optimization by replacing the P1' residue with non-acidic moiety. *Bioorg. Med. Chem. Lett.* **2008**, *18*, 1649-53.

²¹¹ Hamada, Y.; Ohta, H.; Miyamoto, N.; Yamaguchi, R.; Yamani, A.; Hidaka, K.; Kimura, T.; Saito, K.; Hayashi, Y.; Ishiura, S.; Kiso, Y. Novel non-peptidic and small-sized BACE1 inhibitors. *Bioorg. Med. Chem. Lett.* **2008**, *18*, 1643-7.

²¹² Maillard, M.C.; Hom, R.K.; Benson, T.E.; Moon, J.B.; Mamo, S.; Bienkowski, M.; Tomasselli, A.G.; Woods, D.D.; Prince, D.B.; Paddock, D.J.; Emmons, T.L.; Tucker, J.A.; Dappen, M.S.; Brogley, L.; Thorsett, E.D.; Jewett, N.; Sinha, S.; John, V. Design, synthesis, and crystal structure of hydroxyethyl secondary amine-based peptidomimetic inhibitors of human beta-secretase. *J. Med. Chem.* **2007**, *50*, 776-781.

²¹³ Freskos, J.; Brown, D.L.; Fang, L.; Fobian, Y.M.; Varghese, J.; Romero, A.G. *PCT Int. Appl.* **2002**, WO002098849.

²¹⁴ John, V.; Hom, R.; Tucker, J. Methods of treatment of amyloidosis using bi-aryl aspartyl protease inhibitors. US Pat Appl **2006**; US20060014737.

- ²¹⁵ Kortum, S.W.; Benson, T.E.; Bienkowski, M.J.; Emmons, T.L.; Prince, D.B.; Paddock, D.J.; Tomasselli, A.G.; Moon, J.B.; LaBorde, A.; TenBrink, R.E. Potent and selective isophthalamide S2 hydroxyethylamine inhibitors of BACE1. *Bioorg. Med. Chem. Lett.* **2007**, *17*, 3378–3383.
- ²¹⁶ Freskos, J.N.; Fobian, Y.M.; Benson, T.E.; Bienkowski, M.J.; Brown, D.L.; Emmons, T.L.; Heintz, R.; Laborde, A.; McDonald, J.J.; Mischke, B.V.; Molyneaux, J.M.; Moon, J.B.; Mullins, P.B.; Bryan Prince, D.; Paddock, D.J.; Tomasselli, A.G.; Winterrowd, G. Design of potent inhibitors of human beta-secretase. Part 1. *Bioorg. Med. Chem. Lett.* **2007**, *17*, 73–77.
- ²¹⁷ Freskos, J.N.; Fobian, Y.M.; Benson, T.E.; Moon, J.B.; Bienkowski, M.J.; Brown, D.L.; Emmons, T.L.; Heintz, R.; Laborde, A.; McDonald, J.J.; Mischke, B.V.; Molyneaux, J.M.; Mullins, P.B.; Bryan Prince, D.; Paddock, D.J.; Tomasselli, A.G.; Winterrowd, G. Design of potent inhibitors of human beta-secretase. Part 2. *Bioorg. Med. Chem. Lett.* **2007**, *17*, 78–81.
- ²¹⁸ Hussain, I.; Hawkins, J.; Harrison, D.; Hille, C.; Wayne, G.; Cutler, L.; Buck, T.; Walter, D.; Demont, E.; Howes, C.; Naylor, A.; Jeffrey, P.; Gonzalez, M.I.; Dingwall, C.; Michel, A.; Redshaw, S.; Davis, J.B.; Oral administration of a potent and selective non-peptidic BACE1 inhibitor decreases beta-cleavage of amyloid precursor protein and amyloid-beta production in vivo. *J. Neurochem.* **2007**, *100*, 802–809.
- ²¹⁹ (a) Clarke, B.; Demont, E.; Dingwall, C.; Dunsdon, R.; Faller, A.; Hawkins, J.; Hussain, I.; MacPherson, D.; Maile, G.; Matico, R.; Milner, P.; Mosley, J.; Naylor, A.; O'Brien, A.; Redshaw, S.; Riddell, D.; Rowland, P.; Soleil, V.; Smith, K.J.; Stanway, S.; Stemp, G.; Sweitzer, S.; Theobald, P.; Vesey, D.; Walter, D.S.; Ward, J.; Wayne, G. BACE1 inhibitors part 1: identification of novel hydroxy ethylamines (HEAs). *Bioorg. Med. Chem. Lett.* **2008**, *18*, 1011–1016. (b) Clarke, B.; Demont, E.; Dingwall, C.; Dunsdon, R.; Faller, A.; Hawkins, J.; Hussain, I.; MacPherson, D.; Maile, G.; Matico, R.; Milner, P.; Mosley, J.; Naylor, A.; O'Brien, A.; Redshaw, S.; Riddell, D.; Rowland, P.; Soleil, V.; Smith, K.J.; Stanway, S.; Stemp, G.; Sweitzer, S.; Theobald, P.; Vesey, D.; Walter, D.S.; Ward, J.; Wayne, G. BACE1 inhibitors part 2: identification of hydroxy ethylamines (HEAs) with reduced peptidic character. *Bioorg. Med. Chem. Lett.* **2008**, *18*, 1017–1021. (c) Beswick, P.; Charrier, N.; Clarke, B.; Demont, E.; Dingwall, C.; Dunsdon, R.; Faller, A.; Gleave, R.; Hawkins, J.; Hussain, I.; Johnson, C.N.; MacPherson, D.; Maile, G.; Matico, R.; Milner, P.; Mosley, J.; Naylor, A.; O'Brien, A.; Redshaw, S.; Riddell, D.; Rowland, P.; Skidmore, J.; Soleil, V.; Smith, K.J.; Stanway, S.; Stemp, G.; Stuart, A.; Sweitzer, S.; Theobald, P.; Vesey, D.; Walter, D.S.; Ward, J.; Wayne, G. BACE1 inhibitors part 3: identification of hydroxy ethylamines (HEAs) with nanomolar potency in cells. *Bioorg. Med. Chem. Lett.* **2008**, *18*, 1022–1026.
- ²²⁰ Charrier, N.; Clarke, B.; Cutler, L.; Demont, E.; Dingwall, C.; Dunsdon, R.; East, P.; Hawkins, J.; Howes, C.; Hussain, I.; Jeffrey, P.; Maile, G.; Matico, R.; Mosley, J.; Naylor, A.; O'Brien, A.; Redshaw, S.; Rowland, P.; Soleil, V.; Smith, K.J.; Sweitzer, S.; Theobald, P.; Vesey, D.; Walter, D.S.; Wayne, G. Second generation of hydroxyethylamine BACE1 inhibitors: optimizing potency and oral bioavailability. *J. Med. Chem.* **2008**, *51*, 3313–7.
- ²²¹ Ghosh, A.K.; Gemma, S.; Tang, J. beta-Secretase as a therapeutic target for Alzheimer's disease. *Neurotherapeutics.* **2008**, *5*, 399–408.
- ²²² Machauer, R.; Laumen, K.; Veenstra, S.; Rondeau, J.M.; Tintelnot-Blomley, M.; Betschart, C.; Jatton, A.L.; Desrayaud, S.; Staufenbiel, M.; Rabe, S.; Paganetti, P.; Neumann, U. Macrocyclic peptidomimetic beta-secretase (BACE1) inhibitors with activity in vivo. *Bioorg. Med. Chem. Lett.* **2009**, *19*, 1366–1370.
- ²²³ Stachel, S.J.; Coburn, C.A.; Sankaranarayanan, S.; Price, E.A.; Wu, G.; Crouthamel, M.; Pietrak, B.L.; Huang, Q.; Lineberger, J.; Espeseth, A.; Jin, L.; Ellis, J.; Holloway, M.K.; Munshi, S.; Allison, T.; Hazuda, D.; Simon, A.J.; Graham, S.L.; Vacca, J.P. Macrocyclic inhibitors of beta-secretase: functional activity in an animal model. *J. Med. Chem.* **2006**, *49*, 6147–6150.
- ²²⁴ Stauffer, S.R.; Stanton, M.G.; Gregro, A.R.; Steinbeiser, M.A.; Shaffer, J.R.; Nantermet, P.G.; Barrow, J.C.; Rittle, K.E.; Collusi, D.; Espeseth, A.S.; Lai, M.T.; Pietrak, B.L.; Holloway, M.K.; McGaughey, G.B.; Munshi, S.K.; Hochman, J.H.; Simon, A.J.; Selnick, H.G.; Graham, S.L.; Vacca, J.P. Discovery and SAR of isonicotinamide BACE1 inhibitors that bind beta-secretase in a N-terminal 10s-loop down conformation. *Bioorg. Med. Chem. Lett.* **2007**, *17*, 1788–1792.
- ²²⁵ Stanton, M.G.; Stauffer, S.R.; Gregro, A.R.; Steinbeiser, M.; Nantermet, P.; Sankaranarayanan, S.; Price, E.A.; Wu, G.; Crouthamel, M.C.; Ellis, J.; Lai, M.T.; Espeseth, A.S.; Shi, X.P.; Jin, L.; Colussi, D.; Pietrak, B.; Huang, Q.; Xu, M.; Simon, A.J.; Graham, S.L.; Vacca, J.P.; Selnick, H. Discovery of isonicotinamide derived beta-secretase inhibitors: in vivo reduction of beta-amyloid. *J. Med. Chem.* **2007**, *50*, 3431–3433.
- ²²⁶ Miyamoto, M.; Matsui, J.; Fukumoto, H.; Tarui, N. Preparation of 2-[2-amino- or 2-(N-heterocyclyl)ethyl]-6-(4-biphenylmethoxy)tetralin derivatives as b-secretase inhibitors. *PCT Int. Appl.* **2001**; WO2001087293.
- ²²⁷ Miyamoto, M.; Matsui, J.; Fukumoto, H.; Tarui, N. Beta-Secretase inhibitors. *Eur. Pat. Appl.* **2003**, EP1283039.
- ²²⁸ Qiao, L.; Etchenberrigaray, R. Preparation of phosphinylmethyl and phosphorylmethyl succinic and glutaric acid

analogs as b-secretase inhibitors useful in the treatment of Alzheimer's disease. *PCT Int. Appl.* **2002**; WO2002096897.

²²⁹ Etchenberrigaray, R.; Qiao, L. Phosphinylmethyl and phosphorylmethyl succinic and glutaric acid analogs as b-secretase inhibitors. *PCT Int Appl* **2003**; US2003078240.

²³⁰ Bhisetti, G.R.; Saunders, J.O.; Murcko, M.A.; Lepre, C.A.; Britt, S.D.; Come, J.H.; Deninger, D.D.; Wang, T. Preparation of beta-carbolines and other inhibitors of BACE1 aspartic proteinase useful against Alzheimer's and other BACE-mediated diseases. *PCT Int. Appl.* **2002**; WO2002088101.

²³¹ Rajapakse, H.A.; Nantermet, P.G.; Selnick, H.G.; Munshi, S.; McGaughey, G.B.; Lindsley, S.R.; Young, M.B.; Lai, M.T.; Espeseth, A.S.; Shi, X.P.; Colussi, D.; Pietrak, B.; Crouthamel, M.C.; Tugusheva, K.; Huang, Q.; Xu, M.; Simon, A.J.; Kuo, L.; Hazuda, D.J.; Graham, S.; Vacca, J.P. Discovery of oxadiazoyl tertiary carbinamine inhibitors of beta-secretase (BACE1). *J. Med. Chem.* **2006**, *49*, 7270–7273.

²³² Lindsley, S.R.; Moore, K.P.; Rajapakse, H.A.; Selnick, H.G.; Young, M.B.; Zhu, H.; Munshi, S.; Kuo, L.; McGaughey, G.B.; Colussi, D.; Crouthamel, M.C.; Lai, M.T.; Pietrak, B.; Price, E.A.; Sankaranarayanan, S.; Simon, A.J.; Seabrook, G.R.; Hazuda, D.J.; Pudvah, N.T.; Hochman, J.H.; Graham, S.L.; Vacca, J.P.; Nantermet, P.G. Design, synthesis, and SAR of macrocyclic tertiary carbinamine BACE1 inhibitors. *Bioorg. Med. Chem. Lett.* **2007**, *17*, 4057–4061.

²³³ Cole, D.C.; Manas, E.S.; Stock, J.R.; Condon, J.S.; Jennings, L.D.; Aulabaugh, A.; Chopra, R.; Cowling, R.; Ellingboe, J.W.; Fan, K.Y.; Harrison, B.L.; Hu, Y.; Jacobsen, S.; Jin, G.; Lin, L.; Lovering, F.E.; Malamas, M.S.; Stahl, M.L.; Strand, J.; Sukhdeo, M.N.; Svenson, K.; Turner, M.J.; Wagner, E.; Wu, J.; Zhou, P.; Bard, J. Acylguanidines as small-molecule beta-secretase inhibitors. *J. Med. Chem.* **2006**, *49*, 6158-61.

²³⁴ (a) Fobare, W.F.; Solvibile, W.R.; Robichaud, A.J.; Malamas, M.S.; Manas, E.; Turner, J., Hu, Y.; Wagner, E.; Chopra, R.; Cowling, R.; Jin, G.; Bard, J. Thiophene substituted acylguanidines as BACE1 inhibitors. *Bioorg. Med. Chem. Lett.* **2007**, *17*, 5353–5356. (b) Cole, D.C.; Stock, J.R.; Chopra, R.; Cowling, R.; Ellingboe, J.W.; Fan, K.Y.; Harrison, B.L.; Hu, Y.; Jacobsen, S.; Jennings, L.D.; Jin, G.; Lohse, P.A.; Malamas, M.S.; Manas, E.S.; Moore, W.J.; O'Donnell, M.M.; Olland, A.M.; Robichaud, A.J.; Svenson, K.; Wu, J.; Wagner, E.; Bard, J. Acylguanidine inhibitors of beta-secretase: optimization of the pyrrole ring substituents extending into the S1 and S3 substrate binding pockets. *Bioorg. Med. Chem. Lett.* **2008**, *18*, 1063–1066.

²³⁵ Jennings, L.D.; Cole, D.C.; Stock, J.R.; Sukhdeo, M.N.; Ellingboe, J.W.; Cowling, R.; Jin, G.; Manas, E.S.; Fan, K.Y.; Malamas, M.S.; Harrison, B.L.; Jacobsen, S.; Chopra, R.; Lohse, P.A.; Moore, W.J.; O'Donnell, M.M.; Hu, Y.; Robichaud, A.J.; Turner, M.J.; Wagner, E.; Bard, J. Acylguanidine inhibitors of beta-secretase: optimization of the pyrrole ring substituents extending into the S1' substrate binding pocket. *Bioorg. Med. Chem. Lett.* **2008**, *18*, 767–771.

²³⁶ Reitz, A.B.; Luo, C.; Huang, Y.; Ross, T.M.; Baxter, E.E.; Tounge, B.A.; Parker, M.H.; Strobel, E.D.; Reynolds, C.H. Preparation of 2-amino-3,4-dihydropyridol[3,4-d]pyrimidines as inhibitors of beta-secretase (BACE). *PCT Int. Appl.* **2007**, WO2007050612.

²³⁷ Baxter, E.W.; Conway, K.A.; Kennis, L.; Bischoff, F.; Mercken, M.H.; DeWinter, H.L.; Reynolds, C.H.; Tounge, B.A.; Luo, C.; Scott, M.K.; Huang, Y.; Braeken, M.; Pieters, S.M.A.; Berthelot, D.J.C.; Masure, S.; Bruinzeel, W.D.; Jordan, A.D.; Parker, M.H.; Boyd, R.E.; Qu, J.; Alexander, R.S.; Brennehan, D.E.; Reitz, B. 2-Amino-3,4-dihydroquinazolines as inhibitors of BACE1 (b-Site APP cleaving enzyme): use of structure based design to convert a micromolar hit into a nanomolar lead. *J. Med. Chem.* **2007**, *50*, 4261–4264.

²³⁸ Murray, C.W.; Callaghan, O.; Chessari, C.; Cleasby, A.; Congreve, M.; Frederickson, M.; Hartshorn, M.J.; McMennamin, R.; Patel, S.; Wallis, N. Application of fragment screening by X-ray crystallography to beta-secretase. *J. Med. Chem.* **2007**, *50*, 1116–1123.

²³⁹ Chang, W.P.; Downs, D.; Huang, X.P.; Da, H.; Fung, K.M.; Tang, J. Amyloid-beta reduction by memapsin 2 (beta-secretase) immunization. *FASEB J.* **2007**, *21*, 3184-96.

²⁴⁰ Rakover, I.; Arbel, M.; Solomon, B. Immunotherapy against APP beta-secretase cleavage site improves cognitive function and reduces neuroinflammation in Tg2576 mice without a significant effect on brain abeta levels. *Neurodegener Dis.* **2007**, *4*, 392-402.

²⁴¹ Hoyos Flight, M. Neurodegenerative disease: inhibiting beta-secretase where it matters. *Nat. Rev. Neurosci.* **2008**, *9*, 414-415.

²⁴² Morphy, R.; Rankovic, Z. Designed multiple ligands. An emerging drug discovery paradigm. *J. Med. Chem.* **2005**, *48*, 6523–6543.

²⁴³ Schmitt, B.; Bernhardt, T.; Moeller, H.J.; Heuser, I.; Frolich, L. Combination therapy in Alzheimer's disease: a review of current evidence. *CNS Drugs* **2004**, *18*, 827-844.

²⁴⁴ Kola, I.; Landis, J. Can the pharmaceutical industry reduce attrition rates? *Nat. Rev. Drug Discovery* **2004**, *3*, 711–715.

- ²⁴⁵ Morphy, R.; Rankovic, Z. Fragments, network biology and designing multiple ligands. *Drug Discovery Today* **2007**, *12*, 156–160.
- ²⁴⁶ Morphy, R.; Kay, C.; Rankovic, Z. From magic bullets to designed multiple ligands. *Drug Discovery Today* **2004**, *9*, 641–651.
- ²⁴⁷ Bolognesi, M.L.; Rosini, M.; Andrisano, V.; Bartolini, M.; Minarini, A.; Tumiatti, V.; Melchiorre, C. MTDL design strategy in the context of Alzheimer's disease: from lipocrine to memoquin and beyond. *Curr. Pharm. Des.* **2009**, *15*, 601-13.
- ²⁴⁸ Millan, M.J. Dual- and triple-acting agents for treating core and co-morbid symptoms of major depression: novel concepts, new drugs. *Neurotherapeutics* **2009**, *6*, 53-77.
- ²⁴⁹ Morphy, R.; Rankovic, Z.; Designing multiple ligands - medicinal chemistry strategies and challenges. *Curr. Pharm. Des.* **2009**, *15*, 587-600.
- ²⁵⁰ Iqbal, K.; Grundke-Iqbal, I. Developing pharmacological therapies for Alzheimer disease. *Cell. Mol. Life Sci.* **2007**, *64*, 2234-44.
- ²⁵¹ Kitano, H. A robustness-based approach to systems-oriented drug design. *Nat. Rev. Drug. Discovery* **2007**, *6*, 202-10.
- ²⁵² Barabasi, A.L.; Oltvai, Z.N. Network biology: understanding the cell's functional organization. *Nat. Rev. Genet.* **2004**, *5*, 101-13.
- ²⁵³ Korcsmaros, T.; Szalay, M.S.; Böde, C.; Kovacs, I.A.; Csermely, P. How to design multi-target drugs: target search options in cellular networks. *Expert Opin. Drug. Discovery* **2007**, *2*, 1-10.
- ²⁵⁴ Youdim, M.B. The path from anti Parkinson drug selegiline and rasagiline to multifunctional neuroprotective anti Alzheimer drugs ladostigil and m30. *Curr. Alzheimer Res.* **2006**, *3*, 541-550.
- ²⁵⁵ Youdim, M.B.; Buccafusco, J.J.; Multi-functional drugs for various CNS targets in the treatment of neurodegenerative disorders. *Trends Pharmacol. Sci.* **2005**, *26*, 27-35.
- ²⁵⁶ Bar-Am, O.; Weinreb, O.; Amit, T.; Youdim, M.B. The novel cholinesterase-monoamine oxidase inhibitor and antioxidant, ladostigil, confers neuroprotection in neuroblastoma cells and aged rats. *J. Mol. Neurosci.* **2009**, *37*, 135-145.
- ²⁵⁷ Weinreb, O.; Amit, T.; Bar-Am, O.; Yogev-Falach, M.; Youdim, M.B. The neuroprotective mechanism of action of the multimodal drug ladostigil. *Front. Biosci.* **2008**, *13*, 5131-5137.
- ²⁵⁸ Weinreb, O.; Bar-Am, O.; Amit, T.; Drigues, N.; Sagi, Y.; Youdim, M.B. The neuroprotective effect of ladostigil against hydrogen peroxide-mediated cytotoxicity. *Chem. Biol. Interact.* **2008**, *175*, 318-326.
- ²⁵⁹ Van der Schyf, C.J.; Mandel, S.; Geldenhuys, W.J.; Amit, T.; Avramovich, Y.; Zheng, H.; Fridkin, M.; Gal, S.; Weinreb, O.; Bar Am, O.; Sagi, Y.; Youdim, M.B. Novel multifunctional anti-Alzheimer drugs with various CNS neurotransmitter targets and neuroprotective moieties. *Curr. Alzheimer Res.* **2007**, *4*, 522-536.

Chapter 2

Aim of the thesis

The aspartic protease BACE1 (β -secretase) is recognized as one of the most promising targets in the treatment of Alzheimer's disease (AD). The accumulation of β -amyloid peptide ($A\beta$) in the brain is a major factor in the pathogenesis of AD. $A\beta$ is formed by initial cleavage of β -amyloid precursor protein (APP) by BACE1, therefore its inhibition represents one of the therapeutic approach to control progression of AD, by preventing the abnormal generation of $A\beta$. For this reason, in the last decade, many research efforts have focused at the identification of new BACE1 inhibitors as drug candidates. Generally, BACE1 inhibitors are grouped into two families: substrate-based inhibitors, designed as peptidomimetic inhibitors, and non-peptidomimetic ones. The research on non-peptidomimetic small-molecule BACE1 inhibitors remains the most interesting approach, since these compounds hold an improved bioavailability after systemic administration, due to good blood-brain barrier permeability in comparison to peptidomimetic inhibitors.

2.1 Design of heterocycles-based BACE1 inhibitors.

Very recently, our research group discovered a new promising lead compound for the treatment of AD, named lipocrine (**6**), a hybrid compound between lipoic acid and the AChEI tacrine, characterized by a tetrahydroacridinic moiety. Lipocrine was one of the first compounds able to inhibit the catalytic activity of AChE and AChE-induced $A\beta$ aggregation and to protect against reactive oxygen species (See Fig.1).¹ Lipocrine represents one of the best example of Multi-Target-Directed-Ligands (MTDLs) by acting simultaneously on different targets involved in AD pathogenesis. Therefore it emerged as valuable pharmacological tool to investigate AD and as a promising lead compound for new anti-AD drugs.

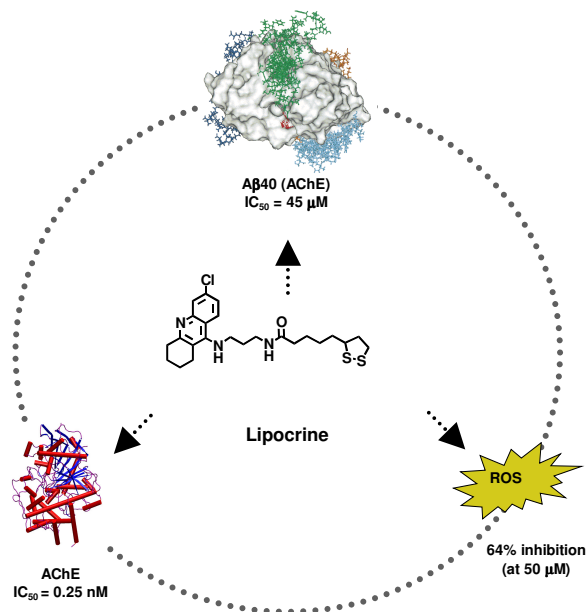


Figure 1. Multi-target profile of lipocrine.

In view of the complexity of AD and the involvement of multiple and interconnected pathological pathways, a new therapeutic approach based on the development of multifunctional molecule able to inhibit BACE1 and to interfere with other pathological event, could be a new paradigm to address this unmet medical need and to slow, or perhaps even halt, the course of the disease.

In view of discover new Multi-Target-Directed-Ligands (MTDLs), lipocrine was also evaluated for BACE1 inhibitory activity, resulting in a potent and selective BACE1 inhibitor ($IC_{50} = 57 \text{ nM}$). Due to its interesting profile, we investigated new scaffold modifications based on this compound in order to obtain useful chemical entities as potent BACE1 inhibitors.

An important structural feature of lipocrine for the optimal inhibition of BACE1 was thought being the dithiolane group; therefore, to confirm this hypothesis the tiophene analogue **7** was designed and synthesised. To evaluate the optimal distance for the inhibitory activity between the tetrahydroacridine moiety and dithiolane fragment, different polymethylene spacers were interposed affording derivatives **1-5** (Fig.2).

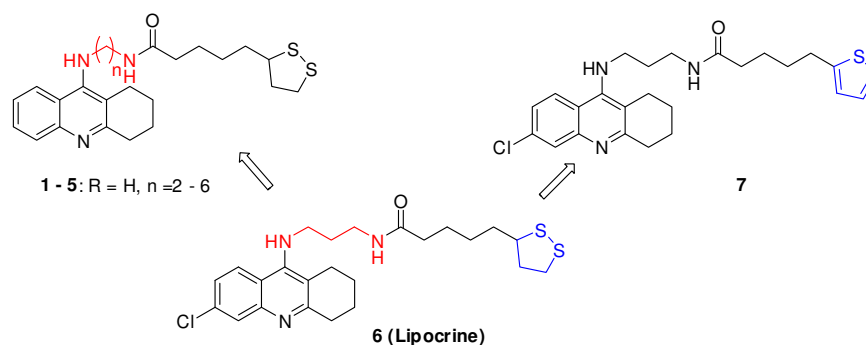


Figure 2. Design strategy of compounds 1-5 and 7

With the aim to obtaining multifunctional compounds able to inhibit not only BACE1 but also the classical targets of AD pathogenesis (i.e. AChE and AChE-mediated A β aggregation inhibition), new ligands bearing lipoic acid as key structure were synthesised. The hybrid derivatives **8** and **9** retain lipoic acid fragment of lipocrine and the aromatic moiety of rivastigmine, a known AChEI used in AD therapy. In particular **8** include the free tertiary amino groups on meta-position of the aromatic ring, whereas **9** displays the methoxy group. These key features are coupled to lipoic acid in two different ways to evaluate the interaction with the enzyme (Fig. 3).

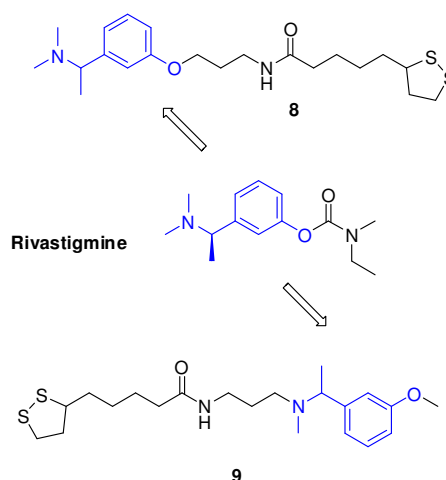


Figure 3. Design strategy of compounds **8** and **9**.

Moreover, derivative **10** represents a hybrid compound incorporating the caproctamine pharmacophore and lipoic acid fragment. Caproctamine was the prototype of the polyamine-based structure AChEIs developed by Melchiorre and co-workers in a study aimed to generate novel polyamine ligands having simultaneously affinity for both AChE active and peripheral sites and for muscarinic M₂ autoreceptors.² Its structure has been discovered applying the universal template approach to AChE, which is a polyamine backbone can recognize different

biological targets through its policationic structure and its selectivity can be achieved by modulating the distance between the amine functions and by inserting appropriate residues on a polyamine backbone. We designed compound **10** by coupling the caproctamine pharmacophore to lipaic acid residue, with the aim to evaluate the potential inhibitory activity towards AD different targets, such as AChE, A β -aggregation and BACE1 (Fig. 4).

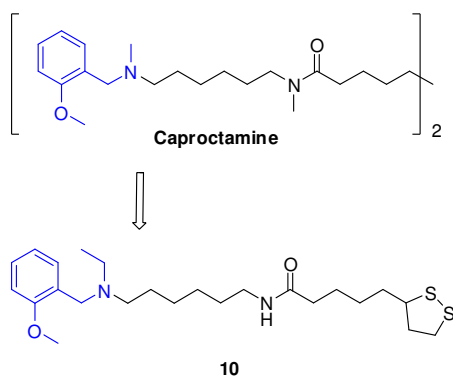


Figure 4. Design strategy of compounds **10**.

To investigate the importance of tetrahydroacridinic moiety of lipocrine for BACE1 inhibitory activity, we applied the concept of molecular simplification as drug design strategy, to synthesise novel heterocyclic compounds. Thus, we designed and synthesized new ligands by replacing the tetrahydroacridine moiety of lipocrine with 4-amino-quinazoline.

In the meanwhile of our investigation on new suitable small molecules for BACE1 inhibition, a work published in 2007 by Johnson & Johnson researchers revealed that 2-amino-3,4-dihydroquinazoline ring is an appropriate moiety for the inhibition of BACE1.³ This fragment was identified by high-throughput screening, and X-ray crystallography of the inhibitor **XLIII** co-crystallized with the enzyme revealed that the 2-amino-3,4-dihydroquinazolines adopted a compact structure bearing a hairpin turn of side chain and the exocyclic amino group participated in a hydrogen bonding array with the two catalytic aspartic acids of BACE1 (Fig. 5)

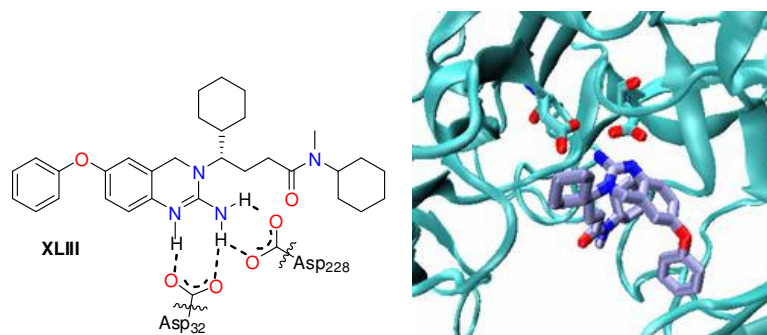


Figure 5. Schematic representation of hydrogen bonding of inhibitor XLIII with two Asp and crystal structure of inhibitor co-crystallised with BACE1 (the two Asp residues are also displayed).

For this reason it was worthwhile to following our investigation upon 2-chloro-4-amino-6,7-dimethoxy-quinazoline in view of chemical similarity to 2-amino-3,4-dihydroquinazoline ring. Therefore, in order to evaluate modifications of the tetrahydroacridinic moiety of lipocrine with a 2-chloro-4-amino-6,7-dimethoxy-quinazoline residue, compound **11** was synthesised revealing an enhanced BACE1 inhibitory activity, compared to lipocrine ($IC_{50} = 18$ nM). Thus, in order to establish structure-activity relationships for BACE1 inhibition, different modifications were carried out on the new prototype. Firstly, we studied the importance of the 2-Cl replacement by inserting different substituents like -H, -CH₃, -NH₂, obtaining compounds **12-14**, respectively (Fig. 7). In addition, structure-activity relationships studies made on the lateral chain allowed exploring the importance of the lipoic acid residue. In view of conferring to the new chemical entity the additional antioxidant property, we replaced the antioxidant moiety of *trans*-ferulic acid in exchange of the dithiolane residue of lipoic acid obtaining compound **15**. Meanwhile, the replacement with acrylic acid led to compounds **16** and **17** which could have the ability to interact to a potential cysteine residue of the enzyme blocking the enzyme in an irreversible mode.

In order to evaluate the effect of changing the position of the lateral chain on inhibitory activity and taking advantage of the interesting activity profile displayed by compound **XLIII** which bears a guanidinic group in its structure, we chose to shift the lateral chain from the 4-position of quinazoline moiety to 2-position, obtaining compound **20** and **21** holding a lipoic acid and *trans*-ferulic acid fragment, respectively (Fig. 7). These compounds bore in their structure a guanidinic moiety that has shown, by X-ray data, to be a key fragment for strong interactions with the catalytic aspartates as displayed by the very potent inhibitors **XL** and **XLV** shown in figure 6.^{4,5}

the new scaffold was coupled to 6-chlorotacrine fragment through a propandiamine spacer affording compound **18** (Fig. 8).

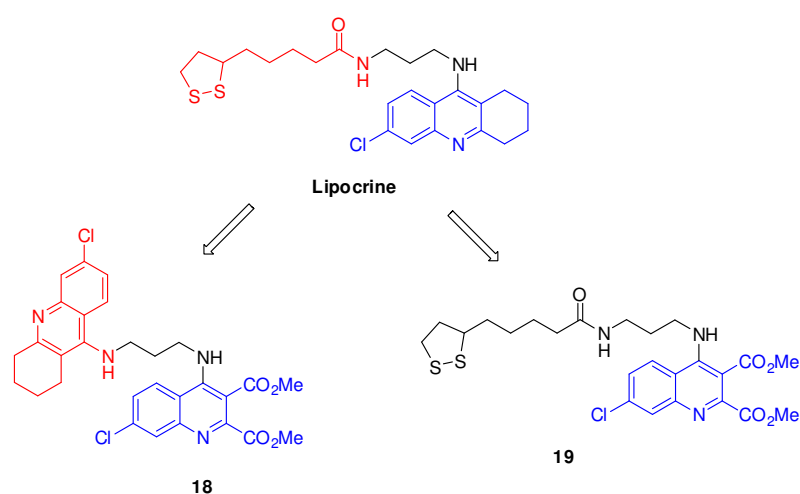


Figure 8. Design strategy of compounds **18** and **19**.

2.2 Design of δ -aminocyclohexane carboxylic acid based BACE1 inhibitors

A side project related to the synthesis of novel enzymatic inhibitors of BACE1 in order to explore the pseudopeptidic transition-state isosteres chemistry was carried out during a research stage at Université de Montréal (Canada) in Hanessian's group.

The availability of structural data from the extracellular domain of BACE1 has greatly enhanced the design of potential inhibitors. The conceptual basis of such a design element has traditionally relied on mimicking the tetrahedral transition state of the enzyme-substrate complex with a suitable surrogate. In fact, a hydroxyethylene isostere in the backbone of the synthetic protease inhibitor has performed an admirable role. Indeed, the first crystal structure of a BACE1-OM99-2 (**A**) complex (Fig. 9), was reported by the Tang and Ghosh⁶ groups in 2000. Valuable insights gleaned from this structural information led to the design and synthesis of several other types of BACE1 inhibitors.

In previous work, Hanessian's group reported on the structure-based design, synthesis, and X-ray crystallographic studies of carbocyclic⁷ and heterocyclic^{8,9} P₁/P₁' truncated variants of the Tang and Ghosh original 1nM BACE1 inhibitor **A** (Fig. 9). Further refinement of these prototypical inhibitors led to consider unnatural, minimally peptidic molecules in which the traditional P₂/P₃ dipeptide subunit in the Tang and Ghosh inhibitor was replaced by a cyclohexane spacer unit. Preliminary results with a prototypical molecule **B** (Fig. 9), resulted in

low μM inhibitory activity against BACE1. In spite of the weak activity, a crystal structure of **B** in complex with BACE1 showed that it was indeed bound in the active site, although the orientation of the *N*-acetyl group was changed. In an effort to study the effect of the nature of steric environment near the *N*-acetyl group, we considered the synthesis of carbocyclic aminoacids represented by the generic structure **C** shown in figure 9.

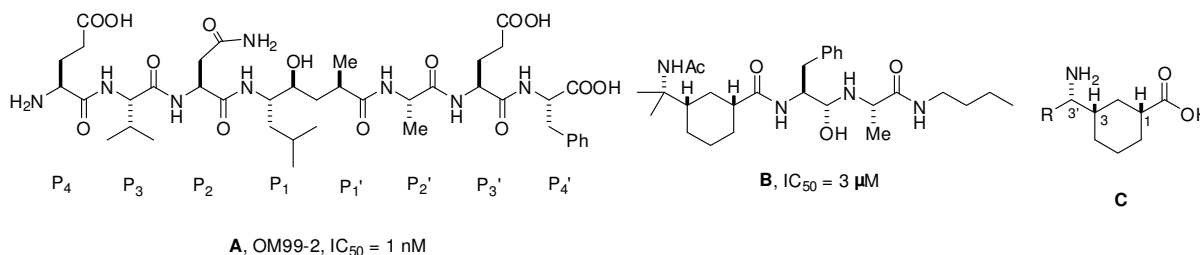


Figure 9. Tang-Ghosh inhibitor OM99-2 (**A**), truncated peptidomimetics bearing carbocyclic aminoacids core **B-C**.

Such carbocyclic δ -aminoacids with stereochemically defined substitution are not known in the context of peptidomimetic design. In this regard, the aim of the project was to incorporate such a constrained carbocyclic aminoacids in a potential inhibitors of BACE1 endowed with reduced peptidic character. This target structure was synthesized previously in Hanessian's lab using a well-know multistep synthesis, starting from the chiral aminoacid as depicted in an exemplar retrosynthetic analysis (Fig.10).¹⁰

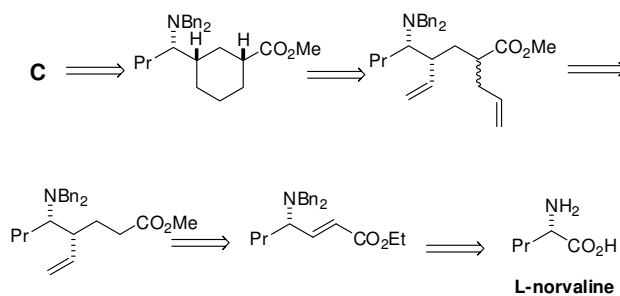


Figure 10. Retrosynthetic analysis of δ -aminocyclohexane carboxylic acid motif **C** starting from a chiral aminoacid (L-norvaline).

The aim of our work has been the synthesis of the δ -aminocyclohexane carboxylic acid motif by a novel asymmetric approach. In particular, we envisioned an alternative route based on an organocatalytic asymmetric conjugate addition of nitroalkanes to cyclohexenone. The obtained 3-(α -nitroalkyl)-cyclohexanones were further functionalized to give the corresponding δ -nitroalkyl cyclohexane carboxylic acids. These intermediates were elaborated to the target structures 3-(α -aminoalkyl)-1-cyclohexane carboxylic acids in a new readily accessible way.

The Michael addition reactions of enolates are some of the most fundamental C-C bond-

forming reactions. Therefore, their catalytic asymmetric versions have been studied extensively.¹¹ Stereoselective Michael additions to α,β -unsaturated ketones represents a challenging objective in asymmetric catalysis. The activation as an iminium ion can in principle constitute a suitable and general method for accomplishing highly stereoselective transformations of enones. However, the inherent problems of forming highly substituted iminium ions from ketones, along with the issue associated with a more difficult control over the configuration of the iminium ion, have complicated the development of an efficient chiral organocatalyst for ketones.

However, the first organocatalyzed addition of 2-nitropropane to cyclohexenone, reported by Yamaguchi and co-workers in 1993,¹² was based on proline catalysis. Using rubidium L-prolinate, they achieved an ee of 59% for cyclohexenone. In 2000, Hanessian and co-workers reported on a substantial improvement in the addition of 2-nitropropane to cyclohexenone in the presence of 10 mol% of L-proline, in conjunction with 2,6-dimethylpiperazine as an additive. The reaction profile exhibited an unusual non-linear effect, before reaching ee values ranging 89-93%.¹³ Since then, the enantioselectivity of this reaction has been extended with *trans*-4,5-methano-L-proline to 99% ee.¹⁴

Applying the organocatalyzed reaction we were able to obtain a separable mixture of isomers: the less polar (*S,S*)-propyl *syn*-isomer (89% ee), and the more polar (*S,R*)-propyl *anti*-isomer (74% ee) that were each separated and characterized. The individual enantiomeric purities were determined by HPLC analysis on a chiral column, using racemic mixtures as controls. A similar protocol with 1-nitrobutane gave the less polar *syn*-(*S,S*)-butyl isomer (89% ee) and the more polar *anti*-(*S,R*)-isomer butyl (71% ee) in a ratio of 1:2, respectively (see Chemistry section 3.2).

Synthetic manipulations to the obtaining nitroketone **D** will be accomplished to reach to the target compound exemplified by motif **C** as depicting in retrosynthetic analysis in figure 11. In particular, the individual nitroketones **D** were each transformed to the corresponding ketene dithioacetals. Successive methanolysis gave the methyl esters that were subjected to reduction and *N*-acetylation.

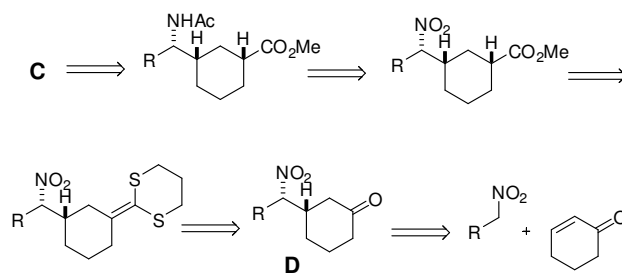


Figure 11. Retrosynthetic analysis of δ -aminocyclohexane carboxylic acid motif **C** featuring the organocatalyzed Michael addition

In the context of the peptidomimetics BACE1 program, this alternative route will represent a practical, shorter and asymmetric approach to the target compound using the enantioselective reaction as synthetic key step.

References

- ¹ Rosini, M.; Andrisano, V.; Bartolini, M.; Bolognesi, M.L.; Hrelia, P.; Minarini, A.; Tarozzi, A.; Melchiorre, C. Rational approach to discover multipotent Anti-Alzheimer drugs. *J. Med. Chem.* **2005**, *48*, 360-363.
- ² Melchiorre, C., Andrisano, V., Bolognesi, M.L., Budriesi, R., Cavalli, A., Cavrini, V., Rosini, M., Tumiatti, V., Recanatini, M. Acetylcholinesterase noncovalent inhibitors based on a polyamine backbone for potential use against Alzheimer's disease. *J. Med. Chem.* **1998**, *41*, 4186-4189.
- ³ Baxter, E.W.; Conway, K.A.; Kennis, L.; Bischoff, F.; Mercken, M.H.; DeWinter, H.L.; Reynolds, C.H.; Tounge, B.A.; Luo, C.; Scott, M.K.; Huang, Y.; Braeken, M.; Pieters, S.M.A.; Berthelot, D.J.C.; Masure, S.; Bruinzeel, W.D.; Jordan, A.D.; Parker, M.H.; Boyd, R.E.; Qu, J.; Alexander, R.S.; Brenneman, D.E.; Reitz, B. 2-Amino-3,4-dihydroquinazolines as inhibitors of BACE1 (b-Site APP cleaving enzyme): use of structure based design to convert a micromolar hit into a nanomolar lead. *J. Med. Chem.* **2007**, *50*, 4261-4264.
- ⁴ Cole, D.C.; Manas, E.S.; Stock, J.R.; Condon, J.S.; Jennings, L.D.; Aulabaugh, A.; Chopra, R.; Cowling, R.; Ellingboe, J.W.; Fan, K.Y.; Harrison, B.L.; Hu, Y.; Jacobsen, S.; Jin, G.; Lin, L.; Lovering, F.E.; Malamas, M.S.; Stahl, M.L.; Strand, J.; Sukhdeo, M.N.; Svenson, K.; Turner, M.J.; Wagner, E.; Wu, J.; Zhou, P.; Bard, J. Acylguanidines as small-molecule beta-secretase inhibitors. *J. Med. Chem.* **2006**, *49*, 6158-61.
- ⁵ Edwards, P.D.; Albert, J.S.; Sylvester, M.; Aharony, D.; Andisik, D.; Callaghan, O.; Campbell, J.B.; Carr, R.A.; Chessari, G.; Congreve, M.; Frederickson, M.; Folmer, R.H.; Geschwindner, S.; Koether, G.; Kolmodin, K.; Krumrine, J.; Mauger, R.C.; Murray, C.W.; Olsson, L.L.; Patel, S.; Spear, N.; Tian, G. Application of fragment-based lead generation to the discovery of novel, cyclic amidine beta-secretase inhibitors with nanomolar potency, cellular activity, and high ligand efficiency. *J. Med. Chem.* **2007**, *50*, 5912-5925.
- ⁶ Hong, L.; Koelsch, G.; Lin, X.; Wu, W. S.; Terzyan, S.; Ghosh, A.K.; Zhang, X. C.; Tang, J. Structure of the protease domain of memapsin 2 (beta-secretase) complexed with inhibitor. *Science* **2000**, *290*, 150-153.
- ⁷ Hanessian, S.; Yun, H.; Hou, Y.; Yang, G.; Bayrakdarian, M.; Therrien, E.; Moitessier, N.; Roggo, S.; Veenstra, S.; Tintelnot-Blomley, M.; Rondeau, J.-M.; Ostermeier, C.; Strauss, A.; Ramage, P.; Paganetti, P.; Neumann, U.; Betschart, C. Structure-based design, synthesis, and memapsin 2 (BACE) inhibitory activity of carbocyclic and heterocyclic peptidomimetics. *J. Med. Chem.*; **2005**; *48*, 5175-5190.
- ⁸ Hanessian, S.; Yun, H.; Hou, Y.; Tintelnot-Blomley, M. Stereoselective synthesis of constrained azacyclic hydroxyethylene isosteres as aspartic protease inhibitors: dipolar cycloaddition and related methodologies toward branched pyrrolidine and pyrrolidinone carboxylic acids. *J. Org. Chem.* **2005**, *70*, 6746-6756.
- ⁹ Hanessian, S.; Hou, Y.; Bayrakdarian, M.; Tintelnot-Blomley, M. Stereoselective synthesis of constrained oxacyclic hydroxyethylene isosteres of aspartic protease inhibitors: aldol and Mukaiyama aldol methodologies for branched tetrahydrofuran 2-carboxylic acids. *J. Org. Chem.* **2005**, *70*, 6735-6745.
- ¹⁰ Hanessian, S.; Maji, D.; Govindan, S.; Matera, R.; Tintelnot-Blomley, M. Substrate-controlled and organocatalytic asymmetric synthesis of carbocyclic amino acid dipeptide mimetics. (*manuscript in preparation*).
- ¹¹ Perlmutter, P. *Conjugate Addition Reactions in Organic Synthesis*; Pergamon Press: Oxford. **1992**.
- ¹² Yamaguchi, M.; Shiraishi, T.; Hiram, M. A Catalytic Enantioselective Michael Addition of a Simple Malonate to Prochiral alpha,beta-Unsaturated Ketones and Aldehydes. *Angew. Chem., Int. Ed. Engl.* **1993**, *32*, 1176-1178.
- ¹³ Hanessian, S.; Pham, V. Catalytic asymmetric conjugate addition of nitroalkanes to cycloalkenones. *Org. Lett.* **2000**, *2*, 2975.
- ¹⁴ Hanessian, S.; Shao, Z.; Warrier, J.S. Optimization of the Catalytic Asymmetric Addition of Nitroalkanes to Cyclic Enones with trans-4,5-Methano-L-proline *Org. Lett.* **2006**, *21*, 4787-90.

Chapter 3

Chemistry

3.1 Synthesis of heterocycles-based BACE1 inhibitors.

Synthesis of compounds 1-7

Nucleophilic aromatic substitution of the tetrahydroacridines **30** or **31** with the opportune chain length diamines, in *n*-pentanol, gave intermediates **23** and **32-36** (Scheme 1). Coupling reaction of tetrahydroacridine intermediates **32-36** with lipoic acid (LA) in the presence of 1-(3-dimethylamino-propyl)-3-ethylcarbodiimide hydrochloride (EDCI·HCl), gave compounds **1-5**, respectively.

Compound **6** and **7** were obtained following the same coupling conditions by condensation of the tetrahydroacridinamine **23** with LA and 5-(thiophen-2-yl)pentanoic acid, respectively (Scheme1).

Synthesis of compounds 8-10

The starting material 1-(3-hydroxyphenyl)ethanone was functionalised under standard reductive amination to the dimethylamine derivative **37**¹. The following alkylation with *tert*-butyl 3-chloropropylcarbamate in DMF gave intermediate **38** which was *N*-deprotected and coupled under standard conditions with LA to give compound **8** (Scheme 2).

Ketone **40** was converted to the known 1-(3-methoxyphenyl)-*N*-methylethanamine **41**² through reductive amination with methylamine and NaBH₄ under H₂ atmosphere. The following alkylation with *tert*-butyl 3-chloropropylcarbamate in DMF, and *N*-deprotection gave intermediate **43** which was coupled with LA under standard conditions to give compound **9** (Scheme 3).

Compound **10** was obtained by coupling the known *N*¹-ethyl-*N*¹-(2-methoxybenzyl)hexane-

1,6-diamine **44**³ with LA under the same conditions (Scheme 4).

Synthesis of compounds 11-15

The readily available 2,4-dichloro-6,7-dimethoxyquinazoline **45** and 4-chloro-6,7-dimethoxyquinazoline **46**⁴ were converted to intermediates **26** and **48** under nucleophilic aromatic substitution with *N*-Boc-1,3-propanediamine, followed by *N*-deprotection (Scheme 5). The substitution of 4-chloro-6,7-dimethoxy-2-methylquinazoline **47**⁴ with free 1,3-propanediamine gave the key intermediate **49**. In order to obtain the 2-amino-quinazoline analogue **51**, an ethanolic solution of the intermediate **24** was heated in autoclave at 140 °C under NH₃ pressure to obtain the analogue **50**. The successive *N*-deprotection afforded **51** as a title compound. The coupling reaction of **26**, **48**, **49** and **51** with LA using EDCI·HCl gave compounds **11-14**, respectively, whereas the amidation of compound **26** with *trans*-ferulic acid in the presence of propylphosphonic anhydride⁵ afforded **15** in moderate yield (Scheme 5).

Synthesis of compounds 16-17

The 4-substitution of dichloroquinazoline **45** with *N*-Boc-1,3-propanediamine or *N*-Boc-1,6-hexanediamine gave intermediate **24** and **52**, respectively. After deprotection, the resulting amine derivatives **26** and **53** were acylated with acryloyl chloride in CH₂Cl₂ in good yield to give acrylamide derivatives **16** and **17**, respectively (Scheme 6).

Synthesis of compounds 18-19

The cyclization of methyl 2-amino-4-chlorobenzoate and dimethyl acetylenedicarboxylate in refluxing *t*-butanol afforded quinolinol **54** that was converted into the chloro analogue **55** in refluxing POCl₃. The substitution with tetrahydroacridinamine **23** gave compound **18**, whereas nucleophilic substitution of **55** with *N*-Boc-1,3-propanediamine gave intermediate **56**. After *N*-deprotection, the resulting amine **57** was coupled with LA under standard conditions to afford compound **19** (Scheme 7).

Synthesis of compounds 20-21

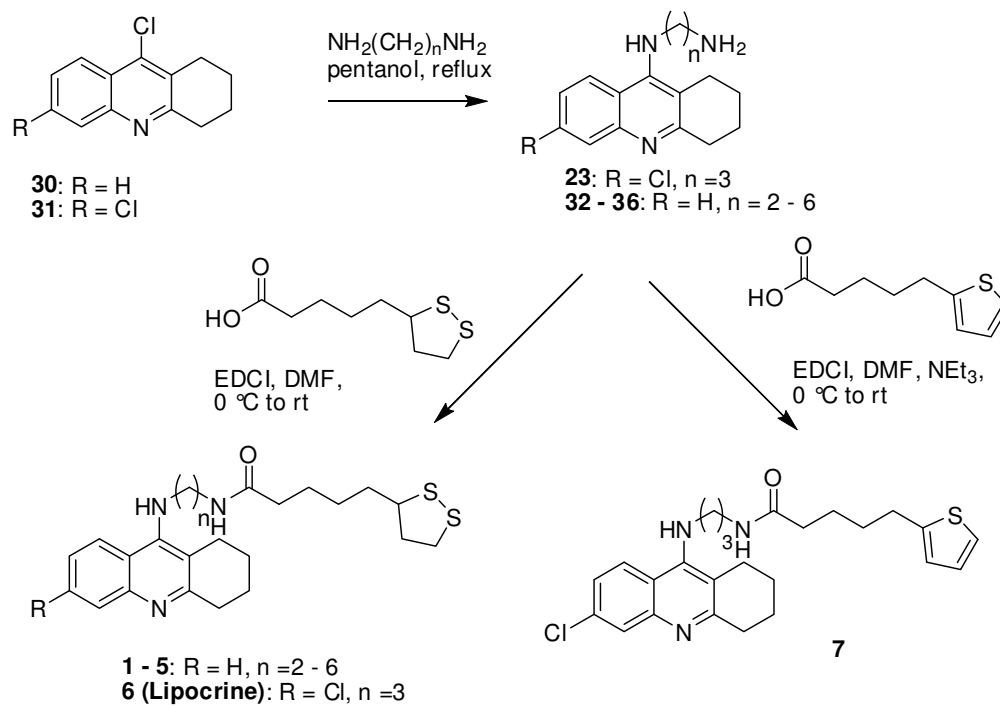
The commercially available dichloroquinazoline **45** was converted to 4-dimethylamino derivative **58**. The following 2-substitution with *N*-Boc-1,3-propanediamine followed by *N*-deprotection afforded amine **60**. The coupling reaction with LA using EDCI·HCl gave compound

20, whereas the condensation with *trans*-ferulic acid in the presence of propylphosphonic anhydride gave compound **21** (Scheme 8).

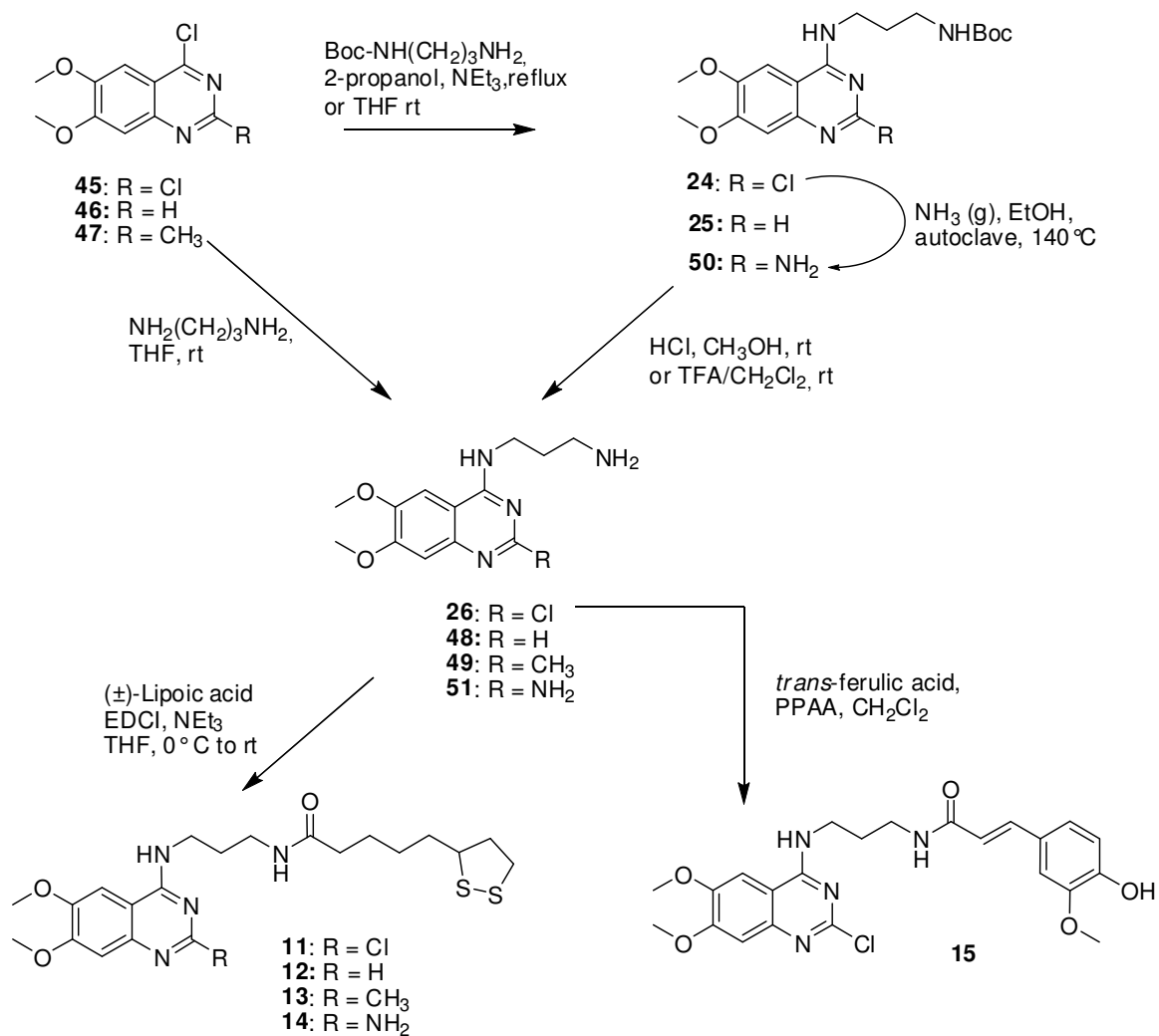
Synthesis of compound **22**

The intermediate **61**⁶ was obtained following the Williamson synthesis by coupling phenol and methyl-5-chloro-2-nitrobenzoate in *N*-methyl-2-pyrrolidone, under basic conditions. The alkaline hydrolysis of the resulting benzoate **61** gave the corresponding acid **62** which was reduced under catalytic hydrogenation to obtain the amino-benzoic acid **63** that was subjected to cyclization in presence of potassium cyanate under basic condition to afford quinazolindiol **64**. Refluxing this intermediate in phosphorous oxychloride gave 2,4-dichloro-6-phenoxyquinazoline **65** that was converted to 4-dimethylamino derivative **66** with dimethylamine. Following the same procedure carried out for compound **20**, the intermediate **66** was converted into amine **68** that was coupled with LA to afford compound **22** (Scheme 9).

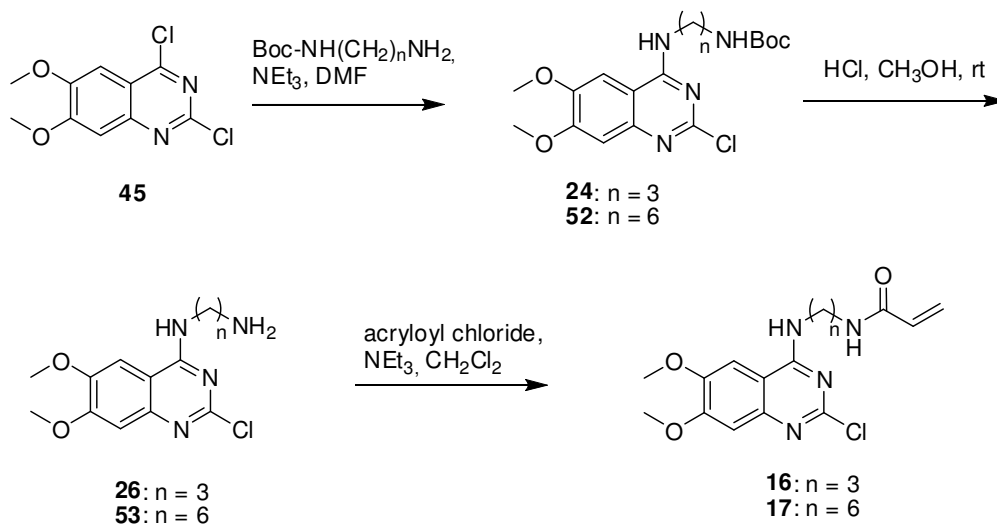
Scheme 1



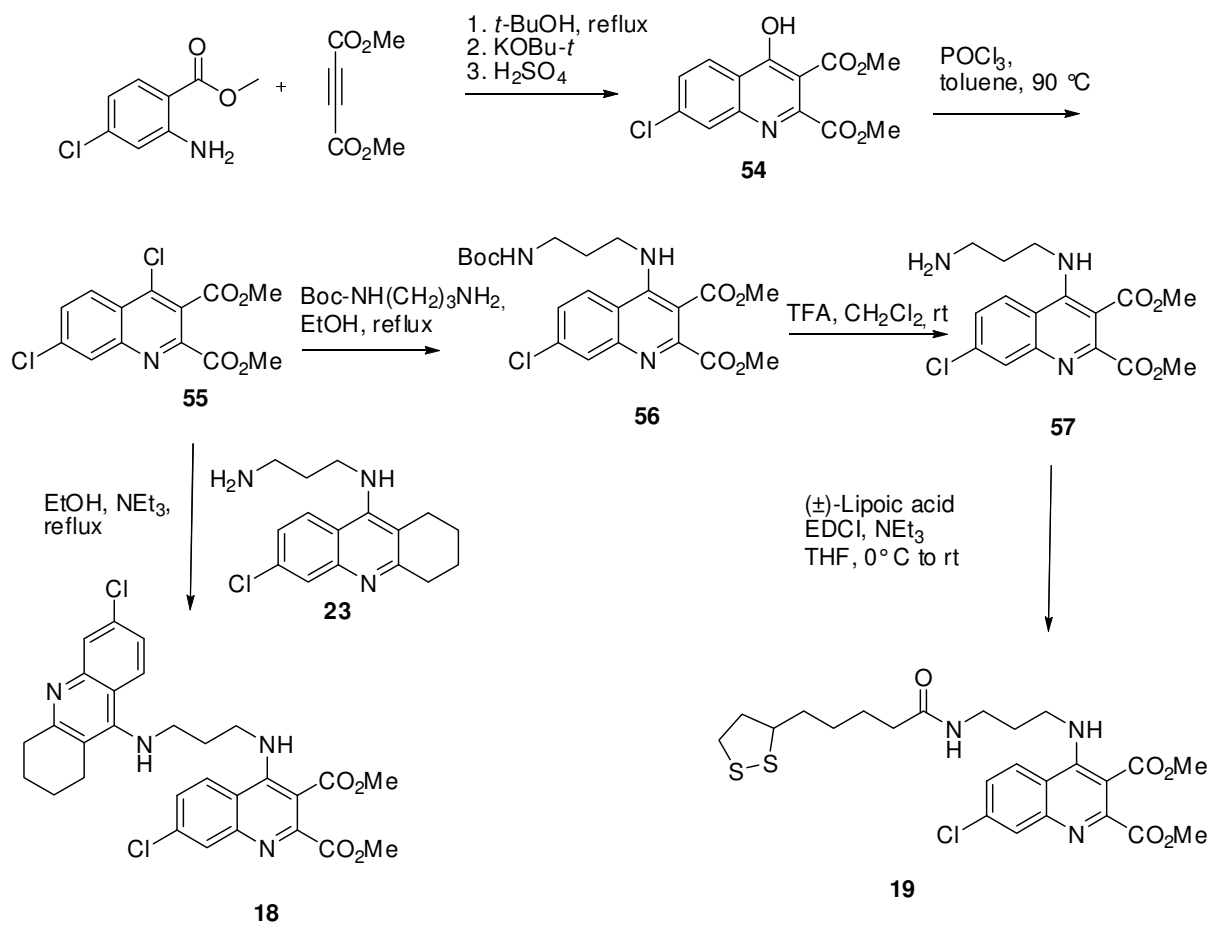
Scheme 5



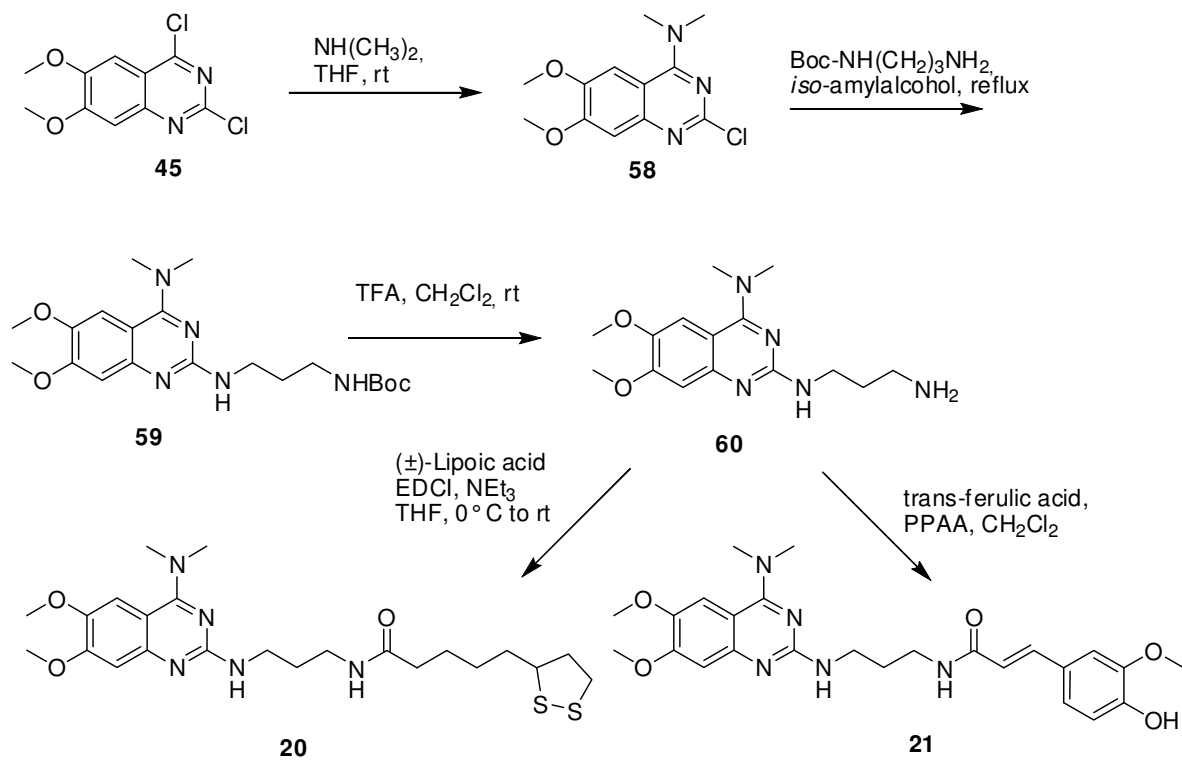
Scheme 6



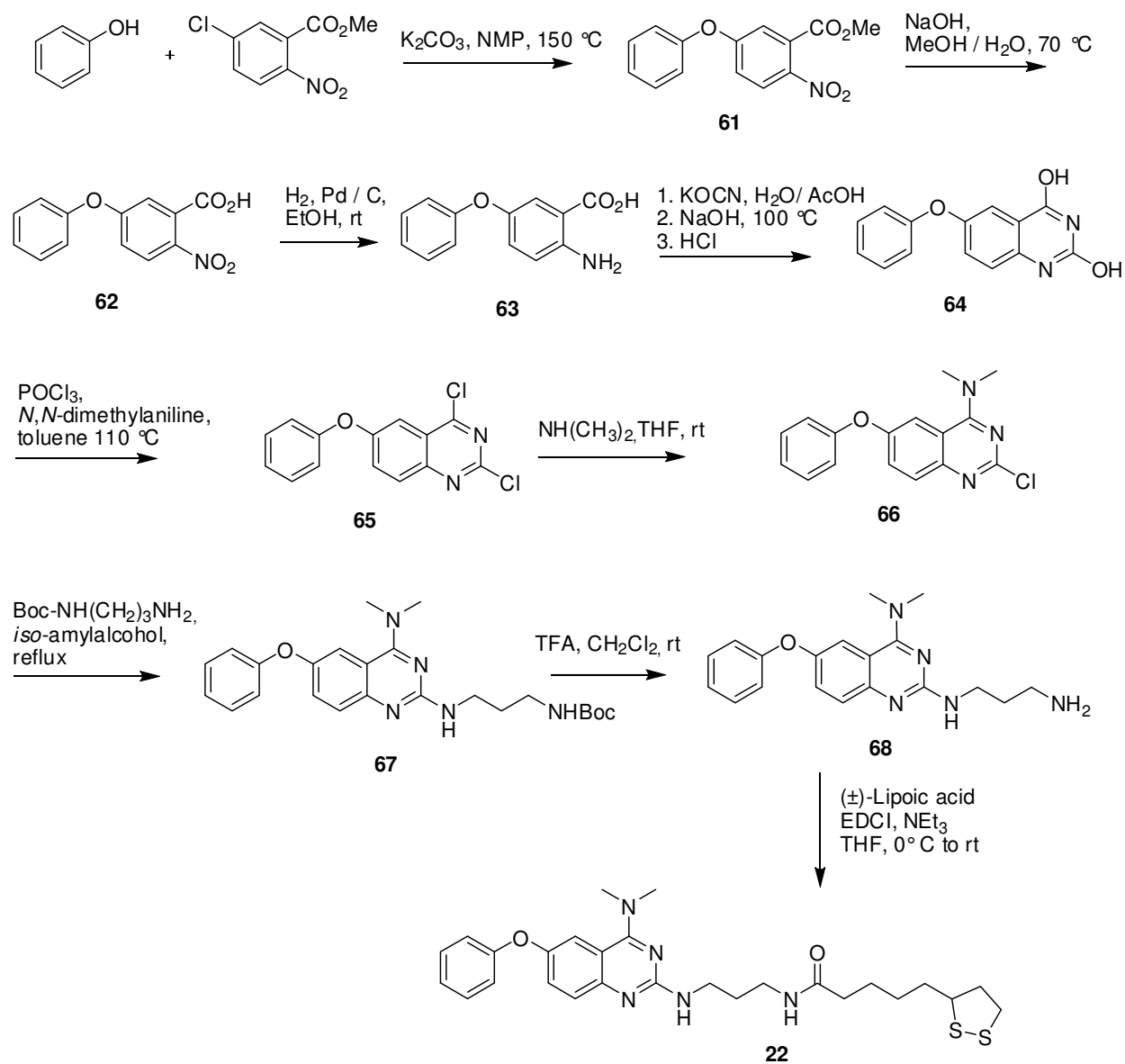
Scheme 7



Scheme 8



Scheme 9



3.2 Synthesis of δ -aminocyclohexane carboxylic acid-based BACE1 inhibitors

The approach followed to get the δ -aminocyclohexane carboxylic acid motif **A** (Fig.1) was based on an organocatalytic asymmetric conjugate addition of nitroalkanes to cyclohexenone.

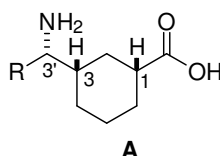


Figure 1. δ -Aminocyclohexane carboxylic acid motif **A**

Addition of 1-nitropropane and 1-nitrobutane to cyclohexenone **69** in the presence of 10 mol % equivalent of D-proline and a stoichiometric amount of *trans*-2,5-dimethylpiperazine in reagent grade CHCl_3 for 48 hours gave, in each case, a separable mixture of isomers in 85-97% combined yield (Scheme 10, Table 1). The less polar (*S,S*)-propyl *syn*-isomer **70** (89% ee), and the more polar (*S,R*)-propyl *anti*-isomer **71** (74% ee), (1:2.2 ratio by ^1H NMR and HPLC, respectively), were each separated and characterized. A similar protocol with 1-nitrobutane gave the less polar *syn*-(*S,S*)-butyl isomer **72** (89% ee) and the more polar *anti*-(*S,R*)-isomer butyl **73** (71% ee) in a ratio of 1:2, respectively (Table 1).

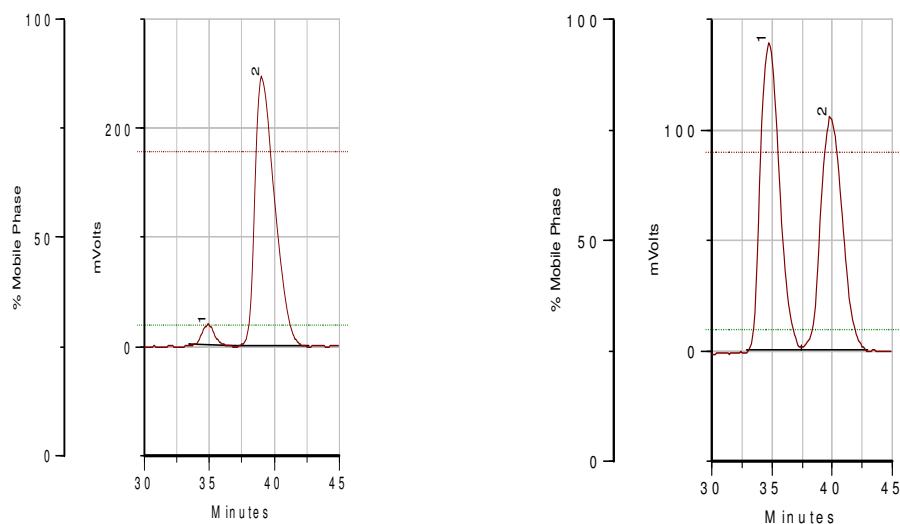
Table 1. Catalytic enantioselective addition of nitroalkane to cyclohexenone catalyzed by D-proline

R	Yield (%)	dr ^a (<i>syn:anti</i>)	ee (%) ^b	
			<i>syn</i>	<i>anti</i>
Ethyl	84	1 : 2.2	89	74
Propyl	97	1 : 2.0	89	71

^a obtained by RP Chiral HPLC and ^1H -NMR at 700 MHz

^b obtained by RP Chiral HPLC (see Experimental Section)

The individual enantiomeric purities were determined by HPLC analysis on a chiral column, using racemic mixtures as controls. An example of HPLC traces of enantioenriched mixture of compounds **70** is shown in figure 2 (see Experimental Section for details of all isomers).



Peak Name	R. Time	Area	Area %
1	34.90	2500539.25	5.39
2	39.02	43910696.00	94.61

Peak Name	R. Time	Area	Area %
1	34.76	25787958.00	53.57
2	39.86	22348432.00	46.43

Figure 2. HPLC profiles of the less polar *syn*-isomer (*S*)-3-((*S*)-1-Nitropropyl)cyclohexanone **70** (enantioenriched in the left side, racemic in the right side). Enantiomeric excesses were determined by RP-HPLC analysis with CHIRALPAK AD-RH column (\varnothing 0.46 cm \times 15 cm) eluting in isocratic mode with 0.1 % Formic acid in CH₃CN / 0.1 % Formic acid in H₂O (30:70), flow = 0.5 mL/min, retention times minor: 34.90 min, major: 39.02 min.

The definitive stereochemical identity of the desired 3*S*,3'*S*-diastereomer was established by correlation with authentic samples obtained from a previous established route starting with the chiral aminoacids as well as from available X-ray structures.

The individual nitroketone less polar *syn*-isomers **70** and **72** were each transformed to the corresponding ketene dithioacetals **74** and **75** (Scheme 10). Methanolysis of **74** and **75** in the presence of HgCl₂ gave the methyl esters **76**, **77**, and **78**, **79**, respectively. Attempts to equilibrate the (*S*,*R*)-isomers **77** and **79** to the desired 1,3-*cis*-(*S*,*S*)-isomers **76** and **78** without affecting the stereochemistry of the carbon centre containing the nitro group were unsuccessful.

In order to establish definitive configurational identity for the desired (*S,S*)-compounds **77** and **78**, they were each subjected to reduction in the presence of 10% Pd/C and ammonium formate, and the resulting amines were *N*-acetylated to give **80** and **81**, respectively. The alkaline hydrolysis of ester and following coupling with the hydroxyethylene based amine gave final compounds **28** and **29**.

The individual more polar *anti*-nitroketone isomers **71** and **73**, as well as their conversion to ketene dithioacetals and methyl esters were also achieved, although these "undesired" diastereomeric nitro alkyl esters were not pursued further in the context of the present peptidomimetic BACE1 project.

References

- ¹ Ciszewska, G.; Pfefferkorn, H.; Tang, Y.S.; Jones, L.; Tarapata, R.; Sunay Ustun B. Synthesis of tritium, deuterium, and carbon-14 labeled (S)-N-ethyl-N-methyl-3-[1-(dimethylamino)ethyl]carbamic acid, phenyl ester, (L)-2,3-dihydroxybutanedioic acid salt (SDZ ENA 713 hta), an investigational drug for the treatment of Alzheimer's Disease *Journal of Labelled Compounds & Radiopharmaceuticals*, **1997**; *39*, 651-668.
- ² Grethe, G.L.; His, L.; Uskokovic, M.; Brossi, A. Syntheses in the isoquinoline series. Synthesis of 2,3-dihydro-4(1H)-isoquinolones *J. Org. Chem.* **1968**, *33*, 491-494.
- ³ Bolognesi, M.L.; Banzi, R.; Bartolini, M.; Cavalli, A.; Tarozzi, A.; Andrisano, V.; Minarini, A.; Rosini, M.; Tumiatti, V.; Bergamini, C.; Fato, R.; Lenaz, G.; Hrelia, P.; Cattaneo, A.; Recanatini, M.; Melchiorre, C. Novel Class of Quinone-Bearing Polyamines as Multi-Target-Directed Ligands To Combat Alzheimer's Disease. *J. Med. Chem.* **2007**, *50*, 4882-4897.
- ⁴ Bridges, A.J.; Zhou, H.; Cody, D.R.; Rewcastle, G.W.; McMichael, A.; Showalter, H.D.H.; Fry, D.W.; Kraker, A.J.; Denny, W.A. Tyrosine kinase inhibitors. 8. An unusually steep structure-activity relationship for analogues of 4-(3-bromoanilino)-6,7-dimethoxyquinazoline (PD 153035), a potent inhibitors of the epidermal growth factor receptor. *J. Med. Chem.* **1996**, *39*, 267-276.
- ⁵ Schwarz, M. *n*-Propane phosphonic acid anhydride. A condensation reagent. *Synlett* **2000**, *9*, 1369.
- ⁶ Dunn, J.P.; Goldstein, D.M.; Stahl, C.M.; Trejo-Martin, T.A. Substituted quinazoline compounds useful as p38 kinase inhibitors. *US Patent* 2004/0209904-A1 (Oct. 21, **2004**).

Chapter 4

Biology

All the compounds were tested for *in vitro* BACE1 inhibitory activity in different protocols of FRET (fluorescence resonance energy transfer) enzymatic assays, varying the nature of substrates and enzyme origin, in order to assess the optimal conditions for a reliable enzymatic test. Moreover, the most active compounds of the series were evaluated also towards cathepsin D (CatD) in order to test their selectivity.

In view of MTDLs drug design approach, the majority of compounds were also evaluated towards the AChE and BChE inhibitory activity, and some of them were investigated in the A β aggregation inhibition test induced by AChE.

In addition, lipocrine (**6**) and hybrid compounds **8-10** were the subjects of an *in vivo* pharmacological investigation in AD mice model.

4.1. BACE1 inhibition

BACE1 activity was measured with a FRET analysis method using a multi well spectrofluorimeter. The peptide substrate of the analyses mimics the APP protein which is the natural substrate of BACE1. The synthetic substrate contains two fluorogenic groups: a group that donates fluorescence (D) and a group that quenches fluorescence (A) as depicted in figure 1. The weakly fluorescent substrate becomes highly fluorescent upon enzymatic cleavage; the increase in fluorescence is linearly related to the rate of proteolysis.

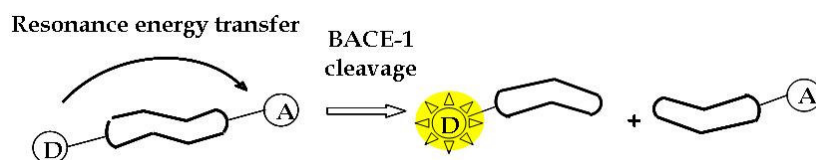


Figure 1. Schematic representation of a FRET-based enzymatic assay.

4.1.1. Method A: Panvera substrate and Invitrogen enzyme

The inhibitory potency against recombinant human BACE1 for compounds **1-10** was evaluated by method (A) based on FRET assay using Rhodamine-Glu-Val-Asn-Leu-Asp-Ala-Glu-Phe-Lys-quencher as fluorogenic substrate (Panvera peptide harbouring rhodamine as donating fluorescent group (Fig. 2)).

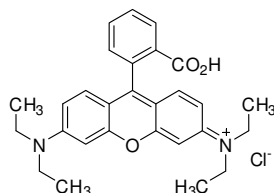


Figure 2. Rhodamine as fluorescence donating group

Purified Baculovirus-expressed BACE1 and rhodamine derivative substrate were purchased from Panvera (Madison, WI, U.S.).

The inhibitory potency of compounds was expressed as IC_{50} values or as a certain % of enzyme inhibition, which represent the concentration of inhibitor required to decrease the maximum enzymatic activity by 50%. Enzyme activity was determined reading the fluorescence emitted by rhodamine at $\lambda = 590$ nm.

Assays were done with a blank containing all components except BACE1 in order to account for non enzymatic reaction. The reaction rates were compared and the percent inhibition due to the presence of test compounds was calculated. Each concentration was analyzed in triplicate. The percent inhibition of the enzyme activity due to the presence of increasing test compound concentration was calculated by the following expression: $100 - (v_i/v_o \times 100)$, where v_i is the initial rate calculated in the presence of inhibitor and v_o is the enzyme activity. To demonstrate inhibition of BACE1 activity, a statine-derived inhibitor was serially diluted into the reactions' wells ($IC_{50} = 18 \pm 1$ nM) or inhibitor IV (Calbiochem, Darmstadt, Germany) was used as reference inhibitor ($IC_{50} = 12.89$ nM) (Fig. 3).

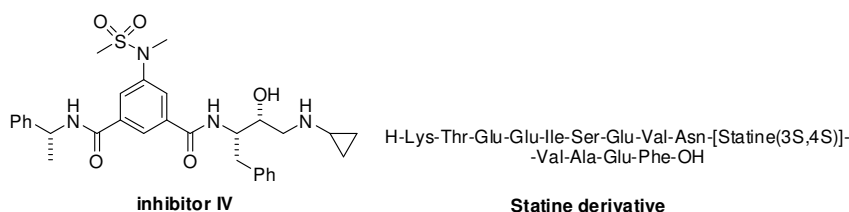


Figure 3. Reference compounds inhibitor IV and statine derivative.

4.1.2. Method B: Casein-FITC substrate and Invitrogen enzyme¹

The inhibitory potency against recombinant human BACE1 for compounds **6, 11-19, 22** and

24-27 was evaluated by a modified method (**B**) employing bovine casein labelled with Fluorescein isothiocyanate (Casein-FITC) as a fluorogenic substrate (Fig.4). The enzyme BACE1 was purchased from Panvera (Madison, WI, U.S).

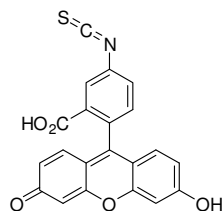


Figure 4. Fluorescein isothiocyanate (FITC) as fluorescence donating group.

The inhibitory potency of compounds was expressed as IC_{50} values or as a certain % of enzyme inhibition. Enzyme activity was determined reading the fluorescence emitted by FITC at $\lambda = 538$ nm.

Assays were done as in method A. To demonstrate inhibition of BACE1 activity donepezil was used as reference inhibitor ($IC_{50} = 586$ nM) (Fig. 5).

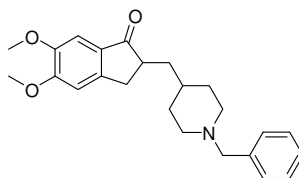


Figure 5. Reference inhibitor: donepezil.

4.1.3. Method C: M-2420 substrate and Sigma enzyme

The inhibitory potency against recombinant human BACE1 for compounds **6**, **11**, **13**, **15**, **20-22** was evaluated by a third method (**C**) based on MCA-SEVNLDAEFK(DNP)-CONH₂ (Fig.6) as fluorogenic substrate called M-2420 that was purchased from Bachem (Torrance, CA, United States). Human recombinant BACE1 was purchased from Sigma Aldrich (Milan, Italy).

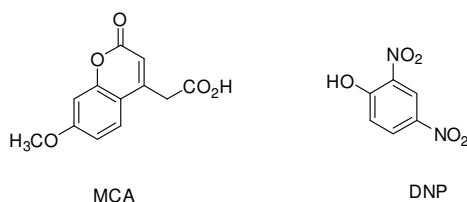


Figure 6. Fluorogenic residues of substrate M-2420

The inhibitory potency of compounds was expressed as IC_{50} values or as a certain % of enzyme inhibition. Enzyme activity was determined reading the fluorescence emitted by the fluorophore at $\lambda = 405$ nm. Assays were done as in method A. To demonstrate inhibition of

BACE1 activity, inhibitor IV (Calbiochem, Darmstadt, Germany) (Fig. 3) was used as reference inhibitor ($IC_{50} = 13.61$ nM).

4.1.4. BACE1 fluorogenic substrate evaluation

The kinetic parameters for the three enzymatic assays were evaluated in order to assess the most reliable assay. Specificity constants (k_{cat}/K_M) were determined under pseudo-first-order conditions, via the “progress curve method”² using a substrate concentration (0.04 or 0.05 μ M) far below K_M , and a final enzyme concentration of 10 or 34 nM (E_0). The {time; fluorescence} data pairs were fitted to equation ($F(t) = \Delta F [1 - \exp(-k_{obs} \cdot t)] + F_{init}$), and the apparent first-order rate constant (k_{obs}) was calculated. The second-order rate constant, k_{cat}/K_M values were calculated according to the following equation: $k_{cat}/K_M = k_{obs}/[E_0]$. Quenching efficiency was determined according to the equation: $q.e.(%) = (1 - F_0/F_1) \times 100$, were $F_0 = F_{init} - F_{buffer}$ and $F_1 = F_{max} - F_{buffer}$.

4.2. Cathepsin D inhibition

Cathepsin D (CatD) activity was measured with a FRET analysis method using a multi well spectrofluorimeter. The inhibitory potency against recombinant for compounds **11**, **14** and **15** was evaluated by a modified B method employing bovine casein labelled with Fluorescein isothiocyanate (Casein-FITC) as a fluorogenic substrate. The inhibitory potency of compounds was expressed as IC_{50} values or as a certain % of enzyme inhibition. Enzyme activity was determined reading the fluorescence emitted by FITC at $\lambda = 538$ nm. Assays were done as in method A. To demonstrate inhibition of CatD activity, pepstatin A was used as a reference inhibitor ($IC_{50} = 0.011 \pm 0.002$ μ M).

4.3. AChE and BChE inhibition

The inhibitory potency against recombinant human AChE and isolated serum BChE for compounds **1-10**, **11**, **13**, **15-19**, **24** and **25** was evaluated by studying the hydrolysis of acetylthiocholine (ATCh) following the colorimetric method of Ellman.³ The inhibitory potency of compounds was expressed as pIC_{50} values, which represent negative logarithm of the

concentration of inhibitor required to decrease the maximum enzymatic activity by 50%. Enzyme activity was determined through the revelation of the formation of an anionic coloured molecular species (2-nitro-4-thiobenzoate, $\lambda_{\text{max}} = 412 \text{ nm}$), which is obtained from the reaction of thiocholine, a product of the enzymatic hydrolysis of acetylthiocholine (substrate of AChE) or butyrylthiocholine (substrate of BChE), and 5,5'-dithio-bis-nitrobenzoic acid (Ellman's reactive). The variation of absorbance at $\lambda = 412 \text{ nm}$ (that is the variation of the absorbance of 2-nitro-4-thiobenzoate per minute, $\Delta A/\text{min}$, enzymatic speed) depends on the substrate concentration, and on the enzymatic activity of AChE or BChE, according to the Michaelis-Menten kinetic.

The nature of AChE inhibition caused by the synthesized compounds was investigated by the graphical analysis of steady-state human AChE inhibition data of **5**. Information regarding the ligand-enzyme interaction was obtained through the determination of K_i ,⁴ which describes the state of equilibrium between the free enzyme, the inhibitor, and the enzyme-inhibitor complex.

4.4. Inhibition of AChE-induced A β aggregation

Anti-aggregation action of compounds **6-10** and **23** was determined in comparison with well-known AChEIs, through a fluorimetric method adapted from Inestrosa.^{5,6} This assay is able to highlight the ability of AChE (recombining human, EC 3.1.1.7) to promote the formation of A β fibrils. Thioflavin-T interacts selectively with amyloid peptide in the β conformation forming a fluorescent complex ($\lambda_{\text{em}} = 490 \text{ nm}$). A compound able to interfere with A β fibrils formation would reduce the fluorescent signal, and this signal is directly proportional to the log of the concentration of the tested compound. The anti-aggregation action is expressed as the inhibitor concentration able to reduce the fluorescent signal of 50%.

4.5. Animal studies

In order to check the efficacy of **6**, **8-10** and **23** in improving the degeneration due to AD, these compounds were administered to anti-NGF mice. Recovery of cholinergic neurons and blockade of tau hyperphosphorylation were studied as anti-AD properties.

This animal model (anti-NGF)⁷ presents a phenotype highly similar to AD in man. In particular, the model consists of a transgenic mouse which expresses antibodies for the nervous growth factor (NGF), and consequently shows an extensive loss of neurones in the cortex,

formation of A β plaques and of intracellular neurofibrillary tangles, as well as behavioural dysfunctions. In particular, in order to produce anti-NGF transgenic mice (AD11), the variable regions in the light and heavy chains of the anti-NGF monoclonal antibody α D11 were linked to the constant human region κ and γ 1, to give the man/rat chimeric antibody α D11, and they were then placed under the transcriptional control of the promoter of the precocious region of the human cytomegalovirus (CMV). Mice expressing functional anti-NGF antibodies (AD11 mice) were obtained by crossing mice that expressed the heavy chain (CMV-VH α D11).

References

- ¹ Mancini, F.; Naldi, M.; Cavrini, V.; Andrisano, V. Multiwell fluorometric and colorimetric microassays for the evaluation of beta-secretase (BACE1) inhibitors. *Anal. Bioanal. Chem.* **2007**, *388*, 1175-1183.
- ² Paschalidou, K.; Neumann, U.; Gerharts, B.; Tzougraki, C. Highly sensitive intramolecularly quenched fluorogenic substrates for renin based on the combination of L-2-amino-3-(7-methoxy-4-coumaryl)propionic acid with 2,4-dinitrophenyl groups at various positions. *Biochem. J.* **2004**, *382*, 1031-1038.
- ³ Ellman, G.L., Courtney, K.D., Andres, V., Featherstone, R.M. *Biochem. Pharmacol.* **1961**, *7*, 88-95.
- ⁴ Dixon, M., Webb, E.C. *Enzymes*, Second Edition **1964**, Chapter VIII, p. 315, Longmans, Green and Co Ltd, London, UK.
- ⁵ Inestrosa, N.C., Alvarez, A, Perez, C.A., Moreno, R.D., Vicente, M., Linker, C., Casanueva, O.I., Soto, C., Garrido, J. *Neuron* **1996**, *16*, 881-891.
- ⁶ Bartolini, M., Bertucci, C., Cavrini, V., Andrisano, V. *Biochem. Pharmacol.* **2003**, *65*, 407-416.
- ⁷ Ruberti, F.; Capsoni, S.; Comparini, A.; Di Daniel, E.; Franzot, J.; Gonfloni, S.; Rossi, G.; Berardi, N.; Cattaneo, A. Phenotypic knockout of nerve growth factor in adult transgenic mice reveals severe deficits in basal forebrain cholinergic neurons, cell death in the spleen, and skeletal muscle dystrophy. *J. Neurosci.* **2000**, *20*, 2589-2601.

Chapter 5

Results and discussion

In order to search new chemical entities able to inhibit BACE1, we designed and synthesised novel heterocyclic compounds related to lipocrine, one of the first examples of MTDLs for AD.¹

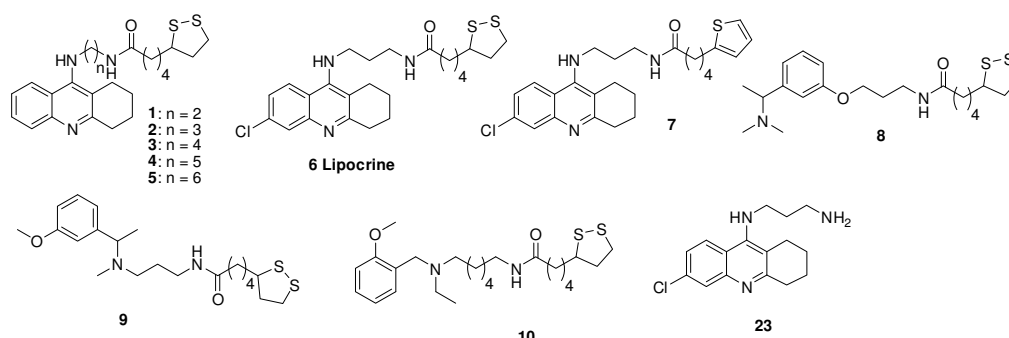
5.1. Biological evaluation of tetrahydroacridine-, rivastigmine- and caproctamine-based compounds (1-10)

Modifying the chain length between the two nitrogen atoms bearing tetrahydroacridine moiety and lipoic acid of lipocrine led to compounds **1-5** and **7**, respectively. Modifications to the tetrahydroacridine moiety afforded hybrid compounds **8** and **9**, bearing the structural features of rivastigmine and lipoic acid, and compound **10** incorporating caproctamine and lipoic acid fragments. All of them were evaluated as BACE1 inhibitors in a FRET (fluorescence resonance energy transfer) enzymatic assay (Method A, for details see Section 4.1.1) and as AChE and BChE inhibitors. Moreover, some of them were evaluated as A β anti-aggregating compounds and were the subjects of an *in vivo* pharmacological investigation in AD mice model.

As shown in Table 1, among the tetrahydroacridine-based compounds **1-6**, derivatives **1** and **2**, bearing a diaminoethylene and diaminopropylene spacer, are endowed with an inhibitory activity in submicromolar range towards BACE1, whereas longer spacers are detrimental for activity. The insertion of a chlorine atom into the acrydine system, affording lipocrine (**6**), led to a very good profile of inhibitory activity towards BACE1, quantified as a 15-fold increase relative to its analogue **2**. In order to define whether the dithiolane group is fundamental for BACE1 activity, the intermediates tacrine and **23** were also evaluated, displaying a total absence of activity. Moreover, the substitution of dithiolane residue with thiophene led to compound **7** which lacked affinity for the enzyme, strengthened the hypothesis that lipoic acid is a key fragment for BACE1

inhibition. As already published,¹ given that the tetrahydroacridine-based derivatives **1-5** and **7** bear the tacrine pharmacophore, are endowed with a good activity profile towards AChE and BChE. To allow comparison of the results shown in Table 1, **23**, tacrine, and LA were used as reference compounds. It is evident that all compounds were effective inhibitors of AChE and BChE, significantly more potent than prototype tacrine. Among compounds **1-5**, optimum inhibition of AChE was observed for **2**, having propylene chain unit. As expected for AChE inhibition,² the insertion of a chlorine atom into the acrydine moiety, as in lipocrine (**6**), produced an 85-, 1676-, and 28-fold increase in AChE inhibition relative to **23**, tacrine, and **2**, respectively.

As one would expect, LA did not inhibit neither AChE nor BACE1 enzyme. On the other hand, the hybrid compounds between rivastigmine and LA **8** and **9**, respectively, displayed a micromolar range of AChE inhibitory activity and a submicromolar range of BACE1 inhibitory activity. The caproctamine-based compound **10** displayed a modest AChE inhibition and a submicromolar BACE1 inhibition (Table 1).

Table 1. AChE, BChE, and BACE1 inhibitory activities of derivative **1-10** and reference compounds.

Compound	n	R	IC ₅₀ ± SEM (nM)		
			AChE	BChE	BACE1 ^a
1	2	H	97.0 ± 3.6	47.5 ± 1.8	772.3 ± 20.7
2	3	H	6.96 ± 0.45	12.0 ± 0.6	867.7 ± 11.2
3	4	H	35.2 ± 2.2	5.04 ± 0.32	> 2000
4	5	H	38.4 ± 2.3	1.48 ± 0.35	> 2000
5	6	H	30.1 ± 1.5	3.24 ± 0.29	> 2000
6 (Lipocrine)	3	Cl	0.253 ± 0.016	10.8 ± 2.5	IC ₅₀ = 57.0 ± 12.0
7			2.66 ± 0.23	30.6 ± 0.7	> 2000
8			25200 ± 1700	82400 ± 6500	
9			74100 ± 3700	398 ± 24	846.5 ± 53.9
10			256 ± 8	2490 ± 110	929.1 ± 28.7
23			21.5 ± 0.8	2580 ± 60	> 3500
Tacrine			424 ± 21	45.8 ± 3.0	inactive at 4000 ^b
Lipoic acid			>1000000	>1000000	> 500

^a = IC₅₀ values obtained by FRET assay following Method A. (for details See Section 4.1.1)

^b = maximum solubility concentration to perform the analysis

Furthermore, as already cited, lipocrine inhibited both the active site and a second distal site of the enzyme. Once verified that lipocrine may interact also with PAS of AChE, it was verified whether there is a concomitant inhibition of Aβ aggregation induced by AChE. As shown in Table 2, it turned out that tacrine and LA, i.e., the pharmacophoric moieties combined in lipocrine, were not able to inhibit at 100 μM the Aβ aggregation induced by AChE, whereas compound **23** at 100 μM caused only a 25 ± 5% inhibition. In contrast, lipocrine was only 3-fold less potent than propidium, used as reference compound being the most potent inhibitor of AChE-induced Aβ aggregation so far available, as revealed by their IC₅₀ values. Furthermore, lipocrine was significantly more potent than all the other AChE inhibitors ever tested.³ Clearly, this finding, together with the results observed for **23**, tacrine, and LA separately, is relevant

because an association of 100 μM tacrine and 100 μM LA or 100 μM **23** and 100 μM LA produced only a weak inhibition of AChE-induced A β aggregation, suggesting that marked A β aggregation inhibition may be achieved only when the two prototypes are combined into the same structure, as in lipocrine.

Lipocrine turned out to be the most potent A β anti-aggregating compound of the series, exhibiting IC₅₀ value around 45 μM . Compounds **7** and **11** exhibited lower, but still significant, A β anti-aggregating effects, while the derivatives bearing methoxybenzylamino groups **8-10** in replacement of the tacrine unit, were weak inhibitors of the AChE-induced A β aggregation.

Table 2. Inhibition of A β 40-aggregation induced by AChE.

Compound [] 100 μM	Inhibition % \pm SEM
Tacrine	< 5
Lipoic acid	< 5
Lipoic acid + Tacrine	15 \pm 6
23	25 \pm 5
Lipoic acid + 23	30 \pm 7
6 (lipocrine)	61.8 \pm 0.8 (IC ₅₀ = 45.0 \pm 14.6 μM)
propidium	(IC ₅₀ = 12.5 \pm 0.5 μM)
7	24.1 \pm 5.7
8	9.0 \pm 6.6
9	15.6 \pm 7.8
10	16.8 \pm 2.2

Animal Studies

As already cited, some selected compounds of the series were the subject of a preliminary *in vivo* pharmacological investigation in AD mice model (For details see Section 4.5). In order to check the efficacy of **6**, **8-10** and **23** in improving the degeneration due to AD, these compounds were administered to anti-NGF mice. Recovery of cholinergic neurons and blockade of tau hyperphosphorylation were studied as anti-AD properties.

The dosage (expressed in mM of solution) was chosen in order to demonstrate that the efficacy of these compounds is better than that the efficacy of the compounds from which they are derived. For this reason Memoquin⁴, which is known for improving all the phenotypic markers in anti-NGF (AD11), was administered in a dose which, based on previous studies, was expected to give only a partial recovery of the phenotype. Moreover, to assess the direct contribution of lipoic acid (LA) alone, in comparison with that of the conjugate of lipoic acid, and to exclude that the effect observed might be due to LA, this compound was administered to the anti-NGF mice as well. The treatment pattern is shown on Experimental section (See Section 6.2.5).

In particular, the administration of LA, tacrine, lipocrine, **8**, rivastigmine and Memoquin did not allow the complete recovery of the cholinergic deficit of the anti-NGF mice. The only compound that allowed a significant recovery, from a statistical point of view, of a number of cholinergic neurones in the basal forebrain was caproctamine-based derivative **10** ($P < 0.05$, Fig. 1). All the compounds administered recovered the phospho-tau phenotype, with the exception of **23** (Figure 2).

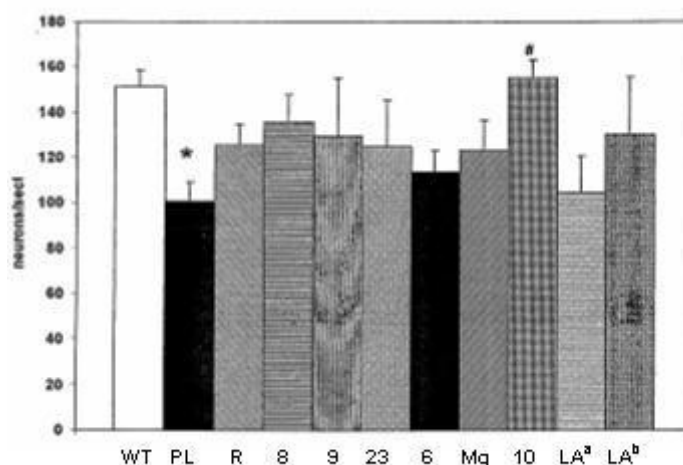


Figure 1. Recovery of cholinergic neurons in AD mice [WT = wild type mice, PL = AD11 mice + placebo, R = AD11 mice + rivastigmine (0.5 mg/Kg/die), 8 = AD11 mice + compound **8** (0.52 mg/Kg/die), 9 = AD11 mice + compound **9** (0.52 mg/Kg/die), 23 = AD11 mice + compound **23** (0.1 mg/Kg/die), 6 = AD11 mice + compound **6** (0.165 mg/Kg/die), Mq = AD11 mice + Memoquin (3.5 mg/Kg/die), 10 = AD11 mice + compound **10** (3.5 mg/Kg/die), LA^a = AD11 mice + LA (0.254 mg/Kg/die), LA^b = AD11 mice + LA (0.114 mg/Kg/die)]

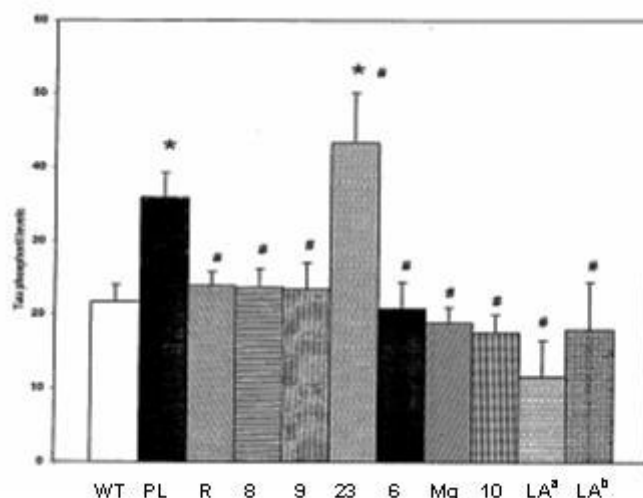


Figure 2 . Recovery of phosphotau phenotype in AD mice [WT = wild type mice, PL = AD11 mice + placebo, R = AD11 mice + rivastigmine (0.5 mg/Kg/die), 8 = AD11 mice + compound **8** (0.52 mg/Kg/die), 9 = AD11 mice + compound **9** (0.52 mg/Kg/die), 23 = AD11 mice + compound **23** (0.1 mg/Kg/die), 6 = AD11 mice + compound **6** (0.165 mg/Kg/die), Mq = AD11 mice + Memoquin (3.5 mg/Kg/die), 10 = AD11 mice + compound **10** (3.5 mg/Kg/die), LA^a = AD11 mice + LA (0.254 mg/Kg/die), LA^b = AD11 mice + LA (0.114 mg/Kg/die)]

5.2. Biological evaluation of 4-amino-quinoline- and 4-amino-quinazoline-based compounds (11-27)

Modification accomplished to the heterocyclic core of lipocrine gave a series of compounds bearing 2-substituted-4-amino-6,7-dimethoxyquinazoline **11-19** and **24-27** (Table 3), that were assayed in modified FRET method (Method B) employing bovine casein labelled with fluorescein isothiocyanate (Casein-FITC) as a fluorogenic substrate. Casein-FITC was selected as new potential substrate of BACE1 because it is already known to be a selective substrate for proteases, it is easily available and it is convenient and versatile for the activity of other aspartic proteases, such as CatD.⁵ Fluorescein isothiocyanate is a good label for proteins because it is highly fluorescent, and it reacts with the amino groups of most proteins in a simple reaction that yields the fluorescein thiocarbamoyl derivative.

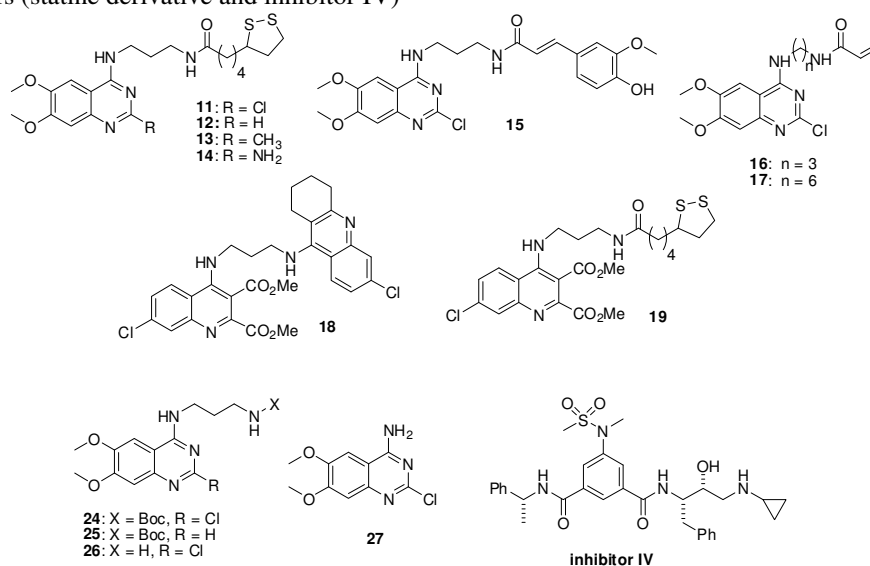
The activity profiles obtained referring to this new method (Method B)⁶ guided the modifications carried out in the quinazoline-based compounds. In addition, inhibitory activity towards CatD was also evaluated for the most potent compounds.

As shown in Table 3, the replacement of the tetrahydroacridinic moiety of lipocrine with 2-chloro-4-amino-6,7-dimethoxyquinazoline residue led to a more potent compound (**11**). Since

this new lead structure exhibited an enhanced BACE1 inhibitory activity relative to lipocrine and a moderate selectivity over CatD ($IC_{50} = 78$ nM), it was chosen for further structure-activity relationship studies.

The replacement of the 2-chloro substituent of **11** with H, CH₃, and NH₂ groups gave compounds **12-14**, respectively, endowed with a lower BACE1 inhibitory activity. In addition, structural modifications on the lateral chain confirmed the importance of the lipoic acid residue, as its replacement with acrylic acid or *tert*-butylcarbonic acid led to less potent analogues (**16**, **17**, **24** and **25**). The amine intermediates **26** and **27** did not exert a remarkable inhibition revealing the importance of lateral chain. Finally, the most intriguing result was the disclosure that the insertion of a different antioxidant residue, such as *trans*-ferulic acid in place of lipoic acid, led to compound **15** with a 9-fold increased selectivity over CatD while retaining a nanomolar BACE1 activity compared to prototype **11** (Table 3).

The replacement of the lipoic acid residue of lipocrine with the 7-chloroquinoline-2,3-dicarboxylic acid dimethyl ester gave compound **18** endowed with a very poor BACE1 inhibitory activity, whereas the substitution of tetrahydroacridinic ring of lipocrine with the same moiety (7-chloroquinoline-2,3-dicarboxylic acid dimethyl ester) provided a less potent analogue **19**.

Table 3. BACE1 and CatD inhibitory activity in different assays by compounds **11-19**, **24-27**, lipocrine and reference inhibitors (statine derivative and inhibitor IV)

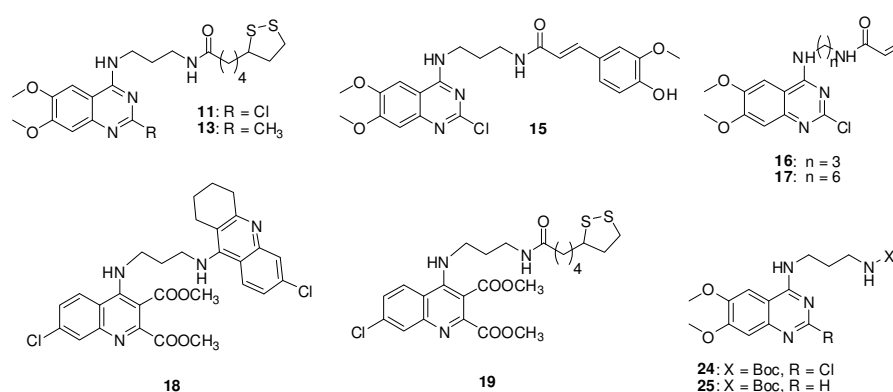
Compound	BACE1 inhibition		CatD inhibition
	Method A Rhodamine Invitrogen substrate	Method B Casein-FITC substrate	Casein-FITC substrate
11	IC ₅₀ = 17.9 ± 3.9 nM	IC ₅₀ = 18 nM	78 nM
12	nd	26 % at 500 nM	
13	no inhibition at 1.13 μM	no inhibition at 18 nM	
14	nd	30 % at 18 nM	18 % at 70 nM
15	10.8 % at 1.05 μM no inhibition at 18 nM	IC ₅₀ = 18 nM	154 nM
16	nd	45 % at 500 nM	
17	nd	20 % at 500 nM	
18	nd	9.04% at 0.493 μM	
19	nd	IC ₅₀ = 490 nM	
24	nd	30 % at 500 nM	
25	nd	22 % at 500 nM	
26	nd	no inhibition at 116 nM	
27	nd	no inhibition at 116 nM	
6 (lipocrine)	IC ₅₀ = 57.0 ± 12.0 nM	IC ₅₀ = 57 nM	
Inhibitor IV	IC ₅₀ = 12.89 nM	IC ₅₀ = 48.86 nM	
Statine derivative^a	IC ₅₀ = 18.0 ± 1.0 nM	IC ₅₀ = 61 ± 2.0 nM	

nd = not detected

^a = (H-Lys-Thr-Glu-Glu-Ile-Ser-Glu-Val-Asn-[Statine(3S,4S)]-Val-Ala-Glu-Phe-OH)

Some selected compounds were also evaluated towards AChE, in view of the fact that such compounds could be seen as molecular simplifications of lipocrine and the results are reported in Table 4. All the quinazoline-based derivatives do not show interesting AChE activity profiles, except the tacrine-based compound **18**. As expected, only compound **18**, bearing the 6-chlorotacrine residue, maintained a strong affinity for AChE, revealing only a 25-fold reduced potency compared to lipocrine, and a good selectivity towards BChE (Table 4).

Table 4. AChE inhibitory activities by 4-amino-quinazoline (**11**, **13**, **15-17**, **24** and **25**) and 4-amino-quinoline derivatives (**18** and **19**) and reference compound lipocrine



Compound	IC ₅₀ AChE M	IC ₅₀ BChE M
11	(1.92 ± 0.25) 10 ⁻⁴	
13	(6.21 ± 0.10) 10 ⁻⁵	
15	1.10 10 ⁻³	
16	(6.94 ± 0.14) 10 ⁻⁴	
17	(3.14 ± 0.55) 10 ⁻⁴	
18	(6.41 ± 0.14) 10 ⁻⁹	(3.70 ± 0.14) 10 ⁻⁶
19	(1.91 ± 0.02) 10 ⁻⁵	
24	(5.70 ± 0.45) 10 ⁻⁴	
25	(3.75 ± 0.58) 10 ⁻⁴	
6 (lipocrine)	(2.53 ± 0.16) 10 ⁻¹⁰	(1.08 ± 0.25) 10 ⁻⁸

In order to evaluate the effect of changing the lateral chain position on BACE1 inhibitory activity and taking advantage of the interesting activity profile displayed by BACE1 inhibitors bearing a dihydroquinazoline moiety,⁷ we designed and synthesised compounds **20** and **21** (Table 5). They bear a lipoic acid and *trans*-ferulic acid fragment, respectively, linked to an aminopropylene spacer in the 2-position of the quinazoline ring. They show in their structure a guanidinic moiety that has shown, by X-ray data, to be a key fragment for strong interactions with the catalytic aspartates. Knowing that the phenoxy group in the 6-position led to an

improved activity profile in dihydroquinazoline-based BACE1 inhibitors, we decided to replace 6-methoxy substituent by 6-phenoxy group, obtaining compound **22**.

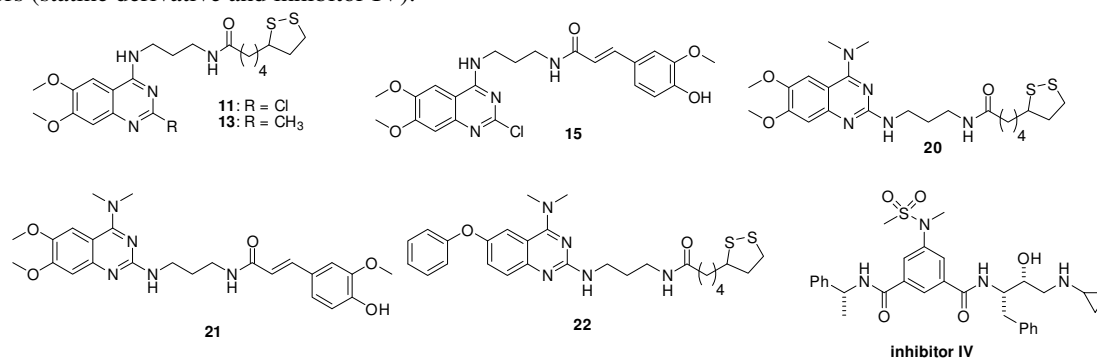
Meanwhile, with the aim of confirming the results of synthesised ligands, the most potent compounds were screened in a well established FRET assay,⁸ prior to be test in a cellular assay. The different FRET tests were studied varying the nature of substrate and of the enzyme origin, in order to evaluate the consistency of results and assess the versatility of the assays.

To this aim, the compounds **6**, **11**, **13** and **15**, together with the 2-amino-quinazoline derivatives **20-22** were evaluated by a new method (Method C, for details see Section 4.1.3.) based on MCA-SEVNLDAEFK(DNP)-CONH₂ as fluorogenic substrate called M-2420.

As shown in Table 5, even though the results on reference inhibitors (Inhibitor IV and statine derivative) displayed a good superimposition, in A, B, and C assays, defining their potency in nanomolar range, surprisingly, the data on behalf of the lead compounds lipocrine and **11**, obtained following the new FRET assay C, led to different results that were not comparable to the previous ones.

While A and B assays seemed to reproduce data for the first lead compounds **6** and **11**, that bear in their structure very similar moiety (i.e. lipoic acid in the lateral chain coupled to tetrahydroacridine and quinazoline, respectively), is not the case for compound **15** that showed a different fragment on lateral chain in the structure (i.e. *trans*-ferulic acid). Very surprisingly, the C assay does not confirm the nanomolar activity profile found with method B for the most promising derivative **15**, which seemed to display a modest inhibitory BACE1 activity.

Within the designed 2-amino-quinazoline compounds **20-22**, only derivative **21**, that bears the *trans*-ferulic acid residue on lateral chain, showed a submicromolar inhibitory BACE1 activity. This data seems to be quite comparable for B and C assays, whereas they are not strengthened by A assay.

Table 5. BACE1 inhibitory activities in different assays by selected compounds **6**, **11**, **13**, **15**, **20-22** and reference inhibitors (statine derivative and inhibitor IV).

Compound	BACE1 inhibition		
	Method A Rhodamine Invitrogen substrate	Method B Casein-FITC substrate	Method C M-2420 substrate (MCA-DNP labelled)
6 (lipocrine)	IC ₅₀ = 57.0 ± 12.0 nM	IC ₅₀ = 57 nM	2.0% at 9.4 μM
11	IC ₅₀ = 17.9 ± 3.9 nM	IC ₅₀ = 18 nM	15.2% at 10.8 μM
13	no inhibition at 1.13 μM	no inhibition at 18 nM	no inhibition at 10.6 μM
15	10.8 % at 1.05 μM n.i at 18 nM	IC ₅₀ = 18 nM	8.27 % at 9.82 μM
20	36.03% at 3 μM 10.82% at 1 μM 6.81% at 3 μM	nd	19.17% at 3 μM 17.78% at 1 μM
21	no inhibition at 1 μM	IC ₅₀ = 0.51 μM	IC ₅₀ = 0.80 ± 0.41 μM
22	10.68% at 3 μM 5.00% at 1 μM	nd	37.53% at 3 μM 21.29% at 1 μM
Inhibitor IV	IC ₅₀ = 12.89 nM	IC ₅₀ = 48.86 nM	IC ₅₀ = 13.61 nM
Statine derivative^a	IC ₅₀ = 18.0 ± 1.0 nM	IC ₅₀ = 61 ± 2.0 nM	IC ₅₀ = 30.8 ± 0.7 nM

nd = not detected; n.i. = no inhibition

^a = (H-Lys-Thr-Glu-Glu-Ile-Ser-Glu-Val-Asn-[Statine(3S,4S)]-Val-Ala-Glu-Phe-OH)

In this regard, it is well known that FRET assays have some disadvantages in term of interference rates that are strongly dependent on compound properties. For example, FRET rhodamine substrate (Method A) has shown to give a 10 times higher rate of potential “false negative” compounds. Subsequent validation assays could be performed in a kinetic mode in order to define with guarantee the correct classification of “false positives” and “false negatives”.⁹ For this reason, BACE1 fluorogenic substrate evaluation assay were carried out to

measure the kinetic parameters and quenching efficiency leading to assess the best conditions for each FRET assay (Table 6). It is well-known that K_M (the Michaelis constant) is often associated with the affinity of the enzyme for substrate, or more accurately is a measure of the substrate concentration required for effective catalysis to occur. On the other hand, K_{cat} gives a direct measure of the catalytic production of product under optimum conditions (saturated enzyme). Consequently, the K_{cat}/K_M ratio is often thought of as a measure of enzyme efficiency. So the higher values for assay C revealed a good specificity and enzymatic efficiency. Moreover the good quenching efficiency, shown in table 6, confirms the correlation between catalytic activity and fluorogenic quenching.

Table 6. Specificity constants for substrates A-C and relative quenching efficiencies

Substrate	K_{cat}/K_M	Q.E. (%)
Invitrogen Peptide (Method A)	1286.13 M ⁻¹ s ⁻¹	98.77
Casein-FITC (Method B)	3298.23 M ⁻¹ s ⁻¹	83.55
M-2420 (Method C)	6221.61 M ⁻¹ s ⁻¹	91.38

Definitely, in search of a FRET assays for the most reliable BACE1 inhibition test, we have investigated on the variability of the results depending on the substrate nature, on changed fluorophores and on different enzyme origin. Among the three FRET evaluated methods, the A assay suffers from a low predictivity but boast a good selective wavelength for fluorescence measure, so the majority of compounds, also intrinsically coloured, could be evaluated. In addition, even though B assay shows modest predictivity, it has been used for a fast screen of inhibitors because it is cheap and versatile for other aspartic proteases, such as CatD. Finally, the C assay has shown to be the most predictive test even though is not suitable for any kind of inhibitors due to its non selective wavelength for the fluorescence measure.

In conclusion, for a preliminary evaluation of compounds is not sufficient to perform experiments only by one specific method because each one has some advantages and disadvantages. The most active compound will have to be investigated on parallel studies with all substrates, prior to cellular assays. Regarding the specific FRET employed assays, we need to exclude that a specific inhibitor could establish some certain interactions with substrate, and compete with the sites where the different fluorophores reside during enzymatic substrate

cleavage. This consideration reflects the variability of emitted fluorescence, and consequently, of the evaluated activity profile.

So far, results variability does not allow us to define which the best assay to be trusted is. Surely, a couple of different assays could give a good consistency of the result, in order to guide structure activity relationship on lead modification, and to select a good candidates for cellular BACE1 inhibition test.

For this reason, we decide to test on cellular assays our first promising candidate, lipocrine. Preliminary data confirmed a micromolar activity on cellular assay ($EC_{50} = 3.7 \mu\text{M}$) strengthening the idea to find a small molecule non-peptidomimetic compound as BACE1 inhibitor. Moreover, after deep investigation on lead modification and validation assay reliability, promising results obtained from compound **22**, seemed to disclose new avenues for the developing a new quinazoline-based BACE1 inhibitor. Definitely 2-amino-quinazoline compounds could represent the starting point for further studies on lead optimization, with the aim of discovery a more potent chemical entity able to inhibit the key enzyme in AD pathogenesis.

5.3 Synthesis of δ -aminocyclohexane carboxylic acid-based BACE1 inhibitors

Carbocyclic δ -aminoacids (Fig. 3) with stereochemically defined substitution are not known in the context of peptidomimetic design. In this regard, the aim of the project was to incorporate such a constrained carbocyclic aminoacids in a potential inhibitors of BACE1 endowed with reduced peptidic character.

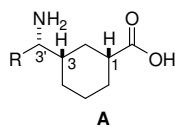


Figure 3. δ -Aminocyclohexane carboxylic acid motif **A**.

The target structure **A** was previously synthesized in Hanessian's lab using a well-known multistep synthesis, starting from a chiral aminoacid as depicted in the retrosynthetic analysis exemplified in figure 4.

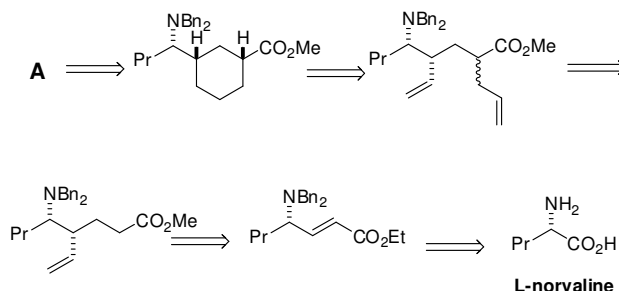


Figure 4. Retrosynthetic analysis of δ -aminocyclohexane carboxylic acid motif **A** starting from a chiral aminoacid (L-norvaline).

The alternative approach to get the δ -aminocyclohexane carboxylic acid motif **A** was based on a novel asymmetric synthesis. In particular, it was envisioned an organocatalytic asymmetric conjugate addition of nitroalkanes to cyclohexenone. The resulting 3-(α -nitroalkyl)-cyclohexanones were further functionalized to give the corresponding δ -nitroalkyl cyclohexane carboxylic acids that were elaborated to the target structures 3-(α -aminoalkyl)-1-cyclohexane carboxylic acids exemplified by **A** (Figure 3) in a new readily accessible way.

The first proline-catalyzed addition of 2-nitropropane to cyclohexenone was reported by Yamaguchi and co-workers in 1993.¹⁰ Using rubidium L-prolinate, they achieved an ee of 59% for cyclohexenone. In 2000, Hanessian and co-workers reported on a substantial improvement in

the addition of 2-nitropropane to cyclohexenone in the presence of 10% mol of L-proline, in conjunction with 2,6-dimethylpiperazine as an additive. The reaction profile exhibited an unusual non-linear effect, before reaching ee values ranging 89-93%.¹¹ Since then, the enantioselectivity of this reaction has been extended with *trans*-4,5-methano-L-proline to 99% ee.¹²

Particularly, in this project we explored the feasibility of 1-nitroalkane additions to 2-cyclohexenones and further functionalisation of the resulting 3-(α -nitroalkyl)-cyclohexanones. These intermediate were elaborated to the corresponding δ -nitroalkyl cyclohexane carboxylic acids as an alternative approach to the target structures 3-(α -aminoalkyl)-1-cyclohexane carboxylic acids exemplified by **A** (Fig. 3). Based on our previous experience,¹² it was expected that the addition of a 1-nitroalkane to 1-cyclohexenone would lead to a diastereomer in which the stereogenic centre at C3 of the resulting cyclohexanone would be fixed as a result of the stereodifferentiating event during the approach of the nitronate anion at the azadienium carboxylate stage (Fig. 5).

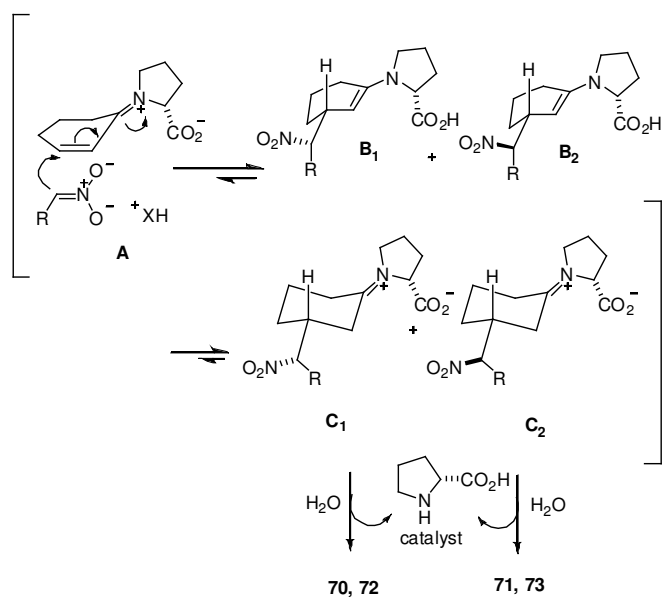
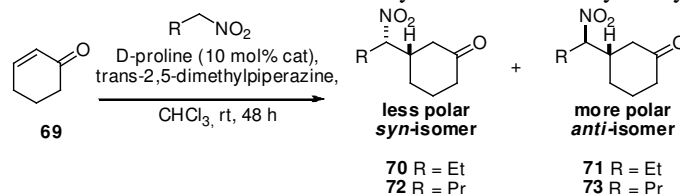


Figure 5. Proposed intermediates in the organocatalytic 1-nitroalkane addition to 2-cyclohexenone in the presence of D-Proline.

However, the stereochemical fate of the carbon atom bearing the C3' residing 1-nitro alkyl appendage would be difficult to predict, since it could undergo proton-abstraction and reprotonation after the initial attack. This appears to be no stereochemical bias to favour one diastereomer over another (Fig. 5). However, the results show that there is a stereochemical

preference for the less polar, minor (*R,S*)-diastereomers in the case of the propyl and butyl chains in **70** and **72**, respectively as evidenced by the higher ee values (Table 5).

Table 5 Catalytic enantioselective addition of nitroalkane to cyclohexenone catalyzed by D-proline



R	Yield (%)	dr ^a (<i>syn:anti</i>)	ee (%) ^b	
			Syn	anti
Ethyl	84	1 : 2.2	89	74
Propyl	97	1 : 2.0	89	71

^a obtained by RP Chiral HPLC and ¹H-NMR at 700 MHz

^b obtained by RP Chiral HPLC (see Experimental Section)

The iminium ion **A** initially formed from 1-cyclohexenone with the 1-nitroalkane provides the necessary bias for a *Si*-face attack by the nitronate anion with its associated bulky conjugate base leading to the corresponding enamines **B1** and **B2** (Fig. 5). Release of the D-proline by the hydrolysis of iminium ions **C1** and **C2** leads to the observed products **70** and **72**, respectively, and the catalytic cycle continues.

In 2000, Hanessian and coworkers¹¹ showed that the conjugate addition of 1-nitropropane to 2-cyclohexenone in the presence of 10 mol% of L-proline and *trans*-1,5-dimethylpiperazine as additive in CHCl₃ afforded a 80% yield of a 1:2 mixture of *ent.***70** and *ent.***71**. The diastereomeric excesses determined by ¹³C NMR analysis of the corresponding ketals with (2*R*,3*R*)-2,3-butanediol, were 85% and 72% for *ent.***70** and *ent.***71**, respectively. In the presence of *trans*-4,5-methano-L-proline as a catalyst, there was a measurable improvement in diastereoselectivity to 91% and 74%, respectively.

In the present study, these results were independently confirmed by HPLC analysis on chiral columns. Furthermore, the stereochemical identity of the less polar *syn*-isomers **70** and **72** were definitively confirmed by comparison with conversion to compounds **80** and **81** prepared from the aminoacid route.

A priori, it is difficult to rationalize the preponderance of the more polar *anti*-isomers **71** and

73 by a ratio of 2:1 over the less polar *syn*-counterparts **70** and **72**, respectively. The ratio appears to be a thermodynamic one under the reaction conditions. Nevertheless, it is interesting that the desired *syn*-isomers **70** and **72** in the context of our intended carbocyclic aminoacid motif **A** (Fig. 3), was produced in an enriched form corresponding to an enantiomeric ratio of approximately 95:5. In this regard, the modest enantiomeric excesses of the *anti*-(3*S*,3'*R*) isomers **71** and **73** (74% and 71%, respectively), were significantly better than the corresponding isomers with Mauroka's *N*-spiro chiral quaternary ammonium bromide phase transfer catalyst, where an ee of 57% was reported.¹³ However, the ratios of diastereomers in Maruoka's study were highly in favour of the enantioenriched *syn*-isomer **70** (*syn/anti* 96:4, 91% and 57% ee, respectively).

In conclusion, proline catalysis has shown an efficient tool to obtain highly enantiopure addition product from nitroalkanes and cyclohexenone. Further straightforward elaboration of nitro alkanes intermediate led us to build an alternative organocatalytic route to access cyclohexane carboxylic δ -aminoacid. In the context of the peptidomimetics BACE1 program, this new asymmetric route was compared to a previous substrate-controlled route resulting in a shorter, asymmetric, and more elegant way to access the δ -aminocyclohexane carboxylic core.

During this thesis drafting, we do not have biological evaluation on behalf of the presented compounds available yet. In the context of the peptidomimetics BACE1 program we are waiting to know activity profiles and selectivity tests of designed ligands in order to guide future work on the δ -aminocyclohexane carboxylic core as structural motif for new small size BACE1 inhibitors.

References

- ¹ Rosini, M.; Andrisano, V.; Bartolini, M.; Bolognesi, M.L.; Hrelia, P.; Minarini, A.; Tarozzi, A.; Melchiorre, C. Rational approach to discover multipotent Anti-Alzheimer drugs. *J. Med. Chem.* **2005**, *48*, 360-363.
- ² Recanatini, M.; Cavalli, A.; Belluti, F.; Piazzini, L.; Rampa, A.; Bisi, A.; Gobbi, S.; Valenti, P.; Andrisano, V.; Bartolini, M.; Cavrini, V. SAR of 9-amino-1,2,3,4-tetrahydroacridine-based acetylcholinesterase inhibitors: synthesis, enzyme inhibitory activity, QSAR, and structure-based CoMFA of tacrine analogues. *J. Med. Chem.* **2000**, *43*, 2007-2018.
- ³ Bartolini, M.; Bertucci, C.; Cavrini, V.; Andrisano, V. Beta-Amyloid aggregation induced by human acetylcholinesterase: inhibition studies. *Biochem. Pharmacol.* **2003**, *65*, 407-416.
- ⁴ Bolognesi, M.L.; Cavalli, A.; Melchiorre, C. Memoquin: a multi-target-directed ligand as an innovative therapeutic opportunity for Alzheimer's disease. *Neurotherapeutics* **2009**, *6*, 152-162.
- ⁵ Twining, S.S. Fluorescein isothiocyanate-labeled casein assay for proteolytic enzymes. *Anal. Biochem.* **1984**, *143*, 30-34.
- ⁶ Mancini, F.; Naldi, M.; Cavrini, V.; Andrisano, V. Multiwell fluorometric and colorimetric microassays for the evaluation of beta-secretase (BACE1) inhibitors. *Anal. Bioanal. Chem.* **2007**, *388*, 1175-1183.
- ⁷ Baxter, E.W.; Conway, K.A.; Kennis, L.; Bischoff, F.; Mercken, M.H.; DeWinter, H.L.; Reynolds, C.H.; Tounge, B.A.; Luo, C.; Scott, M.K.; Huang, Y.; Braeken, M.; Pieters, S.M.A.; Berthelot, D.J.C.; Masure, S.; Bruinzeel, W.D.; Jordan, A.D.; Parker, M.H.; Boyd, R.E.; Qu, J.; Alexander, R.S.; Brenneman, D.E.; Reitz, B. 2-Amino-3,4-dihydroquinazolines as inhibitors of BACE1 (b-Site APP cleaving enzyme): use of structure based design to convert a micromolar hit into a nanomolar lead. *J. Med. Chem.* **2007**, *50*, 4261-4264.
- ⁸ Hanessian, S.; Yun, H.; Hou, Y.; Yang, G.; Bayraktarian, M.; Therrien, E.; Moitessier, N.; Roggo, S.; Veenstra, S.; Tintelnot-Blomley, M.; Rondeau, J.M.; Ostermeier, C.; Strauss, A.; Ramage, P.; Paganetti, P.; Neumann, U.; Betschart, C. Structure-based design, synthesis, and memapsin 2 (BACE) inhibitory activity of carbocyclic and heterocyclic peptidomimetics. *J. Med. Chem.* **2005**, *48*, 5175-5190.
- ⁹ Porcari, V.; Magnoni, L.; Terstappen, G.C.; Fecke, W. A continuous time-resolved fluorescence assay for identification of BACE1 inhibitors. *Assay Drug. Dev. Technol.* **2005**, *3*, 287-297.
- ¹⁰ Yamaguchi, M.; Shiraishi, T.; Hirama, M. A Catalytic Enantioselective Michael Addition of a Simple Malonate to Prochiral alpha,beta-Unsaturated Ketones and Aldehydes. *Angew. Chem., Int. Ed. Engl.* **1993**, *32*, 1176-1178.
- ¹¹ Hanessian, S.; Pham, V. Catalytic asymmetric conjugate addition of nitroalkanes to cycloalkenones. *Org. Lett.* **2000**, *2*, 2975.
- ¹² Hanessian, S.; Shao, Z.; Warrier, J.S. Optimization of the Catalytic Asymmetric Addition of Nitroalkanes to Cyclic Enones with trans-4,5-Methano-L-proline. *Org. Lett.* **2006**, *21*, 4787-90.
- ¹³ Ooi, T.; Takada, S.; Fujioka, S.; Maruoka, K. N-spiro chiral quaternary ammonium bromide catalyzed diastereo- and enantioselective conjugate addition of nitroalkanes to cyclic alpha,beta-unsaturated ketones under phase-transfer conditions. *Org. Lett.* **2005**, *7*, 5143-5146.

Chapter 6

Experimental Section

6.1 Chemistry

Anhydrous solvents were transferred under a positive pressure of Ar from a solvent dispensing system or obtained from commercial suppliers. All commercially available reagents were used without further purification. Melting points were taken in glass capillary tubes on a Büchi SMP-20 apparatus and are uncorrected. Optical rotations were recorded in a 1 dm cell at ambient temperature with a sodium lamp (wavelength of 589 nm) using a 100 mm cell with a 1 mL capacity and are given in units of $10^{-1} \text{ deg cm}^2 \text{ g}^{-1}$.

^1H NMR, ^{13}C NMR, gHSQC and COSY experiments were recorded on Mercury 400 and Varian VXR 200 and 300 instruments (Università di Bologna) or Bruker AMX-300, ARX-400, AV-400 spectrometers (Université de Montréal). Chemical shifts are reported in parts per million (ppm) relative to tetramethylsilane (TMS), and spin multiplicities are given as s (singlet), d (doublet), dd (double doublet), t (triplet), br t (broad triplet), q (quartet) or m (multiplet) and coupling constants (J) were reported in Hertz. When the IR spectra data are not included (because of the lack of unusual features), they were obtained for all compounds reported and were consistent with the assigned structures. The elemental compositions of the compounds agreed to within $\pm 0.4\%$ of the calculated value. When the elemental analysis is not included, crude compounds were used in the next step without further purification.

Analytical thin-layer chromatography was performed on 60F₂₅₄ pre-coated silica gel plates. Visualization was achieved using ultraviolet light and/or staining in a iodine chamber, or with ceric ammonium molybdate, potassium permanganate, ethanolic solution of anisaldehyde or ninhydrin. Flash chromatography was performed on a column of 230-400 mesh silica gel or Kieselgel 40, 0.040-0.063 mm; (Merck) with the indicated solvent system. Gravity column were performed with Kieselgel 60, 0.063-0.200 mm; (Merck). Compounds were named following

IUPAC rules as applied by ChemBioDraw Ultra 11.0, a PC integrated software package for systematic names in organic chemistry.

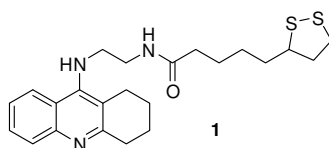
IR, electron impact (EI) and direct infusion ESI-MS analyses performed by Department of Organic Chemistry “A. Mangini” (Università di Bologna) were obtained on Perkin-Elmer 297, VG 7070E, and Waters ZQ 4000 apparatus, respectively. Low and high resolution mass analyses performed by Centre Régional de Spectroscopie de l’Université de Montréal were obtained on AEI-MS 902, MS-50 or LC-MSD-TOF spectrometers using ES or FAB techniques. Either protonated molecular ions $[M+H]^+$ or sodium adducts $[M+Na]^+$ were used for empirical ion confirmation. LC-MS analyses were performed on LC-Gilson apparatus (autoinjector model 234, pump 322), Thermo Finnigan LCQ Advantage MS and TSP UV6000 interface.

General procedure for the synthesis of compounds 1-6 and 8-10. (Procedure A)

A solution of the appropriate amine (1 eq, 0.1 M) and (\pm)-lipoic acid (1.5 eq) in dry DMF (5 mL), under N_2 was cooled to 0 °C and then treated with 1-(3-dimethylaminopropyl)-3-ethylcarbodiimide hydrochloride (EDCI-HCl) (1.2 eq): the mixture was stirred at 0 °C for further 15 min and then at rt for 2 h in the dark. Solvent was then removed under vacuum, avoiding heating up the reaction mixture, affording an oily residue that was purified by gravity column.

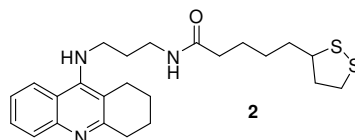
General procedure for the synthesis of compounds 11-13, 19-20 and 22 (Procedure B)

To a solution of the appropriate amine (1 eq, 0.05 M) in anhydrous THF, NEt_3 (1 eq) and (\pm)-lipoic acid (1 eq), under N_2 were added. The reaction mixture was cooled to 0 °C and then treated with 1-(3-dimethylaminopropyl)-3-ethylcarbodiimide hydrochloride (EDCI-HCl) (1 eq): the mixture was stirred at 0 °C for 20 min and then was allowed to reach rt overnight in the dark. Solvent was then removed under vacuum, avoiding heating up the reaction mixture, affording an oily residue that was purified by column chromatography.



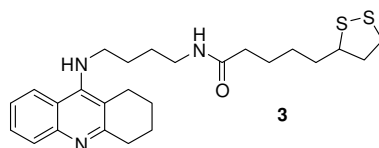
5-(1,2-dithiolan-3-yl)-N-(2-(1,2,3,4-tetrahydroacridin-9-ylamino)ethyl)pentanamide (1). It was synthesized from N^1 -(1,2,3,4-tetrahydroacridin-9-yl)ethane-1,2-diamine **32**¹ (140 mg) following the procedure A. Elution with petroleum ether/ CH_2Cl_2 /MeOH/aqueous 30% ammonia

(6:3:1:0.055) afforded **1** as a foam solid: 35% yield; $^1\text{H NMR}$ (300 MHz, CD_3OD) δ 8.12 (d, $J = 8.8$ Hz, 1H), 7.78 (d, $J = 8.8$ Hz, 1H), 7.58, (t, $J = 8.2$ Hz, 1H), 7.39 (t, $J = 8.2$ Hz, 1H), 3.70 (t, $J = 6.3$ Hz, 2H), 3.28-3.39 (m, 3H), 2.93-3.15 (m, 4H), 2.71-2.79 (m, 2H), 2.26-2.40 (m, 1H), 2.15 (t, $J = 8.6$ Hz, 2H), 1.64-1.93 (m, 5H), 1.30-1.61 (m, 6H); MS (ESI+) m/z 430 $[\text{M}+1]^+$. Calcd. for $\text{C}_{23}\text{H}_{31}\text{N}_3\text{OS}_2$: C, 64.30; H, 7.27; N, 9.78; found C, 64.41; H, 7.28; N, 9.75.



5-(1,2-dithiolan-3-yl)-N-(3-(1,2,3,4-tetrahydroacridin-9-ylamino)propyl)pentanamide (2).

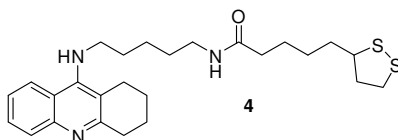
It was synthesized following the procedure A, from N^1 -(1,2,3,4-tetrahydroacridin-9-yl)propane-1,3-diamine **33** (100 mg), obtained from 9-chloro-1,2,3,4-tetrahydroacridine and propane-1,3-diamine following the procedure described in Carlier *et al.*², and purified by flash chromatography with a step gradient system of $\text{CH}_2\text{Cl}_2/\text{MeOH}/\text{aqueous 30\% ammonia}$ (9.5:0.5:0.0 to 7:3:0.1): 65% yield, $^1\text{H NMR}$ (200 MHz, CD_3OD) δ 8.08 (d, $J = 8.8$ Hz, 1H), 7.78 (d, $J = 8.7$ Hz, 1H), 7.53, (t, $J = 8.3$ Hz, 1H), 7.32 (t, $J = 8.3$ Hz, 1H), 3.54 (t, $J = 6.7$ Hz, 2H), 2.87-2.98 (m, 2H), 2.65 (t, $J = 7.5$ Hz, 4H), 1.64-1.93 (m, 6H). Elution with petroleum ether/ $\text{CH}_2\text{Cl}_2/\text{MeOH}/\text{aqueous 30\% ammonia}$ (5:4:1:0.05) afforded **2** as a foam solid: 35% yield; $^1\text{H NMR}$ (200 MHz, CD_3OD) δ 8.15 (d, $J = 8.8$ Hz, 1H), 7.78 (d, $J = 8.8$ Hz, 1H), 7.56-7.64 (m, 1H), 7.37-7.44 (m, 1H), 3.69 (t, $J = 6.6$ Hz, 2H), 3.40-3.52 (m, 1H), 3.23-3.36 (t, $J = 6.6$ Hz, 2H), 2.92-3.18 (m, 4H), 2.74-2.83 (m, 2H), 2.28-2.43 (m, 1H), 2.19 (t, $J = 7.1$ Hz, 2H), 1.73-1.95 (m, 7H), 1.22-1.68 (m, 6H). MS (ESI+) m/z 444 $[\text{M}+1]^+$. Calcd. for $\text{C}_{24}\text{H}_{33}\text{N}_3\text{OS}_2$: C, 64.97; H, 7.50; N, 9.47; found C, 65.18; H, 7.52; N, 9.44.



5-(1,2-dithiolan-3-yl)-N-(4-(1,2,3,4-tetrahydroacridin-9-ylamino)butyl)pentanamide (3).

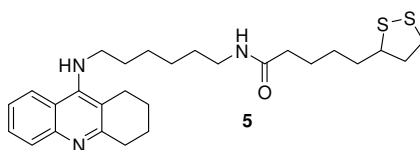
It was synthesized from N^1 -(1,2,3,4-tetrahydroacridin-9-yl)butane-1,4-diamine **34**² (290 mg) following the procedure A. Elution with petroleum ether/ $\text{CH}_2\text{Cl}_2/\text{MeOH}/\text{aqueous 30\% ammonia}$ (6:3:1:0.06) afforded **3** as a foam solid: 38% yield; $^1\text{H NMR}$ (200 MHz, CD_3OD) δ 8.12 (d, $J = 8.6$ Hz, 1H), 7.78 (d, $J = 8.6$ Hz, 1H), 7.52-7.62 (m, 1H), 7.32-7.43 (m, 1H), 3.41-3.60 (m, 3H),

2.90-3.21 (m, 6H), 2.68-2.77 (m, 2H), 2.31-2.46 (m, 1H), 2.17 (t, $J = 6.9$ Hz, 2H), 1.38-1.95 (m, 15H); MS (ESI+) m/z 458 $[M+1]^+$. Calcd. for $C_{25}H_{35}N_3OS_2$: C, 65.60; H, 7.71; N, 9.18; found C, 65.67; H, 7.69; N, 9.15.



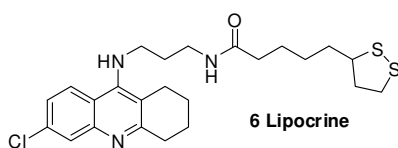
5-(1,2-dithiolan-3-yl)-N-(5-(1,2,3,4-tetrahydroacridin-9-ylamino)pentyl)pentanamide (4).

It was synthesized from N^1 -(1,2,3,4-tetrahydroacridin-9-yl)pentane-1,5-diamine **35**² (480 mg) following the procedure A. Elution with petroleum ether/ CH_2Cl_2 /MeOH/aqueous 30% ammonia (6:3:1:0.055) afforded **4** as a foam solid: 40% yield; 1H NMR (200 MHz, CD_3OD) δ 8.09 (d, $J = 8.6$ Hz, 1H), 7.78 (d, $J = 8.6$ Hz, 1H), 7.52-7.60 (m, 1H), 7.33-7.41 (m, 1H), 3.40-3.57 (m, 3H), 2.87-3.18 (m, 6H), 2.63-2.75 (m, 2H), 2.25-2.43 (m, 1H), 2.17 (t, $J = 6.8$ Hz, 2H), 1.35-1.95 (m, 17H); MS (ESI+) m/z 472 $[M+1]^+$. Calcd. for $C_{26}H_{37}N_3OS_2$: C, 66.20; H, 7.91; N, 8.91; found C, 66.41; H, 7.89; N, 8.88.



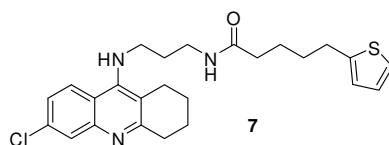
5-(1,2-dithiolan-3-yl)-N-(6-(1,2,3,4-tetrahydroacridin-9-ylamino)hexyl)pentanamide (5).

It was synthesized from N^1 -(1,2,3,4-tetrahydroacridin-9-yl)hexane-1,6-diamine **36**² (370 mg) following the procedure A. Elution with petroleum ether/ CH_2Cl_2 /MeOH/aqueous 30% ammonia (6:3:1:0.05) afforded **5** as a foam solid: 30% yield; 1H NMR (200 MHz, $CDCl_3$) δ 7.83 (apparent t, $J = 9.3$ Hz, 2H), 7.47-7.56 (m, 1H), 7.28-7.37 (m, 1H), 5.89 (t, $J = 3.2$ Hz, 1H, exchangeable with D_2O), 4.15 (br s, 2H, exchangeable with D_2O), 3.40-3.57 (m, 3H), 3.01-3.23 (m, 6H), 2.60-2.75 (m, 2H), 2.31-2.48 (m, 1H), 2.15 (t, $J = 7.3$ Hz, 2H), 1.35-1.96 (m, 19H); MS (ESI+) m/z 486 $[M+1]^+$. Calcd. for $C_{27}H_{39}N_3OS_2$: C, 66.76; H, 8.09; N, 8.65; C, 66.87; H, 8.12; N, 8.62.

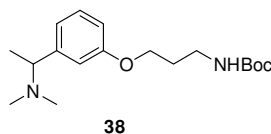


N-(3-(6-chloro-1,2,3,4-tetrahydroacridin-9-ylamino)propyl)-5-(1,2-dithiolan-3-

yl)pentanamide (6). It was synthesized following the procedure A, from *N*¹-(6-chloro-1,2,3,4-tetrahydroacridin-9-yl)propane-1,3-diamine **23** (180 mg), obtained from 6,9-dichloro-1,2,3,4-tetrahydroacridine and propane-1,3-diamine following the procedure described in Carlier *et al.*,² and purified by flash chromatography with a step gradient system of CH₂Cl₂/MeOH/aqueous 30% ammonia (9.5:0.5:0.0 to 8:2:0.03): 70% yield, ¹H NMR (200 MHz, CDCl₃) δ 7.93 (d, *J* = 9.1 Hz, 1H), 7.86 (d, *J* = 2.4 Hz, 1H), 7.22 (dd, *J* = 9.0, 2.3 Hz, 1H), 3.62 (t, *J* = 6.8 Hz, 2H), 2.88-3.05 (m, 4H), 2.60-2.68 (m, 2H), 1.71-1.95 (m, 6H). Elution with petroleum ether/CH₂Cl₂/EtOH/aqueous 30% ammonia (7:2:1:0.03) afforded **6** as a foam solid: 35% yield; ¹H NMR (200 MHz, CD₃OD) δ 8.08 (d, *J* = 8.9 Hz, 1H), 7.72 (d, *J* = 2.1 Hz, 1H), 7.28 (dd, *J* = 8.9, 2.1 Hz, 1H), 3.42-3.58 (m, 3H), 3.27 (t, *J* = 6.5 Hz, 2H), 2.89-3.17 (m, 4H), 2.65-2.77 (m, 2H), 2.27-2.43 (m, 1H), 2.19 (t, *J* = 7.2 Hz, 2H), 1.73-1.91 (m, 7H), 1.31-1.65 (m, 6H); MS (ESI+) *m/z* 478 [M+1]⁺. Calcd. for C₂₄H₃₂ClN₃OS₂: C, 60.29; H, 6.75; N, 8.79; found C, 60.45; H, 6.74; N, 8.77.

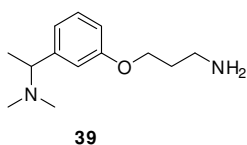


***N*-(3-(6-chloro-1,2,3,4-tetrahydroacridin-9-ylamino)propyl)-5-(thiophen-2-yl)pentanamide (7).** It was synthesized from *N*¹-(6-chloro-1,2,3,4-tetrahydroacridin-9-yl)propane-1,3-diamine **23** (0.350 g, 1.21 mmol), 5-(thiophen-2-yl)pentanoic acid (0.334 g, 1.82 mmol) and EDCI·HCl (0.278 g, 1.45 mmol) following the procedure A. Purification by flash chromatography (petroleum ether/CH₂Cl₂/MeOH/aqueous 30% ammonia, 6.0:3.5:0.5:0.007) afforded **7** (0.441 g, 80 %) as a yellowish wax. ¹H NMR (CDCl₃, 200 MHz) δ 8.70 (br t, 1H, exchangeable with D₂O) 7.96 (d, 1H, *J* = 8.8 Hz), 7.88 (d, 1H, *J* = 2.2 Hz), 7.23 (d, 1H, *J* = 1.8 Hz), 7.09-7.01 (m, 1H), 6.91 (t, 1H, *J* = 3.6 Hz), 6.76-6.78 (m, 1H), 6.05 (br t, 1H, exchangeable with D₂O), 3.48-3.52 (m, 4H), 3.02-3.05 (m, 2H), 2.85 (t, 2H, *J* = 6.6 Hz), 2.71-2.76 (m, 2H), 2.25 (t, 2H, *J* = 6.6 Hz), 1.71-1.90 (m, 10H). MS (ESI+) : *m/z* 456 [M+1]⁺.

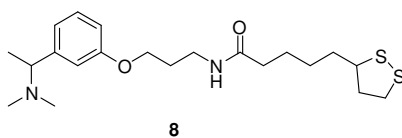


***tert*-Butyl 3-(3-(1-(dimethylamino)ethyl)phenoxy)propylcarbamate (38).** A solution of

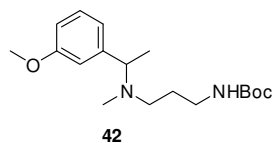
compound **37** was synthesised following the procedure described for the corresponding (*R,S*)-3-(1-(Di-(²H₃)methylamino)ethyl)phenol in Ciszewska *et al.*³ (0.350 g, 2.17 mmol), *tert*-butyl 3-chloropropylcarbamate (0.420 g, 2.17 mmol) and K₂CO₃ (0.300 g, 2.17 mmol) in DMF (10 mL) was stirred under reflux conditions for 24 h. Evaporation of the solvent afforded a residue which was purified by gravity column. Elution with CHCl₃/MeOH/aqueous 30% ammonia (9:1:0.02) afforded **38** (0.454 g, 65 %) as an oil. ¹H NMR (CDCl₃, 200 MHz) δ 7.20 (t, *J* = 8.0 Hz, 1H), 6.79-6.89 (m, 3H), 4.92 (br s, 1H, exchangeable with D₂O), 4.02 (t, *J* = 6.4 Hz, 2H), 3.20-3.33 (m, 3H), 2.20 (s, 6H), 1.93-1.99 (m, 2H), 1.44 (s, 9H), 1.35 (d, *J* = 6.6 Hz, 3H).



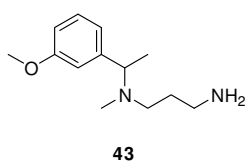
3-(3-(1-(Dimethylamino)ethyl)phenoxy)propan-1-amine (39). To a solution of **38** (0.200 g, 0.62 mmol) in CH₂Cl₂ (5 mL) trifluoroacetic acid (1.5 mL) was added. The reaction mixture was stirred at rt for 2 hr and evaporated in vacuum. The obtained residue was dissolved in water, made basic by adding 2N NaOH and then extracted with CHCl₃ (3 × 20 mL). Evaporation of the dried solvent afforded **39** (0.137 g, quantitative). ¹H NMR (CDCl₃, 200 MHz) δ 7.20 (t, *J* = 8.0 Hz, 1H), 6.72-6.88 (m, 3H), 4.04 (t, *J* = 6.2 Hz, 2H), 3.12-3.22 (m, 1H), 2.91 (t, *J* = 6.6 Hz, 2H), 2.19 (s, 6H), 1.88-1.95 (m, 2H), 1.43 (br s, 2H, exchangeable with D₂O), 1.34 (d, *J* = 6.6 Hz, 3H).



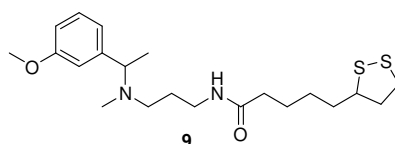
***N*-(3-(3-(1-(Dimethylamino)ethyl)phenoxy)propyl)-5-(1,2-dithiolan-3-yl)pentanamide (8).** It was synthesized from **39** (0.150 g, 0.67 mmol) and (±)-lipoic acid (0.210 g, 1.02 mmol) following the procedure A. Elution with petroleum ether/toluene/CH₂Cl₂/MeOH/aqueous 30% ammonia (6:1:1.5:1.5:0.01) afforded **8** (0.080 g, 30 %) as a waxy solid. ¹H NMR (CDCl₃, 200 MHz) δ 7.27 (t, *J* = 8.2 Hz, 1H), 6.98-6.78 (m, 3H), 5.99 (br t, 1H), 4.09 (t, *J* = 6.0 Hz, 2H), 3.62-3.21 (m, 5H), 3.19-3.05 (m, 3H), 2.53-2.40 (m, 1H), 2.32 (s, 6H), 2.22 (t, *J* = 7.2 Hz, 2H), 1.99-1.81 (m, 3H), 1.73-1.65 (m, 4H), 1.47 (d, *J* = 6.6 Hz, 3H). MS (ESI⁺) : *m/z* 411 [M+1]⁺. Calcd for C₂₁H₃₄N₂O₂S₂: C, 61.42; H, 8.35; N, 6.82. found: C, 61.62; H, 8.36; N, 6.80.



tert-Butyl 3-((1-(3-methoxyphenyl)ethyl)(methyl)amino)propylcarbamate (42). A solution of 1-(3-methoxyphenyl)-*N*-methylethanamine **41**⁴ (0.320 g, 1.9 mmol), *tert*-butyl 3-chloropropylcarbamate (0.370 g, 1.9 mmol) and K₂CO₃ (0.260 g, 1.9 mmol) and a catalytic amount of KI in DMF (10 mL) was stirred under reflux conditions for 24 h. Evaporation of the solvent afforded a residue which was purified by gravity column. Elution with CHCl₃/MeOH/aqueous 30% ammonia (9:1:0.005) afforded **42** (0.245 g, 40 %) as an oil. ¹H NMR (CDCl₃, 200 MHz) δ 7.20 (t, *J* = 8.0 Hz, 1H), 6.95-6.74 (m, 3H), 5.38 (br s, 1H, exchangeable with D₂O), 3.80 (s, 3H), 3.50 (q, *J* = 7.0 Hz, 1H), 3.13 (q, *J* = 6.2 Hz, 2H), 2.52-2.30 (m, 2H), 2.19 (s, 3H), 1.68-1.54 (m, 2H), 1.44 (s, 9H), 1.35 (d, *J* = 6.6 Hz, 3H).

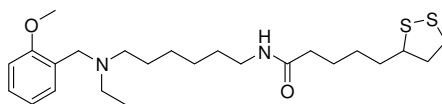


N¹-(1-(3-Methoxyphenyl)ethyl)-N¹-methylpropane-1,3-diamine (43). It was obtained as an oil from **42** (0.230 g, 0.62 mmol) and trifluoroacetic acid (1.5 mL) in CH₂Cl₂ (5 mL) following the procedure described for **39**; (0.137 g, quantitative yield). ¹H NMR (CDCl₃, 200 MHz) δ 7.27 (t, *J* = 8.0 Hz, 1H), 6.97-6.80 (m, 3H), 3.85 (s, 3H), 3.54 (q, *J* = 6.6 Hz, 1H), 2.74 (t, *J* = 6.6 Hz, 2H), 2.58-2.30 (m, 2H), 2.25 (s, 3H), 1.67-1.55 (m, 2H+2H exchangeable with D₂O), 1.39 (d, *J* = 7.0 Hz, 3H).



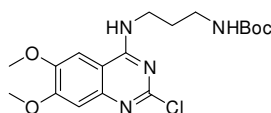
5-(1,2-Dithiolan-3-yl)-N-(3-((1-(3-methoxyphenyl)ethyl)(methyl)amino)propyl)pentanamide (9). It was synthesised from **43** (0.130 g, 0.59 mmol) and (±)-lipoic acid (0.240 g, 1.47 mmol) following the procedure A, and purified by gravity column chromatography. Elution with petroleum ether/CH₂Cl₂/EtOH/aqueous 30% ammonia (5.5:3.5:1:0.015) afforded **9** (0.133 g, 55 %) as a waxy solid. ¹H NMR (CDCl₃, 200 MHz) δ 7.23

(t, $J = 7.8$ Hz, 1H), 6.90-6.75 (m, 3H), 6.56 (br s, 1H, exchangeable with D_2O), 3.79 (s, 3H), 3.58-3.47 (m, 2H), 3.25-3.05 (m, 4H), 2.45-2.37 (m, 3H), 2.20 (s, 3H), 2.03 (t, $J = 7.2$ Hz, 2H), 1.97-1.82 (m, 1H), 1.73-1.38 (m, 8H), 1.34 (d, $J = 6.4$ Hz, 3H). MS (ESI+) : m/z 411 $[M+1]^+$. Calcd for $C_{21}H_{34}N_2O_2S_2$: C, 61.42; H, 8.35; N, 6.82. Found: C, 61.65; H, 8.36, N, 6.81.



10

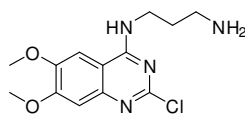
5-(1,2-dithiolan-3-yl)-N-(6-(ethyl(2-methoxybenzyl)amino)hexyl)pentanamide (10). It was synthesized from N^1 -ethyl- N^1 -(2-methoxybenzyl)hexane-1,6-diamine **44**⁵ (0.300 g, 1.13 mmol) and lipoic acid (0.350 g, 1.70 mmol) following the procedure A, and purified by gravity column chromatography. Elution with a gradient of mobile phase petroleum ether/toluene/ CH_2Cl_2 /EtOH/aqueous 30% ammonia (7:2:1:1:0.05 to 7:1:1:1:0.05) afforded **10** (0.219 g, 43 %) as a waxy solid. 1H NMR ($CDCl_3$, 200 MHz) δ 7.48-7.42 (m, 1H), 7.26-7.18 (m, 1H), 6.99-6.85 (m, 2H), 5.43 (br s, 1H, exchangeable with D_2O), 3.84 (s, 3H), 3.64-3.53 (m, 1H + s, 2H), 3.27-3.08 (m, 4H), 2.57-2.43 (m, 5H), 2.17 (t, $J = 7.4$ Hz, 2H), 2.00-1.82 (m, 1H), 1.73-1.29 (m, 14H), 1.07 (t, $J = 7.0$ Hz, 3H). MS (ESI+) : m/z 453 $[M+1]^+$. Calcd for $C_{24}H_{40}N_2O_2S_2$: C, 63.67; H, 8.91; N, 6.19. Found: C, 63.79; H, 8.93, N, 6.17.



24

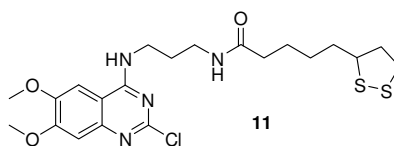
tert-Butyl 3-(2-chloro-6,7-dimethoxyquinazolin-4-ylamino)propylcarbamate (24). To a stirred solution of 2,4-dichloro-6,7-dimethoxyquinazoline **45** (1.00 g, 3.86 mmol) in anhydrous DMF (15 mL) was added a solution of *tert*-butyl 3-aminopropylcarbamate (1.01 g, 5.79 mmol) in DMF and NEt_3 (0.54 mL, 3.86 mmol). The resulting mixture was stirred at rt overnight, then was poured in ice-water and extracted with CH_2Cl_2 (2×100 mL), washed with water. The organic phase was dried over Na_2SO_4 and concentrated. Diethyl ether was added to the residue and the obtained suspension was stirred to remove DMF traces from solid, then filtered and dried to obtain **24** (1.33 g, 86 %) as a crystalline white solid. 1H NMR ($CDCl_3$, 200 MHz) δ 7.63 (br s, 1H, exchangeable with D_2O), 7.32 (s, 1H), 7.14 (s, 1H), 4.89 (br t, 1H, exchangeable with D_2O), 4.05 (s, 3H), 4.00 (s, 3H), 3.77 (q, $J = 5.4$ Hz, 2H), 3.36 (q, $J = 6.2$ Hz, 2H), 1.79 (m, $J = 4.6$ Hz,

2H), 1.50 (m, 9H). MS (ESI+) : m/z 397 [M+1]⁺.



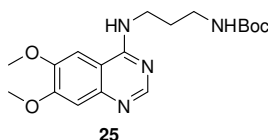
26

***N*¹-(2-chloro-6,7-dimethoxyquinazolin-4-yl)propane-1,3-diamine (26).** To a stirred solution of **24** (0.18 g, 0.45 mmol) in MeOH (3 mL) was added 3 N HCl solution (6 mL) and was allowed to stir at rt overnight. The reaction mixture was diluted with 40% NaOH aq. solution and extracted with CH₂Cl₂ (5 × 50 mL). The organic layer was dried over Na₂SO₄ and concentrated to obtain the free amine **26** (0.103 g, 77%) as a off-white solid. Mp = 210°-215 °C (dec.). ¹H NMR (CDCl₃, 200 MHz) δ 8.53 (br s, 1H, exchangeable with D₂O) 7.13 (s, 1H), 6.98 (s, 1H), 3.99 (s, 3H), 3.96 (s, 3H), 3.80 (q, *J* = 4.4 Hz, 2H), 3.10 (t, *J* = 5.6 Hz, 2H), 1.87 (m, 2H), 1.64 (br s, 2H, exchangeable with D₂O). MS (ESI+) : m/z 297 [M+1]⁺.

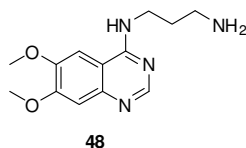


11

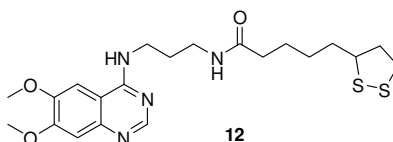
***N*-(3-(2-chloro-6,7-dimethoxyquinazolin-4-ylamino)propyl)-5-(1,2-dithiolan-3-yl)pentanamide (11).** It was synthesised from **26** (0.15 g, 0.505 mmol), NEt₃ (70 μL, 0.505 mmol), (±)-lipoic acid (0.104 g, 0.505 mmol) and EDCI-HCl (0.097 g, 0.505 mmol) following the procedure B. Purification by gravity column chromatography (petroleum ether/CH₂Cl₂/EtOH/aqueous 30% ammonia, 5:4.5:0.5:0.01) afforded **11** (0.110 g, 45 %) as a yellowish oil. ¹H NMR (CDCl₃, 300 MHz) δ 7.46 (br t, *J* = 5.8 Hz, 1H, exchangeable with D₂O), 7.34 (s, 1H), 7.14 (s, 1H), 6.22 (t, 1H, exchangeable with D₂O), 4.06 (s, 3H), 4.00 (s, 3H), 3.73 (q, *J* = 4.8 Hz, 2H), 3.58 (m, *J* = 6.3 Hz, 1H), 3.45 (q, *J* = 6.0 Hz, 2H), 3.24-2.91 (m, 2H), 2.53-2.42 (m, 1H), 2.32 (t, *J* = 7.5 Hz, 2H), 2.30-1.61 (m, 7H), 1.60-1.47 (m, 2H). ¹³C-NMR (CDCl₃, 75 MHz) δ 174.52, 160.58, 157.02, 155.07, 149.27, 147.93, 107.54, 107.22, 101.08, 56.63, 56.57, 56.47, 40.52, 38.74, 37.34, 36.78, 36.21, 34.86, 29.69, 29.13, 25.75. MS (ESI+) : m/z 486 [M+1]⁺.



tert-Butyl 3-(6,7-dimethoxyquinazolin-4-ylamino)propylcarbamate (25). To a stirred solution of **46**⁶ (0.15 g, 0.67 mmol) in 2-propanol (20 mL) was added a solution of *tert*-butyl 3-aminopropylcarbamate (0.12 g, 0.67 mmol) in 2-propanol. The resulting mixture was refluxed for 8 hr. After adding further amount of amine (0.04 g, 0.23 mmol) and refluxing another 16 hr the reaction mixture was allowed to cool to rt. The solvent was removed under reduced pressure, then diethyl ether was added, and the obtained suspension was stirred for a while. The precipitated formed was filtered under vacuum allowing to collect the title compound **25** (0.19 g, 78 %) as a white solid. ¹H NMR (CDCl₃, 200 MHz) δ 8.52 (s, 1H), 8.13 (br s, 1H, exchangeable with D₂O), 7.49 (s, 1H), 7.36 (s, 1H) 5.10 (br s, 1H, exchangeable with D₂O), 4.07 (s, 3H), 4.04 (s, 3H), 3.80 (q, *J* = 5.6 Hz, 2H), 3.35 (q, *J* = 5.6 Hz, 2H), 1.82 (m, *J* = 4.6 Hz, 2H), 1.48 (m, 9H).

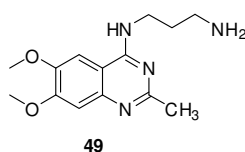


N1-(6,7-Dimethoxyquinazolin-4-yl)propane-1,3-diamine (48). To a stirred solution of **25** (0.18 g, 0.50 mmol) in MeOH (3 mL) was added 3 N HCl solution (7 mL) and was allowed to stir at rt overnight. The reaction mixture was diluted with 40% NaOH aq. solution and extracted with CH₂Cl₂ (5 × 50 mL). The organic layer was dried over Na₂SO₄ and concentrated to obtain the free amine **48** (0.10 g, 77%) as a colourless oil. ¹H NMR (CDCl₃, 300 MHz) δ 8.57 (s, 1H), 7.83 (br s, 1H, exchangeable with D₂O) 7.21 (s, 1H), 7.04 (s, 1H), 4.04 (s, 3H), 4.00 (s, 3H), 3.81 (q, *J* = 3.9 Hz, 2H), 3.08 (q, *J* = 5.4 Hz, 2H), 1.99 (m, 2H), 1.80 (br s, 2H, exchangeable with D₂O). MS (ESI+) : *m/z* 263 [M+1]⁺.

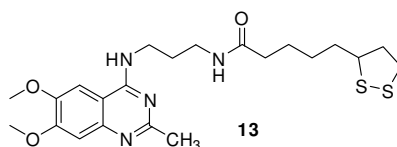


N-(3-(6,7-Dimethoxyquinazolin-4-ylamino)propyl)-5-(1,2-dithiolan-3-yl)pentanamide (12). It was synthesised from **48** (0.08 g, 0.30 mmol), NEt₃ (42 μL, 0.30 mmol), (±)-lipoic acid

(0.063 mg, 0.30 mmol) and EDCI·HCl (0.058 g, 0.30 mmol) following the procedure B. Purification by flash chromatography (CH₂Cl₂/MeOH 9.8:0.2) gave **12** (0.060 g, 44 %) as a yellowish oil. ¹H NMR (CDCl₃, 300 MHz) δ 8.51 (s, 1H), 7.57 (br s, 1H, exchangeable with D₂O), 7.45 (s, 1H), 7.20 (s, 1H), 6.57 (t, *J* = 6.3 Hz, 1H, exchangeable with D₂O), 4.05 (s, 3H), 4.01 (s, 3H), 3.72 (q, *J* = 5.4 Hz, 2H), 3.56 (m, 1H), 3.47-3.25 (m, 3H), 3.22-3.07 (m, 2H), 2.46 (m, 1H), 2.29 (t, *J* = 7.3 Hz, 2H), 2.00-1.40 (m, 8H). ¹³C-NMR (CDCl₃, 50 MHz) δ 174.24, 158.92, 154.53, 153.43, 149.21, 145.01, 108.20, 106.66, 101.08, 56.47, 56.29, 43.41, 40.33, 38.56, 37.26, 36.62, 36.21, 34.69, 29.40, 28.97, 25.56. MS (ESI+) : *m/z* 451 [M+1]⁺.

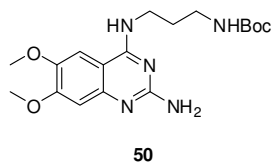


***N*-(6,7-dimethoxy-2-methylquinazolin-4-yl)propane-1,3-diamine (49)**. Following the procedure described in Millen *et al.*⁷, to a solution of **47**⁶ (0.60 g, 2.51 mmol) in anhydrous THF (20 mL) was added propane-1,3-diamine (420 μL, 5.03 mmol). Within 10 min the hydrochloric salt of diamine began precipitating out of the mixture. After stirring overnight at rt the solvent was removed *in vacuo*. The resulting crude was purified by flash column chromatography (CH₂Cl₂/MeOH 9.8:0.2) to obtain **49** (0.27 g, 40%) as an off-white solid. Mp = 110°-112 °C. ¹H NMR (CDCl₃, 200 MHz) δ 7.53 (s, 1H, exchangeable with D₂O), 7.15 (s, 1H), 6.96 (s, 1H), 4.00 (s, 3H), 3.97 (s, 3H), 3.82 (q, *J* = 5.4 Hz, 2H), 3.04 (t, *J* = 6.0 Hz, 2H), 2.62 (s, 3H), 1.87 (m, *J* = 6.0 Hz, 2H), 1.64 (br s, 2H, exchangeable with D₂O).



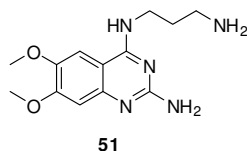
***N*-(3-(6,7-Dimethoxy-2-methylquinazolin-4-ylamino)propyl)-5-(1,2-dithiolan-3-yl)pentanamide (13)**. It was synthesised from **49** (0.24 g, 0.87 mmol), NEt₃ (121 μL, 0.87 mmol), (±)-lipoic acid (0.179 g, 0.87 mmol) and EDCI·HCl (0.167 g, 0.87 mmol) following the procedure B. Purification by flash chromatography (CH₂Cl₂/MeOH 9.3:0.7) afforded **13** (0.170 g, 42 %) as a yellowish oil. ¹H NMR (CDCl₃, 200 MHz) δ 7.30 (s, 1H), 7.13 (s, 1H), 7.05 (t, *J* = 5.8 Hz, 1H, exchangeable with D₂O), 6.57 (t, *J* = 5.8 Hz, 1H, exchangeable with D₂O), 4.01 (s, 3H), 3.97 (s, 3H), 3.73 (q, *J* = 6.0 Hz, 2H), 3.52 (m, 1H), 3.40 (q, *J* = 5.8 Hz, 2H), 3.25-3.03 (m,

2H), 2.60 (s, 3H), 2.52-2.23 (m, 5H), 1.97-1.45 (m, 7H). ^{13}C -NMR (CDCl_3 , 50 MHz) δ 173.89, 162.46, 159.09, 154.41, 151.08, 148.51, 106.84, 106.62, 100.81, 56.48, 56.36, 56.21, 40.33, 38.55, 37.05, 36.68, 36.03, 34.70, 29.72, 28.98, 26.34, 25.60. MS (ESI+) : m/z 465 $[\text{M}+1]^+$.

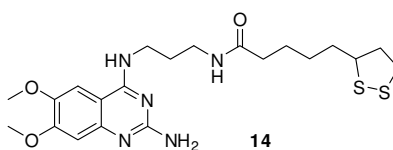


tert-Butyl 3-(2-amino-6,7-dimethoxyquinazolin-4-ylamino)propylcarbamate (50).

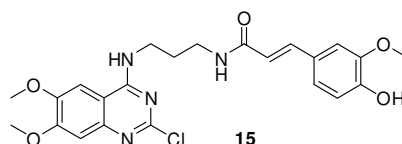
Following the procedure described in Ife *et al.*⁸, the chloroquinazoline **24** (0.45 g, 1.13 mmol) was dissolved in ethanolic ammonia (8 %) and heated in a sealed reactor at 140 °C for 24 hr. After cooling, solvent was evaporated off under vacuum and the obtained crude was purified by gravity column chromatography ($\text{CH}_2\text{Cl}_2/\text{MeOH}/\text{aqueous 30\% ammonia}$, 9.5:0.5:0.07) to obtain the title compound **50** (160 mg, 37%) as a white solid. Mp = 105°-108 °C. ^1H NMR (CDCl_3 , 300 MHz) δ 7.15 (s, 1H), 6.87 (s, 1H), 6.85 (br s, 1H, exchangeable with D_2O), 5.31 (br s, 1H, exchangeable with D_2O), 4.76 (br s, 2H, exchangeable with D_2O), 3.98 (s, 3H), 3.96 (s, 3H), 3.70 (q, $J = 5.8$ Hz, 2H), 3.30 (q, $J = 5.8$ Hz, 2H), 1.77 (m, $J = 6.0$ Hz, 2H), 1.49 (s, 9H). MS (ESI+) : m/z 378 $[\text{M}+1]^+$.



N^4 -(3-aminopropyl)-6,7-dimethoxyquinazolin-2,4-diamine (51). To a stirred solution of **50** (0.20 g, 0.529 mmol) in MeOH (2 mL) was added 3 N HCl solution (6 mL) and was allowed to stir at rt overnight. Concentration of the mixture under vacuum, using EtOH for the azeotropic removal of water, allowed to obtain the hydrochloride amine salt **51** (0.170 g, 91%) as a white solid. Mp = 280°-285 °C (dec.). ^1H NMR (CD_3OD , 200 MHz) δ 7.63 (s, 1H), 6.92 (s, 1H), 3.99 (s, 3H), 3.96 (s, 3H), 3.80 (t, $J = 7.0$ Hz, 2H), 3.07 (t, $J = 7.4$ Hz, 2H), 2.11 (m, $J = 7.4$ Hz, 2H).

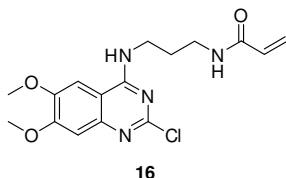


***N*-(3-(2-amino-6,7-dimethoxyquinazolin-4-ylamino)propyl)-5-(1,2-dithiolan-3-yl)pentanamide (14)**. Following the procedure described in Karamanska *et al.*,⁹ to a stirred suspension of **51** hydrochloride (0.170 g, 0.485 mmol) in anhydrous DMF (15 mL) at 0 °C was added NEt₃ (27 μL, 1.94 mmol), (±)-lipoic acid (0.100 g, 0.485 mmol) and EDCI·HCl (0.093 g, 0.485 mmol) under nitrogen atmosphere. After stirring at 0 °C for 20 min, the resulting mixture was allowing to reach rt overnight in the dark. After adding a further amount of NEt₃ (100 μL, 7.18 mmol) and EDCI·HCl (0.050 g, 0.260 mmol) and stirring at rt for 8 hr, solvent was removed under vacuum, avoiding heating up the reaction mixture. The residue was taken up in CH₂Cl₂ and washed with water (2 × 20 mL). The aqueous phase was re-extracted with CHCl₃ to recover 80 mg of starting amine whereas the organic phase was dried (Na₂SO₄), dried and concentrated to afford a crude that was purified by gravity chromatography (CH₂Cl₂/MeOH/aqueous 30% ammonia, 9.2:0.8:0.03) to obtain **14** (0.050 g, 22 %, 46 % borsm) as a yellowish oil. ¹H NMR (CDCl₃, 300 MHz) δ 7.25 (s, 1H), 7.10 (br s, 1H, exchangeable with D₂O), 6.89 (s, 1H), 5.98 (br t, *J* = 6.6 Hz, 1H, exchangeable with D₂O), 4.96 (br s, 2H, exchangeable with D₂O), 4.02 (s, 3H), 3.98 (s, 3H), 3.67 (q, *J* = 6.0 Hz, 2H), 3.57 (t, *J* = 6.3 Hz, 1H), 3.45 (q, *J* = 6.0 Hz, 2H), 3.25-3.11 (m, 3H), 2.48 (m, 1H), 2.27 (t, *J* = 8.4 Hz, 2H), 2.00-1.40 (m, 8H). MS (ESI+) : *m/z* 466 [M+1]⁺.

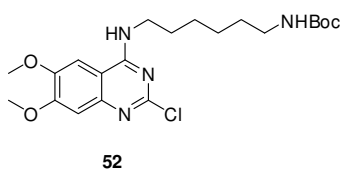


(*E*)-*N*-(3-(2-chloro-6,7-dimethoxyquinazolin-4-ylamino)propyl)-3-(4-hydroxy-3-methoxyphenyl)acrylamide (15). To a stirred solution of **26** (0.18 g, 0.607 mmol), *trans*-ferulic acid (0.118 g, 0.607 mmol) and NEt₃ (254 μL, 1.82 mmol) in CH₂Cl₂ (50 mL), a 50% solution of propylphosphonic anhydride¹⁰ in DMF (0.464 mL, 0.728 mmol) was added. The resulting mixture was allowed to stir at rt for 8 hr, then was quenched with water, diluted with CH₂Cl₂ and washed with water (3 × 20 mL). The organic phase was dried over Na₂SO₄ and concentrated to obtain a crude that was purified by gravity column chromatography (CH₂Cl₂/MeOH 9.6:0.4) to obtain **15** (0.150 g, 53 %) as a white solid. Mp = 185°-188 °C. ¹H NMR (CDCl₃, 400 MHz) δ 7.56 (d, *J* = 15.6 Hz, 1H), 7.44 (br t, 1H, exchangeable with D₂O), 7.35 (s, 1H), 7.12 (s, 1H), 7.08 (dd, *J* = 8.4, 1.5 Hz, 1H), 7.00 (d, *J* = 1.5 Hz, 1H), 6.92 (d, *J* = 8.4 Hz, 1H), 6.39 (d, *J* = 15.6 Hz, 1H), 6.28 (br t, 1H, exchangeable with D₂O), 5.83 (br s, 1H, exchangeable with D₂O),

4.09 (s, 3H), 3.98 (s, 3H), 3.93 (s, 3H), 3.75 (q, $J = 4.8$ Hz, 2H), 3.54 (q, $J = 6.0$ Hz, 2H), 1.87 (m, 2H). ^{13}C -NMR (CDCl_3 , 100 MHz) δ 166.70, 159.60, 158.80, 155.70, 151.50, 151.30, 147.30, 144.90, 141.92, 128.80, 120.10, 118.80, 118.03, 109.63, 115.00, 111.92, 101.05, 56.59, 56.43, 56.20, 37.31, 36.35, 29.71. MS (ESI-) : m/z 471 $[\text{M}-1]^-$.

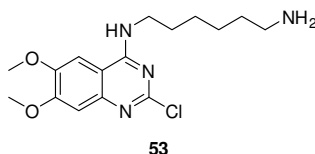


***N*-(3-(2-chloro-6,7-dimethoxyquinazolin-4-ylamino)propyl)acrylamide (16).** To a stirred solution of **26** (0.10 g, 0.337 mmol) in CH_2Cl_2 (15 mL) at 0°C was added NEt_3 (70 μL , 0.505 mmol) and acryloyl chloride (40 μL , 0.50 mmol). After stirring at 0°C for 20 min, the resulting mixture was allowing to reach rt in 6 hr. The reaction was quenched with water, diluted with CH_2Cl_2 and washed with water (3×20 mL). The organic phase was dried over Na_2SO_4 and concentrated to obtain a crude that was subjected to gravity column purification ($\text{CH}_2\text{Cl}_2/\text{MeOH}$ 9.5:0.5) to obtain **16** (0.080 g, 68 %) as a white solid. ^1H NMR ($(\text{CD}_3)_2\text{SO}$, 200 MHz) δ 8.35 (br t, 1H, exchangeable with D_2O), 8.19 (br t, 1H, exchangeable with D_2O), 7.62 (s, 1H), 7.07 (s, 1H), 6.30-6.17 (dd, $J = 16.0, 10.0$ Hz, 1H), 6.12-6.02 (dd, $J = 16.0, 3.0$ Hz, 1H), 5.62-5.55 (dd, $J = 10.0, 3.0$ Hz, 1H), 3.89 (s, 6H), 3.52 (q, $J = 5.4$ Hz, 2H), 3.25 (q, $J = 5.4$ Hz, 2H), 1.83 (m, 2H). MS (ESI+) : m/z 351 $[\text{M}+1]^+$.

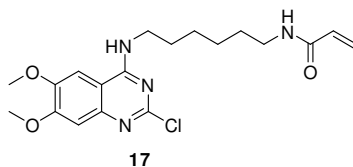


***tert*-Butyl 6-(2-chloro-6,7-dimethoxyquinazolin-4-ylamino)hexylcarbamate (52).** To a stirred solution of 2,4-dichloro-6,7-dimethoxyquinazoline **45** (0.20 g, 0.77 mmol) in anhydrous DMF (10 mL) was added *tert*-butyl 6-aminohexylcarbamate (0.519 mL, 2.32 mmol). The resulting mixture was stirred at rt for 2 hr. To the reaction mixture ice water was added until a suspension could be seen. The solid was filtered out and the filtrate was extracted with CH_2Cl_2 (2×20 mL). The organic phase were dried over Na_2SO_4 , concentrated and joined to the filtered solid. The overall residue was purified by flash column chromatography (petroleum ether/EtOAc, gradient from 8.8 :1.2 to 100% EtOAc) to obtain **52** (0.20 g, 60 %) as a white

solid. ^1H NMR (CDCl_3 , 300 MHz) δ 7.29 (s, 1H), 7.12 (s, 1H), 6.78 (br s, 1H, exchangeable with D_2O), 4.65 (br s, 1H, exchangeable with D_2O), 3.96 (s, 6H), 3.63 (q, $J = 6.0$ Hz, 2H), 3.18 (q, $J = 6.0$ Hz, 2H), 1.70 (t, $J = 6.6$ Hz, 2H), 1.49-1.33 (m, 15H). ^{13}C NMR (CDCl_3 , 50 MHz) δ 160.32, 156.67, 156.36, 154.75, 148.93, 147.73, 107.33, 106.83, 101.14, 79.41, 56.31, 56.18, 40.52, 39.66, 30.12 (2C), 28.51 (3C), 25.46, 25.15. MS (ESI+) : m/z 461 [$\text{M}+23$] $^+$.

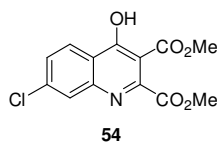


***N*¹-(2-chloro-6,7-dimethoxyquinazolin-4-yl)hexane-1,6-diamine (53).** To a stirred solution of **52** (0.070 g, 0.159 mmol) in MeOH (5 mL) was added 3 N HCl solution (5 mL) and was allowed to stir at rt overnight. MeOH was evaporated off under vacuum, then diluted and extracted with CH_2Cl_2 (3×10 mL). The organic layer was dried over Na_2SO_4 and concentrated to obtain the hydrochloride amine salt **53** (0.040 g, 75%) as a white solid. ^1H NMR (CDCl_3 , 200 MHz) δ 7.10 (s, 1H), 7.05 (s, 1H), 6.42 (t, 1H, exchangeable with D_2O), 3.91 (s, 3H), 3.90 (s, 3H), 3.60 (q, $J = 6.2$ Hz, 2H), 2.66 (t, $J = 6.2$ Hz, 2H), 1.91 (br s, 3H, exchangeable with D_2O), 1.70 (m, 2H), 1.40-1.20 (m, 6H). MS (ESI+) : m/z 263 [$\text{M}+1$] $^+$.

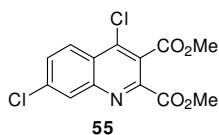


***N*-(6-(2-chloro-6,7-dimethoxyquinazolin-4-ylamino)hexyl)acrylamide (17).** To a stirred solution of **53** (0.30 g, 0.885 mmol) in CH_2Cl_2 (30 mL) at 0 °C was added NEt_3 (72 μL , 1.33 mmol) and acryloyl chloride (72 μL , 0.885 mmol). After stirring at 0 °C for 20 min, the resulting mixture was allowing to reach rt in 3 hr. The reaction was quenched with water, diluted with CH_2Cl_2 and washed with water (3×20 mL). The organic phase was dried over Na_2SO_4 and concentrated to obtain a crude that was subjected to gravity column purification ($\text{CH}_2\text{Cl}_2/\text{MeOH}$ 9.5:0.5) to obtain **17** (0.20 g, 58 %) as a white solid. Mp = 155°-158 °C. ^1H NMR (CDCl_3 , 300 MHz) δ 7.52 (s, 1H), 7.13 (s, 1H), 7.01 (br t, 1H, exchangeable with D_2O), 6.35-6.29 (dd, $J = 17.1, 1.5$ Hz, 1H), 6.20-6.11 (dd, $J = 17.1, 9.9$ Hz, 1H), 5.86 (br t, 1H, exchangeable with D_2O), 5.71-5.67 (dd, $J = 9.9, 1.2$ Hz, 1H), 3.98 (s, 3H), 3.95 (s, 3H), 3.63 (q, $J = 6.3$ Hz, 2H), 3.44 (q,

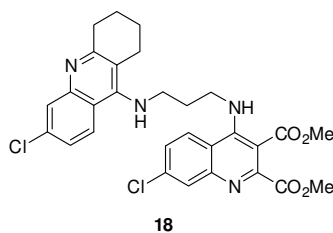
$J = 6.6$ Hz, 2H), 1.80-1.25 (m, 8H). MS (ESI+) : m/z 393 [M+1]⁺.



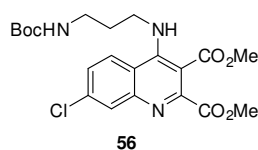
Dimethyl 7-chloro-4-hydroxyquinoline-2,3-dicarboxylate (54).¹¹ A stirred mixture of methyl 2-amino-4-chlorobenzoate (5.0 g, 27 mmol) and dimethyl acetylenedicarboxylate (5.1 g, 35 mmol) in *t*-butanol (44 mL) was refluxed for 7 hr under a nitrogen atmosphere. After adding additional dimethyl acetylenedicarboxylate (2.32 g, 16 mmol) and refluxing another 9 hr the reaction mixture was allowed to cool to rt and potassium *t*-butoxide (3.0 g, 26.7 mmol) was added in one portion. A violet precipitate formed and the resulting mixture was refluxed for 1.5 hr. The mixture was cooled to rt and filtered to separate the solids which are washed with *t*-butanol and ether. The solids were dissolved in water and acidified with 1N sulfuric acid to form a green precipitate. The resulting mixture was extracted with CH₂Cl₂ and the combined extracts were washed with brine and water, dried over Na₂SO₄, filtered and concentrated to give a green solid. Recrystallization of this material from MeOH provided **54** (2.00 g, 25%) as an off-white solid. Mp = 225-228 °C. ¹H NMR (CDCl₃, 200 MHz) δ 8.30 (d, $J = 9.0$ Hz, 1H), 8.06 (s, 1H), 7.58 (d, $J = 9.0$, 1H), 4.03 (s, 6H). MS (ESI-) : m/z 294 [M-1]⁻.



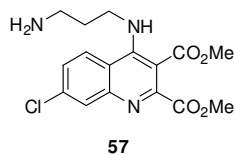
Dimethyl 4,7-dichloroquinoline-2,3-dicarboxylate (55).¹¹ A mixture of **54** (1.31 g, 4.43 mmol), phosphorous oxychloride (5 mL, 53.64 mmol) and toluene (2 mL) was heated briefly at 90 °C. After cooling at rt, the reaction mixture was quenched with ice-water and extracted with EtOAc. The combined extracts were dried over Na₂SO₄, filtered and concentrated to lead the title dichloroquinoline **55** (1.39 g, quantitative) as a crystalline yellow solid. Mp = 110-113 °C. ¹H NMR (CDCl₃, 200 MHz) δ 8.33 (dd, $J = 4.0, 1.4$ Hz, 1H), 8.27 (s, 1H), 7.77 (dd, $J = 8.8, 2.2$ Hz, 1H), 4.08 (s, 6H). MS (ESI+) : m/z 338 [M+23]⁺.



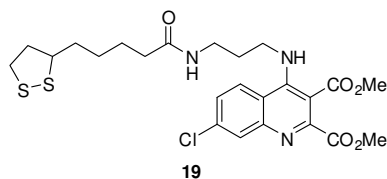
Dimethyl 7-chloro-4-(3-(6-chloro-1,2,3,4-tetrahydroacridin-9-ylamino)propylamino)quinoline-2,3-dicarboxylate (18). A stirred solution of **55** (0.23 g, 0.73 mmol) and N^1 -(6-chloro-1,2,3,4-tetrahydroacridin-9-yl)propane-1,3-diamine **23**¹² (0.21 g, 0.73 mmol) in EtOH (50 mL) and NEt₃ (0.10 mL, 0.73 mmol) was refluxed for 24 hr. After the solvent removal under vacuum the crude was purified by flash chromatography (CH₂Cl₂/MeOH, 9.5:0.5) to obtain 0.17 g of **18** (0.17 g, 40 %) as a white crystalline solid. Mp = 230-235 °C (dec.). ¹H NMR (CDCl₃, 200 MHz) δ 9.48 (br t, 1H, exchangeable with D₂O) 8.20 (d, $J = 9.2$ Hz, 1H), 8.15-8.00 (m, 2H), 7.83 (d, $J = 2.2$ Hz, 1H), 7.35 (d, $J = 9.2$ Hz, 1H), 7.20 (d, $J = 9.2$ Hz, 1H), 6.30 (br t, 1H, exchangeable with D₂O), 4.10-3.95 (m, 7H), 3.89 (s, 3H), 3.08 (t, 2H), 2.65 (t, 2H) 2.34 (m, 2H), 1.81 (m, 4H). MS (ESI+) : m/z 569 [M+1]⁺.



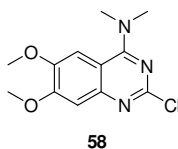
Dimethyl 4-(3-(tert-butoxycarbonylamino)propylamino)-7-chloroquinoline-2,3-dicarboxylate (56). To a stirred solution of **55** (0.46 g, 1.46 mmol) in EtOH (100 mL) was added a solution of *tert*-butyl 3-aminopropylcarbamate (0.25 g, 1.46 mmol) in EtOH. The resulting mixture was refluxed for 5 hr. After adding an additional amine (0.10 g, 0.57 mmol) and refluxing another 8 hr the reaction mixture was allowed to cool to rt. The solvent was removed under pressure and the crude was purified by flash chromatography (petroleum ether/EtOAc 88:12 to 100% EtOAc) to furnish title compound **56** (0.23 g, 40 %) as a yellow solid. Mp = 144-146 °C. ¹H NMR (CDCl₃, 200 MHz) δ 9.48 (br s, 1H, exchangeable with D₂O) 8.35 (d, $J = 9.2$ Hz, 1H), 8.20 (s, 1H), 7.41 (d, $J = 9.2$ Hz, 1H), 5.25 (br s, 1H, exchangeable with D₂O), 4.01 (s, 3H), 3.90 (s, 3H), 3.82 (m, 2H), 3.30 (q, $J = 5.4$ Hz, 2H), 1.98 (m, 2H), 1.40 (m, 9H). MS (ESI+) : m/z 452 [M+1]⁺.



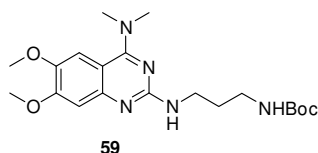
Dimethyl 4-(3-aminopropylamino)-7-chloroquinoline-2,3-dicarboxylate (57). To a stirred solution of **56** (0.23 g, 0.50 mmol) in CH₂Cl₂ (10 mL) at 0 °C was carefully added trifluoroacetic acid (2 mL) and was allowed to stir at rt in 2 hr. The solvent were evaporated under pressure, adding heptane for the azeotropic removal of trifluoroacetic acid to obtain **57** as trifluoroacetate salt. The product was dissolved in alkaline water (K₂CO₃) and extracted with CH₂Cl₂. The solvent was removed under pressure to furnish the free amine **57** (0.17 g, quantitative) as a colourless oil. ¹H NMR (CDCl₃, 300 MHz) δ 9.13 (br s, 1H, exchangeable with D₂O) 8.15 (d, *J* = 9.0 Hz, 1H), 8.00 (s, 1H), 7.41 (d, *J* = 9.0 Hz, 1H), 4.00 (s, 3H), 3.90 (s, 3H), 3.78 (q, *J* = 6.3 Hz, 2H), 2.99 (t, *J* = 6.0 Hz, 2H), 1.89 (m, 2H), 1.48 (br s, 2H, exchangeable with D₂O). MS (ESI+) : m/z 352 [M+1]⁺.



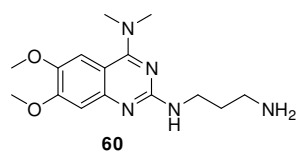
Dimethyl 4-(3-(5-(1,2-dithiolan-3-yl)pentanamido)propylamino)-7-chloroquinoline-2,3-dicarboxylate (19). It was synthesised from **57** (0.20 g, 0.57 mmol), NEt₃ (79 μL, 0.57 mmol), (±)-lipoic acid (0.117 g, 0.57 mmol) and EDCI·HCl (0.109 g, 0.57 mmol) following the procedure B. Purification by flash chromatography (CH₂Cl₂/MeOH 98:2) afforded **19** (0.21 g, 68 %) as a yellowish oil. ¹H NMR (CDCl₃, 400 MHz) δ 8.67 (t, *J* = 4.4 Hz, 1H, exchangeable with D₂O), 8.11 (d, *J* = 9.2 Hz, 1H), 7.88 (d, *J* = 1.6 Hz, 1H), 7.35 (dd, *J* = 8.4, 1.6 Hz, 1H), 6.01 (t, *J* = 6.0 Hz, 1H, exchangeable with D₂O), 3.94 (s, 3H), 3.86 (s, 3H), 3.70 (q, *J* = 5.6 Hz, 2H), 3.51 (m, *J* = 8.0 Hz, 1H), 3.39 (q, *J* = 6.4 Hz, 2H), 3.15-3.05 (m, 2H), 2.41 (m, *J* = 6.0 Hz, 1H), 2.16 (t, *J* = 7.6 Hz, 2H), 1.94-1.82 (m, 3H), 1.70-1.52 (m, 4H), 1.40 (q, *J* = 7.6 Hz, 2H). ¹³C-NMR (CDCl₃, 100 MHz) δ 173.70, 168.38, 167.99, 155.40, 153.15, 149.66, 137.83, 129.14, 126.60, 126.55, 118.02, 101.97, 56.63, 53.12, 52.69, 45.86, 40.46, 38.68, 36.76, 36.54, 34.77, 31.15, 29.10, 25.59. MS (ESI+) : m/z 541 [M+1]⁺.



2-chloro-6,7-dimethoxy-*N,N*-dimethylquinazolin-4-amine (58). Following the procedure described in Kanuma *et al.*,¹³ to a stirred solution of 2,4-dichloro-6,7-dimethoxyquinazoline **45** (0.50 g, 1.93 mmol) in THF (25 mL) was added 50 % aq. dimethylamine solution (0.49 mL, 3.86 mmol). After stirring at rt for 2 hr, the solvent was removed under vacuum. The obtained residue was taken up in CHCl₃ (100 mL) and washed with brine, the aqueous phase was re-extracted with CHCl₃ (3 × 50 mL). The combined organic extracts were dried over Na₂SO₄ and concentrated to obtain the title compound **58** (0.48 g, 93 %) as a yellow solid. Mp = 155°-160 °C. ¹H NMR (CDCl₃, 300 MHz) δ 7.28 (s, 1H), 7.18 (s, 1H), 4.01 (s, 3H), 3.98 (s, 3H), 3.37 (s, 6H).

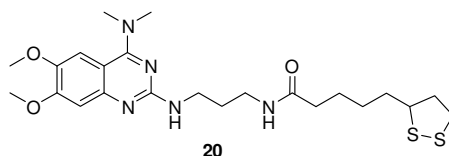


tert-Butyl 3-(4-(dimethylamino)-6,7-dimethoxyquinazolin-2-ylamino)propylcarbamate (59). To a stirred solution of **58** (0.40 g, 1.49 mmol) in iso-amylalcohol (5 mL) was added a solution of *tert*-butyl 3-aminopropylcarbamate (0.49 g, 2.91 mmol) iso-amylalcohol and NEt₃ (0.21 mL, 1.49 mmol). The resulting mixture was stirred at 160 °C for 6 hr. After cooling at rt, the reaction mixture was concentrated and the obtained residue was taken up in CHCl₃ (100 mL) and washed with brine. The organic phase was dried over Na₂SO₄ and concentrated to obtain a crude that was purified by flash chromatography (CH₂Cl₂/toluene/MeOH/aqueous 30% ammonia, 9:1:0.5:0.05) to obtain **59** (0.34 g, 56 %) as a white solid. ¹H NMR (CDCl₃, 200 MHz) δ 7.15 (s, 1H), 6.92 (s, 1H), 5.75 (br s, 1H, exchangeable with D₂O), 5.05 (br s, 1H, exchangeable with D₂O), 3.99 (s, 3H), 3.93 (s, 3H), 3.58 (q, *J* = 6.2 Hz, 2H), 3.25-3.16 (m, 8H), 1.68-1.82 (m, 2H), 1.48 (m, 9H).

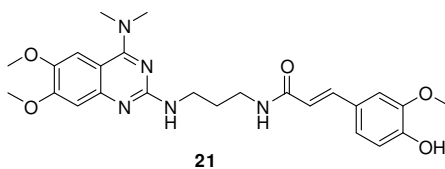


***N*²-(3-aminopropyl)-6,7-dimethoxy-*N*⁴,*N*⁴-dimethylquinazoline-2,4-diamine (60).** To a

stirred solution of **59** (0.34 g, 0.806 mmol) in CH₂Cl₂ (5 mL) at 0 °C was carefully added trifluoroacetic acid (1 mL) and was allowed to stir at rt in 5 hr. The solvent was evaporated under pressure, adding heptane for the azeotropic removal of trifluoroacetic acid to obtain the trifluoroacetate salt. The product was dissolved in alkaline water (K₂CO₃) and extracted with CH₂Cl₂ (3 × 50 mL). The organic extract was dried over Na₂SO₄ and concentrated in vacuo to furnish the free amine **60** (0.26 g, quantitative) as a colourless oil. ¹H NMR (CDCl₃, 300 MHz) δ 7.15 (s, 1H), 6.90 (s, 1H), 5.22 (br s, 1H, exchangeable with D₂O), 3.99 (s, 3H), 3.93 (s, 3H), 3.58 (q, *J* = 6.2 Hz, 2H), 3.17 (s, 6H), 2.82 (t, *J* = 5.4 Hz, 2H), 1.89 (s, 2H, exchangeable with D₂O), 1.83-1.70 (m, 2H).

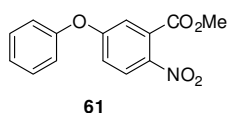


***N*-(3-(4-(dimethylamino)-6,7-dimethoxyquinazolin-2-ylamino)propyl)-5-(1,2-dithiolan-3-yl)pentanamide (20)**. It was synthesised from **60** (0.27 g, 0.882 mmol), NEt₃ (123 μL, 0.882 mmol), (±)-lipoic acid (0.182 g, 0.882 mmol) and EDCI·HCl (0.170 g, 0.882 mmol) following the procedure B. Purification by gravity chromatography (gradient elution from CH₂Cl₂/petroleum ether/MeOH 7.5:2:0.5 to 7.2: 2:0.8) to obtain **20** (0.200 g, 46 %) as a yellowish oil. ¹H NMR (CDCl₃, 300 MHz) δ 7.22 (s, 1H), 7.16 (s, 1H), 6.96 (br m, 1H, exchangeable with D₂O), 6.72 (br m, 1H, exchangeable with D₂O), 4.01 (s, 3H), 3.93 (s, 3H), 3.60-3.45 (m, 2H), 3.45 (s, 6H), 3.45-3.35 (m, 2H), 3.09-3.18 (m, 2H), 2.50-2.40 (m, 1H), 2.24 (t, *J* = 7.0 Hz, 2H), 2.00-1.20 (m, 10H). MS (ESI+) : *m/z* 494 [M+1]⁺.

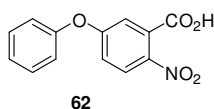


***(E)*-N-(3-(4-(dimethylamino)-6,7-dimethoxyquinazolin-2-ylamino)propyl)-3-(4-hydroxy-3-methoxyphenyl)acrylamide (21)**. To a stirred solution of **60** (0.21 g, 0.69 mmol), *trans*-ferulic acid (0.13 g, 0.69 mmol) and NEt₃ (290 μL, 2.01 mmol) in CH₂Cl₂ (30 mL), a 50% solution of propylphosphonic anhydride¹⁰ in DMF (0.52 mL, 0.82 mmol) was added. The resulting mixture was allowed to stir at rt for 8 hr. After adding further amount of propylphosphonic anhydride in DMF (0.26 mL, 0.41 mmol) and stirring for 8 hr, the reaction

mixture was quenched with water, washed with water, diluted K_2CO_3 , and 1N HCl. The organic phase was dried over Na_2SO_4 and concentrated to obtain a crude that was purified by flash column chromatography ($CH_2Cl_2/MeOH$ 9:1 to $CH_2Cl_2/MeOH/$ aqueous 30% ammonia 9:1:0.1) to obtain **21** (0.175 g, 53 %) as a off-white solid. Mp = 140°-145 °C. 1H NMR ($CDCl_3$, 400 MHz) δ 8.05 (br s, 1H, exchangeable with D_2O), 7.41 (d, J = 15.6 Hz, 1H), 7.25 (br s, 1H, exchangeable with D_2O), 7.22 (s, 1H), 7.16 (s, 1H), 6.98 (s, 1H), 6.90 (d, J = 1.8 Hz, 1H), 6.89 (br s, 1H, exchangeable with D_2O), 6.80 (d, J = 1.8 Hz, 1H), 6.45 (d, J = 15.6 Hz, 1H), 3.89 (s, 3H), 3.87 (s, 3H), 3.85 (s, 3H), 3.70-3.55 (q, J = 5.4 Hz, 2H), 3.55-3.45 (q, J = 5.4 Hz, 2H), 3.40 (s, 6H), 1.95 (t, J = 5.4 Hz, 2H). ^{13}C -NMR ($CDCl_3$, 100 MHz) δ 166.93, 147.53, 147.08, 145.58, 140.10 (2C), 127.78 (2C), 122.29 (2C), 119.25 (2C), 114.91 (2C), 109.83 (2C), 107.34, 56.63, 56.56, 56.18, 42.23 (2C), 39.54, 37.69, 29.90. MS (ESI+) : m/z 482 $[M+1]^+$.

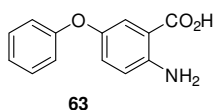


Methyl 2-nitro-5-phenoxybenzoate (61). Following the procedure described in Dunn *et al.*,¹⁴ to a stirred solution of phenol (4.18 g, 44.4 mmol) in *N*-methyl-2-pyrrolidone (40 mL) K_2CO_3 powder (8.20 g, 59.4 mmol) was added in small portions. The obtained suspension was stirred at rt for 30 min, then methyl 5-chloro-2-nitrobenzoate (8.00 g, 59.4 mmol) was added in small portions to obtain a orange solution that was stirred at 160 °C for 3 hr. The reaction mixture was cooled to rt, poured in ice-water (150 mL) and extracted with EtOAc (2 \times 70 mL). The organic layer was washed with water (2 \times 50 mL), brine (2 \times 50 mL), dried over Na_2SO_4 , concentrated in vacuo, and the obtained residue was purified by flash chromatography (petroleum ether/EtOAc, 95:5) to obtain **61** (5.46 g, 54%) as a yellow oil. 1H NMR ($CDCl_3$, 300 MHz) δ 8.04 (d, J = 8.4 Hz, 1H), 7.41 (m, 2H), 7.30 (t, J = 7.5 Hz, 1H), 7.13-7.06 (m, 4H), 3.93 (s, 3H). ^{13}C NMR ($CDCl_3$, 50 MHz) δ 166.17, 162.26, 154.41, 151.08, 131.23, 130.57 (2C), 126.79, 125.86, 120.65 (2C), 118.71, 117.14, 53.46.

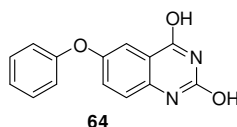


2-Nitro-5-phenoxybenzoic acid (62). Following the procedure described in Dunn *et al.*,¹⁴ to a solution of **61** (3.36 g, 13.2 mmol) in MeOH/water (15/15 mL) was added NaOH pellets (1.58 g, 39.56 mmol) at 0 °C. The reaction mixture was heated at 70 °C for 2 hr. After cooling to rt, the

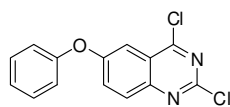
reaction was acidified with 3 N HCl and extracted with EtOAc (3 × 100 mL). The organic layer was washed with brine, dried over Na₂SO₄, concentrated in vacuo. The obtained residue was purified by flash chromatography (petroleum ether/EtOAc/toluene/AcOH, 60:30:10:1.5) to obtain **62** (2.82 g, 83%) as a brown solid. Mp = 145°-147 °C. ¹H NMR (CDCl₃, 200 MHz) δ 9.41 (br s, 1H), 8.00 (d, *J* = 8.8 Hz, 1H), 7.44-7.52 (m, 2H), 7.25-7.35 (m, 2H), 7.11-7.17 (m, 3H). ¹³C NMR (CDCl₃, 75 MHz) δ 170.85, 162.28, 154.53, 141.95, 130.81 (2C), 129.81, 126.97, 126.16, 120.83 (2C), 119.56, 117.72.



2-Amino-5-phenoxybenzoic acid (63). To a solution of **62** (2.82 g, 10.9 mmol) in EtOH (110 mL) was added palladium on activated carbon, and the mixture was stirred under hydrogen for 6 hr. The suspension was filtered through celite and the filtrate concentrated and dried in vacuo to yield **63** (2.39 g, 96 %) as a light brown solid. Mp = 140°-142 °C. ¹H NMR (CDCl₃, 200 MHz) δ 7.65 (d, *J* = 3.0 Hz, 1H), 7.34 (d, *J* = 8.2 Hz, 2H), 6.93-7.16 (m, 4H), 6.71 (d, *J* = 8.8 Hz, 1H). ¹³C NMR (CDCl₃, 75 MHz) δ 172.75, 158.76, 148.13, 146.51, 129.87 (2C), 128.77, 126.61 (2C), 118.49, 117.42 (2C), 109.95.

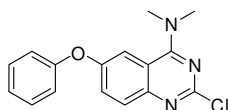


6-Phenoxyquinazoline-2,4-diol (64). Following the procedure described in Wéber *et al.*,¹⁵ to a mechanically stirred suspension of **63** (1.73 g, 7.55 mmol) in water (30 mL) and acetic acid (1 mL, 17.5 mmol) a solution of KOCN (1.35 g, 16.6 mmol) in water (10 mL) was added dropwise. After stirring at rt for 90 min, NaOH pellets (15.31 g, 383 mmol) were added in one portion and the solution was allowed to heat at 90-100 °C for 5 hr. After cooling to rt, the reaction was acidified with 6 N HCl until a brown precipitated was formed. The suspension was filtered under vacuum, the collected solid was washed repeatedly with water to obtain **64** (1.51 g, 61%) as a light brown solid. Mp = >260 °C. ¹H NMR ((CD₃)₂SO, 200 MHz) δ 11.34 (s, 1H), 11.17 (s, 1H), 7.32-7.45 (m, 5H), 7.23-7.13 (m, 2H), 7.05-7.01 (d, *J* = 7.6 Hz, 1H).



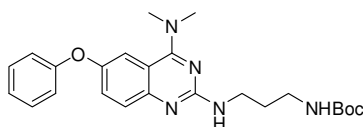
65

2,4-Dichloro-6-phenoxyquinazoline (65). Following the procedure described in Wéber *et al.*,¹⁵ to compound **64** (0.62 g, 2.43 mmol) was added POCl₃ (3.34 mL, 36.0 mmol) dropwise and *N,N*-dimethylaniline (0.15 mL, 1.21 mmol) and toluene (2 mL). The reaction mixture was heated at 115 °C for 7 hr. After adding a further amount of POCl₃ (3.00 mL, 32.3 mmol) and *N,N*-dimethylaniline (0.15 mL, 1.21 mmol) and refluxing another 16 hr the reaction mixture was allowed to cool to rt, and POCl₃ was distilled off, then the residue was poured into ice-water. The slurry was stirred, then the solid was filtered under vacuum, washed with water and dried to yield **65** (0.56 g, 80%) as a yellow solid. Mp = 98°-100 °C. ¹H NMR (CDCl₃, 200 MHz) δ 8.0 (d, *J* = 9.2 Hz, 1H), 7.81-7.70 (dd, *J* = 9.2, 2.4 Hz, 1H), 7.58-7.44 (m, 2H), 7.40-7.28 (m, 2H), 7.14 (d, *J* = 8.0 Hz, 2H).



66

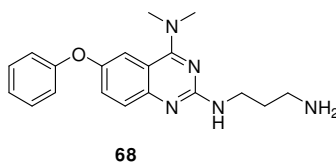
2-Chloro-*N,N*-dimethyl-6-phenoxyquinazolin-4-amine (66). Following the procedure described in Kanuma *et al.*,¹³ to a stirred solution of **65** (0.35 g, 1.20 mmol) in THF (15 mL) was added 50 % aq. dimethylamine solution (0.30 mL, 2.40 mmol). After stirring at rt for 2 hr, the solvent was removed under vacuum. The obtained residue was taken up in CHCl₃ (70 mL) and washed with brine. The organic extracts were dried over Na₂SO₄ and concentrated to obtain the title **66** (0.34 g, 94 %) as a white solid. Mp = 106°-108 °C. ¹H NMR (CDCl₃, 200 MHz) δ 7.80 (d, *J* = 9.2 Hz, 1H), 7.59-7.30 (m, 4H), 7.18 (t, *J* = 7.4 Hz, 1H), 7.05 (d, *J* = 8.2 Hz, 2H), 3.32 (s, 6H).



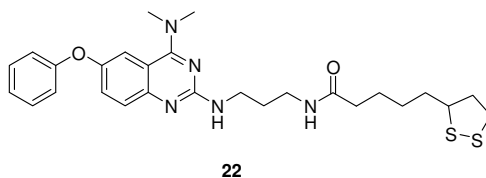
67

***tert*-Butyl 3-(4-(dimethylamino)-6-phenoxyquinazolin-2-ylamino)propylcarbamate (67).** To a stirred solution of **66** (0.34 g, 1.13 mmol) in iso-amylalcohol (3 mL) was added a solution of *tert*-butyl 3-aminopropylcarbamate (0.30 g, 1.70 mmol) iso-amylalcohol and NEt₃ (0.1 mL,

0.70 mmol). The resulting mixture was stirred at 160 °C for 4 hr. After adding further amount of *tert*-butyl 3-aminopropylcarbamate (0.17 g, 0.97 mmol) and refluxing another hour, the reaction mixture was allowed to cool to rt and concentrated. The obtained residue was taken up in CHCl₃ (50 mL) and washed with brine. The organic phase was dried over Na₂SO₄ and concentrated to obtain a crude that was purified by flash chromatography (CH₂Cl₂/toluene/MeOH 9.7:1:0.3) to obtain **67** (0.36 g, 73 %) as a yellow oil. ¹H NMR (CDCl₃, 200 MHz) δ 7.58 (d, *J* = 9.2 Hz, 1H), 7.45 (d, *J* = 2.2 Hz, 1H), 7.35-7.26 (m, 3H), 7.08 (t, *J* = 7.4 Hz, 1H), 6.98 (d, *J* = 7.8 Hz, 2H), 6.25 (br s, 1H, exchangeable with D₂O), 5.39 (br s, 1H, exchangeable with D₂O), 3.60 (q, *J* = 6.2 Hz, 2H), 3.25-3.15 (m, 8H), 1.69-1.81 (m, 2H), 1.47 (m, 9H).

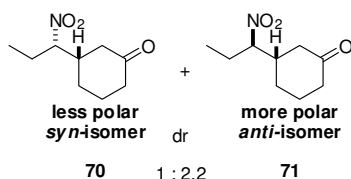


***N*²-(3-Aminopropyl)-*N*⁴,*N*⁴-dimethyl-6-phenoxyquinazoline-2,4-diamine (68).** To a stirred solution of **67** (0.36 g, 0.82 mmol) in CH₂Cl₂ (5 mL) at 0 °C was carefully added trifluoroacetic acid (0.64 mL, 8.32 mmol) and was allowed to stir at rt in 3 hr. The solvent were evaporated under pressure, adding heptane for the azeotropic removal of trifluoroacetic acid traces to obtain the trifluoroacetate salt. The product was dissolved in alkaline water (40 % NaOH) and extracted with CH₂Cl₂ (5 × 20 mL). The organic extract was dried over Na₂SO₄ and concentrated to obtain a residue that was purified by flash chromatography (CH₂Cl₂/toluene/MeOH/30% aq. ammonia, 9:1:1:0.1) to obtain **68** (0.23 g, 83 %) as a yellow oil. ¹H NMR (CDCl₃, 200 MHz) δ 7.47 (d, *J* = 10.0 Hz, 2H), 7.31-7.27 (m, 3H), 7.10-6.93 (m, 3H), 5.22 (br s, 1H, exchangeable with D₂O), 3.58 (q, 2H, *J* = 6.2 Hz), 3.17 (s, 6H), 2.82 (t, 2H, *J* = 5.4 Hz), 1.88 (s, 2H, exchangeable with D₂O), 1.83-1.70 (m, 2H).



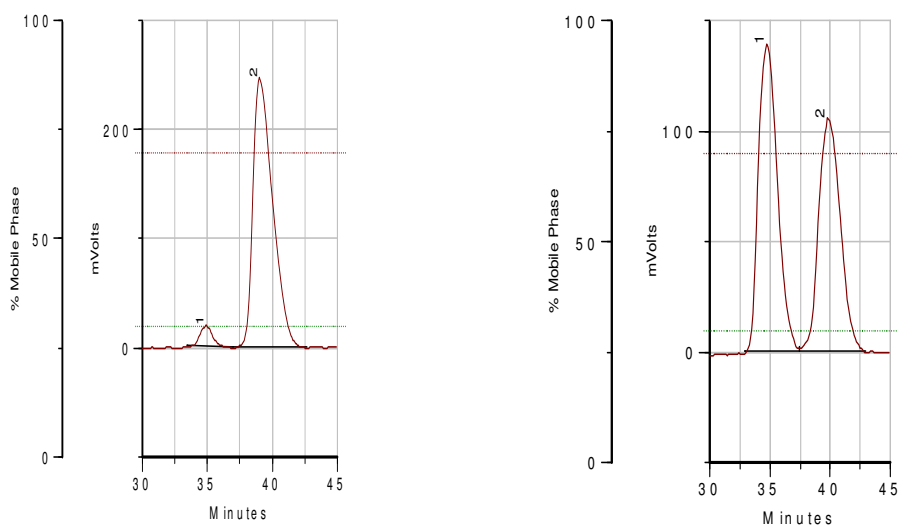
***N*-(3-(4-(Dimethylamino)-6-phenoxyquinazolin-2-ylamino)propyl)-5-(1,2-dithiolan-3-yl)pentanamide (22).** It was synthesised from **68** (0.23 g, 0.68 mmol), NEt₃ (95 μL, 0.68 mmol), (±)-lipoic acid (0.140 g, 0.068 mmol) and EDCI·HCl (0.130 g, 0.68 mmol) following the

procedure B. Purification by flash chromatography (CH₂Cl₂/petroleum ether/MeOH 8:1.5:0.5) gave **22** (0.200 g, 54 %) as a yellowish oil. ¹H NMR (CDCl₃, 200 MHz) δ 7.55-7.44 (m, 2H), 7.40-7.04 (m, 4H), 6.97 (d, *J* = 8.2 Hz, 2H), 5.91 (br s, 2H, exchangeable with D₂O), 3.56 (t, *J* = 5.8 Hz, 2H), 3.45-3.20 (m+s, 8H), 3.10 (q, *J* = 6.2 Hz, 2H), 2.50-2.30 (m, *J* = 6.2 Hz, 1H), 2.24 (t, *J* = 6.8 Hz, 2H), 2.00-1.20 (m, 10H). ¹³C-NMR (CDCl₃, 50 MHz) δ 177.71, 175.61, 172.66, 157.05, 150.12, 146.66, 128.57 (2C), 127.83, 125.33, 121.95, 117.55 (2C), 116.43, 104.07, 56.35, 40.20, 42.12, 40.66 (2C), 37.74, 36.55, 35.23, 31.14, 28.84, 25.22, 24.61. MS (ESI+) : *m/z* 526 [M+1]⁺.



(*S*)-3-((*S*)-1-Nitropropyl)cyclohexanone (**70**) and (*S*)-3-((*R*)-1-nitropropyl)cyclohexanone (**71**). A mixture of 2-cyclohexene-1-one **69** (0.100 mL, 1.04 mmol), 1-nitropropane (0.195 mL, 2.18 mmol), 2,5-dimethylpiperazine (0.120 g, 1.04 mmol) and a catalytic amount of D-proline (10 mol%) was stirred in reagent grade chloroform (8 mL) for 48 h at rt. The reaction mixture was diluted with CH₂Cl₂ and washed with aqueous HCl (3%). The organic phase was dried (MgSO₄), filtered, evaporated and the residue was purified by chromatography (EtOAc:hexanes 1:4) to obtain 1:2.2 diastereomeric mixture of **70** and **71** as a colourless oil (0.162 g, 84%). A portion of the crude product was separated by column chromatography for characterization.

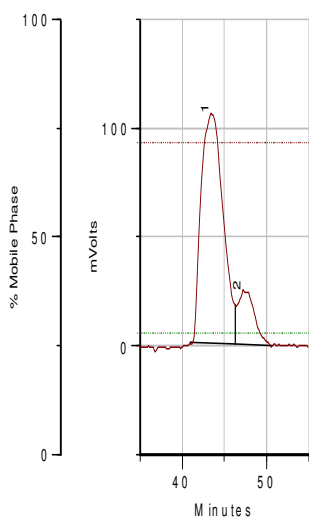
For less polar *syn*-isomer **70**: [α]_D²⁰ -26 (c 0.1, CHCl₃); IR (CHCl₃) 1542, 1714, cm⁻¹; ¹H NMR (400 MHz, CDCl₃) δ 4.31 (m, 1H), 2.54-2.40 (m, 2H), 2.37-2.24 (m, 2H) 2.16-2.08 (m, 2H), 2.03-1.78 (m, 3H), 1.72-1.60 (m, 1H), 1.55-1.45 (m, 1H), 0.97 (t, *J* = 7.2 Hz, 3H); ¹³C NMR (100 MHz, CDCl₃) δ 208.32, 93.86, 43.52, 41.16, 40.59, 27.13, 23.83, 23.74, 9.89. MS (FAB): *m/z* 186 [M+1]⁺, ee = 89%. The enantiomeric excess of the less polar *syn*-isomer was determined by RP-HPLC analysis with CHIRALPAK AD-RH column (\varnothing 0.46 cm \times 15 cm) eluting in isocratic mode with 0.1 % Formic acid in CH₃CN / 0.1 % Formic acid in H₂O (30:70), flow = 0.5 mL/min, retention times minor 34.90 min, major 39.02 min.



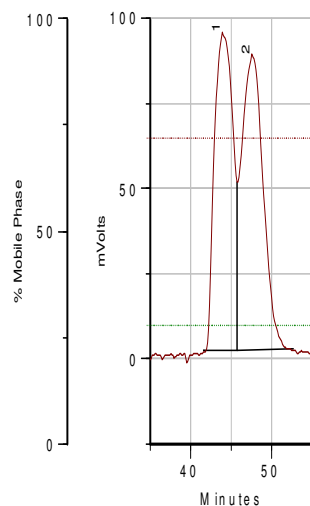
Peak Name	R. Time	Area	Area %
1	34.90	2500539.25	5.39
2	39.02	43910696.00	94.61

Peak Name	R. Time	Area	Area %
1	34.76	25787958.00	53.57
2	39.86	22348432.00	46.43

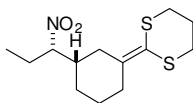
For more polar *anti*-isomer **71**: $[\alpha]_D^{20} +15$ (c 0.1, CHCl_3); IR (CHCl_3) 1542, 1714, cm^{-1} ; ^1H NMR (400 MHz, CDCl_3) δ 4.36 (m, 1H), 2.45-2.34 (m, 2H), 2.32-2.20 (m, 3H), 2.17-2.08 (m, 1H), 2.05-1.95 (m, 2H), 1.86-1.78 (m, 1H), 1.73-1.61 (m, 1H), 1.50-1.36 (m, 1H), 0.97 (t, $J=7.2$ Hz, 3H); ^{13}C NMR (100 MHz, CDCl_3) δ 208.33, 93.87, 43.02, 40.98, 40.53, 27.33, 24.09, 23.73, 10.01; MS (FAB): m/z 186 $[\text{M}+1]^+$, ee = 74%. The enantiomeric excess of the more polar *anti*-isomer was determined by RP-HPLC analysis with CHIRALPAK AD-RH column (\varnothing 0.46 cm \times 15 cm) eluting in isocratic mode with 0.1 % Formic acid in CH_3CN / 0.1 % Formic acid in H_2O (28:72), flow = 0.5 mL/min, retention times minor 44.33 min, major 47.25 min.



Peak Name	R. Time	Area	Area %
1	44.33	2203832.50	12.95
2	47.26	14813406.00	87.05

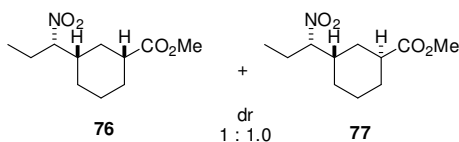


Peak Name	R. Time	Area	Area %
1	43.92	24985658.00	48.27
2	47.66	26776176.00	51.73



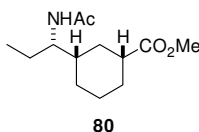
74

2-((*S*)-3-((*S*)-1-nitropropyl)cyclohexylidene)-1,3-dithiane (74). In a stirring solution of [1,3]dithian-2-yl-phosphonic acid diethyl ester (0.097 g, 0.378 mmol) in THF (2 mL) at $-78\text{ }^{\circ}\text{C}$ was added *n*-BuLi (0.258 mL, 0.412 mmol, 1.6 M in hexane) dropwise during 15 min. After 1 h **70** (0.07 g, 0.378 mmol) in THF (1 mL) was added, stirred for 15 min at $-78\text{ }^{\circ}\text{C}$ and was allowed to warm to rt. The reaction mixture was quenched after 1 h by adding saturated solution of NH_4Cl (2 mL) and extracted with EtOAc ($3\times 10\text{ mL}$). The organic phase was washed with brine, dried, concentrated and the residue was purified by chromatography (5% EtOAc in hexanes) to give **74** as colourless oil (0.092 g, 85%) $[\alpha]_{\text{D}}^{20} -0.91$ (c 1, CHCl_3); IR (CHCl_3) 1547 cm^{-1} ; ^1H NMR (CDCl_3) δ 4.33-4.25 (m, 1H), 3.09-2.88 (m, 5H), 2.16-1.66 (m, 9H), 1.40-1.26 (m, 2H), 0.98 (t, $J=7.0\text{ Hz}$, 3H); ^{13}C NMR (CDCl_3) δ 140.04, 122.90, 94.19, 40.96, 33.57, 31.12, 29.93, 29.85, 28.57, 24.78, 24.61, 24.29, 10.00. MS (FAB): m/z 288 $[\text{M}+1]^+$, HRMS (FAB) Calc. for $\text{C}_{13}\text{H}_{22}\text{NO}_2\text{S}_2$ $[\text{M}+1]^+$ 288.1086, found 288.1101.

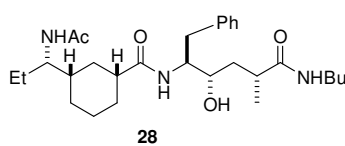


(1*R*,3*S*)-Methyl 3-((*S*)-1-nitropropyl)cyclohexanecarboxylate (76) and (1*S*,3*S*)-methyl 3-((*S*)-1-nitropropyl)cyclohexanecarboxylate (77) A solution of **74** (0.09 g, 0.313 mmol), mercuric chloride (0.591 g, 1.25 mmol), MeOH (6 mL), and perchloric acid (0.132 mL of a 70% aqueous solution, 0.939 mmol) was heated at reflux for 2 hr. After cooling and filtration, the reaction mixture was neutralized with saturated solution of NaHCO_3 and extracted with CH_2Cl_2 . The combined organic extracts were washed with brine, dried, concentrated and the residue was purified by chromatography (EtOAc:hexanes 1:4) to give 1:1 mixture of ester **76** and **77** as colourless oils (0.057g, 80%). A portion of the crude product was separated by column chromatography for characterization. For **76** (0.027 g): $[\alpha]_{\text{D}}^{20} -9.0$ (c 1, CHCl_3); IR (CHCl_3) $1549, 1735\text{ cm}^{-1}$; ^1H NMR (CDCl_3) δ 4.21 (m, 1H), 3.68 (s, 3H), 2.34 (m, 1H), 2.18-1.84 (m, 6H), 1.65-1.58 (m, 1H), 1.33-1.04 (m, 4H), 0.94 (t, $J=7.2\text{ Hz}$, 3H); ^{13}C NMR (CDCl_3) δ 175.91, 96.03, 52.17, 43.07, 31.36, 29.06, 28.93, 25.05, 24.39, 10.79; MS (FAB): m/z 288 $[\text{M}+1]^+$.

HRMS (FAB) Calc. for $C_{11}H_{19}NO_4$ $[M+1]^+$ 229.1314 found 229.1309.

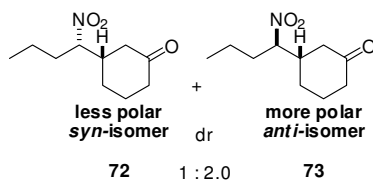


(1R,3S)-Methyl 3-((S)-1-acetamidopropyl)cyclohexanecarboxylate (80). To a solution of nitro compound **76** (14.8 mg, 0.065 mmol) in dry MeOH (0.3 mL) was added successively under Argon atmosphere, ammonium formate (28 mg, 0.45 mmol), and 10% palladium-on-carbon (10 mg). The suspension was stirred for 4h at rt then filtered through a short pad of Celite, then washed with MeOH (10 mL). Concentration of the solvent afforded the corresponding amine (13 mg, quantitative) which was dissolved in CH_2Cl_2 , then Ac_2O (18.4 μL , 0.105 mmol) Et_3N (27 μL , 0.195 mmol) and DMAP (catalytic amount). The solution was stirred at rt for 3 h then quenched with NH_4Cl . The organic phase was diluted with EtOAc (10 mL), washed with HCl (1N) and $NaHCO_3$, dried, concentrated, and residue was purified by chromatography (EtOAc/hexanes, 1/1) to give **80** as a colourless solid (12 mg, 76%); $[\alpha]_D^{20}$ -36.1 (c 1, $CHCl_3$); IR (neat) 3285, 1739, 1648 cm^{-1} ; 1H NMR ($CDCl_3$) δ 5.20-5.18 (d, $J = 8.5$ Hz, 1H), 3.79-3.73 (m, 1H), 3.66 (s, 3H), 2.30 (m, 1H), 2.00 (s, 3H), 1.92-1.87 (m, 2H), 1.71-1.55 (m, 2H), 1.47-1.36 (m, 1H), 1.33-1.13 (m, 4H), 1.00-0.94 (m, 1H), 0.89 (t, $J = 7.3$ Hz, 3H); ^{13}C NMR ($CDCl_3$) δ 176.6, 170.2, 55.2, 51.9, 43.6, 41.3, 32.1, 29.2, 27.9, 25.6, 24.9, 23.9, 11.0; MS (FAB): m/z 242 $[M+1]^+$; HRMS (FAB) Cald. for $C_{13}H_{23}NO_3$ 241.1677, found 241.1672.



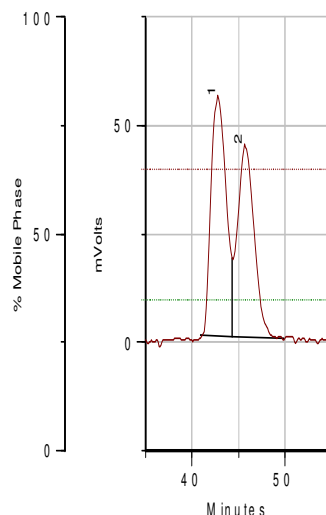
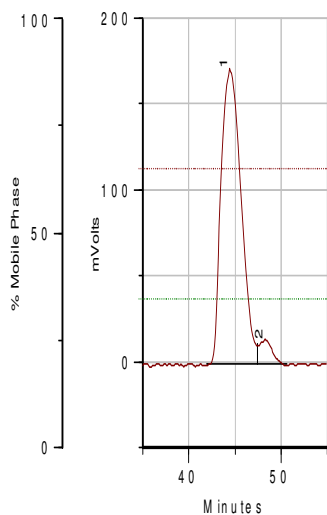
(1R,3S)-3-((S)-1-Acetamidopropyl)-N-((2S,3S,5R)-6-(butylamino)-3-hydroxy-5-methyl-6-oxo-1-phenylhexan-2-yl)cyclohexanecarboxamide (28). In a solution of ester **80** (8 mg, 0.0332 mmol) in MeOH (1 mL) was added LiOH solution (100 μL , 1N solution in water) and stirred for 12 h at rt. The reaction mixture was diluted with EtOAc (10 mL) and neutralized with diluted HCl, washed with brine, dried (Na_2SO_4) and concentrated. The crude product was used directly for coupling without purification. In a solution of Boc protected amine (26 mg, 0.0664 mmol) in CH_2Cl_2 (1 mL) was added TMSI (38 μL , 0.26 mmol) at rt for 30 min. The reaction mixture was quenched with $Na_2S_2O_3$ solution and extracted with EtOAc. The organic layer was washed with

NHCO₃ solution, brine, dried (Na₂SO₄) and concentrated. It was used immediately without purification. The acid and amine were taken in a solution of co-solvent (CH₂Cl₂:H₂O, 1:1, 1 mL). HOBt (9 mg, 0.065 mmol) and EDC (13 mg, 0.066 mmol) were added and stirred at 4 °C for 24 h. The reaction mixture was diluted with EtOAc (10 mL) and washed with diluted HCl, NaHCO₃, brine and dried (Na₂SO₄). After concentration, the crude product was purified by careful column chromatography (5% MeOH in CH₂Cl₂) to give amide **28** (8 mg, 50%) as white solid. $[\alpha]_D^{20}$ -24 (c 0.22, MeOH); ¹H NMR (CD₃OD) δ 7.26-7.16 (m, 5H), 4.04-4.03 (m, 1H), 3.54 (t, *J* = 4.0 Hz, 2H), 3.12 (t, *J* = 7.1 Hz, 2H), 2.73 (dd, *J* = 5.8, 5.7 Hz, 1H), 2.73 (dd, *J* = 9.4, 9.3 Hz, 1H), 2.57-2.52 (m, 1H), 2.15-2.10 (m, 1H), 1.95 (s, 3H), 1.85-1.75 (m, 1H), 1.75-1.60 (m, 3H), 1.60-1.50 (m, 2H), 1.50-1.40 (m, 4H), 1.40-1.20 (m, 7H), 1.08 (d, *J* = 6.9 Hz, 2H), 1.05-0.99 (m, 1H), 0.93 (t, *J* = 7.2 Hz, 3H), 0.87 (t, *J* = 7.4 Hz, 3H); ¹³C NMR (MeOD) δ 177.9, 177.7, 172.1, 139.2, 129.3 (2C), 128.3 (2C), 126.2, 69.9, 55.6, 54.9, 45.4, 41.3, 39.0, 38.1, 37.7, 37.0, 32.6, 31.6, 29.6, 27.8, 25.4, 24.4, 21.5, 20.0, 17.5, 13.0, 9.8; MS (ESI) *m/z* 502.2 [M+1]⁺; HRMS (FAB) Calcd. for C₂₉H₄₈N₃O₄ [M+1]⁺ 502.3567, found 502.3599.



(S)-3-((S)-1-Nitrobutyl)cyclohexanone (72) and **(S)-3-((R)-1-nitrobutyl)cyclohexanone (73)**. A mixture of 2-cyclohexene-1-one **69** (0.100 mL, 1.04 mmol), 1-nitrobutane (0.220 mL, 2.08 mmol), 2,5-dimethylpiperazine (0.120 g, 1.04 mmol) and a catalytic amount of D-proline (10 mol%) were stirred in reagent grade chloroform (8 mL) for 48 h at rt. The reaction mixture was diluted with CH₂Cl₂ and washed with aqueous HCl (3%). The organic phase was dried (MgSO₄), filtered, evaporated and purified by chromatography (hexanes:EtOAc, 4:1) to obtain a 1:2 diastereomeric mixture of **72** and **73** as colourless oil (0.200 g, 97%). A portion of the crude product was separated by column chromatography for characterization. For the less polar *syn*-isomer **72**: $[\alpha]_D^{20}$ -18 (c 0.1, CHCl₃); IR (CHCl₃) 1548, 1717, cm⁻¹; ¹H NMR (400 MHz, CDCl₃) δ 4.42-4.36 (m, 1H), 2.54-2.40 (m, 2H), 2.35-2.24 (m, 2H), 2.16-2.06 (m, 2H) 2.05-1.84 (m, 2H), 1.73-1.44 (m, 3H), 1.40-1.24 (m, 2H), 0.96 (t, *J* = 7.2 Hz, 3H); ¹³C NMR (100 MHz, CDCl₃) δ 208.26, 92.11, 44.56, 41.36, 40.57, 32.32, 27.07, 23.83, 18.72, 13.01; MS (FAB): *m/z* 200 [M+1]⁺, ee = 89 %. The enantiomeric excess of the less polar *syn*-isomer was determined by RP-

HPLC analysis with CHIRALPAK AD-RH column (\varnothing 0.46 cm \times 15 cm) eluting in isocratic mode with 0.1 % Formic acid in CH₃CN / 0.1 % Formic acid in H₂O (35:65), flow = 0.5 mL/min, retention times minor 48.32 min, major 44.50 min.

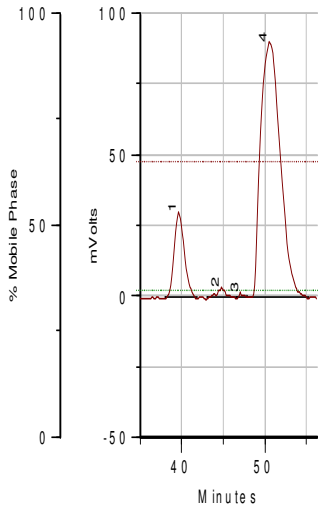


Peak Name	R. Time	Area	Area %
1	44.50	43450976.00	94.66
2	48.32	2452799.75	5.34

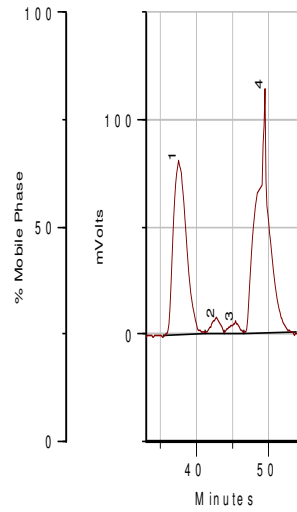
Peak Name	R. Time	Area	Area %
1	42.80	10646814.00	53.29
2	45.72	9333523.00	46.71

For the more polar *anti*-isomer **73**: $[\alpha]_D^{20} + 20$ (c 0.1, CHCl₃); IR (CHCl₃) 1548, 1717, cm⁻¹; ¹H NMR (400 MHz, CDCl₃) δ 4.48-4.43 (m, 1H), 2.48-2.37 (m, 2H), 2.33-2.20 (m, 3H), 2.19-2.11 (m, 1 H), 2.10-1.98 (m, 2H), 1.76-1.62 (m, 2H), 1.52-1.20 (m, 3H), 0.98 (t, J = 7.2 Hz, 3H); ¹³C NMR (75 MHz, CDCl₃) δ 209.52, 93.25, 44.17, 42.37, 41.75, 33.50, 28.58, 25.29, 20.05, 14.25; MS (FAB): m/z 200 [M+1]⁺, ee = 71 %. The enantiomeric excess of the more polar *anti*-isomer was determined by RP-HPLC analysis with CHIRALPAK AD-RH column (\varnothing 0.46 cm \times 15 cm) eluting in isocratic mode with 0.1 % Formic acid in CH₃CN / 0.1 % Formic acid in H₂O (35:65), flow = 0.5 mL/min, retention times minor 39.65 min, major 50.59 min.

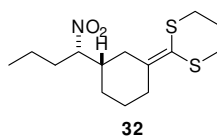
Chapter 6



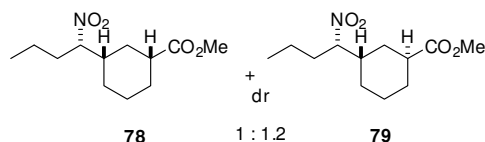
Peak Name	R. Time	Area	Area %
1	39.65	4311732.50	14.36
2	44.86	550930.88	1.83
3	47.10	126960.65	0.42
4	50.59	25034252.00	83.38



Peak Name	R. Time	Area	Area %
1	37.55	17431646.00	41.24
2	42.85	1262070.88	2.99
3	45.51	1007719.69	2.38
4	49.57	22563528.00	53.39

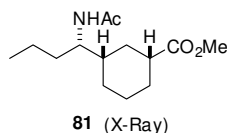


2-((S)-3-((S)-1-Nitrobutyl)cyclohexylidene)-1,3-dithiane (75). In a stirring solution of [1,3]dithian-2-yl-phosphonic acid diethyl ester (0.129 g, 0.502 mmol) in THF (2 mL) at $-78\text{ }^{\circ}\text{C}$ was added *n*-BuLi (0.48 mL, 0.552 mmol, 1.6 M in hexane) dropwise during 15 min. After 1 h, ketone **72** (0.100 g, 0.502 mmol) in THF (1 mL) was added and stirred for 15 min at $-78\text{ }^{\circ}\text{C}$ and then cooling bath was removed. The reaction mixture was quenched after 1 h by adding saturated solution of NH_4Cl (2 mL) and extracted with EtOAc (3 \times 10 mL). The organic phase was washed with brine, dried over Na_2SO_4 and concentrated. The purification of crude product by column chromatography (5% EtOAc in hexanes) furnished a ketene dithioacetal **75** as colourless oil (0.124 g, 82%). $[\alpha]_{\text{D}}^{20} -1.3$ (c 1, CHCl_3); IR (CHCl_3) 1547 cm^{-1} ; $^1\text{H NMR}$ (CDCl_3) δ 4.30 (m, 1H), 3.0 (m, 1H), 2.67-2.56 (m, 3H), 1.99-1.73 (m, 9H), 1.41-1.28 (m, 6H), 0.95 (t, $J=7.2\text{ Hz}$, 3H); $^{13}\text{C NMR}$ δ 140.66, 119.54, 93.20, 41.92, 34.36, 33.61, 31.88, 30.60, 29.28, 28.30, 25.52, 25.37, 19.66, 13.91; MS (FAB): m/z 302 $[\text{M}+1]^+$, HRMS (FAB) Calc. for $\text{C}_{14}\text{H}_{24}\text{NO}_2\text{S}_2$ $[\text{M}+1]^+$ 302.1243, found 302.1351.

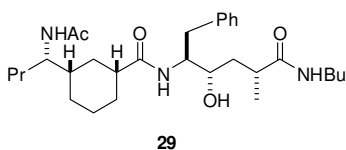


(1R,3S)-Methyl 3-((S)-1-nitrobutyl)cyclohexanecarboxylate (78) and **(1S,3S)-methyl 3-((S)-1-nitrobutyl)cyclohexanecarboxylate (79).** A solution of **75** (0.120 g, 0.398 mmol), mercuric chloride (0.752 g, 1.59 mmol), MeOH (7 mL), and perchloric acid (0.17 mL of a 70% aqueous solution, 1.19 mmol) was heated at reflux for 2 h. After cooling and filtration, the reaction mixture was neutralized with saturated solution of NaHCO_3 and extracted with CH_2Cl_2 . The combined organic extract were washed with brine, dried (Na_2SO_4) and concentrated to give a 1:1 diastereomeric mixture of the ester **78** and **79** as colourless oils (0.069 g, 72%). A portion of the crude product was separated by column chromatography for characterization. For **75** (0.32 g): $[\alpha]_{\text{D}}^{20} -13.7$ (c 1, CHCl_3); IR (CHCl_3) $1548, 1733\text{ cm}^{-1}$; $^1\text{H NMR}$ (CDCl_3) δ 4.27 (m, 1H), 3.68 (s, 3H), 2.34 (m, 1H), 2.03-1.56 (m, 7H), 1.33-1.15 (m, 1H), 0.94 (t, $J=7.3\text{ Hz}$, 3H); $^{13}\text{C NMR}$ (CDCl_3) δ 175.76, 94.16, 52.02, 43.04, 40.90, 32.95, 31.38, 28.96, 28.91, 25.03, 19.57,

13.76; MS (FAB): m/z 244 $[M+1]^+$, HRMS (FAB) Calc. for $C_{12}H_{22}NO_4$ $[M+1]^+$ 244.1543, found 244.1601.



(1R,3S)-Methyl 3-((S)-1-acetamidobutyl)cyclohexanecarboxylate (81). To a solution of nitro compound **78** (14.8 mg, 0.061 mmol) in MeOH (0.3 mL) was added successively under Ar atmosphere, ammonium formate (28 mg, 0.45 mmol), and 10% palladium on carbon (10 mg). The suspension was stirred for 4h at rt then filtered through a short pad of Celite, then washed with MeOH (10 mL). Concentration of the combined organic phase afforded an amine (13 mg, quantitative) which was dissolved in CH_2Cl_2 , and Ac_2O (18.4 μL , 0.105 mmol) was added followed by Et_3N (27 μL , 0.195 mmol) and DMAP (catalytic amount). The reaction mixture was stirred at rt for 3 h then quenched by adding NH_4Cl . The organic phase was diluted with EtOAc (10 mL) and was washed with HCl (1N) and $NaHCO_3$, dried, concentrated and the residue was purified by chromatography (EtOAc/hexanes, 1/1) to give **81** as colourless solid (12 mg, 76%); $[\alpha]_D^{20}$ -34.5 (c 1, $CHCl_3$); IR (neat) 3282, 1734, 1641 cm^{-1} ; 1H NMR ($CDCl_3$) δ 5.22 (d, $J = 8.6$ Hz, 1H), 3.83 (m, 1H), 3.65 (s, 3H), 2.28 (m, 1H), 1.98-1.70 (m, 6H), 1.49-1.15 (m, 9H), 0.97-0.87 (m, 4H); ^{13}C NMR ($CDCl_3$) δ 176.62, 170.08, 53.47, 51.98, 43.62, 41.68, 34.29, 32.01, 29.23, 27.99, 25.59, 23.93, 19.83, 14.39; MS (FAB): m/z 256 $[M+1]^+$ (X-ray provided).

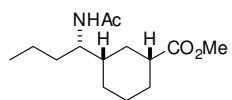


(1R,3S)-3-((S)-1-Acetamidobutyl)-N-((2S,3S,5R)-6-(butylamino)-3-hydroxy-5-methyl-6-oxo-1-phenylhexan-2-yl)cyclohexanecarboxamide (29). In a solution of ester **81** (10 mg, 0.039 mmol) in MeOH (1 mL) was added LiOH solution (150 μL , 1N solution in water) and stirred for 12 h at rt. The reaction mixture was diluted with EtOAc (10 mL) and neutralized with diluted HCl, washed with brine, dried (Na_2SO_4) and concentrated. The crude product was used directly for coupling without purification. In a solution of Boc protected amine (16 mg, 0.039 mmol) in CH_2Cl_2 (1 mL) was added TMSI (22 μL) at rt for 30 min. The reaction mixture was quenched with $Na_2S_2O_3$ solution and extracted with EtOAc. The organic layer was washed with $NaHCO_3$

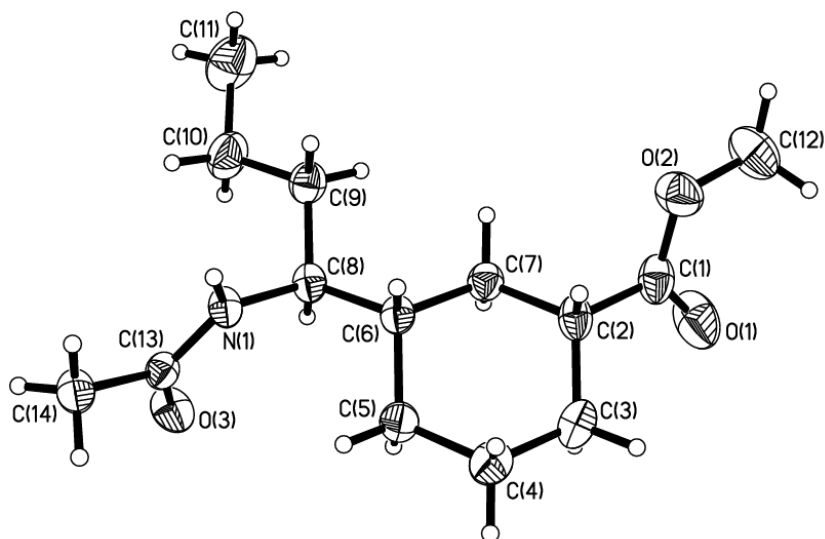
solution, brine, dried (Na_2SO_4) and concentrated. It was used immediately without purification. The acid and amine were taken in a solution of co-solvent ($\text{CH}_2\text{Cl}_2:\text{H}_2\text{O}$, 1:1, 1 mL). HOBt (5.3 mg, 0.039 mmol) and EDC (7.5 mg, 0.039 mmol) were added and stirred at 4 °C for 24 h. The reaction mixture was diluted with EtOAc (10 mL) and washed with diluted HCl, NaHCO_3 , brine and dried (Na_2SO_4). After concentration, the crude product was purified by careful column chromatography (5% MeOH in CH_2Cl_2) to give amide **29** (8 mg, 40%) as white solid. $[\alpha]_{\text{D}}^{20}$ -50 (c 0.25, MeOH: CHCl_3 [1:1]); IR (neat) 3315, 1648, 1630 cm^{-1} ; ^1H NMR (MeOD: CDCl_3 [5:1]) δ 8.11 (s, 1H), 7.59-7.48 (m, 4H), 4.38 (t, $J = 6.7$ Hz, 1H), 3.97 (bs, 1H), 3.86 (m, 1H), 3.44 (t, $J = 7.1$ Hz, 2H), 3.22 (dd, $J = 5.7, 6.0$ Hz, 1H), 3.00 (dd, $J = 9.3, 9.2$ Hz, 1H), 2.85-2.80 (m, 1H), 2.55 (s, 1H), 2.50-2.40 (m, 1H), 2.28 (s, 3H), 2.20-2.10 (m, 1H), 2.05-1.95 (m, 3H), 1.90 (d, $J = 12.5$ Hz, 1H), 1.80-1.50 (m, 12H), 1.40 (d, $J = 6.8$ Hz, 4H), 1.25 (t, $J = 7.0$ Hz, 6H); ^{13}C NMR ($\text{CD}_3\text{OD}:\text{CDCl}_3$ [5:1]) δ 177.2, 177.0, 171.2, 138.2, 128.6 (2C), 127.6 (2C), 125.6, 68.9, 53.9, 52.9, 44.6, 40.8, 38.3, 37.5, 36.8, 36.5, 32.9, 31.7, 30.8, 29.3, 28.8, 27.1, 24.7, 21.1, 19.4, 18.7, 16.8, 12.8, 12.6; MS (ESI) m/z 516 $[\text{M}+1]^+$; HRMS (FAB) Calc. for $\text{C}_{30}\text{H}_{50}\text{N}_3\text{O}_4$ $[\text{M}+1]^+$ 516.3723, found 516.3720.

Crystal structure determination and refinement of compound 81 and ORTEP representation

Identification code	han408 (81)	
Empirical formula	C ₁₄ H ₂₅ NO ₃	
Formula weight	255.35	
Temperature	293(2)K	
Wavelength	1.54178 Å	
Crystal system	Orthorhombic	
Space group	P2 ₁ 2 ₁ 2 ₁	
Unit cell dimensions	a = 5.0354(14) Å	α = 90°
	b = 16.767(4) Å	β = 90°
	c = 17.907(5) Å	γ = 90°
Volume	511.9(7) Å ³	
Z	4	
Density (calculated)	1.122 Mg/m ³	
Absorption coefficient	0.624 mm ⁻¹	
F(000)	560	
Crystal size	0.62 × 0.11 × 0.09 mm	
Theta range for data collection	3.61 to 69.94°	
Index ranges	-6 < h < 6, -20 < k < 20, -21 < l < 21	
Reflections collected	21134	
Independent reflections	2865 [R _{int} = 0.039]	
Absorption correction	None	
Max. and min. transmission	0.9500 and 0.7000	
Refinement method	Full-matrix least-squares on F ²	
Data / restraints / parameters	2865 / 0 / 167	
Goodness-of-fit on F ²	0.717	
Final R indices [I > 2σ(I)]	R ₁ = 0.0387, wR ₂ = 0.0769	
R indices (all data)	R ₁ = 0.0723, wR ₂ = 0.0853	
Absolute structure parameter	0.1(4)	
Extinction coefficient	0.0043(3)	
Largest diff. peak and hole	0.165 and -0.107 e/Å ³	



81 (X-Ray)



6.2 Biology

6.2.1. BACE1 inhibition

Method A: Panvera peptide and Invitrogen Enzyme

Purified Baculovirus-expressed BACE1 (β -secretase) and rhodamine derivative substrate were purchased from Panvera (Madison, WI, U.S). Sodium acetate and DMSO were from Sigma Aldrich (Milan, Italy). Purified water from Milli-RX system (Millipore, Milford, MA, USA) was used to prepare buffers and standard solutions. Spectrofluorometric analyses were carried out on a Fluoroskan Ascent multiwell spectrofluorimeter (excitation: 544 nm; emission: 590 nm) by using black microwell (96 wells) Corning plates (Sigma, Italy). Stock solutions of the tested compounds were prepared in DMSO and diluted with 50 mM sodium acetate buffer pH = 4.5.

Specifically, 20 μ L of BACE1 enzyme (25 nM) were incubated with 20 μ L of test compound for 60 minutes. To start the reaction, 20 μ L of substrate (0.25 μ M) were added to the well. The mixture was incubated at 37 °C for 60 minutes. To stop the reaction, 20 μ L of BACE1 stop solution (sodium acetate 2.5 M) were added to each well. Then the spectrofluorometric assay was performed by reading the fluorescence signal at 590 nm.

Assays were done with a blank containing all components except BACE1 in order to account for non enzymatic reaction. The reaction rates were compared and the percent inhibition due to the presence of test compounds was calculated. Each concentration was analyzed in triplicate. The percent inhibition of the enzyme activity due to the presence of increasing test compound concentration was calculated by the following expression: $100 - (v_i/v_o \times 100)$, where v_i is the initial rate calculated in the presence of inhibitor and v_o is the enzyme activity. To demonstrate inhibition of BACE1 activity, inhibitor IV (Calbiochem, Darmstadt, Germany) was used as reference inhibitor (IC_{50} =12.89 nM).

Method B: Casein-FITC and Invitrogen Enzyme

Purified Baculovirus-expressed BACE1 (β -secretase) in 50 mM Tris (pH = 7.5), 10% glycerol (5 Units) was purchased from Panvera (Madison, WI, U.S). Casein from bovine milk, labelled with Fluorescein isothiocyanate (Casein-FITC) type III (61 μ g FITC per mg solid) and sodium acetate were from Sigma Aldrich (Milan, Italy). Methanol was grade pure from Carlo Erba (Milan, Italy). Purified water from Milli-RX system (Millipore, Milford, MA, USA) was used to

prepare buffers and standard solutions. Spectrofluorometric analyses were carried out on a Fluoroskan Ascent multiwell spectrofluorimeter (excitation: 485 nm; emission: 538 nm) by using black microwell (96 wells) Cliniplate plates (Thermo LabSystems, Helsinki, Finland).

Stock solutions of the tested compounds were prepared in methanol and diluted with 50 mM sodium acetate buffer pH = 4.5.

Specifically, 20 μ L of BACE1 enzyme (1 U/mL) were incubated with 20 μ L of test compound for 60 minutes. To start the reaction, 20 μ L of Casein-FITC (400 nM) were added to the well. The mixture was incubated at 37 °C for 60 minutes. To stop the reaction, 20 μ L of BACE1 stop solution (sodium acetate 2.5 M) were added to each well. Then the spectrofluorometric assay was performed by reading the fluorescence signal at 538 nm.

Assays were done with a blank containing all components except BACE1 in order to account for non enzymatic reaction. BACE1 maximum activity was expressed as $\Delta F/h$ at 538 nm. The reaction rates were compared and the percent inhibition due to the presence of test compounds was calculated. Each concentration was analyzed in triplicate. The percent inhibition of the enzyme activity due to the presence of increasing test compound concentration was calculated by the following expression: $100 - (v_i/v_o \times 100)$, where v_i is the initial rate calculated in the presence of inhibitor and v_o is the enzyme activity. To demonstrate inhibition of BACE1 activity Donepezil was used as reference inhibitor ($IC_{50}=586$ nM) or a statine-derived inhibitor ($IC_{50} = 61 \pm 2.0$ nM).

Method C: M-2420 substrate and Sigma enzyme

Human recombinant BACE1 (β -secretase), sodium acetate, CHAPS and DMSO were purchased from Sigma Aldrich (Milan, Italy). The substrate, M-2420, was from Bachem, (Torrance, CA, USA). Purified water from Milli-RX system (Millipore, Milford, MA, USA) was used to prepare buffers and standard solutions. Spectrofluorometric analyses were carried out on a Fluoroskan Ascent multiwell spectrofluorimeter (excitation: 320 nm; emission: 405 nm) by using black microwell (96 wells) Corning plates (Sigma, Italy).

Stock solutions of the tested compounds were prepared in DMSO and diluted with DMSO.

Specifically, 175 μ L of BACE1 enzyme (25 nM in NaOAc 20 mM pH 4.5, containing 0.1% w/v CHAPS) were incubated with 5 μ L of test compound for 60 minutes. To start the reaction, 20 μ L of M-2420 (3 μ M in Hepes 10 mM pH 7.5) were added to the well. The mixture was

incubated at room temperature for 15 minutes and the fluorescence signal was read at 405 nm.

Assays were done with a blank containing all components except BACE1 in order to account for non enzymatic reaction. The reaction rates were compared and the percent inhibition due to the presence of test compounds was calculated. Each concentration was analyzed in duplicate. The percent inhibition of the enzyme activity due to the presence of increasing test compound concentration was calculated by the following expression: $100 - (v_i/v_o \times 100)$, where v_i is the initial rate calculated in the presence of inhibitor and v_o is the enzyme activity. To demonstrate inhibition of BACE1 activity, inhibitor IV (Calbiochem, Darmstadt, Germany) was used as reference inhibitor ($IC_{50}=13.61$ nM).

BACE1 fluorogenic substrate evaluation

The kinetic parameters for the three enzymatic assays (**A**, **B** and **C**) were evaluated in order to optimize the test conditions. Hydrolysis of the fluorogenic substrates was monitored in a 200 μ L reaction volume by measuring the fluorescence increase in a Fluoroskan Ascent spectrofluorimeter (beam diameter: 3 mm) by using black microwells (96 wells) Corning plates. $\lambda_{ex}/\lambda_{em}$ pairs were set at 544/590, 485/538 and 320/405 nm when substrates **A** (Invitrogen peptide, Panvera), **B** (Casein-FITC, Sigma) or **C** (M-2420, Bachem) were employed.

Specificity constants (k_{cat}/K_M) were determined under pseudo-first-order conditions, via the “progress curve method”¹⁶ using a substrate concentration (0.04 or 0.05 μ M) far below K_M , and a final enzyme concentration of 10 or 34 nM (E_0). The {time; fluorescence} data pairs were fitted to equation ($F(t) = \Delta F [1 - \exp(-k_{obs} \cdot t)] + F_{init}$), and the apparent first-order rate constant (k_{obs}) was calculated. The second-order rate constant, k_{cat}/K_M values were calculated according to the following equation: $k_{cat}/K_M = k_{obs}/[E_0]$. Quenching efficiency was determined according to the equation: $q.e.(%) = (1 - F_0/F_1) \times 100$, where $F_0 = F_{init} - F_{buffer}$ and $F_1 = F_{max} - F_{buffer}$.

6.2.2. Cathepsin D inhibition

20 μ L of CatD (0.05 μ M) were incubated with 20 μ L of test compound for 30 minutes. To start the reaction, 20 μ L of Casein-FITC (1.44 μ M) were added to the well. The mixture was incubated at 37 °C for 90 min. To stop the reaction, 20 μ L of BACE1 stop solution (sodium acetate 2.5 M) were added to each well. Pepstatin A was used as a reference inhibitor ($IC_{50}=0.011 \pm 0.002$ μ M).

6.2.3. AChE and BChE inhibition

The method of Ellman *et al.* was followed.¹⁷ Five different concentrations of each compound were used in order to obtain inhibition of AChE or BChE activity comprised between 20-80%. The assay solution consisted of a 0.1 M phosphate buffer pH 8.0, with the addition of 340 μM 5,5'-dithio-bis(2-nitrobenzoic acid), 0.02 unit/mL of human recombinant AChE or human serum BChE (Sigma Chemical), and 550 μM of substrate (acetylthiocholine iodide or butyrylthiocholine iodide). Test compounds were added to the assay solution and pre-incubated at 37 °C with the enzyme for 20 min followed by the addition of substrate. Assays were done with a blank containing all components except AChE or BChE in order to account for non-enzymatic reaction. The reaction rates were compared and the percent inhibition due to the presence of test compounds was calculated. Each concentration was analyzed in triplicate, and IC_{50} values were determined graphically from log concentration–inhibition curves.

Determination of Steady State Inhibition Constant. To obtain estimates of the competitive inhibition constant K_i , reciprocal plots of $1/V$ versus $1/[S]$ were constructed at relatively low concentration of substrate (below 0.5 mM). The plots were assessed by a weighted least square analysis that assumed the variance of V to be a constant percentage of V for the entire data set. Slopes of these reciprocal plots were then plotted against the concentration of **6** (range 0 – 0.344 nM) in a weighted analysis and K_i was determined as the ratio of the replot intercept to the replot slope. Reciprocal plots involving tacrine (not shown) or **6** inhibition show both increasing slopes (decreased V_{max} at increasing inhibitor's concentrations) and increasing intercepts (higher K_m) with higher inhibitor concentration. This pattern indicates mixed inhibition, arising from significant inhibitor interaction with both the free enzyme and the acetylated enzyme. Replots of the slope versus the concentration of **6** or tacrine gives estimate of competitive inhibition constant, $K_i = 0.155 \pm 0.046$ nM or $K_i = 0.151 \pm 0.016$ μM , respectively. So the pattern in the graphical representation shows **6** able to bind to the peripheral anionic site as well as the active site of AChE.

6.2.4. Inhibition of AChE-induced A β aggregation

Aliquots of 2 μL A β peptide, lyophilized from 2 mg mL⁻¹ 1,1,1,3,3,3-hexafluoro-2-propanol solution and dissolved in DMSO, were incubated for 24 h at room temperature in 0.215 M sodium phosphate buffer (pH 8.0) at a final concentration of 230 μM . For co-incubation

experiments aliquots (16 μL) of AChE (final concentration 2.30 μM , $\text{A}\beta/\text{AChE}$ molar ratio 100:1) and AChE in the presence of 2 μL of the tested inhibitor in 0.215 M sodium phosphate buffer pH 8.0 solution (final inhibitor concentration 100 μM) were added. Blanks containing $\text{A}\beta$, AChE, and $\text{A}\beta$ plus inhibitors at various concentrations, in 0.215 M sodium phosphate buffer (pH 8.0) were prepared. The final volume of each vial was 20 μL . Each assay was run in duplicate. To quantify amyloid fibril formation, the thioflavin T (ThT) fluorescence method was then applied.¹⁸ After dilution with glycine-NaOH buffer (pH 8.5), containing 1.5 mM ThT, the fluorescence intensities due to β -sheet conformation was monitored for 300 s at $\lambda_{\text{em}} = 490$ nm ($\lambda_{\text{ex}} = 446$ nm). The percent inhibition of the AChE induced aggregation due to the presence of the test compound was calculated by the following expression: $100 - (\text{IF}_i/\text{IF}_0 \times 100)$ where IF_i and IF_0 are the fluorescence intensities obtained for $\text{A}\beta$ plus AChE in the presence and in the absence of inhibitor, respectively, minus the fluorescent intensities due to the respective blanks.

6.2.5. Animal studies

All the mice used in these experiments were housed at constant temperature (22 ± 1 °C) and relative humidity ($60 \pm 1\%$) under a 12 hours light/dark cycle. Food and water were provided *ad libitum*. Effects of treatment on body weight and mortality were recorded. All the experiments were conducted according to the guidelines of the European Animal Health and Welfare Act.

AD11 anti-NGF mice were produced as described in Section 4.3.¹⁹ The treatment pattern shown below was therefore followed.

Table 4. Treatment pattern of selected compound in anti-NGF mice.

Compound	Numbers of mice	Administration route ^a	Dosage ^b	Duration
6 (lipocrine)	4	i.p.	0.165 mg/kg/day (0.104 mM)	15
8	5	i.p.	0.52 mg/kg/day (0.37 mM)	15
9	4	i.p.	0.52 mg/kg/day (0.37 mM)	15
10	4	i.p.	2.5 mg/kg/day (1.658 mM)	15
23	3	i.p.	0.1 mg/kg/day (0.104 mM)	15
Rivastigmine	4	i.p.	0.5 mg/kg/day (0.37 mM)	15
Memoquin	3	i.p.	3.5 mg/kg/day (1.658 mM)	15
LA	4	i.p.	0.254 mg/kg/day (0.37 mM)	15
LA	4	i.p.	1.14 mg/kg/day (1.658 mM)	15

^a i.p. = indicates intraperitoneal injection

^b duration of treatment expressed in days, and molarity refers to solution administered to the anti-NGF mice.

After the treatment, the mice were anaesthetised with 2,2,2-tribromoethanol (8 $\mu\text{L}/\text{g}$ of body

weight) and the encephala were removed from the cranial box. The front part of the brain, containing the basal forebrain and one of the two occipital poles was fixed in 4% paraformaldehyde, cryoprotected in 30% in saccharose and treated for immunohistochemistry. The second occipital pole was frozen on dry ice and treated so as to be subjected to Western Blot to assess the presence of phosphorylated tau.

Immunohistochemistry was carried out to show the number of cholinergic neurones in the basal forebrain. For this purpose, sections were incubated with the monoclonal antibody anticholine acetyltransferase (1 : 500, Chemicon International Inc., Temecula, CA). The reaction was developed using the avidin-biotin alkaline phosphatase Elite standard kit (Vector laboratories, Burlingame, CA), followed by a development with 3, 3' diaminobenzidine HCl (Sigma, Saint Louis, MO) and 5-bromo-4-chloro-3-indolyl phosphate toluidine salt (Sigma).

To carry out a Western blot analysis an iced solution was prepared (50 mM Tris-HCl, pH 7.5, 50 mM EDTA, 250 mM Spermidine, 1 mM phenylmethylsulphonyl fluoride (PMSF), 1 mM iodoacetamide, 10 µM/mL turkey egg white inhibitor, 0.1 % Triton X-100).

The homogenates were centrifuged at 13,400 rpm for 30 minutes at 4 °C, collecting the supernatant, re-centrifuged and kept at -80 °C until use. The proteic content was determined by diluting the samples ten times and using the BIO-RAD "DC protein assay kit" (Hercules, CA, USA). The samples (20 µg protein) were loaded on polyacrylamide gel NuPAGE 10% (Invitrogen, Carlsbad, CA) and SDS-PAGE and a Western blot were carried out in order to detect phosphorylated tau. In particular, phosphorylated tau was found using monoclonal antibodies AT270 (1:1000, Innogenetics, Gand, Belgium) which detect the phosphorylated tau in the Thr181 residue. A pre-stained proteic marker (New England Biolabs, Ipswich, MA) was loaded to find the dimension of the bands. The reaction was developed using an anti-mouse HRP (1:5000, GE Healthcare, Little Chalfont, England) and a developing solution ECL (GE, Healthcare).

References

- ¹ Steinberg, G.M.; Mednick, M.L.; Maddox, J.; Rice, R. A hydrophobic binding site in acetylcholinesterase. *J. Med. Chem.* **1975**, *18*, 1057-1061.
- ² Carlier, P. R.; Du, D. M.; Han, Y.; Liu, J.; Pang, Y. P. Potent, easily synthesized huperzine A-tacrine hybrid acetylcholinesterase inhibitors. *Bioorg. Med. Chem. Lett.* **1999**, *9*, 2335-2338.

- ³ Ciszewska, G.; Pfefferkorn, H.; Tang, Y.S.; Jones, L.; Tarapata, R.; Sunay Ustun B. Synthesis of tritium, deuterium, and carbon-14 labeled (S)-N-ethyl-N-methyl-3-[1-(dimethylamino)ethyl]carbamic acid, phenyl ester, (L)-2,3-dihydroxybutanedioic acid salt (SDZ ENA 713 hta), an investigational drug for the treatment of Alzheimer's Disease *Journal of Labelled Compounds & Radiopharmaceuticals*, **1997**; *39*, 651-668.
- ⁴ Grethe, G.L.; His, L.; Uskokovic, M.; Brossi, A. Syntheses in the isoquinoline series. Synthesis of 2,3-dihydro-4(1H)-isoquinolones *J. Org. Chem.* **1968**, *33*, 491-494.
- ⁵ Bolognesi, M.L.; Banzi, R.; Bartolini, M.; Cavalli, A.; Tarozzi, A.; Andrisano, V.; Minarini, A.; Rosini, M.; Tumiatti, V.; Bergamini, C.; Fato, R.; Lenaz, G.; Hrelia, P.; Cattaneo, A.; Recanatini, M.; Melchiorre, C. Novel Class of Quinone-Bearing Polyamines as Multi-Target-Directed Ligands To Combat Alzheimer's Disease. *J. Med. Chem.* **2007**, *50*, 4882-4897.
- ⁶ Bridges, A.J.; Zhou, H.; Cody, D.R.; Rewcastle, G.W.; McMichael, A.; Showalter, H.D.H.; Fry, D.W.; Kraker, A.J.; Denny, W.A. Tyrosine kinase inhibitors. 8. An unusually steep structure-activity relationship for analogues of 4-(3-bromoanilino)-6,7-dimethoxyquinazoline (PD 153035), a potent inhibitors of the epidermal growth factor receptor. *J. Med. Chem.* **1996**, *39*, 267-276.
- ⁷ Millen, J.; Riley, T.N.; Waters, I.W.; Hamrick, M.E. 2-(β -arylethylamino)-and 4-(β -arylethylamino)quinazoline as phosphodiesterase inhibitors. *J. Med. Chem.* **1985**, *28*, 12-17.
- ⁸ Ife, R.J.; Brown, T.H.; Blurton, P.; Keeling, D.K.; Leach, C.A.; Meeson, M.L.; Parsons, M.E.; Theobald, C.J. Reversible inhibitors of the gastric (H⁺/K⁺)-ATPase. 5. Substituted 2,4-diaminoquinazolines and thienopyrimidines. *J. Med. Chem.* **1995**, *38*, 2763-2773.
- ⁹ Karamanska, R.; Mukhopadhyay, B.; Russell, D.A.; Field, R.A.; Thioctic acid amide: Convenient tethers for achieving low non-specific protein binding to carbohydrates presented on gold surfaces. *Chem.Comm.* **2005**, *26*, 3334-3336.
- ¹⁰ Schwarz, M. *n*-Propane phosphonic acid anhydride. A condensation reagent. *Synlett* **2000**, *9*, 1369.
- ¹¹ Bare, T.M.; Sparks, R.B. Pyridazinedione compounds useful in treating neurological disorders. *US Patent* 5,739,133 (Apr. 14, **1998**)
- ¹² Rosini, M.; Andrisano, V.; Bartolini, M.; Bolognesi, M.L.; Hrelia, P.; Minarini, A.; Tarozzi, A.; Melchiorre C. Rational approach to discover multipotent anti-Alzheimer drugs. *J. Med. Chem.* **2005**, *48*, 360-363.
- ¹³ Kanuma, K.; Omodera, K.; Nishiguchi, M.; Funakoshi, T.; Chaki, S.; Semple, G.; Tran, T.-A.; Kramer, B.; Hsu, D.; Casper, M.; Thomsen, B.; Beeley, N.; Sekiguchi, Y. Discovery of 4-(dimethylamino)quinazolines as potent and selective antagonists for the melanin-concentrating hormone receptor 1. *Bioorg. Med. Chem. Lett.* **2005**, *15*, 2565-2569.
- ¹⁴ Dunn, J.P.; Goldstein, D.M.; Stahl, C.M.; Trejo-Martin, T.A. Substituted quinazoline compounds useful as p38 kinase inhibitors. *US Patent* 2004/0209904-A1 (Oct. 21, **2004**).
- ¹⁵ Wéber, C.; Bielik, A.; Demeter, A.; Borza, I.; Szendrei, G.I.; Keserù, G.M.; Greiner, I. Solid-phase synthesis of 6-hydroxy-2,4-diaminoquinazolines. *Tetrahedron* **2005**, *61*, 9375-9380.
- ¹⁶ Paschalidou, K.; Neumann, U.; Gerharts, B.; Tzougraki, C. Highly sensitive intramolecularly quenched fluorogenic substrates for renin based on the combination of L-2-amino-3-(7-methoxy-4-coumaryl)propionic acid with 2,4-dinitrophenyl groups at various positions. *Biochem. J.* **2004**, *382*, 1031-1038.
- ¹⁷ Ellman, G. L.; Courtney, K. D.; Andres, V.; Featherstone, R. M. A new rapid colorimetric determination of acetylcholinesterase activity. *Biochem. Pharmacol.* **1961**, *7*, 88-95.
- ¹⁸ Bartolini, M.; Bertucci, C.; Cavrini, V.; Andrisano, V. Beta-Amyloid aggregation induced by human acetylcholinesterase: inhibition studies. *Biochem. Pharmacol.* **2003**, *65*, 407-416.
- ¹⁹ Ruberti, F.; Capsoni, S.; Comparini, A.; Di Daniel, E.; Franzot, J.; Gonfloni, S.; Rossi, G.; Berardi, N.; Cattaneo, A. Phenotypic knockout of nerve growth factor in adult transgenic mice reveals severe deficits in basal forebrain cholinergic neurons, cell death in the spleen, and skeletal muscle dystrophy. *J. Neurosci.* **2000**, *20*, 2589-2601.